The importance of the time-effect in electrochemical studies of corrosion inhibitors

Meeusen, Mats

DOI
10.4233/uuid:990fdc2d-bae1-4de2-9ac1-3f649bb980cf

Publication date
2020

Document Version
Final published version

Citation (APA)
Meeusen, M. (2020). *The importance of the time-effect in electrochemical studies of corrosion inhibitors*. [Dissertation (TU Delft), Delft University of Technology]. https://doi.org/10.4233/uuid:990fdc2d-bae1-4de2-9ac1-3f649bb980cf

Important note
To cite this publication, please use the final published version (if applicable).
Please check the document version above.

The importance of the time-effect in electrochemical studies of corrosion inhibitors

PhD thesis

Mats Meeusen

This research was performed in Delft University of Technology
Department of Materials Science and Engineering
Mekelweg 2, 2628 CD Delft,
the Netherlands

This research was carried out under project number F81.6.13503 in the framework of the Partnership Program of the Materials innovation institute M2i (www.m2i.nl) and the Foundation for Fundamental Research on Matter (FOM), which is part of the Netherlands Organization for Scientific Research NWO (www.nwo.nl).

The cover presents an optical microscopy image of the hot-dip galvanized steel surface.

The importance of the time-effect in electrochemical studies of corrosion inhibitors

Dissertation

for the purpose of obtaining the degree of doctor

at Delft University of Technology

by the authority of the Rector Magnificus Prof. dr. ir. T.H.J.J. van der Hagen,

chair of the Board of Doctorates

to be defended publicly on

Friday 27 March 2020 at 12:30 o'clock

by

Mats MEEUSEN

Master of Science in Chemical and Materials Engineering,

Vrije Universiteit Brussel, Brussels, Belgium

born in Wilrijk (Antwerp), Belgium

This dissertation has been approved by the promotors:

Prof. dr. ir. J.M.C. Mol
Prof. dr. ir. H.A. Terryn

Composition of the doctoral committee:

Rector Magnificus	chairman
Prof. dr. ir. J.M.C. Mol	Delft University of Technology, promotor
Prof. dr. ir. H. Terryn	Delft University of Technology, promotor

Independent members:

Prof. dr. M.J. Santofimia Navarro	Delft University of Technology, the Netherlands
Prof. dr. F. Deflorian	University of Trento, Italy
Prof. dr. M. Olivier	University of Mons, Belgium
Prof. dr. T. Breugelmans	Universiteit Antwerpen, Belgium
Prof. dr. ir. J. Sietsma	Delft University of Technology, the Netherlands (reserve member)

Other member:

Dr. ir. B. Boelen	Tata Steel, the Netherlands

Keywords: corrosion inhibitors, aluminium alloy AA2024-T3, galvanized steel, ORPEIS, (in)stability, time-effect

ISBN 978-94-6332-615-5
Cover design: Koffie bij Tine/Tine Van Kerkhoven
Printed by: GVO drukkers & vormgevers B.V.

Table of Contents

Summary

The corrosion protection of metallic substrates with corrosion inhibitors, either in solution or dispersed in a coating formulation, has been the focus of many research topics for many decades and has intensified in recent years even more with industry moving away from hexavalent chromium (Cr(VI))- based corrosion inhibitors. While mainly concentrating on the electrochemical behaviour and the underlying corrosion protective mechanism, the study of the time-effect, i.e. the study of how the electrochemical system behaves and the stabilization of the electrochemical system is altered over time, is often not taken into account when studying corrosion inhibitor-containing electrochemical systems.

To gain a better understanding of the kinetic aspect of corrosion inhibitors changing the overall electrochemistry, this study focusses on the quantification of the time-effect of corrosion inhibitors' electrochemical behaviour. Therefore odd random phase electrochemical impedance spectroscopy (ORP-EIS) is selected, a multisine alternative to the classical electrochemical impedance spectroscopy (EIS) technique, capable to measure and quantify the stability of electrochemical systems over time. Two different electrochemical systems are considered: lithium-based corrosion inhibitor technology on aluminium alloy AA2024-T3 and silica- and phosphate-based corrosion inhibitors for hot-dip galvanized steel. The former, already well-understood system, served as the proof of concept to design a well-defined methodology to study corrosion inhibitor-containing electrochemical systems, and gain deeper knowledge of the latter system.

First EIS measurements on organically coated aluminium alloy AA2024-T3 with dispersed lithium-carbonate corrosion inhibitor inside an artificial defect were unable to describe the initial, rapidly evolving stages of corrosion (protection) due to the instability of the system and the shortcoming of the EIS technique in that perspective. Therefore it was opted to use ORP-EIS measurements and develop a quantification approach for the (in)stability of the electrochemical behaviour over time, described by the behaviour of the non-linearities and non-stationarities. This provided not only an estimation of the stabilization time an electrochemical system needs and a reliable EIS measurement can be obtained but also allowed linking the presence of non-stationarities in a certain frequency range to the (un)stable behaviour of the different electrochemical processes governing the overall system's instability and trends in the parameter evolution of the electrical equivalent circuits (EECs) describing the system.

Different macroscopic electrochemical techniques such as potentiodynamic polarization (PP), continuous open circuit potential (OCP) with superimposed linear polarization resistance (LPR), electrochemical noise (EN) and EIS were applied together with ORP-EIS to study a number of commercially available silica- and phosphate-based corrosion inhibitors for the corrosion protection of hot-dip galvanized steel. ORP-EIS measurements served as the electrochemical tool to evaluate the stability of each respective electrochemical system under investigation and as the basis for the interpretation of the results from the different macroscopic electrochemical techniques. As such, initially unstable and fluctuating results with high relative error prior to the system's stabilization point on the one hand and the stable results in terms of the polarization resistance (R_p) obtained from LPR and EIS measurements could be explained.

Overall, the presented results indicate that the time-effect cannot be overlooked when studying and interpreting corrosion inhibitor-containing electrochemical systems.

Samenvatting

De bescherming tegen corrosie van metallische substraten met corrosie inhibitoren, ofwel in oplossing ofwel in een coating formulering, is het onderwerp van verscheidene onderzoeken geweest door de jaren heen en is enkel versterkt de laatste jaren als gevolg van de industriële verschuivingen weg van zesvoudig chroom (Cr(VI)-) houdende corrosie inhibitoren. Deze studies focussen grotendeels op het elektrochemische gedrag en het onderliggende mechanisme beschermend tegen corrosie maar nemen de studie van het zogenaamde tijdseffect, dat bestudeert hoe een elektrochemisch systeem zich gedraagt en hoe de stabiliteit ervan verandert als functie van de tijd, niet in rekening tijdens het bestuderen van corrosie inhibitor-houdende elektrochemische systemen.

Om een beter inzicht te krijgen in het kinetische aspect van de corrosie inhibitoren en de daarbij horende veranderingen veroorzaakt in de globale elektrochemie richt deze studie zich op de kwantificering van het tijdseffect van het elektrochemische gedrag van deze inhibitoren. Om die reden werd odd random phase elektrochemische impedantiespectroscopie (ORP-EIS) geselecteerd, een alternatief op de klassieke elektrochemische impedantie spectroscopie (EIS) techniek, die het mogelijk maakt om de stabiliteit van elektrochemische systemen in rekening te brengen en te kwantificeren als functie van de tijd. Twee verschillende elektrochemische systemen werden beschouwd in dit werk: lithium-gebaseerde corrosie inhibitie technologie op aluminium legering AA2024-T3 en silica- en fosfaat-gebaseerde corrosie inhibitoren op verzinkt staal. Het eerste systeem, reeds welbekend, diende als proof of concept om een goed gedefinieerde methodologie te ontwerpen om corrosie inhibitor-bevattende elektrochemische systemen te bestuderen en om meer diepgaande kennis te vergaren omtrent het laatstgenoemde systeem.

Aanvankelijke EIS metingen op organisch gecoate aluminium legering AA2024-T3 met geïmpregneerde lithiumcarbonaat corrosie inhibitoren in een artificieel defect waren niet in staat om de initiële, snel evoluerende stadia van corrosie(bescherming) te beschrijven te wijten aan de instabiliteit van het systeem en de tekortkomingen van de techniek in dat perspectief. Om die reden werd gekozen voor ORP-EIS metingen en het ontwikkelen van een kwantificatie methode voor de (in)stabiliteit van elektrochemische systemen als functie van de tijd, die worden beschreven door het gedrag van de niet-lineariteiten en niet-stationariteiten. Dit zorgde niet alleen voor een schatting van de tijd die een elektrochemisch systeem nodig heeft om te stabiliseren en om een betrouwbare EIS meting op te leveren maar liet ook toe om de aanwezigheid van de non-stationariteiten in een bepaald

frequentiedomein te koppelen met het (in)stabiele gedrag van de elektrochemische processen die de globale (in)stabiliteit overheersen en met de trends in het verloop van de parameters van het equivalent elektrisch circuit (EEC) die het systeem fysisch beschrijven.

Verschillende macroscopische elektrochemische technieken zoals potentiodynamische polarisatie (PP), continue potentiaalmetingen bij evenwicht met gesuperponeerde lineaire polarisatie weerstandsmetingen (LPR), elektrochemische ruismetingen (EN) en EIS werden aangewend, tegelijkertijd met ORP-EIS, om een aantal commercieel beschikbare silica- en fosfaat-gebaseerde corrosie inhibitoren voor de corrosiebescherming van verzinkt staal te bestuderen. ORP-EIS metingen dienden als het elektrochemische middel om de stabiliteit van de respectievelijke elektrochemische systemen te bestuderen en als de basis voor de interpretatie van de resultaten van de verschillende macroscopische elektrochemische technieken. Op die manier konden de initieel instabiele en fluctuerende polarisatieweerstandswaarden met grote relatieve fout en de stabiele polarisatieweerstandswaarden, verkregen respectievelijk voor en na stabilisatie van het systeem, verklaard worden.

De resultaten in dit werk tonen aan dat het tijdseffect niet buiten beschouwing gelaten kan worden bij het bestuderen en interpreteren van corrosie inhibitor-houdende elektrochemische systemen.

List of figures

List of tables

Abbreviations and acronyms

ATR	Attenuated total reflection
BED	Backscatter electron detector
CE	Counter electrode
CPE	Constant phase element
DWT	Discrete wavelet transform
EC	Equivalent circuit
E_{corr}	Corrosion potential
EEC	Equivalent electrical circuit
ECN	Electrochemical current noise
EDX	Energy dispersive X-ray spectroscopy
EIS	Electrochemical impedance spectroscopy
EN	Electrochemical noise
EPN	Electrochemical potential noise
FESEM	Field emission scanning electron microscopy
FTIR	Fourier transform infrared spectroscopy
GDOES	Glow discharge optical emission spectroscopy
GDP	Gross Domestic Product
HVLP	High volume low pressure
i_{corr}	corrosion current density
IE	Inhibition efficiency
IMPACT	International measures of prevention, application and economics of corrosion technologies
K-K	Kramers-Kronig
LPR	Linear polarization resistance

NACE	National Association of Corrosion Engineers
NL	Non-linearities
NS	Non-stationarities
NSS	Neutral salt spray
OCP	Open circuit potential
ORP-EIS	Odd random phase electrochemical impedance spectroscopy
PP	Potentiodynamic polarization
PVC	Pigment volume concentration
RE	Reference electrode
REACH	Registration, Evaluation, Authorization and Restriction of Chemicals
RMS	Root mean square
R_n	Noise resistance
ROI	Return of Investment
R_p	Polarization resistance
SCE	Saturated calomel electrode
SEM	Scanning electron microscopy
TSA	Tartaric-sulphuric acid
WE	Working electrode
wt%	Weight percent
XPS	X-ray photoelectron spectroscopy
XRF	X-ray fluorescence
ZRA	Zero resistance ammeter

Chapter 1

Introduction

1.1. Industrial relevance and research objective

Corrosion is one of the major problems of global economy at the moment. The latest International Measures of Prevention, Application and Economics of Corrosion Technologies (IMPACT) report of 2016 by the National Association of Corrosion Engineers (NACE) estimated the global cost of corrosion to be $2.5 trillion, equivalent to 3.4 % of the world's Gross Domestic Product (GDP) in 2013. However, it is estimated that an astronomical saving of 15 up to 35 % could be realized on the cost of corrosion by using available corrosion control practices [1]. Corrosion inhibitor management is one of the main corrosion prevention and protection strategies that could reduce the overall cost of corrosion effectively. It is calculated that a return on investment (ROI) of 9.4 could be achieved by using non-hazardous corrosion inhibitors in the framework of green water treatment [1]. Because of the severity of the corrosion problem on the economical scale currently, academia and industries are striving towards using durable and sustainable corrosion control measures. Among those measures, 'green' corrosion inhibitor management is one of the top priorities of the industries suffering from corrosion related issues.

The use of hexavalent chromium (Cr(VI)-) based corrosion inhibitors has been common practice during the last decades. However, in 2007, the European Union adapted stricter international health and safety legislations including the Registration, Evaluation, Authorization and Restriction of Chemicals (REACH), aiming to create a new legal framework for the use of hazardous chemical substances [2]. A variety of Cr(VI)-containing chemicals, used as active protective pigments in many coating formulations, have been phased out either January 2017 or January 2019 because of their toxic and/or carcinogenic nature [3]. For the steel industry especially, this implicates that all branded organic coated galvanized steel products must be Cr(VI)-free by the end of 2017.

Corrosion inhibitors, either in solution or dispersed in a coating system, react with the underlying metallic substrate and are able to prevent or minimize the corrosion processes [4]. They act on the system in such a way that the kinetics of the processes controlling the overall system's electrochemical behaviour are significantly modified compared to the situation without corrosion inhibitors present. A distinction can be made between anodic, cathodic and mixed-type corrosion inhibitors in terms of their effect on the respective partial electrochemical reactions based on the mixed potential theory, although other inhibitor classifications are possible. Evans diagrams are able to graphically represent the mixed potential theory, predicting corrosion potential and corrosion rate taking into account the thermodynamics and kinetics of all reactions taking place. In these diagrams, the Tafel lines

for both the anodic and cathodic branches of either the hydrogen evolution/oxygen reduction reaction or the metal dissolution/plating reaction are shown, respectively. The corrosion potential and corrosion rate can then be defined as the potential at which the anodic line of the metal dissolution intersects with the cathodic line of hydrogen evolution or oxygen reduction and the rate of anodic metal dissolution at the corrosion potential, respectively [4][5][6][7][8].

Anodic-type corrosion inhibitors work by blocking the oxidation reaction, i.e. metal dissolution, through the reaction of the corrosion inhibitor with the produced metallic ions Me^{n+}, produced at the anode, resulting in the formation of an adsorbed film on the metallic surface. The Evans diagram in Fig. 1.1 schematically represents the effect of an anodic inhibitor on the partial oxidation reaction, resulting in a shift of the corrosion potential (E_{corr}) towards more noble values and a reduction of the corrosion current density (i_{corr}). Cathodic-type corrosion inhibitors, on the other hand, work by slowing down or blocking the reduction reaction of the metal, commonly oxygen reduction or hydrogen evolution. Increased alkalinity at cathodic surface spots causes these inhibitors to react with OH^- ions of water and produce compounds selectively precipitating on cathodic areas, creating a barrier for oxygen diffusion and preventing electron transfer from the metal.

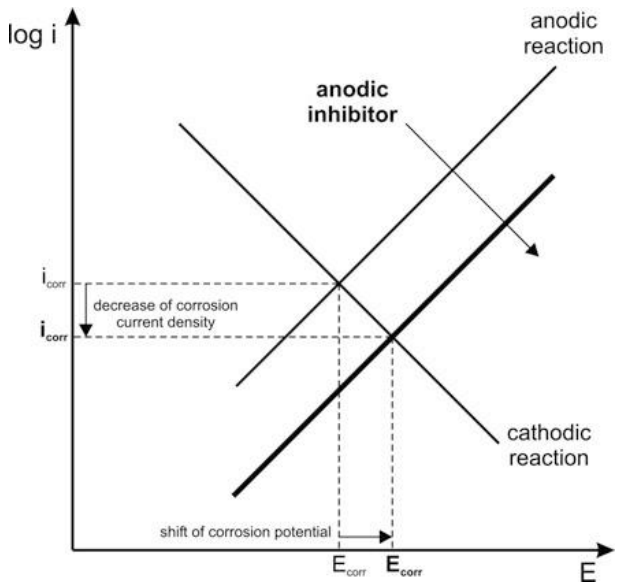

Figure 1.1 Schematic representation of the effect of a anodic-type inhibitor in the Evans diagram [8].

The Evans diagram in Fig. 1.2 schematically represents the effect of a cathodic inhibitor on the partial reduction reaction, resulting in a shift of the corrosion potential (E_{corr}) towards more active values and a reduction of the corrosion current density (i_{corr}). Mixed-type corrosion inhibitors are film forming compounds on both corrosion half-reactions. The Evans diagram in Fig. 1.3 schematically represents the effect of a mixed-type inhibitor on the partial oxidation and reduction reactions, resulting in a decrease of the corrosion current density (i_{corr}). The relative extent of each corrosion half-reaction determines the overall effect on the corrosion potential (E_{corr}) [4][5][6][7][8].

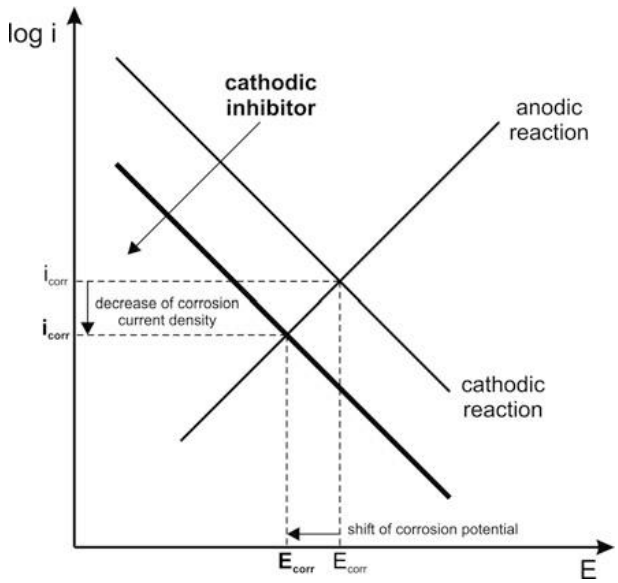

Figure 1.2 Schematic representation of the effect of a cathodic-type inhibitor in the Evans diagram [8].

In any case, the thermodynamics and kinetics dictating the course and rate of corrosion of the electrochemical system are altered over time by the protective action of the corrosion inhibitors. The introduction of newly produced intermediate anodic and/or catholic products in the overall process causes changes in the reversible potentials of the reactions, the exchange current densities and in the (slopes of the) Tafel lines representing the reactions. This results in a modified corrosion potential E_{corr} and corrosion current density i_{corr} and consequently an adapted corrosion rate with time characterizing the time-varying (non-stationary) character of corrosion inhibitor- containing electrochemical systems (Figure 1.4)

[6][8]. This emphasizes the importance of taking into account the time-effect, describing how the electrochemical system behaves and alters the electrochemical stability over time.

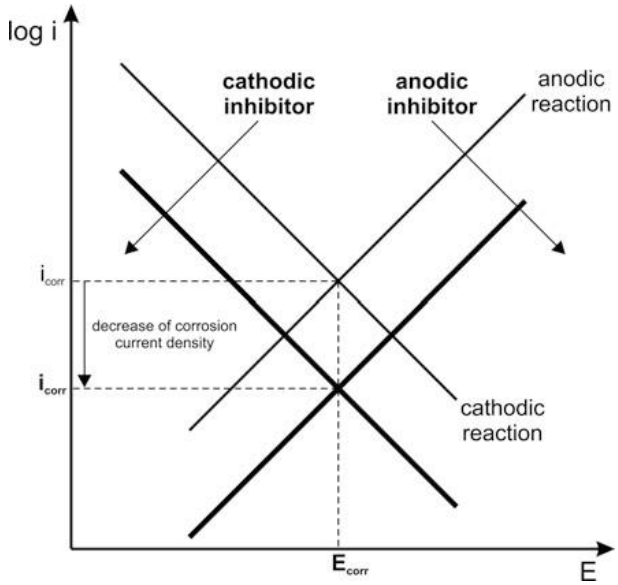

Figure 1.3 Schematic representation of the effect of a mixed-type inhibitor in the Evans diagram [8].

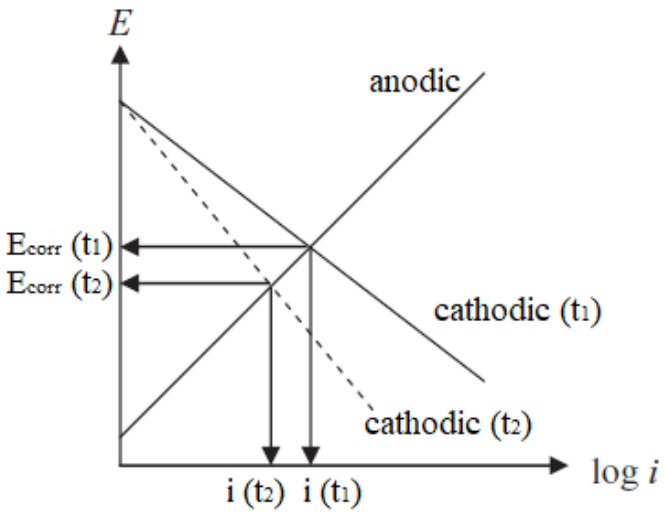

Figure 1.4 Schematic representation of the time-varying effect of a cathodic-type inhibitor on the corrosion potential (E_{corr}) and corrosion current density (i_{corr}) in the Evans diagram.

The linear Tafel lines presented in the preceding Evans diagrams are described by the Tafel equations:

$$\eta_a = b_a \log(\frac{i}{i_0}) \quad (1)$$

and

$$\eta_c = -b_c \log(\frac{|i|}{i_0}) \quad (2)$$

where b_a and b_c are the anodic and cathodic Tafel slopes, respectively. However, it needs to be remarked that these equations present a simplification, in the case of a sufficiently large anodic or cathodic polarization (η > 50 mV), of the Butler-Volmer equation, which expresses the relation between the overpotential η and the current density i at the electrode:

$$i = i_0 \exp[\frac{\alpha n F(E-E_{rev})}{RT}] - i_0 \exp[\frac{-(1-\alpha) n F(E-E_{rev})}{RT}] \quad (3)$$

$$i = i_0 \exp[\frac{\alpha n F \eta}{RT}] - i_0 \exp[\frac{-(1-\alpha) n F \eta}{RT}] \quad (4)$$

where i_0 is the exchange current density, α is the charge transfer coefficient, n is the number of exchanged electrons in the electrode reaction, F is the Faraday constant, R is the gas constant and T is the temperature [8]. However, in the vicinity of the corrosion potential E_{corr}, this linearization is not valid since anodic and cathodic reactions are occurring at similar rates and the net current, being the sum of the anodic and cathodic currents, deviates from the Tafel relationship. This indicates intrinsic non-linear behaviour. Polarization curves, measured by scanning the potential of a sample from a potential well under the corrosion potential to a potential well above the corrosion potential, are able to describe the overall behaviour at different potentials. In Figure 1.5, a polarization diagram is shown together with the Tafel lines, indicating the non-linear behaviour of corroding electrochemical systems [8].

Since corrosion processes are thus intrinsically non-stationary and non-linear, these phenomena can only be described adequately if they can be studied with appropriate electrochemical techniques or combinations of electrochemical techniques taking into account these deviations from linear and time-invariant behaviour [9][10][11]. We aim to create a framework taking into account the non-linear and time-varying character in corrosion inhibitor research. Therefore it is crucial to focus not only on the time-effect when studying corrosion inhibitor containing electrochemical systems but also on the selection of the electrochemical techniques to study this behaviour.

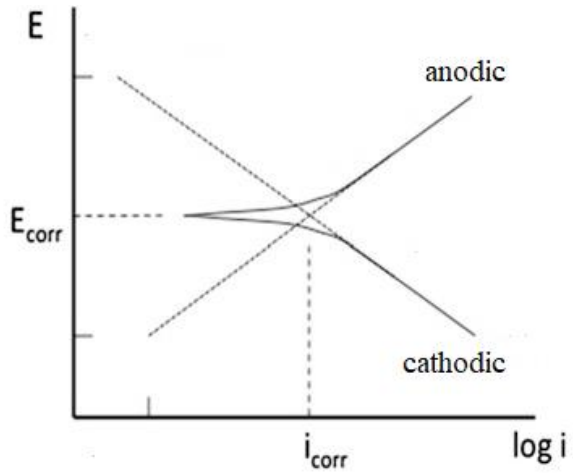

Figure 1.5 Schematic representation of the Tafel lines (dashed lines) resulting from the Tafel extrapolation of a polarization diagram (full line) [8].

Most corrosion inhibitor studies, however, focus on the electrochemical mechanism, i.e. retrieving the underlying corrosion mechanism, and the overall system's performance resulting in the application of (a combination of) conventional electrochemical techniques such as potentiodynamic polarization (PP) and electrochemical impedance spectroscopy (EIS) to retrieve that information and/or surface analysis techniques such as scanning electron microscopy coupled with energy dispersive x-ray spectroscopy (SEM-EDX), Fourier-transform infrared spectroscopy (FTIR) and glow-discharge optical emission spectroscopy (GDOES). We want to take corrosion inhibitor research one step further and follow the inhibitor's electrochemical behaviour over time in a quantitative way emphasizing the importance of the time-effect in inhibitor-containing electrochemical systems before focussing on protective mechanisms and overall performance. The selection of the appropriate electrochemical tool able to follow the inhibitor's electrochemical behaviour over time in a qualitative way is therefore crucial.

In the end, we want to study the influence of the corrosion inhibitor's behaviour over time on the electrochemical behaviour obtained from not only PP and EIS measurements but also from electrochemical noise (EN) measurements and the newly introduced open circuit potential (OCP) with superimposed linear polarization resistance (LPR) measurements and the impact on the interpretation of the performance of those inhibitor-containing electrochemical systems. As such, a rigorous methodology can be developed to study these kind of systems and acquire time-resolved information in a correct and reliable way.

1.2. Experimental approach

This work aims to study the inhibitor-metal interactions, focussing on both the methodology or strategy to study these interactions in a reliable way and the intrinsic protective behaviour of the corrosion inhibitors taking into account the electrochemical time-effect. Two different electrochemical systems are therefore studied: lithium-based corrosion inhibitor technology on aluminium alloy AA2024-T3 and silica- and phosphate-based corrosion inhibitors for the corrosion protection of hot-dip galvanized steel. The former, for which basic knowledge is available, serves as the proof of concept for the quantitative analysis of the time-effect and to develop a methodology or strategy to study the latter, relatively unknown, system.

EIS measurements on lithium-carbonate pigmented organic coatings in a coating defect serve as the starting point, indicating the shortcomings of the technique to take into account the time-effect of inhibitor-containing electrochemical systems. These measurements allow to follow electrochemical processes based on impedance measurements. Based on a small perturbation alternating voltage (1-10 mV), the current response is monitored as a function of frequency. The deviation of amplitude and phase from the applied signal allows us to calculate the impedance, which is the proportion between the applied perturbation voltage and the current response [12]. This permits one to study different electrochemical processes, for example kinetic and diffusion processes, having different characteristic time-constants and consequently occurring at different frequencies, dictating the overall electrochemical process [13]. Using EIS, the response of the electrochemical system can also be modelled by means of an electrical equivalent circuit (EEC). This circuit incorporates combinations of different components accounting for the different contributions of physical phenomena taking place [13][14].

However, to perform a reliable EIS measurement, it is necessary that the system fulfils the conditions of causality, linearity and stationarity, to define correctly the transfer function of the electrochemical system and to obtain a satisfactory model. Therefore, in general, classical EIS measurements are performed by applying only a small amplitude perturbation signal (to ensure linearity) in the stationary regime of the process (to ensure time-invariance). This might result in measurements having poor signal-to-noise ratios. Moreover, the measurement will not be able to describe the initial, rapidly evolving stages of electrochemical processes, such as corrosion phenomena [9][15]. Since we wanted to focus on the time-effect in a quantitative way, classical EIS is not sufficient anymore at this point.

At this point, odd random phase electrochemical impedance spectroscopy (ORP-EIS) was selected, a multisine alternative to classical EIS able to present this non-linear and time-

varying behaviour, for the in-depth analysis of the stability of corrosion inhibitor-containing electrochemical systems over time while also exploring the possibility of quantifying this information.

ORP-EIS is based on the parallel measurement of multiple frequency components, using the sum of multiple sinusoidal signals as an excitation, also referred to as multisine EIS. With this technique, the level of disturbing noise, the level of non-linear distortions and the level of non-stationary behaviour can be measured and quantified and eventually taken into account when interpreting the resulting data when fitting according to a physically suitable EEC. The working principle of applying such a 'multisine' excitation signal is schematically represented below (Fig. 1.6). Rather than applying each excitation frequency subsequently, all excitation frequencies are summed and applied together. But there are some more particularities to the applied signal, i.e. only the odd harmonics are excited and per group of 3 consecutive odd harmonics, one is randomly omitted as represented in Fig. 1.7 [9]. This generates a periodic broadband signal consists of the sum of N harmonically related sine waves with an amplitude U(k), a maximum frequency f_{max} and random phases φ_k:

$$u(t) = \sum_{k=-N}^{N} \frac{U(k)}{2} e^{j\left(\frac{2\pi f_{max} k t}{N} + \varphi_k\right)} \quad (5)$$

$$= \sum_{k=1}^{N} U(k) \cos(2\pi f_k t + \varphi_k) \quad (6)$$

The phases φ_k are randomly chosen in the interval $[0,2\pi]$ such that $E[e^{j\varphi k}]=0$. This provides an odd random phase multisine excitation signal with a random harmonic grid which has a logarithmic distribution. The determination and quantification of the level of disturbing noise, non-linearities and non-stationarities of the electrochemical system is then perfromed through a statistical data analysis. Direct consequence of this multsine excitation signal is that the higher frequencies are excited many times more than the lower frequencies and therefore measurement time is drastically reduced compared to classical EIS, making ORP-EIS especially useful to retrieve quantified time-resolved electrochemical information [9][15][16].

The findings related to the use of ORP-EIS as the electrochemical tool to study the time-effect serve as the proof of concept and are then put into practice defining an adequate methodology or strategy to screen different commercially available silica- and phosphate-based corrosion inhibitors for hot-dip galvanized steel with conventional macroscopic electrochemical techniques. The information obtained from the quantification of the ORP-EIS data related to the stability of different corrosion inhibitor-containing systems serves as the starting point for the interpretation of the electrochemical data of the selected

macroscopic electrochemical techniques: potentiodynamic polarization (PP), open circuit potential (OCP) with superimposed linear polarization resistance (LPR), electrochemical noise (EN) and electrochemical impedance spectroscopy (EIS).

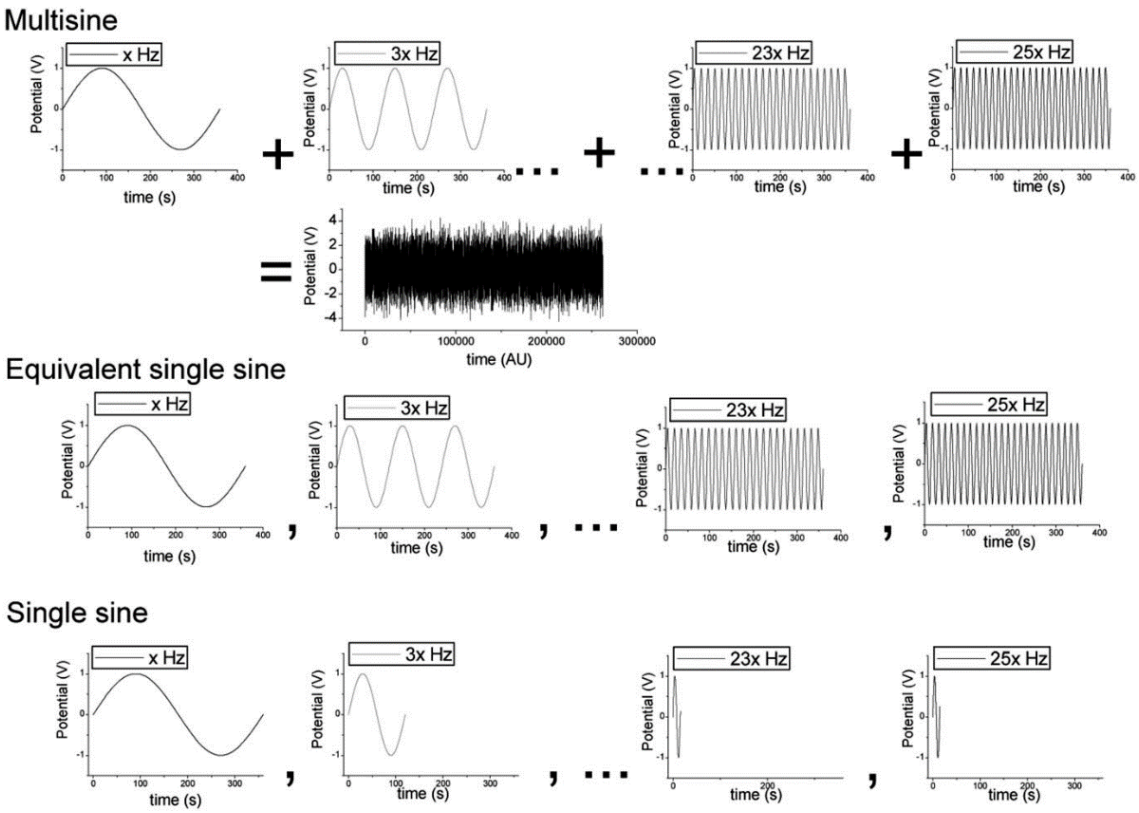

Figure 1.6 Schematic representation of the principle of ORP-EIS [9].

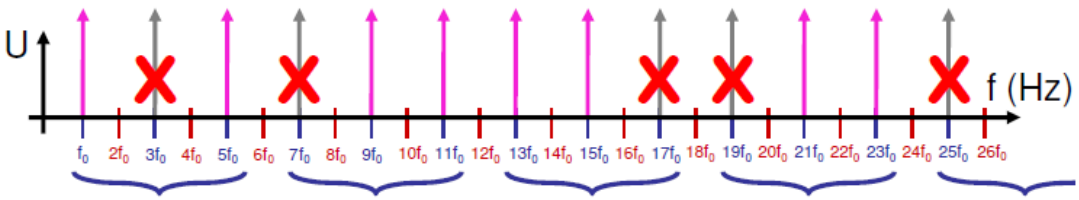

Figure 1.7 Schematic representation of the principle of omitting 1 out of 3 consecutive odd harmonics in ORP-EIS. The purple arrows represent the excited odd harmonics and the grey arrows represent the omitted odd harmonics, respectively [15].

PP measurements are capable to describe the kinetic behaviour by decoupling the anodic and cathodic reactions as well as the corrosion inhibition mechanism at discrete moments in time. A continuous OCP measurement, describing the thermodynamic stability in terms of a potential value, are extended with LPR measurements over hour, able to describe the corrosion protective properties over time. EN measurements are capable of performing in-depth corrosion analysis, through analysis of the noise resistance or through alternative transient analysis methods. EIS has established itself as an effective technique to provide time-resolved information about the corrosion protective properties of inhibitor-containing electrochemical systems both qualitatively, in terms of the magnitude of the impedance modulus at low frequencies, and quantitatively, in terms of fitting the data to an equivalent electrical circuit with a physicochemical meaning.

Finally, a number of silica- and phosphate-based corrosion inhibitors are then screened on their intrinsic protective behaviour for organic coated galvanized steels with the developed methodology or strategy. The followed experimental approach is presented in Fig. 1.8.

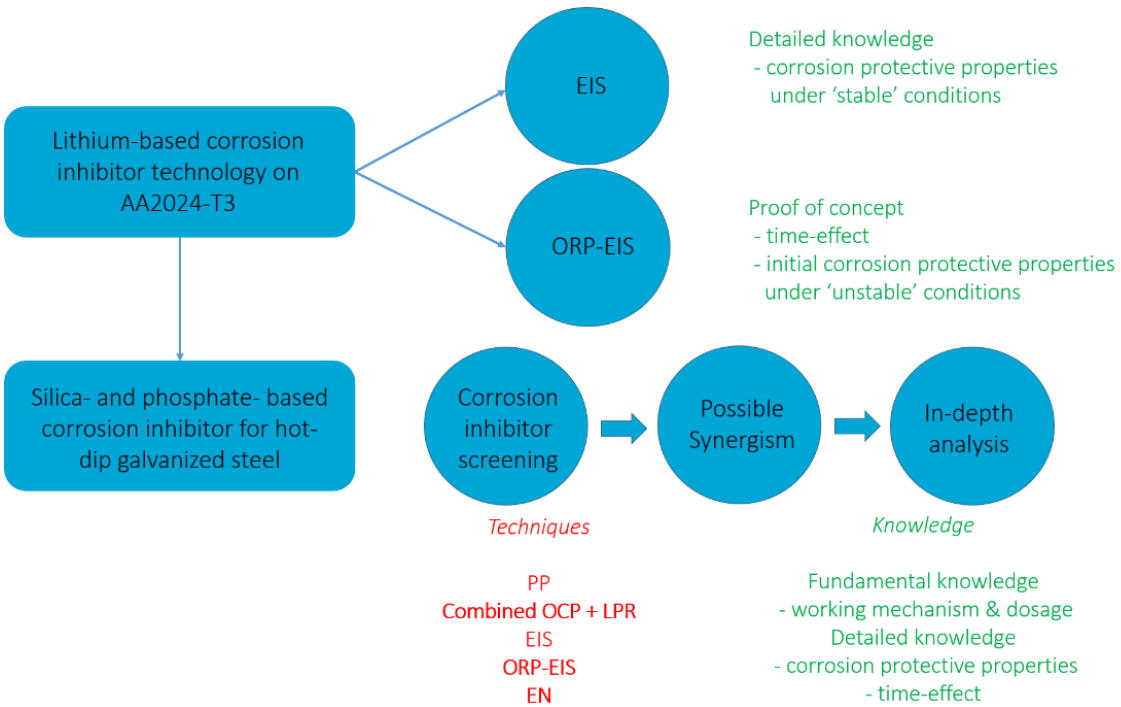

Figure 1.8 Schematic illustration of the different experimental steps followed to study corrosion inhibitor- containing electrochemical systems.

1.3. Outline of the thesis

A graphical representation of the structure of this PhD thesis is presented in Figure 1.9. In Chapter 1, a general introduction is given discussing the industrial relevance, the aim and the experimental approach of this work. The experimental results are presented in the format of scientific papers throughout chapters 2 to 5.

The first part of the experimental work focusses on lithium- based corrosion inhibitor technologies for the protection of aluminium alloy AA2024-T3. In Chapter 2 a classical electrochemical approach is followed using electrochemical impedance spectroscopy (EIS) measurements for the electrochemical evaluation of the protective layers generated in an artificial coating defect from lithium-carbonate leaching organic coatings on aluminium alloy 2024-T3 on the macroscopic scale. The electrochemical behaviour is initially described qualitatively and quantitatively, by linking the proposed physical model to an equivalent electrical circuit (EEC). Chapter 3 introduces a novel approach using odd random phase electrochemical impedance spectroscopy (ORP-EIS) measurements to follow now also the time-dependant behaviour in a quantitative way by examination of the non-linearities and non-stationarities present in the system and investigate the influence of the (in)stabilities on the proposed model.

The second part of the experimental work focusses on commercially available silica- and phosphate-based corrosion inhibitors for the corrosion protection of hot-dip galvanized steel. Chapter 4 discusses the methodology or strategy to evaluate the previously introduced electrochemical tool as the starting point for the screening of corrosion inhibitors taking into account also the time-effect and the influence on the results and interpretation of a number of macroscopic electrochemical techniques. In Chapter 5 this methodology or strategy is followed to study the intrinsic electrochemical behaviour of a variety of corrosion inhibitors. A general overview, conclusions and recommendations about the methodology to study the electrochemical behaviour of corrosion inhibitor-containing electrochemical systems and the intrinsic behaviour of both electrochemical systems is discussed in Chapter 6.

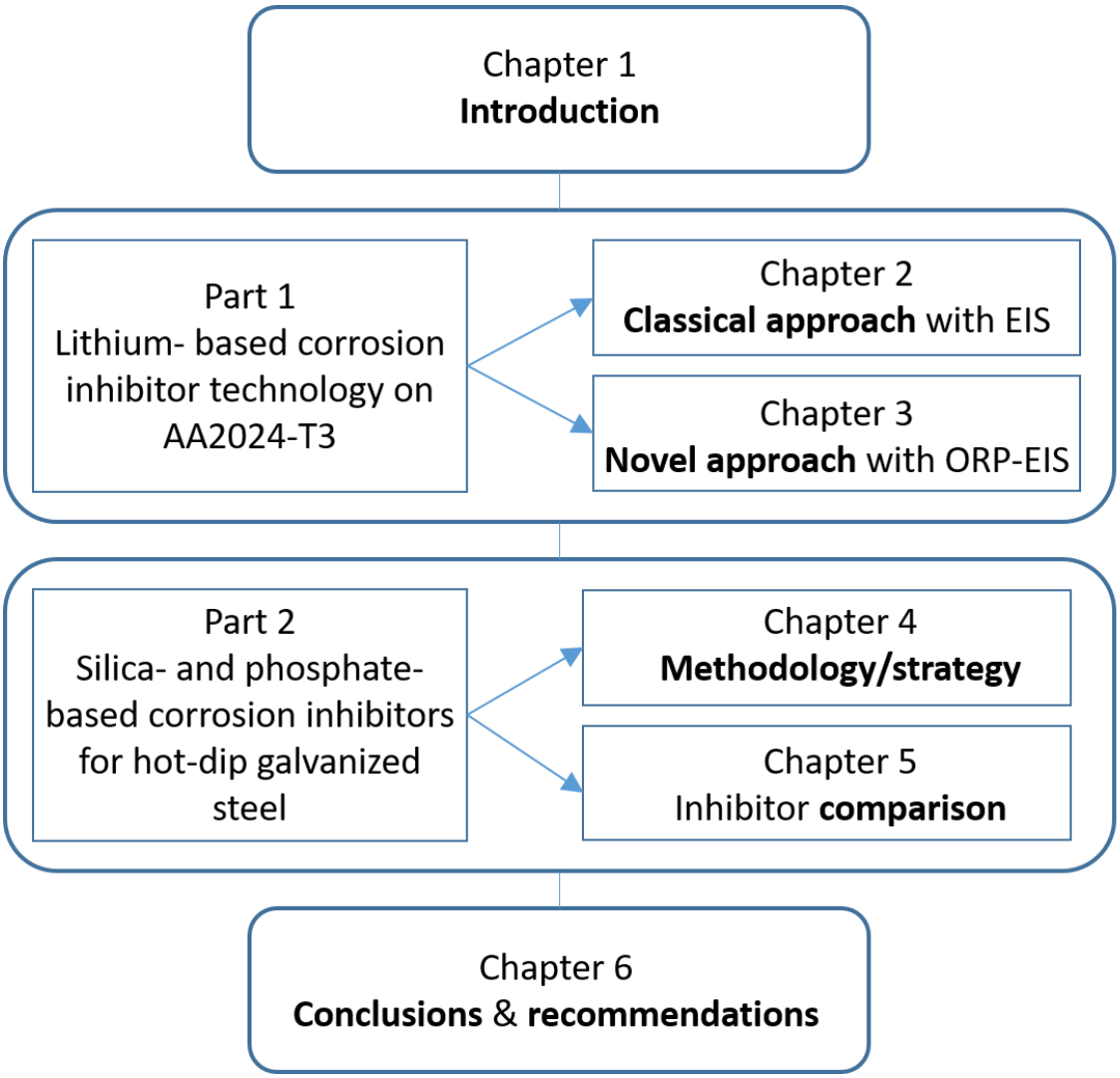

Figure 1.9 Graphical representation of the PhD thesis outline.

References

1. Gerhardus, K., Jeff, V., Thopson, N., Moghissi, O., Gould, M., & Payer, J. (2016). International Measures of Prevention , Application , and Economics of Corrosion Technologies Study. *NACE international*, 1–216.
2. Humphries, P. (2018). REACH Authorisation and Hexavalent Chrome.
3. Baghni, I. M., Lyon, S. B., & Ding, B. (2004). The effect of strontium and chromate ions on the inhibition of zinc. *Surface and Coatings Technology*, *185*(2–3), 194–198.
4. Dariva, G., Gallo, A. (2014). Corrosion Inhibitors – Principles, Mechanisms and Applications. *Developments in Corrosion Protection*. Intech Open
5. Roberge, P. R. (1999). Handbook of corrosion engineering. New York: Mc Graw Hill Handbook.
6. Talbot, D., & Talbot, J. (2000). Corrosion science and technology. C. Press.
7. Bardal, E. (2004). *Corrosion and protection*. Springer.
8. Andreatta, F., & Fedrizzi, L. (2016). Corrosion Inhibitors. In *Active Protective Coatings* (pp. 59–83). Springer.
9. Van Ingelgem, Y., Tourwé, E., Blajiev, O., Pintelon, R., & Hubin, A. (2009). Advantages of odd random phase multisine electrochemical impedance measurements. *Electroanalysis*, *21*(6), 730–739.
10. Wolff, N., Harting, N., & Fridolin, R. (2019). Understanding nonlinearity in electrochemical systems, *The European Physical Journal Special Topics, 2640*, 2617–2640.
11. Varela, H., & Krischer, K. (2001). Nonlinear phenomena during electrochemical oxidation of hydrogen on platinum electrodes, *Catalysis Today, 70*, 411–425.
12. Orazem, M. E., & Tribollet, B. (2008). *Electrochemical Impedance Spectroscopy*. Wiley.
13. Brett, C., Maria, A. N. ., & Brett, O. (1993). Electrochemistry Principles, Methods and Applications. Oxford University Press.
14. Macdonald, D. D. (2006). Reflections on the history of electrochemical impedance spectroscopy, *Electrochimica Acta, 51*, 1376–1388.
15. Bruegelmans, T. (2010). An identification approach as a prerequisite for quantitative electrochemical studies. PhD Thesis, Vrije Universiteit Brussel.
16. Breugelmans, T., Tourwé, E., Van Ingelgem, Y., Wielant, J., Hauffman, T., Hausbrand, R., Terryn, H., Hubin, A. (2010). Odd random phase multisine EIS as a detection method for the onset of corrosion of coated steel. *Electrochemistry Communications*, *12*(1), 2–5.

Chapter 2

Electrochemical evaluation of corrosion inhibiting layers formed in a defect from lithium-leaching organic coatings

This chapter is based on a published scientific paper:
P. Visser, M. Meeusen, Y. Gonzalez-Garcia, H. Terryn and J.M.C. Mol (2017). Electrochemical evaluation of corrosion inhibiting layers formed in a defect from lithium-leaching organic coatings. *Journal of the Electrochemical Society, 164 (7)*. C369-C406.

Abstract

This work presents the electrochemical evaluation of protective layers generated in a coating defect from lithium-leaching organic coatings on AA2024-T3 aluminum alloys as a function of neutral salt spray exposure time. Electrochemical impedance spectroscopy was used to study the electrochemical properties on a macroscopic scale. An electrochemical model allowed to quantitatively link the electrochemical behavior with the physical model of the layer in the damaged area as studied by scanning electron microscopy.

2.1. Introduction

In 2010, lithium salts were introduced as possible alternative to chromates as leachable corrosion inhibitor from organic coatings by Visser and Hayes [1]. It was found that organic coatings loaded with lithium salts demonstrated effective corrosion inhibition in a defect under neutral salt spray (NSS) conditions. Further investigations revealed that under NSS corrosive conditions lithium salts leached from the organic coating into an artificial defect and increased the pH in the defect to values between 9 and 10 [2]. Under these alkaline conditions a hydrated aluminum oxide layer is formed in the defect area with a final thickness of 0.5-1.5 µm after 168 h NSS exposure. The protective layer has a typical physical morphology consisting of a dense barrier layer at the aluminum interface, a porous middle layer and a columnar outer layer [3]. NSS testing according to aerospace standards demonstrated that this protective layer provides long-term corrosion protection comparable with chromate based inhibitor technology [4]. X-ray photoelectron spectroscopy (XPS) indicated that the formed layers have the characteristics of a hydrated aluminum oxide like (pseudo)boehmite [2].

Protective aluminum oxide/hydroxide layers have been of interest since the late 1950s. It was reported at that time that the native aluminum oxide film is hydrated to form pseudoboehmite and boehmite upon immersion in water at elevated temperatures [5]. Alwit and Kudo [6, 7] studied the formation of these pseudoboehmite layers at 50-100°C and prepared TEM cross-sections demonstrating a duplex structure with a dense inner layer and a porous outer layer. Buchheit et al. [8] studied protective layers prepared by a chemical conversion process from alkaline lithium salt solutions and demonstrated good corrosion protection on several aluminum alloys. Such conversion coatings showed clearly a two-layer morphology comprising a thin amorphous inner layer and an outer crystalized hydrotalcite layer [9]. Din et. al. generated boehmite layers with a similar duplex morphology with the accelerated oxide film growth method, using steam [10]. In their work, they demonstrated that these layers provide corrosion protection on AA6060 alloys by electrochemical analysis and standard corrosion testing such as acid assisted salt spray and filiform corrosion resistance. Potentiodynamic polarization measurements showed a reduction in anodic and cathodic activity and the pitting potential shifted to more noble values [11].

While our previous studies focused on the structure, morphology, and formation of the protective hydrated aluminum oxide layer in a defect, the development of the electrochemical response of these layers over time has not yet been studied [2, 4, 12, 13]. Therefore, the aim of this work is to study the development of the electrochemical

characteristics and to link these with the physical properties of the protective layer during and after its formation in an artificial coating defect on AA2024-T3, using field emission scanning electron microscopy (FESEM) and electrochemical impedance spectroscopy (EIS). To this aim, artificially damaged lithium-leaching organic model coatings applied on AA2024-T3 aluminum alloys were exposed to a neutral salt spray corrosion test (ASTM B-117). Cross-sectional analysis of the defect area using FESEM showed the thickness evolution and morphological formation of the protective layer over time. The evolution of the electrochemical response of the layer in the defect area as a function of time and the quantification of the electrochemical characteristics of the hydrated aluminum oxide in the coating defect on a macroscopic scale were studied with EIS. This study provides pivotal information on the electrochemical and physical development of the layer in a coating defect aimed to develop our insights into the corrosion protective properties of these lithium-leaching organic coatings.

2.2. Experimental

2.2.1. Materials and sample preparation

Polyurethane model coatings with a composition as listed in Table 2.1 were used for this work. The lithium-salt loaded coatings have a total pigment volume concentration (PVC) of 30 vol %, comprising 15 vol % inorganic pigments and fillers and 15 vol % lithium salt respectively. Analytical grade lithium carbonate and lithium oxalate purchased from Sigma Aldrich were used as lithium-leaching compounds for active inhibition.

The pigmented organic coatings were prepared according to the following procedure. The raw materials of Component A were added sequentially while stirring into a 370 ml glass jar. Subsequently, 400 grams Zirconox® pearls (1.7 -2.4 mm) were added to the mixture for grinding and dispersion of the pigments. The samples were shaken for 20 minutes on a Skandex® paint shaker to achieve a fineness of grind less than 25 μm. After shaking the pearls were separated from the coating. Component B was added separately, and the paint was stirred to a homogeneous mixture.
AA2024-T3 bare aluminum alloy (Alcoa) was anodized in tartaric-sulphuric acid (TSA) according to aerospace requirements (AIPI 02-01-003). The model coatings were applied with a high volume low pressure (HVLP) spray gun at ambient conditions (23 °C and 55 % RH). After the application and a 1 h flash-off period, the coated panels were cured at 80°C for 16 h. The dry film thickness of the coatings after drying was 20-25 μm.

An artificial damage was made on the coated panels with a mechanical milling device leaving a U-shaped scribe of 1 mm wide and 100-150 μm deep. After scribing, the samples were exposed to the neutral salt spray test (ASTM-B117) for varying periods of time, from 2 h up to 168 h. Before each sample analysis, the corrosion process was quenched and any residual chlorides were removed by rinsing the panels with flowing deionized water for 2 min and air-drying.

Table 2.1 Composition of uninhibited reference and the lithium-leaching organic model coatings.

	Non-inhibiting reference	**Lithium carbonate**	**Lithium oxalate**
Component A			
N-Butylacetate	75.0 g	75.0 g	75.0 g
Desmophen 650MPA	47.7 g	47.7 g	47.7 g
Lithium carbonate		23.6 g	
Lithium oxalate			32.0 g
Magnesium oxide		16.4 g	16.4 g
Tioxide TR 92		5.9 g	5.9 g
Blanc Fixe N ($Ba(SO_4)$)		15.4 g	15.4 g
Component B			
Tolonate HDB 75 MX	28.5 g	28.5 g	28.5 g
Dynasilan Glymo	5.2 g	5.2 g	5.2 g

2.2.2. Scanning electron microscopy (SEM)

Cross-sectional observations of the scribed region were carried out using a JEOL JSM-7100F field emission SEM using the backscatter electron detector (BED-C) at 5 kV and a working distance of 3 mm. The samples were sectioned using a diamond saw and consecutively ion milled using a Hitachi IM4000 ion milling system at 6kV Ar-ion acceleration, a 3 times-per-minute sample rotation speed and a swing angle of +/- 30º.

2.2.3. Electrochemical impedance spectroscopy (EIS)

The electrochemical behaviour of coated AA2024-T3 samples in the presence of a coating defect was studied with EIS before and after different periods of neutral salt spray (NSS) exposure. EIS measurements were performed at OCP using a Gamry Interface 1000 computer-controlled potentiostat over a frequency range from 10-2 Hz to 3·104 Hz, 7 points per decade and a sinusoidal amplitude of 10 mV, using a three-electrode set-up in a Faraday cage, equipped with a saturated calomel electrode (SCE) as the reference electrode, platinum wire as the counter electrode and a scribed panel as the working electrode using a 0.05 M NaCl electrolyte. The area exposed to the electrolyte was 12.5 cm2, the effective bare electrode (i.e. the coating defect) area was 0.48 cm2 and the volume of electrolyte was 60 cm3. Measurements were recorded after 4 to 8 hours exposure to the 0.05M NaCl electrolyte on at least three samples for each exposure condition. The impedance plots were fitted using different equivalent circuits with Zview from Scribner Associates Inc.

2.3. Results and discussion

2.3.1. Visual and microscopic coating defect analysis as a function of NSS exposure time

In the aerospace industry, the active protective properties of coatings are tested by means of neutral salt spray (NSS) exposure according to ASTM B-117 [14]. Prior to exposure, an artificial defect is made through the coating into the metal and the degree of corrosion is assessed after various periods of exposure. Fig.2.1a-d shows the rapid formation of corrosion products in such a defect when exposed to corrosive conditions as a function of time in case a coating has no inhibitive capabilities for protection of AA2024-T3 bare aluminum alloy. The first signs of corrosion are evident after only 2 h of exposure (Fig. 2.1a) illustrating the intrinsic high corrosion susceptibility of the AA2024-T3 alloy. The corrosion continues with time and results in a large amount of voluminous corrosion products in the scribe after 48 and 168 h of exposure (Fig. 2.1c and d). In contrast to the coating without corrosion inhibitor, both model coating formulations, loaded with lithium carbonate (Fig. 2.1e-h) and lithium oxalate (Fig. 2.1i-l) as leachable corrosion inhibitor, showed no corrosion products in the scribed area after 168 h of NSS exposure. This demonstrates the effective active protective properties of these lithium-based inhibitor loaded coatings.

Fig. 2.2 shows micrographs of cross-sections of defect areas before and after NSS exposure. Fig. 2.2a shows the general overview of the cross-sectional edge region of the defect prior to exposure. Fig. 2.2b shows the typical surface of the unexposed scribe bottom. Fig 2.2c shows the cross-sectional edge region of the defect in case lithium-leaching coatings are applied and exposed to NSS after 168 h of exposure. The cross-sectional micrographs of a coating defect of a lithium oxalate loaded coating covered samples confirm the absence of corrosion and reveal the protective layer that was formed throughout the scribed area. Fig 2.2d shows the typical morphology of the hydrated aluminum oxide layer that is formed from this lithium oxalate loaded coating covered sample under these corrosive conditions [3]. The layer covers the entire surface of the damaged alloy. This characteristic layer is formed rapidly from the lithium-leaching coating technology and protects the damaged area effectively.

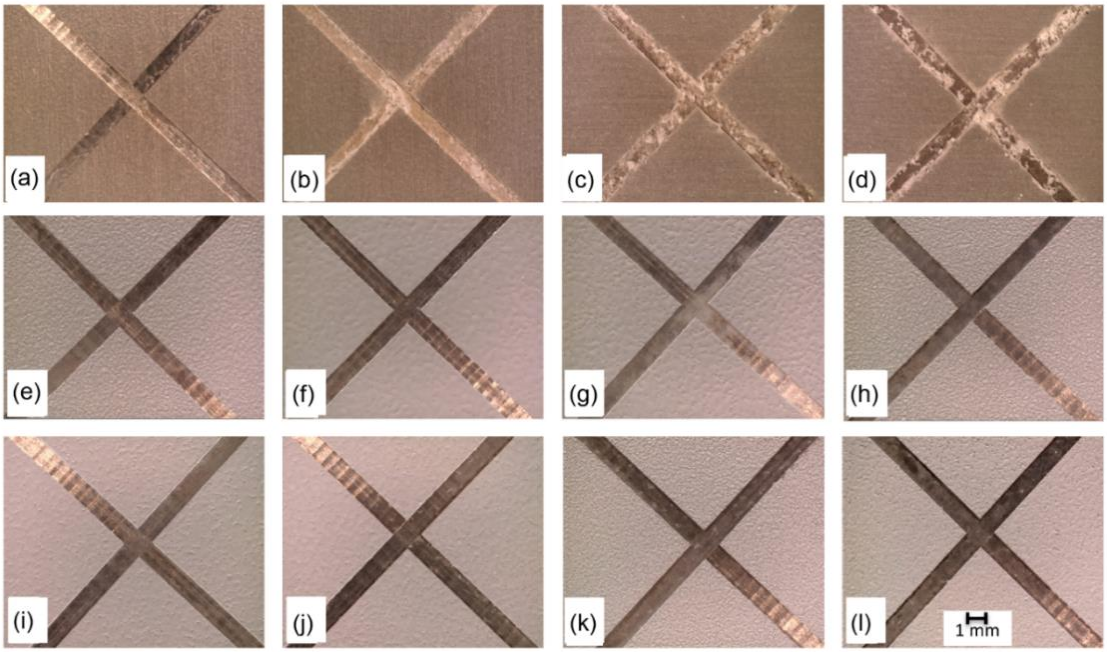

Figure 2.1 Top view of scribe area after neutral salt spray exposure: non-inhibited coating after **(a)** 2 h, **(b)** 8 h, **(c)** 48 h, and **(d)** 168 h; lithium carbonate loaded coating after **(e)** 2 h, **(f)** 8 h, **(g)** 48 h, and **(h)** 168 h; lithium oxalate loaded coating after **(i)** 2 h, **(j)** 8 h, **(k)** 48 h, and **(l)** 168 h.

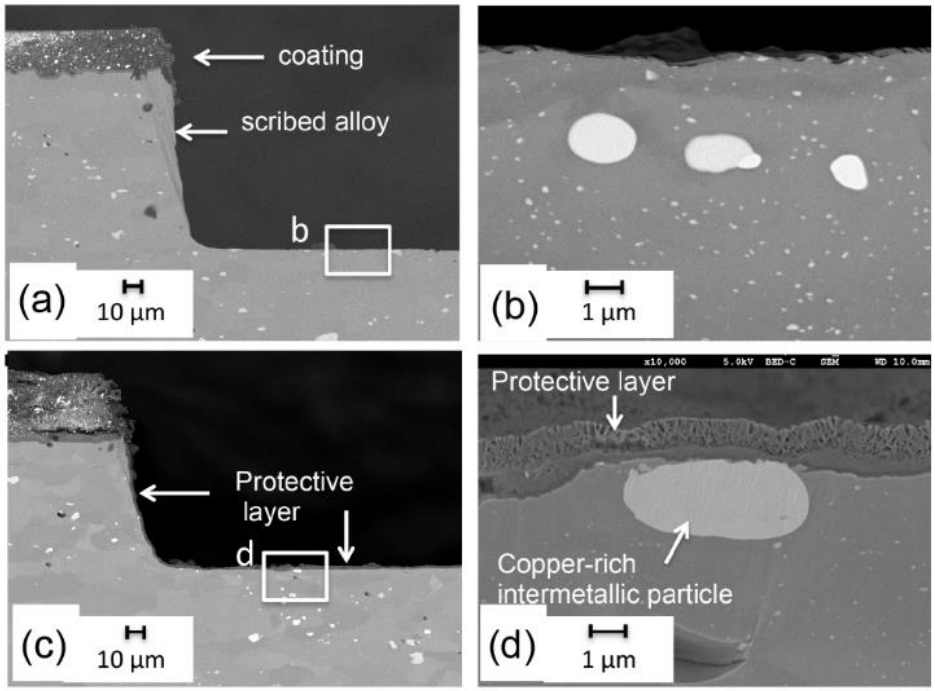

Figure 2.2 Microscopic cross-sectional view of the coating scribe area: **(a)** edge region of the defect and **(b)** defect bottom region before NSS exposure; **(c)** edge region of the defect and **(d)** defect bottom region after 168 h NSS exposure for the lithium oxalate loaded coating covered sample.

2.3.2. Protective layer formation as a function of NSS exposure time

To study the formation and the characteristics of the protective layer in the defect area over time, ion-milled cross-sections of lithium carbonate and lithium oxalate loaded coatings were analyzed after 2, 8, 48, and 168 h of NSS exposure. Fig. 2.3 shows cross-sectional micrographs of the protective layer during its formation over this period of time. The micrographs show that after 2 h NSS exposure a layer of 0.3 to 0.5 µm has been formed on the aluminum surface of the scribe. (Fig. 2.3 a,e). The layer has a dense morphology at the aluminum metal/oxide interface of ~ 0.1 µm and a more porous morphology at the outer surface. As result of longer exposure, the layer develops in thickness and morphology on the outer side. After 8 to 48 h of exposure, the layer thickness varies between 0.6-0.8 µm and both the lithium carbonate and lithium oxalate loaded samples shows the development of a columnar structure at the outer surface and maintaining a dense layer at the aluminum

interface (~0.1 µm) (Fig. 2.3b and f, 8 h; Fig 2.3. c and g, 48 h). After 168 h the protective layers have grown to a thickness of about 1.0-1.2 µm and show the characteristic morphology of a dense inner layer (~0.1 µm), a porous middle layer and a columnar outer layer as observed in our previous studies [4]. It is important to notice that the thickness of the dense inner layer remains similar, ~0.1 µm, for both lithium-leaching coatings for the full exposure time of 168 h.

Fig. 2.4 shows the quantitative development of the thickness of the layer derived from the micrographs of the cross-sections. It can be noted that after 2 and 8 h NSS exposure, the thickness of the layers from the lithium oxalate loaded coating are thicker compared to the layers generated from the lithium carbonate loaded coatings. This can be explained by the lower initial pH in the defect area of the lithium oxalate coatings as observed by local pH measurements in previous work [2]. The development of the aluminum hydroxide gel layer is a result of the competitive film formation process of chemical dissolution at aluminum hydroxide gel/solution interface and film growth at the metal/aluminum hydroxide gel interface. This in line with the results of Hurlen and Haug, who observed that thickness of the layer is related to the pH of the solution. A higher pH accelerates the chemical dissolution at the aluminum hydroxide gel/solution interface resulting in thinner layers [15, 16].

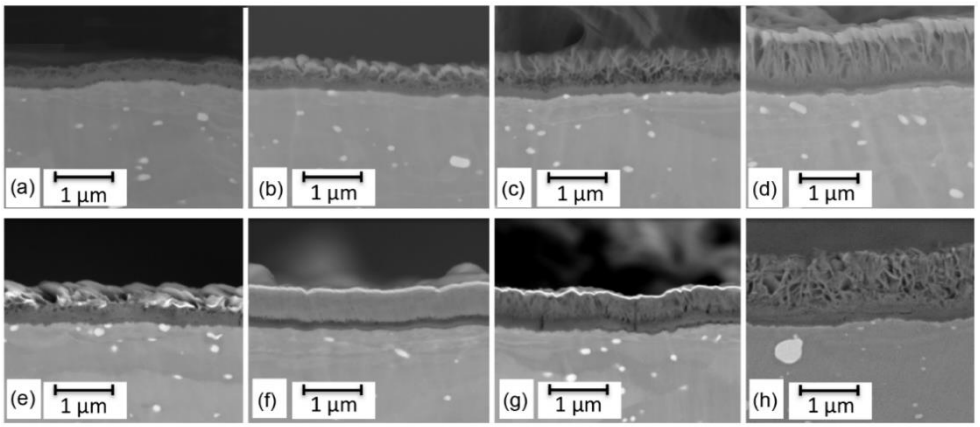

Figure 2.3 Cross-sectional scanning electron micrographs of the protective layer in the scribe: lithium carbonate loaded coating after **(a)** 2, **(b)** 8, **(c)** 48, and **(d)** 168 hours of NSS exposure; lithium oxalate loaded coating after **(e)** 2, **(f)** 8, **(g)** 48, and **(h)** 168 hours of NSS exposure.

The results confirm the previously proposed multistep-process to comprise basically 4 steps [2]: oxide thinning, anodic dissolution, formation of an aluminum hydroxide gel layer, and finally the aging of this gel into a hydrated aluminum oxide [16, 17]. The cross-sections revealed the formation of the protective aluminum hydroxide gel on the alloy in the early stages, followed by the ageing process resulting in the characteristic three-layered morphology of the protective layer with a dense layer at the aluminum interface, a porous transition layer in the middle and a columnar morphology at the top.

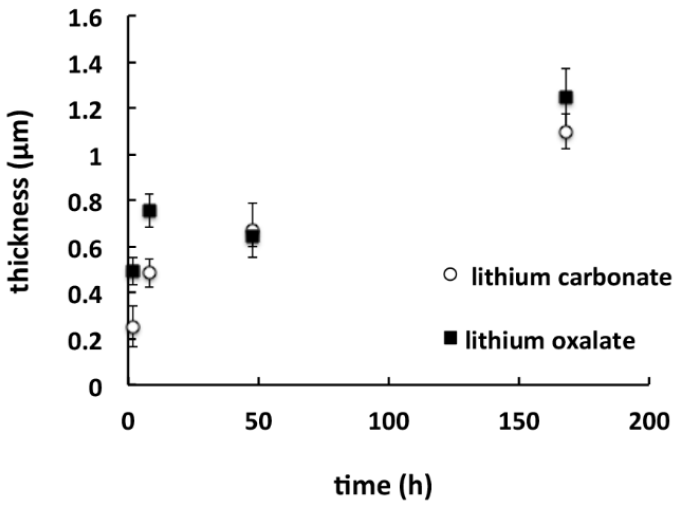

Figure 2.4 Measured thickness of the protective layers from lithium carbonate and lithium oxalate loaded coatings after different periods of NSS exposure.

2.3.3. Corrosion protective properties as a function of NSS exposure time

The electrochemical characteristics of the layers formed in a defect from coatings with and without lithium-leaching compounds were measured by EIS. Fig. 2.5 shows the Bode plots of the coatings with and without lithium-leaching compounds after 168 h NSS exposure. A non-exposed reference sample was measured to show the initial state of the scribe (damaged area) representing the alloy with a native oxide. After exposure to the corrosive NSS conditions, the Bode plots of the impedance modulus (Fig. 2.5a) of both lithium-leaching coatings show an increase of impedance values in the middle frequency (10^{1}-10^{3} Hz) and low frequency (10^{-1}-10^{-2} Hz) ranges compared to the unexposed sample and the sample without

inhibitor. This increase of the impedance modulus in the middle frequency range can be associated with the formation of an (oxide) layer in the damaged area [18]. The increase of the impedance modulus at low frequencies by approximately one order of magnitude can be associated with the increased corrosion resistance of the layers generated from the lithium-leaching coatings [19].

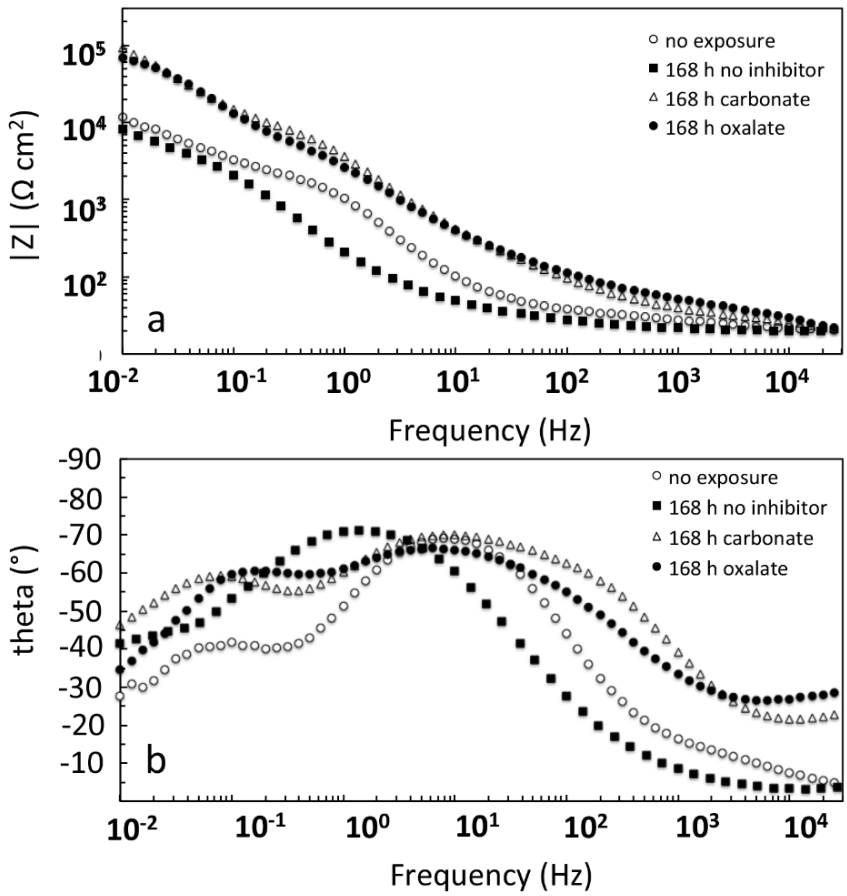

Figure 2.5 Electrochemical impedance spectra of the defect areas of coatings with and without lithium salts on AA2024 aluminum alloy before and after 168h NSS exposure measured in a 0.05M NaCl solution: **(a)** impedance modulus **(b)** phase angle plot.

The accompanying phase angle plots of these measurements are shown in Fig. 2.5b. In case of the unexposed scribe the phase angle diagram shows clearly two time-constants, one at 10^{1} Hz for the thin oxide layer and one at 10^{-1} Hz related to the electrochemical activity at

the aluminum interface in the coating defect, which are characteristic for the native oxide on aluminium [20]. After NSS exposure, the Bode phase angle diagram of the coating without inhibitor shows still two time-constants. However, the time-constant at the middle frequency shifted to a lower frequency and the second time-constant at the low frequency increased slightly. This behavior can be explained due to the formation of corrosion products in the defect area. The Bode phase angle plots for both lithium-leaching coatings show a broadening of the phase angle around $10^1 – 10^3$ Hz as a result of the generated layer in the defect area. It can be noted that this phase angle peak has an asymmetric shape and shows a shoulder in the higher frequency area around 10^2 to 10^3 Hz. This asymmetry suggests that there are possibly two overlapping time-constants in this frequency range. The phase angle of the time-constant observed at the low frequency range (10^{-1}Hz) has increased. This increase of the phase angle in the low frequency range can be associated with an improved corrosion protection.

Fig. 2.6 shows the Bode plots representing the behavior of the impedance of the samples with and without lithium-leaching coatings before and after the various exposure times in the NSS. The coating without inhibitor (Fig. 2.6a and d) shows a decrease of the impedance in the mid frequency range and the time-constant shifts to lower frequencies over time. This phenomenon can be explained by the dissolution of the native oxide. When analysing the Bode impedance modulus plots of the lithium-leaching coatings (Fig. 2.6b and c) it can be noticed that impedance modulus values increase almost instantaneously for both samples due to the NSS exposure. After only 2 h NSS exposure, the impedance modulus values have increased significantly in the middle and low frequency range and increased further as a result of longer exposure times. After 168 h the impedance modulus reaches a maximum. Compared to the sample with the native oxide, the impedance modulus of the hydrated aluminum oxide layer increased by about one order of magnitude in the low frequency range and increased a half order of magnitude in the middle frequency range. The lithium carbonate and lithium oxalate coatings show similar protective behavior independent of the anion used. The Bode phase angle plots of the lithium-leaching coatings are shown in Fig. 2.6d and e. It can be noted that the phase angle of the respective time-constants increased and broadened as a result of the NSS exposure time. Overall, this indicates that the electrochemical characteristics can be linked with the formation of the protective layer as observed in the FESEM cross sections (Fig. 2.3).

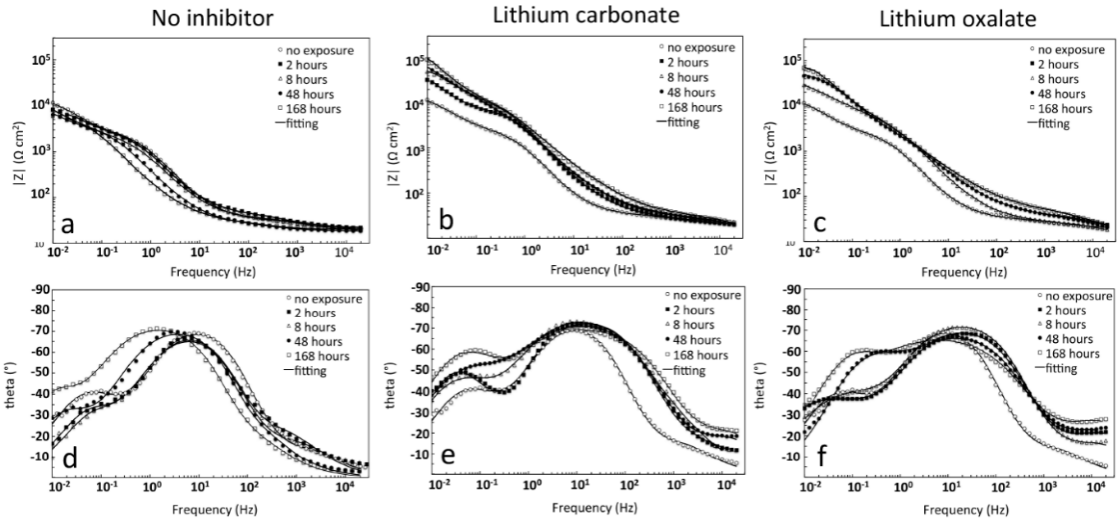

Figure 2.6 Electrochemical impedance spectra of the defect areas of lithium salt loaded coatings on AA2024-T3 aluminum alloy before and after NSS exposure for 2 h up to 168 h: coating with no inhibitor coating **(a)** impedance modulus **(d)** phase angle plot; lithium carbonate loaded coating **(b)** impedance modulus **(e)** phase angle plot; lithium oxalate loaded coating **(c)** impedance modulus **(f)** phase angle plot

The EIS spectra of these measurements were fitted with equivalent circuits (ECs) to quantitatively describe the electrochemical properties of the generated layers in the defect during the formation [21]. Fig. 2.7 shows the two equivalent circuit models used to fit the data from the EIS measurements. EC1, a two time-constant circuit, was used to describe the effect in the defect of a damaged coating without inhibitor prior and after NSS exposure. R_{sol} represents the resistance of the electrolyte; R_{oxide} is the resistance of the (native) oxide layer and the CPE_{oxide} is the constant phase element (CPE) describing the capacitance of the oxide layer using parameters Q_{oxide} and n_{oxide}, the electrochemical processes at the aluminum interface are represented by R_{pol} and CPE_{dl}. R_{pol} is the polarization resistance and CPE_{dl} is accounting for the double layer capacitance. CPE's are commonly used to describe the frequency dependence of elements with a non-ideal capacitive behavior [22]. In this work, CPE is used to account for the dispersive behavior of the time-constants due to the non-uniformity of the layers generated in the defect [2, 12].

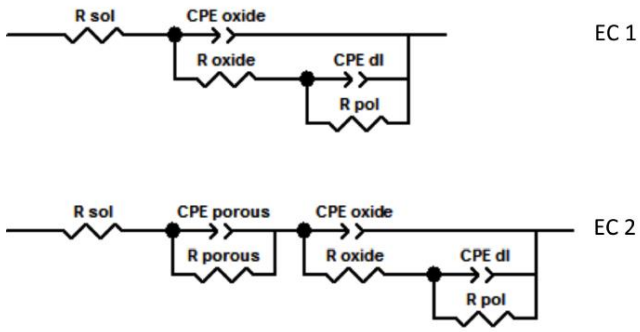

Figure 2.7 Equivalent electric circuits used to fit EIS spectra for coating defect areas: **(a)** EC1 for unexposed scribe and coating without inhibitor **(b)** EC2 for the lithium-based inhibitor generated protective layers.

An equivalent circuit model (EC2) with three time-constants was used for the fitting of the EIS spectra of the lithium-leaching samples. The physical morphology of the protective hydrated aluminum oxide layer observed in the defect by FESEM and represented by the Bode phase angle plots (Fig. 6e and f) indicate that a three time-constant equivalent circuit model (EC2) is more appropriate compared to the two time-constant model (EC1). The metal/oxide layer interface and dense barrier layer are represented by two clearly defined time-constants at the low ($5 \cdot 10^{-2}$ – 10^{-1} Hz) and middle (10^{1}-10^{3} Hz) frequency range respectively. The third time-constant of EC2 describes the contribution of the broader phase angle at the higher frequencies (10^{2} - 10^{3} Hz) related to the porous outer layer. EC2 can be interpreted as: R_{sol} for the solution resistance, R_{porous} and CPE_{porous} describe the contribution of the porous middle layer, R_{oxide} and CPE_{oxide} represent the dense inner layer, and CPE_{dl} and R_{pol} describe the double layer capacitance and polarization resistance at the metal/oxide interface. The fitted curves are displayed as solid lines in the Bode plots of Fig. 2.6. The numerical values of the fittings from these spectra are listed in Table 2.2, 2.3 and 2.4.

The results for the coating without inhibitor (Table 2.2) showed an initial decrease of R_{oxide} followed by a gradual increase. This behavior could indicate the process of oxide thinning followed by the precipitation of the corrosion products in the defect area. Table 2.3 and 2.4 show the fitting results of the lithium-leaching coatings. The most important observation from these data is the significant increase of R_{oxide} and R_{pol} over time for both coatings related to the generation of a dense oxide layer at the aluminum interface. R_{oxide} increases by a factor 7 and 10 for the lithium carbonate and lithium oxalate loaded coatings respectively. In addition, the polarization resistance increased by a factor 20 for the lithium

carbonate loaded coating and a factor 10 for the lithium oxalate loaded coating compared to the native oxide and the coating without inhibitor.

Table 2.2 Fitted parameters for EIS spectra of the scribed coating without inhibitor after different periods of NSS exposure.

		T= 0	T= 2 h	T= 8 h	T= 48 h	T= 168 h
EC		**1**	**1**	**1**	**1**	**1**
R_{sol}	Ωcm^2	27	28	24	20	21
$Q(CPE_{Oxide})$	$Ssncm^{-2}$	1.16×10^{-4}	1.33×10^{-4}	1.80×10^{-4}	2.38×10^{-4}	3.50×10^{-4}
n_{oxide}		0.87	0.82	0.78	0.83	0.82
R_{oxide}	Ωcm^2	3846	3799	3990	4506	9931
$Q(CPE_{dl})$	$Ssncm^{-2}$	4.30×10^{-4}	1.0×10^{-3}	1.15×10^{-3}	1.69×10^{-3}	2.10×10^{-3}
n_{dl}		0.85	0.90	0.92	0.89	0.95
R_{pol}	Ωcm^2	9683	3820	6954	6591	11609
χ^2		3.5×10^{-3}	6.0×10^{-3}	5.1×10^{-3}	$4{,}5 \times 10^{-3}$	5.7×10^{-3}

Table 2.3 Fitted parameters for EIS spectra of the scribed lithium carbonate loaded coating after different periods of NSS exposure.

		T= 0	T= 2 h	T= 8 h	T= 48 h	T= 168 h
EC		**1**	**2**	**2**	**2**	**2**
R_{sol}	Ωcm^2	26	19	21	15	15
$Q(CPE_{porous})$	$Ssncm^{-2}$	-	1.30×10^{-4}	1.95×10^{-4}	1.42×10^{-5}	1.35×10^{-5}
n_{porous}		-	0.69	0.67	0.76	0.75
R_{Porous}	Ωcm^2	-	13	18	15	17
$Q(CPE_{Oxide})$	$Ssncm^{-2}$	1.06×10^{-4}	3.40×10^{-5}	2.89×10^{-5}	3.47×10^{-5}	2.82×10^{-5}
n_{oxide}		0.84	0.87	0.86	0.84	0.81
R_{oxide}	Ωcm^2	3788	9153	17009	17562	29636
$Q(CPE_{dl})$	$Ssncm^{-2}$	4.80×10^{-4}	1.76×10^{-4}	8.18×10^{-5}	5.21×10^{-5}	3.30×10^{-5}
n_{dl}		0.85	0.88	0.76	0.73	0.86
R_{pol}	Ωcm^2	12515	62248	105030	129400	237430
χ^2		3.9×10^{-3}	9.4×10^{-4}	1.1×10^{-3}	1.73×10^{-4}	7.8×10^{-4}

Table 2.4 Fitted parameters for EIS spectra of the scribed lithium oxalate loaded coating after different periods of NSS exposure.

		T= 0	T= 2 h	T= 8 h	T= 48 h	T= 168 h
EC		**1**	**2**	**2**	**2**	**2**
R_{sol}	Ωcm^2	26	15	15	13	13
$Q(CPE_{porous})$	$Ssncm^{-2}$	-	9.31×10^{-6}	9.98×10^{-6}	1.97×10^{-5}	1.74×10^{-5}
n_{porous}		-	0.76	0.82	0.70	0.70
R_{Porous}	Ωcm^2	-	23	12	24	34
$Q(CPE_{Oxide})$	$Ssncm^{-2}$	1.06×10^{-4}	2.11×10^{-5}	3.55×10^{-5}	3.98×10^{-5}	4.22×10^{-5}
n_{oxide}		0.84	0.83	0.86	0.80	0.77
R_{oxide}	Ωcm^2	3788	10775	8160	9942	37847
$Q\ (CPE_{dl})$	$Ssncm^{-2}$	4.80×10^{-4}	1.54×10^{-4}	1.31×10^{-4}	2.71×10^{-5}	2.03×10^{-5}
n_{dl}		0.85	0.72	0.70	0.82	0.97
R_{pol}	Ωcm^2	12515	58012	42597	50748	96352
χ^2		7.1×10^{-3}	1.56×10^{-4}	2.7×10^{-4}	5.2×10^{-4}	7.4×10^{-4}

For further analysis and comparison, the equivalent capacitance of the different elements in the equivalent circuit was calculated using the CPE parameters (Q and n) and the resistance corresponding to each time-constant using the equation:

$$C = R^{\frac{(1-n)}{n}} Q^{\frac{1}{n}} \quad (1)$$

This is equation is applicable to a normal time-constant distribution through a surface layer according to Hirschorn et al. [23]. The resistance and capacitance of the dense oxide layer (R_{oxide} and C_{oxide}) and the metal/oxide interface (R_{pol} and C_{dl}) was calculated from at least 3 replicate measurements. Fig. 2.8 shows the evolution and scatter of the resistance and capacitance of the oxide layer and the metal/oxide interface as a function of NSS exposure time. Fig. 2.8a shows that resistance of the oxide (R_{oxide}) increased over time due to the formation of the dense layer from the lithium-leaching coatings. Whereas the defect area has a R_{oxide} of about 3.7 $k\Omega\ cm^2$ before NSS exposure, the resistance almost tripled after only 2 h NSS exposure. Over prolonged exposure, R_{oxide} shows a gradual increase to values of 25-

30 kΩ cm^2 after 168 h (Fig. 2.8a). At the same time, the capacitance of the formed dense layer (C_{oxide}) is reduced by a factor 5 lower after 2 h NSS exposure compared the native oxide and remains stable over time around 20-30 µF/cm^2 (Fig. 2.8c). This behavior can be related to the rapid formation of the dense layer on the substrate and a gradual further densification and reducing porosity increasing the oxide resistance while maintaining its thickness as reflected by the FESEM cross-sectional analysis in Fig. 2.3. The resistance of the oxide (R_{oxide}) of the coating without inhibitor remains at a level of 5 to 9 kΩ cm^2. In addition, the oxide capacitance of the coating without inhibitor is increasing rapidly indicating degradation of the oxide layer (inset Fig. 2.8c). The corrosion activity at the substrate can be characterized by the time-constant consisting of the polarization resistance (R_{pol}) and the double layer capacitance (C_{dl}). Fig. 2.8b and d show the evolution of the R_{pol} and C_{dl} during the formation of the protective layer in the defect. Compared to the defect prior to NSS exposure, both lithium-leaching coatings show increasing polarization resistance (Fig. 2.8b) and decreasing double layer capacitance (Fig. 2.8d) over time indicating improved corrosion protective properties of the formed layer on the aluminum in the defect area. For the coatings without inhibitor the polarization resistance (R_{pol}) remained around the initial level and the double layer capacitance (C_{dl}) increased to very large values (inset Fig. 2.8d), indicating the presence of the corrosion process. The observed trend of increasing resistances and decreasing capacitances of the lithium-leaching coatings is consistent with the formation and densification of the protective layer in the defect area. The observed effect corresponds with the trend of increasing layer thickness over time in Fig. 2.4.

The inhibition efficiency (IE) of the generated layers in the defect was calculated from the impedance data at the various intervals using the following equation [24, 25]:

$$IE\ (\%) = \frac{R_{pol\ (lithium)} - R_{pol\ (no\ inhibitor)}}{R_{pol\ (lithium)}} \times 100\% \qquad (2)$$

where $R_{pol(lithium)}$ represents the polarization resistance of the protective layer generated from a lithium-leaching coating and $R_{pol(no\ inhibitor)}$ represents the polarization resistance in the defect from a coating without inhibitor after the same NSS exposure time. The inhibiting efficiency of the layers generated in a defect area from lithium leaching coatings are shown in Fig. 2.9. The inhibition efficiency of the lithium carbonate loaded coating demonstrates an inhibiting efficiency of around 80% after only 2 hours which develops further up to 95% after 48 h and remains at a similar level upon longer exposure. The inhibition efficiency of the protective layer from the lithium oxalate loaded coating develops faster in the first hours this can be related to the faster layer thickness development of these lithium oxalate loaded

coatings in Fig. 2.4. The development of the inhibition efficiency confirms the fast and effective inhibition provided by protective layers generated in the defect area.

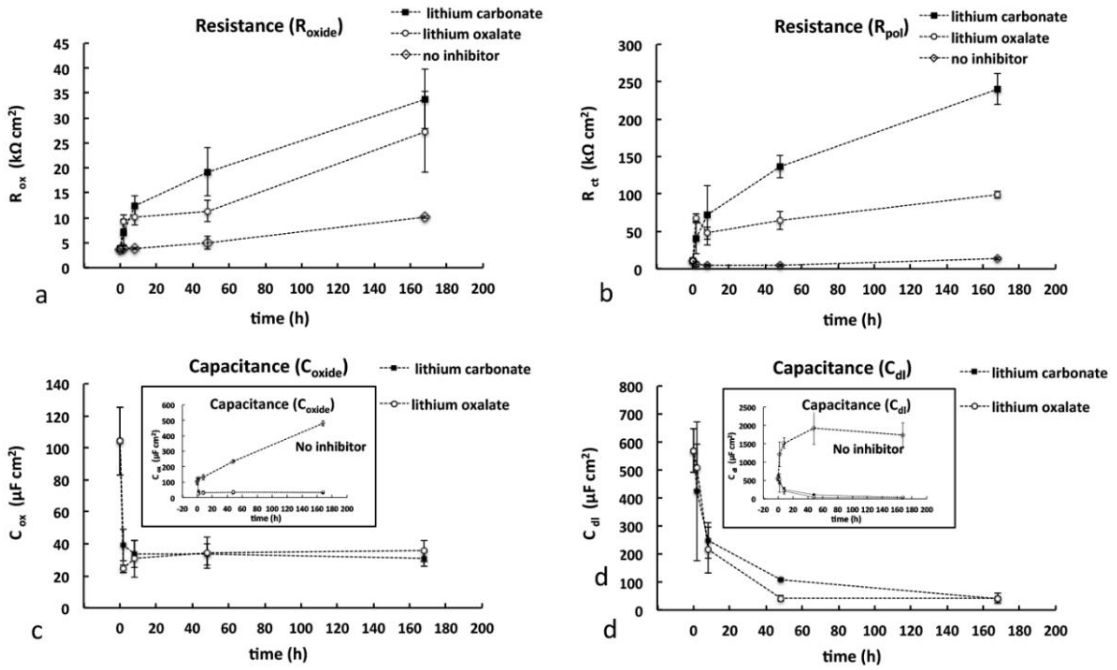

Figure 2.8 Evolution of **(a)** the dense layer resistance (R_{oxide}), **(b)** polarization resistance (R_{pol}) of coatings with and without lithium salts, **(c)** dense layer capacitance (C_{oxide}), and **(d)** double layer capacitance (C_{dl}) of scribed lithium-leaching coatings during NSS exposure. The insets of **(c)** and **(d)** show the evolution of C_{oxide} and C_{dl} in the defect of coatings without inhibitor compared to the lithium leaching coatings.

Fig. 2.10 shows the schematic equivalent circuit that can be related with the physical morphology of the corrosion protective layer in the defect. Considering the physical morphology of the protective layers and the quantitative EIS results, it can be concluded that the improved corrosion protective properties of the formed layer can be attributed to the rapid formation of the dense and compact layer at the aluminum interface. The impedance part related from the porous part plays only a minor role in the overall corrosion resistance.

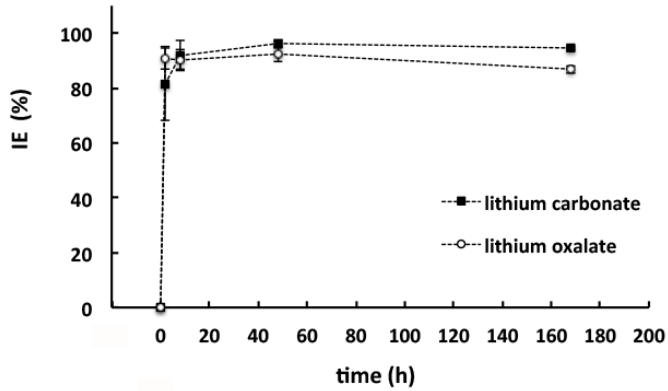

Figure 2.9 Evolution of inhibition efficiency in the defect area of the lithium leaching coatings during NSS exposure.

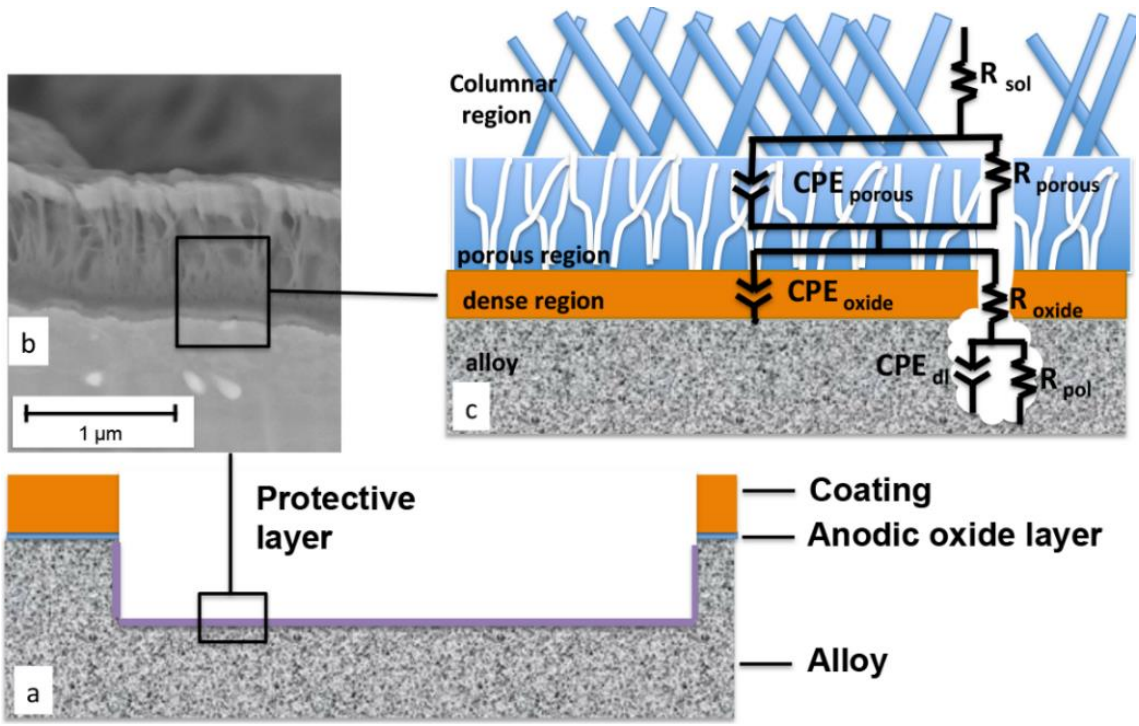

Figure 2.10 Schematic representation of the fitted equivalent circuit based on the physical properties of the protective layer generated in the defect from lithium-leaching organic coatings **(a)** the defect area with protective layer, **(b)** the physical coating morphology and **(c)** schematic representation of EC in protective layer.

2.4. Conclusions

The electrochemical characteristics of the corrosion protective layers generated in a coating defect from lithium-leaching coatings on AA2024-T3 aluminum alloys when exposed to neutral salt spray conditions over time were studied. The electrochemical properties were linked with the physical properties of the protective properties using microscopy and electrochemical impedance spectroscopy. Effective corrosion inhibition from these lithium-leaching coatings was observed after NSS exposure. Cross-sectional microscopic analysis revealed the fast and effective growth of protective layers in thickness and morphology covering the entire damaged area. The results obtained from EIS demonstrate the development of the corrosion resistant properties due to the generation of a protective layer in the defect area and this layer exhibits an irreversible long-term resistance to corrosive conditions. The corrosion protective properties of this layer can be attributed to the dense inner layer of the protective layer. There were no significant differences in corrosion protection observed between lithium carbonate and lithium oxalate salts. The results of this study confirm the fast and effective active protective nature of these lithium-leaching coatings.

References

1. Visser, P., & Hayes, S. A., WO2010112605-A1, (2010).
2. Visser, P., Lutz, A., Mol, J. M. C., & Terryn, H. (2016). Study of the formation of a protective layer in a defect from lithium-leaching organic coatings. *Progress in Organic Coatings*, *99*, 80–90.
3. Visser, P., Liu, Y., Zhou, X., Hashimoto, T., Mol, A. J. M. C., & Terryn, H. A. (2015). The corrosion protection of AA2024-T3 aluminium alloy by leaching of lithium- containing salts from organic coatings. *Faraday Discussions*, *180*, 511–526.
4. Visser, P., Liu, Y., Terryn, H., & Mol, J. M. C. (2016). Lithium salts as leachable corrosion inhibitors and potential replacement for hexavalent chromium in organic coatings for the protection of aluminum alloys. *Journal of Coatings Technology and Research*, *13*(4), 557–566.
5. Hart, R. K. (1957). The formation of films on aluminium immersed in water. *Transactions of the Faraday Society, 53*, 1020-1027.
6. Kudo, T., Alwitt, R.S. (1978). Cross-sections of hydrous and composite aluminum oxide films. *Electrochimica Acta*, *23(4),* 341–345.
7. Alwitt, R.S. (1974). The Growth of Hydrous Oxide Films on Aluminum. *Journal of the Electrochemical Society, 121*, 1322–1328.
8. Buchheit, R. G., Bode, M. D., & Stoner, G. E. (1993). Corrosion-resistant, chromate-free talc coatings for Aluminum. *Corrosion Science*, *50(3)*, 205-214.
9. Drewien, C. A., Eatough, M. O., Tallant, D. R., Hills, C. R., & Buchheit, R. G. (1996). Lithium-aluminum-carbonate-hydroxide hydrate coatings on aluminum alloys: Composition, structure, and processing batch chemistry. *Journal of Materials Research, 11,* 1507–1513.
10. Din, R. U., Gudla, V. C., Jellesen, M. S., & Ambat, R. (2015). Accelerated growth of oxide film on aluminium alloys under steam : Part I : Effects of alloy chemistry and steam vapour pressure on microstructure. *Surface & Coatings Technology*, *276*, 77–88.
11. Din, R. ., Bordo, K., Jellesen, M. S., & Ambat, R. (2015). Accelerated growth of oxide film on aluminium allows under steam: part II: effects of alloy chemistry and steam vapour pressure on corrosion and adhesion performance. *Surface and Coatings Technology*, *276*, 106–115.
12. Liu, Y., Visser, P., Zhou, X., Lyon, S. B., Hashimoto, T., Curioni, M., Gholinia, A., Thompson, G.E., Smyth, G., Gibbon, S.R., Graham, D., Mol, J.M.C., Terryn, H. (2016). Protective Film Formation on AA2024-T3 Aluminum Alloy by Leaching of Lithium Carbonate from an Organic Coating. *Journal of The Electrochemical Society*, *163*(3), C45–C53.

13. Liu, Y., Visser, P., Zhou, X., Lyon, S. B., Hashimoto, T., Gholinia, A., Thompson, G.E., Smyth, G., Gibbon, S.R., Graham, D., Mol, J.M.C., Terryn, H. (2016). An investigation of the corrosion inhibitive layers generated from lithium oxalate-containing organic coating on AA2024-T3 aluminium alloy. *Surface and Interface Analysis*, *48*(8), 798–803.
14. Visser, P., Terryn, H., & Mol, J. M. C. (2016). *Active Protective Coatings: New-Generation Coatings for Metals,* Springer.
15. Hurlen, T., Haug, A.T. (1984). Corrosion and passive behaviour of aluminium in weakly alkaline solution, *Electrochimica Acta, 29*, 1133-1138.
16. Tabrizi, M. R., Lyon, S. B., Thompson, G. E., & Ferguson, J. M. (1991). The long-term corrosion of aluminium in alkaline media. *Corrosion Science, 32(7)*, 733–742.
17. Foley, R. T., Nguyen, T. H. (1982). The Chemical Nature of Aluminum Corrosion. *Journal of the electrochemical society, 129*, 464–467.
18. Van der linden, B., Terryn, H., Vereecken, J. (1990). Investigation of anodic aluminium oxide layers by electrochemical impedance spectroscopy. *Journal of applied electrochemistry, 20*, 798–803.
19. Tedim, J., Zheludkevich, M. L., Bastos, A. C., Salak, A. N., Lisenkov, A. D., & Ferreira, M. G. S. (2014). Influence of preparation conditions of Layered Double Hydroxide conversion films on corrosion protection. *Electrochimica Acta*, *117*, 164–171.
20. Zheludkevich, M. L., Yasakau, K. A., Poznyak, S. K., & Ferreira, M. G. S. (2005). Triazole and thiazole derivatives as corrosion inhibitors for AA2024 aluminium alloy. *Corrosion Science*, *47*(12), 3368–3383.
21. Kuznetsov, B., Serdechnova, M., Tedim, J., Starykevich, M., Kallip, S., Oliveira, M. P., Hack, T., Nixon, S., Ferreira, M.G.S, Zheludkevich, M. L. (2016). *RSC Advances, 6,* 13942–13952.
22. Hsu, C. H., & Mansfeld, F. (2001). Technical Note : Concerning the Conversion of the Constant Phase Element Parameter Y_0 into a Capacitance. *Corrosion 57(9)*, 747–748.
23. Hirschorn, B., Orazem, M. E., Tribollet, B., Vivier, V., Frateur, I., & Musiani, M. (2010). Determination of effective capacitance and film thickness from constant-phase-element parameters. *Electrochimica Acta, 55(21)*, 6218–6227.
24. Al-amiery, A. A., Kassim, F. A. B., Kadhum, A. A. H., Mohamad, A.B. (2016). Synthesis and characterization of a novel eco-friendly corrosion inhibition for mild steel in 1 M hydrochloric acid. *Scientific Reports, 6*, 1–13.
25. Martinez, S., Metikos-Hukovic, M. (2003). A nonlinear kinetic model introduced for the corrosion inhibitive properties of some organic inhibitors. *Journal of Applied Electrochemistry, 33,* 1137–1142.

Chapter 3

The use of odd random phase electrochemical impedance spectroscopy to study lithium-based corrosion inhibition by active protective coatings

This chapter is published as a scientific paper:
M. Meeusen, P. Visser, L. Fernández Macía, A. Hubin, H. Terryn and J.M.C. Mol (2018). The use of odd random phase electrochemical impedance spectroscopy to study lithium-based corrosion inhibition by active protective coatings. *Electrochimica Acta, 278*. 363-373.

Abstract

In this work, the study of the time-dependent behaviour of lithium carbonate based inhibitor technology for the active corrosion protection of aluminium alloy 2024-T3 is presented. Odd random phase electrochemical impedance spectroscopy (ORP-EIS) is selected as the electrochemical tool to study the corrosion protective properties of a model organic coating with and without lithium carbonate as a function of immersion time, by examination of the non-linearities and non-stationarities in the system. A dedicated qualitative and quantitative analysis allows linking the presence of non-stationarities in a certain frequency range with the (un)stable behaviour of different electrochemical processes. Monitoring of the system with and without lithium corrosion inhibitors during the first 12 hours after immersion in a 0.05 M NaCl aqueous solution and modelling the ORP-EIS data with equivalent electrical circuit (EEC) models revealed a relation between the trends in the parameter evolution and the (un)stable behaviour of the morphological changes taking place. This paper shows that the ORP-EIS based methodology allows us to study the behaviour of corrosion inhibitors in an alternative way; the time-dependent behaviour of corrosion inhibitor containing electrochemical systems is highlighted, proving that this a useful approach for further corrosion inhibitor and active protective coating research.

3.1. Introduction

Among the wide variety of electrochemical techniques, electrochemical impedance spectroscopy (EIS) has proven to be a suitable and powerful technique to screen corrosion inhibitors and study the protective properties and efficiency of (self-healing) coatings on metal substrates over time [1–3]. EIS can provide both qualitative and quantitative information. The qualitative description refers to monitoring the efficiency of electrochemical systems by comparing, e.g., the magnitude of the impedance modulus at low frequencies, i.e., the polarization resistance. Any decrease or increase in the polarization resistance can be related to a decrease or increase in corrosion protection, respectively [1–3]. Quantitatively, the system can be studied by fitting the experimental data to an equivalent electrical circuit (EEC) model describing the physical phenomena occurring in the electrochemical system, in such a way that the individual contributions to the global system's performance can be studied [1, 3]. This makes EIS a very powerful technique to study electrochemical systems. Garcia et al. studied the corrosion inhibition mechanism of cerium-based bi-functional inhibitors on AA2024-T3 alloy with EIS, proposing a systematic strategy in selecting the most probable EEC. Doing so, it is crucial that the most probable EEC has a physical meaning, with minimal model error and parameter errors on all circuit elements [4]. Balaskas et al. applied EIS to study the effect of various organic compounds on the corrosion process of AA2024-T3 alloy, in order to rank them according to the degree of corrosion protection they provide [5]. Lamaka et al. screened different organic corrosion inhibitors for aluminium 2024 alloys with EIS to reveal the effectiveness and working mechanism of each inhibitor [1]. In a later study, EIS was used to study the synergistic effect of inhibitor mixtures for the protection of AA2024-T3 [6]. Lopez-Garrity et al. completed a similar study, to reveal the mechanism of the protective action of sodium molybdate corrosion inhibitor on AA2024-T3 alloys [7].

Recently, lithium-based corrosion inhibitor technology has become of interest as possible alternative to chromium based corrosion inhibitor technology and protect aluminium AA2024-T3 against (localized) corrosion [8–10]. Visser et al. have proven that when dispersed in a model organic coating, lithium carbonate and lithium oxalate pigments can ensure fast and effective corrosion protection in an artificial damage under neutral salt spray (NSS) exposure according to ASTM B-117 [11]. These lithium-salts are able to leach from the coating matrix through a specific leaching mechanism, providing active corrosion protection by rapid formation of a three-layered morphology, consisting of an inner dense layer close to the aluminium alloy metal surface, a porous middle layer and a very porous columnar

outer layer [12, 13]. The coverage, growth process and surface chemistry of the protective layer were studied in detail with a variety of surface analysis and spectroscopic techniques [13, 14]. Finally, electrochemical impedance spectroscopy (EIS) was used to study the electrochemical properties of the generated three-layered protective morphology, its formation and properties as a function of NSS exposure time [15]. However, a more in depth study of the initial stability as a function of time of this protective layer after NSS is required. Since corrosion processes are intrinsically de facto non-linear and non-stationary, these phenomena can only be described adequately by means of EIS if it is proven that the system is linear and stationary within the measurement time, since these are crucial requirements to have reliable EIS measurements [16].

The application of Kramers-Kronig (K-K) transforms could provide a possible solution to verify electrochemical impedance data with respect to the conditions of causality, linearity and time-invariance. If a system fulfils these conditions and if the impedance is finite in the frequency domain under investigation, the EIS data will transform following the K-K relationships. On the contrary, the converse is not true [17][18]. It has been demonstrated that the linearity can always be guaranteed, but that the conformity with the causality and time-invariance conditions is more difficult, limiting the K-K transforms' applicability [17][18][19]. Besides, with that approach it is not possible to quantify the level of non-linear and non-stationary distortions at each frequency.

Odd random phase electrochemical impedance spectroscopy (ORP-EIS) is an electrochemical tool providing linearity and time-invariance information that can be used to evaluate the suitability of the equivalent electrical circuit models. ORP-EIS is a different technique to measure impedance compared to the classical EIS method. Rather than exciting the system at each subsequent frequency, as in classical EIS, the system is excited with a multisine signal over the entire frequency range. This periodic broadband signal consists of harmonically related sine waves whereof only the odd harmonics are excited and out of every group of three consecutive odd harmonics, one is randomly omitted [20]. This method provides two benefits. Firstly, applying a broadband rather than a single sine signal decreases the measurement time drastically while exciting the higher frequencies even more. This reduces the standard deviation, compared to a single-sine excitation, since the standard deviation is inversely proportional to the number of samples taken. Secondly, through a dedicated data analysis procedure, extra information regarding the noise, non-linearities and non-stationarities present in the system under investigation can be evaluated and quantified [21–24]. To investigate the reliability of the modelling results, it is important to verify whether the experimental data are correct and to evaluate whether the EEC model is able to describe

the experimental data within the experimental error. This information is also available by the application of the ORP-EIS technique. The concept of ORP-EIS has already demonstrated to be a successful tool for a number of practical applications. Van Gheem et al. studied non-linear and non-stationary electrochemical systems using an especially designed excitation signal [21]. By exciting the system with an odd random phase multisine with a random harmonic grid, it was possible to detect both non-linearities and non-stationarities, as was concluded from the application on the pitting corrosion of aluminium in an aerated sodium chloride solution [22]. Breugelmans et al. successfully applied it as a rapid corrosion screening test of metal-coated steel [25] and to analyse (self-healing) organic coatings [20]. Hauffman et al. employed ORP-EIS to investigate the time-varying process of self-assembling monolayers on aluminium oxide, a process which is essentially non-stationary [26, 27]. In addition, a detailed study of the early stages of copper corrosion and the mechanism of adsorption on copper by ORP-EIS has been reported [28, 29].

In this paper, ORP-EIS is used to study the initial stability as a function of time of the protective morphology formed in coating defects of model coatings with and without lithium leaching coating technology on an AA2024-T3 substrate. The application of this technique is crucial to investigate the initial stages of the stability of the multi-layered protective morphology provided by inhibitor based corrosion protective technologies and to achieve more reliable measurements for corrosion inhibitor systems in general. In a first step, the experimental data are examined, both qualitatively and quantitatively, through the analysis of the additional information regarding the non-linearities and non-stationarities provided by ORP-EIS about the correctness of the data. Furthermore, the impact and advantages of using the additional information regarding the non-linearities and non-stationarities in the modelling is assessed in order to study and improve the modelling reliability. A parallel is drawn between the stationarity of the different electrochemical processes and the parameter evolution of the equivalent electrical circuit elements.

3.2. Experimental details

3.2.1. Materials and sample preparation

AA2024-T3 aluminium alloy with nominal composition from Alcoa was anodized in tartaric-sulphuric acid (TSA) according to aerospace requirements (AIPI 02-01-003). The anodized samples were coated with a polyurethane based model coating (Table 3.1) with a dry film

thickness of 20-25 µm [15]. Coatings without corrosion inhibitors, used as non-inhibited reference, and lithium carbonate containing coatings were applied. To study the active corrosion protective properties of these coatings, an artificial damage from corner to corner was made with a mechanical milling device yielding a U-shaped scribe of 1 mm width and approximately 100-150 µm depth. Afterwards, the scribed lithium carbonate containing samples were exposed to the neutral salt spray test (NSS) according to ASTM B-117 for 168 hours [11]. The 0.05 M NaCl solution used during the ORP-EIS measurements was prepared from J.T. Baker NaCl crystals with a purity of at least 99% and demineralized water.

Table 3.1 Composition of the organic model coatings with and without lithium carbonate.

	Without corrosion inhibitors	**Lithium carbonate**
Component A		
N-Butylacetate	75.0 g	75.0 g
Desmophen 650MPA	47.7 g	47.7 g
Lithium carbonate		23.6 g
Magnesium oxide	16.4 g	16.4 g
Tioxide TR 92	5.9 g	5.9 g
Blanc Fixe N ($Ba(SO_4)$)	66.0 g	15.4 g
Component B		
Tolonate HDB 75 MX	28.5 g	28.5 g
Dynasilan Glymo	5.2 g	5.2 g

3.2.2. Odd random phase electrochemical impedance spectroscopy (ORP-EIS)

A typical three electrode set-up was used for the electrochemical experiments with an Ag/AgCl 3 M KCl reference electrode (RE), a platinum grid as the counter electrode (CE) and the mechanically scribed coated AA2024-T3 sample as the working electrode (WE) with an exposed area of 3.14 cm^2 and a scribed area of 0.48 cm^2. The set-up was placed in a Faraday cage. Measurements were recorded immediately after immersion in 0.05 M NaCl and for 12 subsequent hours. In the case of the system without corrosion inhibitors, a measurement

was taken every 10 minutes and, in the case of the lithium carbonate inhibited system, a measurement was taken every 15 minutes.

The ORP-EIS measurements were performed with a MATLAB controlled set-up composed of a Bio-Logic SP-200 potentiostat and a National Instruments PCI-6110 DAQ-card. The frequency range is from 10^{-2} Hz to $2 \cdot 10^{3}$ Hz. The amplitude of the excitation signal was set to 10 mV (7.07 mV RMS) applied at the free corrosion potential, to have a good signal-to-noise ratio while keeping the non-linearities confined. The MATLAB written software to build the odd random phase multisine excitation signal, record the impedance measurements and perform the modelling was developed at the Vrije Universiteit Brussel. A more detailed description of the technique can be found elsewhere [16, 21].

3.3. Results and discussion

3.3.1. Qualitative interpretation of ORP-EIS noise distortions

To study the system's evolution in meeting the three requirements needed for a correct EIS measurement, both the system without corrosion inhibitors and the lithium carbonate inhibited system were intensively monitored during the first hours after immersion in the electrolyte. In Fig. 3.1, the ORP-EIS results of the coated AA2024-T3 sample without inhibitors after 0, 2, 4 and 6 hours of immersion in 0.05 M NaCl are presented. The black line and the grey line correspond to the magnitude of the impedance modulus and the phase angle, respectively, as usually plotted by classical EIS. The other characteristics of the experimental data of an ORP-EIS measurement are provided by the curves representing the noise, the noise plus the non-linearities and the noise plus the non-stationarities [30, 31]. Data interpretation can be described in the following way. The system is fully linear if the noise curve and the *noise+non-linearities* curve overlap; the system is fully time-invariant (stationary) if the noise curve and the *noise+non-stationarities* curve overlap.

For the first measurement at Time = 0 (Fig. 3.1a), neither the *noise+non-linearities* curve nor the *noise+non-stationarities* curve overlap the noise curve. This suggests the presence of significant non-linearities and non-stationarities in the system right at the start. After 2 hours of immersion (Fig. 3.1b), the *noise+non-linearities* curve approaches the noise curve, almost fulfilling the condition of linearity. Nevertheless, the *noise+non-stationarities* curve does not overlap the noise curve, indicating that the system behaves non-stationary. After 4 hours

(Fig. 3.1c), the *noise+non-linearities* curve overlaps completely the noise curve, indicating a linear behaviour of the system. The *noise+non-stationarities* curve does not overlap the noise curve yet, meaning the stationarity condition still must be fulfilled. After 6 hours of immersion (Fig. 3.1d), the system behaves fully linearly and stationary, as observed by the overlap of the noise, *noise+non-linearities* and *noise+non-stationarities* curves.

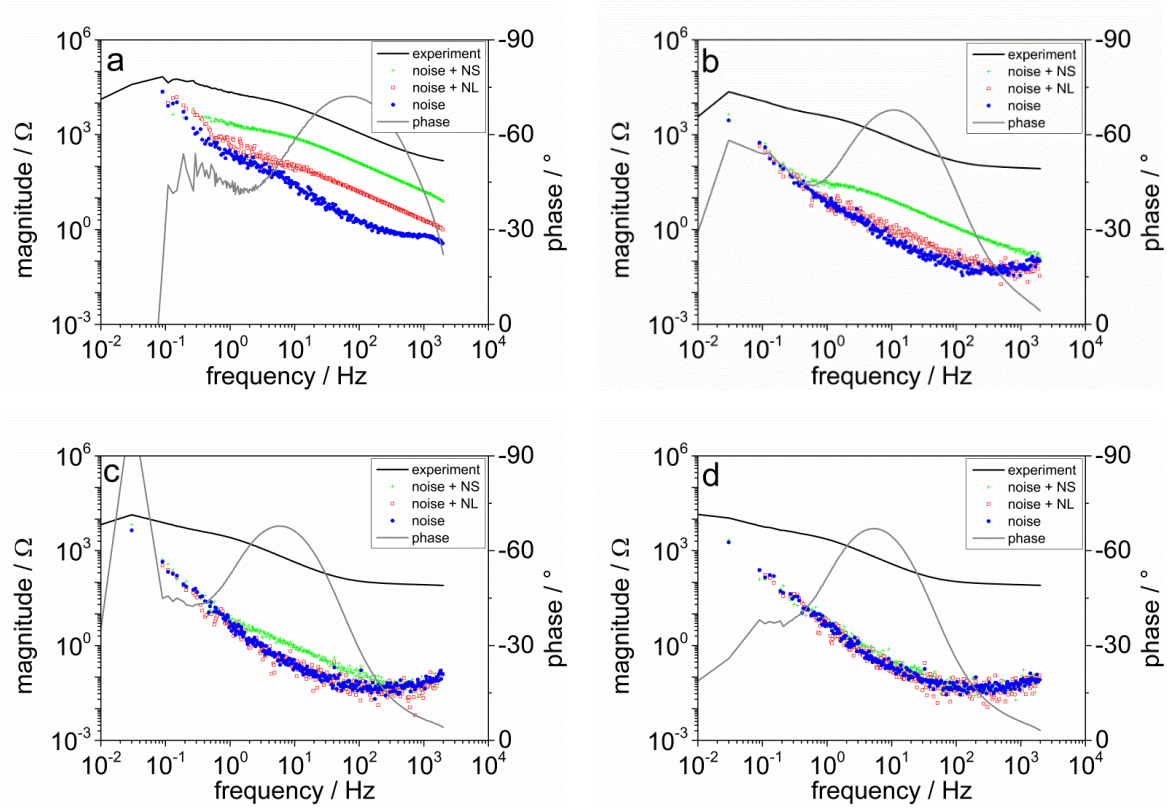

Figure 3.1 Bode plots of the system without corrosion inhibitors after 0h **(a)**, 2h **(b)**, 4h **(c)** and 6h **(d)** in 0.05 M NaCl with the experimental impedance and noise distortion curves.

In Fig. 3.2, the ORP-EIS results of the sample with the lithium carbonate containing coating after different times of immersion in 0.05 M NaCl are presented. It can be seen that, right at the start of the measurement, neither the *noise+non-linearities* curve nor the *noise+non-stationarities* curve completely overlaps the noise curve (Fig. 3.2a). The system did not reach the linearity and stationarity condition yet. In the case of the *noise+non-stationarities* curve, the mismatch is especially apparent at high frequencies, from 20 Hz to 2 kHz. The non-

stationarities observed at the higher frequencies suggest that the electrochemical processes with low characteristic time constants (fast processes) mainly cause the time-variant behaviour of the system.

After 2 hours of immersion (Fig. 3.2b), the *noise+non-linearities* curve clearly overlaps the noise curve, meaning that the system has a linear behaviour under the given experimental conditions. However, the same observation about the stationarity condition can be made as before, with the non-stationary behaviour related to the high frequency region and thus the unstable behaviour linked to the electrochemical processes with low characteristic time constants. After 4 hours of immersion (Fig. 3.2c), the *noise+non-stationarities* curve approaches the noise curve, indicating that the system has reached the condition of stationarity. After 6 hours of immersion (Fig. 3.2d), the system behaves fully linearly and stationary, since the *noise+non-linearities* curve and the *noise+non-stationarities* curve overlap with the noise curve.

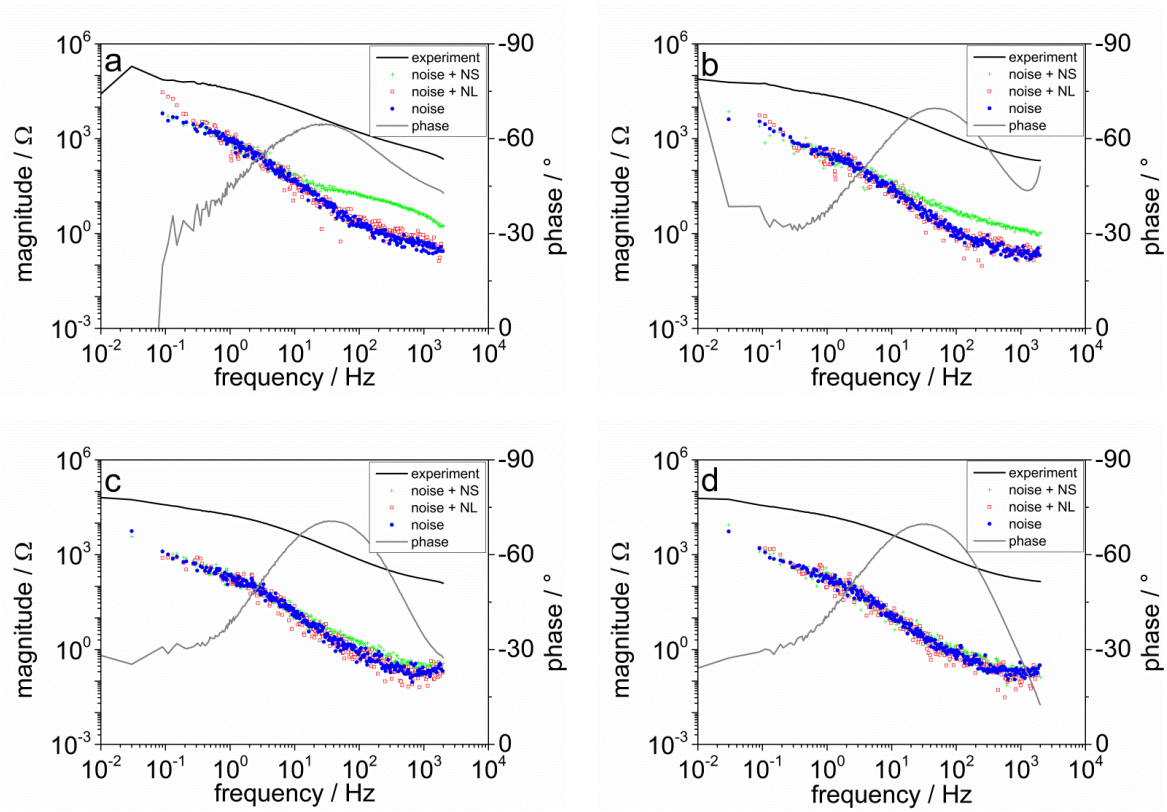

Figure 3.2 Bode plots of the lithium carbonate inhibited system after 0h **(a)**, 2h **(b)**, 4h **(c)** and 6h **(d)** in 0.05 M NaCl with the experimental impedance and noise distortion curves.

From this qualitative interpretation, it can be seen that for both the system without corrosion inhibitors and the lithium carbonate inhibited system, it takes approximately 6 hours to reach a stationary behaviour and, thus, fulfil the condition of time-invariance. At this point, both systems also behave linearly. This time designates the duration to reach a stable degradation process of the (native) oxide on the sample without corrosion inhibitors or the three-layered protective morphology formed during 168 hours of NSS on the lithium carbonate inhibited sample. It corresponds to the stabilization time needed before a reliable EIS measurement is obtained. However, the non-linear and non-stationary behaviour of both systems in the initial hours of immersion requires further study by means of a quantitative interpretation of the noise distortions in the ORP-EIS data.

3.3.2. Quantitative interpretation of ORP-EIS noise data

The qualitative analysis of the experimental data obtained for both the system without corrosion inhibitors and the inhibitor containing systems provides an estimation of the time each system needs to 'stabilize' and fulfil the conditions of linearity and time-invariance. Yet, in order to study the reliability of EIS data in more detail, the information in Fig. 3.1 and Fig. 3.2 regarding the noise, non-linearities and non-stationarities present in the system needed to be quantified. The discrete information was calculated for each measurement separately by a numerical integration through interpolation using the trapezoidal rule [32]. The individual contributions of the noise, non-linearities and non-stationarities were calculated, as absolute values, by subtracting the noise curve from the noise+non-linearities and the noise+non-stationarities curve. This information was then expressed relative to the magnitude of the impedance modulus (N/|Z|; NL/|Z|; NS/|Z|), which is also quantified by a numerical integration through interpolation. This approach was followed for the first 12 hours of every measurement, both for the system without corrosion inhibitors and the lithium carbonate inhibited system. The resulting curves of the relative contributions of the noise, non-linearities and non-stationarities as a function of time are presented in Fig. 3.3.

3.3.2.1. ORP-EIS noise data analysis of the system without corrosion inhibitors

For the system without corrosion inhibitors (Fig. 3.3a), it can be observed that in the first hour after immersion, the non-stationarities have the highest relative contribution of the three, with an absolute value only 1 order of magnitude lower than the magnitude of the Bode impedance modulus, corresponding to a contribution of almost 10%. For the noise, the contribution is almost 2 orders of magnitude lower compared to the magnitude of the impedance modulus and for the non-linearities almost 3 orders of magnitude. All contributions tend to fluctuate during the initial stages.

Following the initial stages after immersion, all individual contributions start decreasing over time. The relative contribution of the noise decreases quite strongly, before reaching a stable value after nearly 1 hour, approximately 3 orders of magnitude lower than the measured impedance modulus, corresponding to approximately 0.1%. Afterwards, the noise contribution remains stable for the rest of the measurement time.

The relative contribution of non-linearities decreases strongly in the first 2 hours, reaching a relative contribution of approximately 2·10-4 or less until the end of the measurement, corresponding to approximately 0.02% or less of the impedance modulus. This point in time is indicated by the full vertical line in Fig. 3.3a and from this point, the system behaves fully linearly.

The contribution of the non-stationarities decreases from only 1 to almost 3 orders of magnitude difference compared to the impedance modulus during the first 2 hours of immersion. Afterwards, its contribution keeps decreasing up to 5 hours after immersion, reaching a relative contribution of approximately 4 orders of magnitude lower than the impedance modulus, comparable to what is observed for the non-linearities. This point in time is indicated by the dashed vertical line in Fig. 3.3a, corresponding to a fully time-invariant behaviour of the system from this moment on.

The high relative contributions and high fluctuations during the initial stages of immersion are due to the unstable behaviour of the system right after immersion in the electrolyte. Considering these trends, the system's behaviour can be described as non-linear and non-stationary during the initial stages. The non-stationarities represent the main contributor to the system's distortion. After 2 hours, the system's behaviour is still unstable, but the system behaves fully linearly with an excitation signal amplitude of 10 mV.

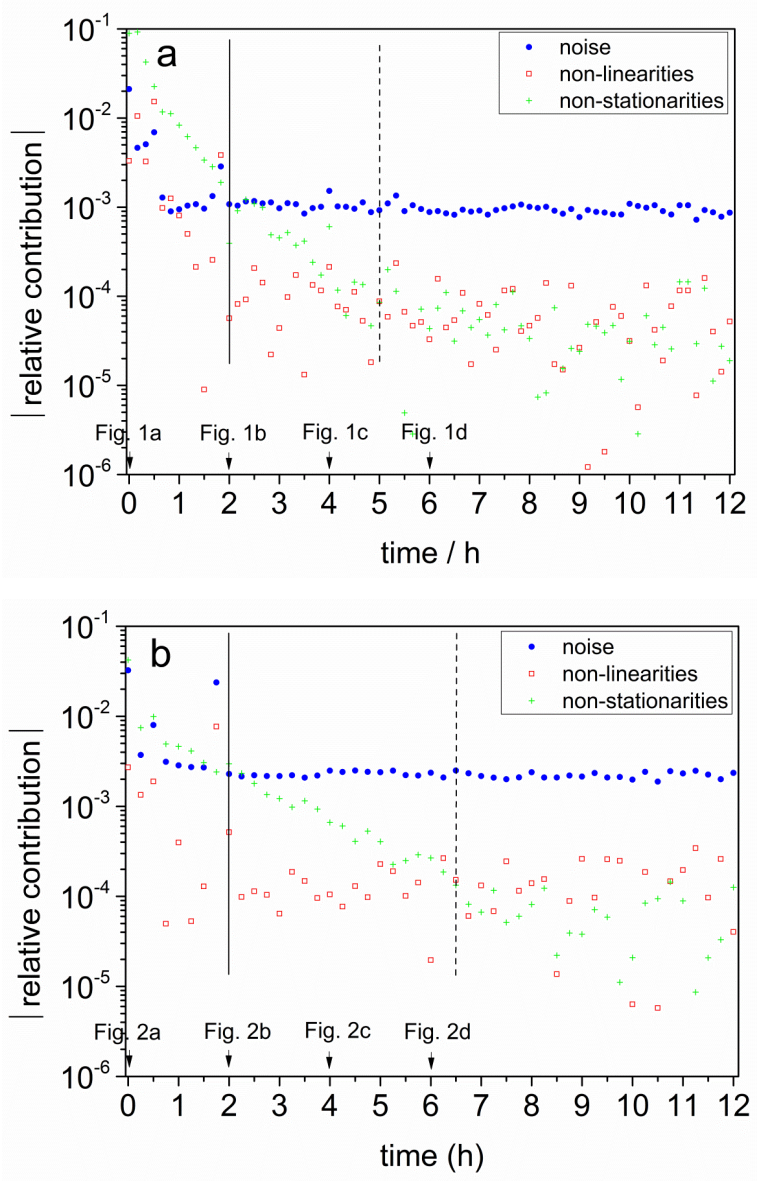

Figure 3.3 Evolution of the contribution of the noise (N), non-linearities (NL) and non-stationarities (NS) relative to the impedance modulus for **(a)** the system without corrosion inhibitors and **(b)** the lithium carbonate inhibited system for the first 12 hours of immersion in 0.05 M NaCl. The full- and dashed- vertical line represent the point in time where the system is fully linear and fully stationary, respectively.

The information concerning the non-stationarities accounts for the instability of the electrochemical processes. Yet, processes with different time constants are visible in different frequency regions of the impedance spectrum; thus, non-stationarities in a certain frequency region could be associated to a particular electrochemical process. To analyse the contribution of the different processes to the overall system stability, the data regarding the non-stationarities was also quantified per frequency decade. The impedance data were, therefore, divided into 6 frequency decades. The first frequency decade, from 10 mHz to 100 mHz, was included in this analysis, because there were only three data points present, providing no statistically significant information. In addition to that, the data between 1 kHz and 2 kHz were not taken into account, since they comprise only one tenth of a frequency decade. The relative contribution (NS/|Z|) is calculated for each frequency decade separately and displayed in Fig. 3.4.

It can be observed that the contribution of the non-stationarities decreases for every frequency decade with time (Fig. 3.4a). For the highest (V) and the lowest (II) frequency decades it strongly decreases in the first hours and stabilizes after approximately 4 hours. On the other hand, for the two mid frequency regions (III and IV) it decreases more slowly and stabilizes after more than 6 hours. This corresponds to what is already observed in a qualitative way: after 2 hours (Fig. 3.1b) the system behaves non-stationary over the entire frequency range, while after 4 hours (Fig. 3.1c), the system behaves only non-stationary in the 1 Hz - 100 Hz range. Consequently, the electrochemical processes with time constants corresponding to the mid-frequency regions take the longest to stabilize, prolonging the instability of the system.

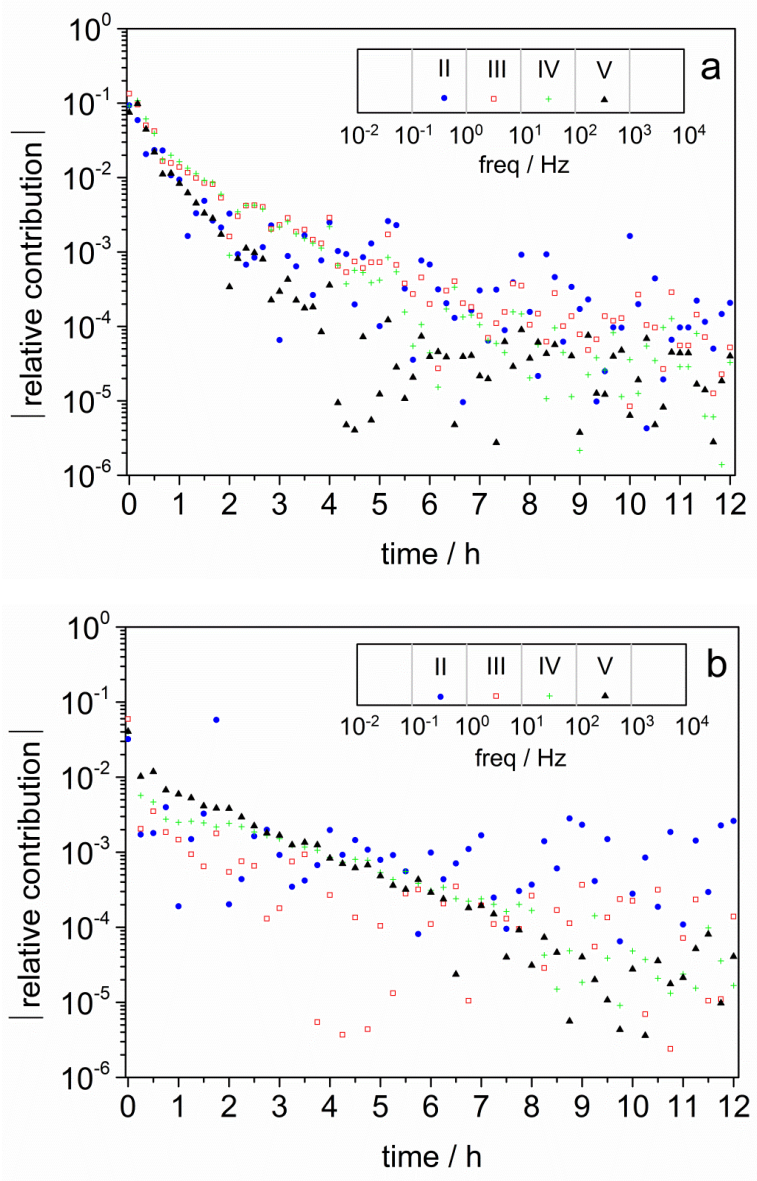

Figure 3.4 Evolution of the relative contribution of the non-stationarities for the different frequency decades for **(a)** the system without corrosion inhibitors and **(b)** the lithium carbonate inhibited system for the first 12 hours of immersion in 0.05 M NaCl.

3.3.2.2. ORP-EIS noise data analysis of the lithium carbonate loaded system

For the lithium carbonate loaded system (Fig. 3.3b), the relative contributions of the noise and non-stationarities are the highest right after the start of immersion, about 3-4%. The relative contribution of the non-linearities, on the other hand, is already 2 orders of magnitude lower than the impedance modulus.

During the initial stages, the individual contribution of the noise undergoes some fluctuations, before decreasing to a stable value after 2 hours of immersion, more than 2 orders of magnitude lower than the impedance modulus with a relative contribution of approximately 0.3%. The noise relative contribution remained equal for the remaining time of the measurement. The contribution of the non-linearities is only present in the first hours after immersion and rapidly decreases over time, reaching a stable contribution with a value of $3 \cdot 10^{-4}$ or less after 2 hours of immersion. This point in time is indicated by the full vertical line in Fig. 3.3b and from this moment on, the system behaves fully linearly. Here again the non-stationarities account for the largest contribution right after the start of immersion, with less than 2 orders of magnitude difference with the impedance modulus, corresponding to approximately 4%. However, this contribution decreases as a function of time, more than 3 orders of magnitude lower after 3 hours and reaches a stable contribution with a value of $1 \cdot 10^{-4}$ or less after 6.5 hours, fulfilling the condition of time-invariance. This point in time is indicated by the dashed vertical line in Fig. 3.3b.

Similarly to the system without corrosion inhibitors, the same quantification per decade was carried out for the contribution of the non-stationarities of the lithium carbonate loaded system. In Fig. 3.4b, it can be observed that for the lowest (II) frequency decade, the contribution of the non-stationarities remains the same over time, while for the other frequency decades, the contribution of the non-stationarities decreases for each frequency decade with time. The contribution of the non-stationarities of frequency decade III decreases rapidly and reaches a more or less stable value after approximately 4 hours. The contribution of the non-stationarities of frequency decades IV and V decreases more slowly and reaches a pseudo-plateau between 6 and 8 hours and stabilizes around 8 hours after immersion. The trend for the frequency decades IV and V is in accordance with what is observed in a qualitative way (Fig. 3.2), with a non-stationary behaviour in the higher frequency decades initially. This implies that the electrochemical processes with characteristic time constants related to frequency decades IV and V dominate the overall instability of the system.

When studying the data quality of the ORP-EIS measurements in a quantitative way, the point in time when the three requirements for a reliable classical EIS measurement are fulfilled can be determined more adequately. This information must be used correctly in practice when fitting the experimental data to an equivalent electrical circuit (EEC). This will be discussed in the next section.

3.3.3. Corrosion protective properties of the system without corrosion inhibitors and the lithium carbonate inhibited system

The ORP-EIS data of the system without corrosion inhibitors were fitted with an equivalent electrical circuit (EEC1) with two time-constants to model quantitatively the behaviour of the (native) oxide layer on aluminium alloys in a defect without the presence of corrosion inhibitors [6, 15]. In EEC1 (Fig. 3.5a), R_s is the electrolyte resistance, R_{oxide} is the resistance of the oxide layer consisting of the native oxide layer and the formed corrosion products upon exposure to the electrolyte, CPE_{oxide} is the constant phase element representing the capacitive behaviour of this oxide layer, R_{pol} is the polarization resistance and CPE_{dl} is the constant phase element accounting for capacitive behaviour of the double layer [15]. A constant phase element (CPE) rather than a capacitor is chosen here to allow deviations from the ideal capacitive behaviour [18]. The impedance of a constant phase element (Z_{CPE}) is given by:

$$Z_{CPE} = \frac{1}{(j\omega)^n Q} \quad (1)$$

where Q is the CPE-constant, n is the power value ($0<n\leq1$), j is the imaginary number ($j^2=-1$) and ω is the angular frequency.

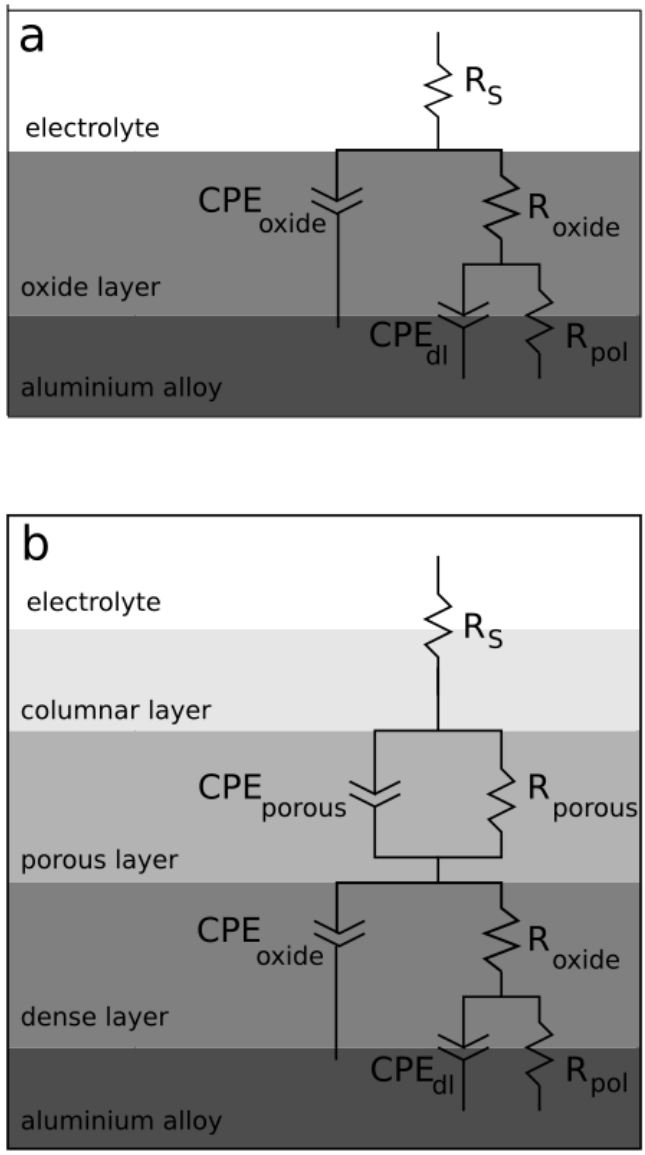

Figure 3.5 The equivalent electrical circuit used to perform the fittings for **(a)** the system without corrosion inhibitors (EEC1) and **(b)** the lithium carbonate inhibited system (EEC2).

During the first 5 hours of immersion, the system without corrosion inhibitors does not meet the requirements of a reliable impedance measurement, as discussed above, and the

straightforward application of the EEC models is not possible. Initially, the system behaves both non-linearly and non-stationary and it only meets the linearity and stationarity conditions after 2 and 5 hours, respectively. Moreover, the individual contribution of the non-stationarities is always predominant over that of the non-linearities. This must be taken into account in the modelling and an alternative fitting approach has to be followed for the first hours of immersion. Because the non-stationary contribution is dominant over the non-linearity contribution, the experimental data are weighted according to the *noise+non-stationarities* in every frequency point rather than with the magnitude of the impedance modulus, as commonly used for EIS fittings. The quality of the fitting can be determined by the evaluation of the model residual, i.e., the difference between the best-fit model and the experiment curves [33]. The approach is illustrated in Fig. 3.6 for the impedance after 1 hour of immersion. It can be seen that the model residual and the *noise+non-stationarities* curves are laying around the same level, indicating that the only difference between the experimental data and the fitting results can be associated to the measurement of the noise present in the system and the non-stationarity behaviour of the system. The parameter values of the circuit elements and their relative errors for the system without corrosion inhibitors after 1 hour of immersion are shown in Table 3.2. For all the EIS data during the first 5 hours of immersion, similar modelling results are obtained. Besides, all model parameters are estimated with low relative errors, below 5% for R_{oxide}, Q_{oxide}, n_{oxide} and n_{dl}, below 10% for Q_{dl} and below 20% for R_{pol}. So, the proposed EEC1 model is able to match the experimental data within the level of the noise distortions and the model can be accepted.

After 5 hours of immersion, the system without corrosion inhibitors behaves in a fully linear and time-invariant manner, as shown in Fig. 3.3a. Since the requirements for a correct EIS measurement are fulfilled, a classical data fitting approach can be followed and a weighting factor corresponding to the inverse of the magnitude of the impedance modulus in each frequency point is attributed. Yet, here again, the reliability of the fitting procedure must be evaluated. The model residual is evaluated and compared to the noise curve in this case. The approach is illustrated in Fig. 3.7 for the impedance after 8 hours of immersion. The model residual overlaps the noise curve only in the low frequency region, and differs from it in the middle and high frequency regions. Nevertheless, the model residual relative to the impedance magnitude is always below 10%, relative to the impedance magnitude, proving the EEC is statistically correct. The parameter values and the relative errors on each of the circuit elements for the system without corrosion inhibitors after 8 hours of immersion are shown in Table 3.2. For all the EIS data obtained between 5 and 12 hours after immersion, similar modelling results are obtained. In any case, all model parameters are estimated with low relative errors, below 5% for R_{oxide}, Q_{oxide}, n_{oxide} and n_{dl}, and below 15% for R_{pol} and Q_{dl}.

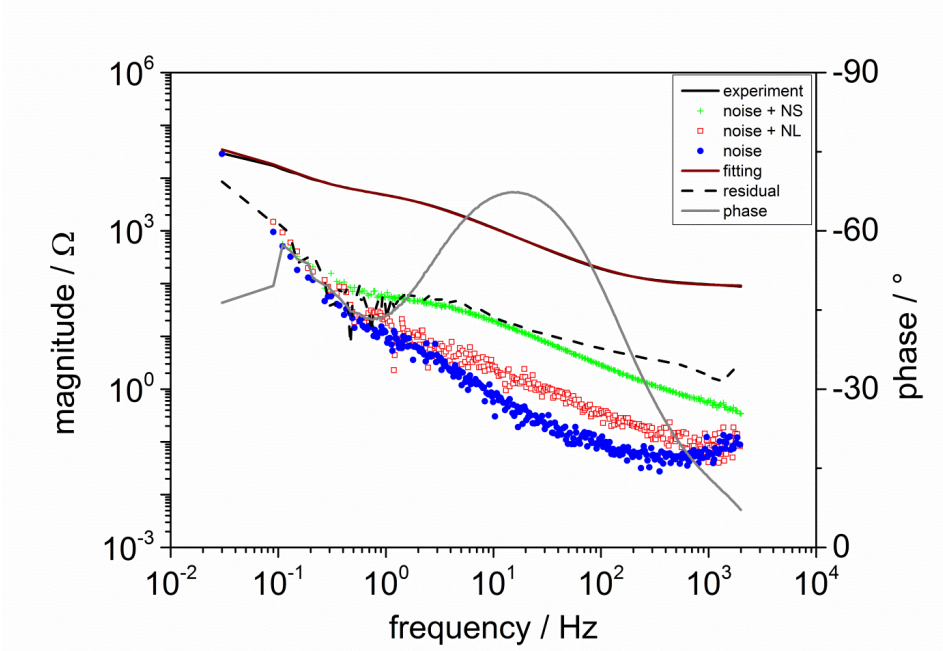

Figure 3.6 Bode plot of the system without corrosion inhibitors after 1 hour of immersion in 0.05 M NaCl with the experimental impedance and noise distortion curves and the fitted impedance and model residual curves.

Table 3.2 Fitting results of the system without corrosion inhibitors after 1 hour and 8 hours of immersion in 0.05 M NaCl, showing the parameter values and the relative errors on each of the circuit elements, respectively.

		1 hour		8 hours	
		value	**error (%)**	**Value**	**error (%)**
R_s	Ω.cm²	44.26	0.16	41.48	0.30
R_{oxide}	kΩ.cm²	3.67	0.54	2.10	0.67
Q_{oxide}	$Ss^n.cm^{-2}$	$4.83 \cdot 10^{-5}$	0.80	$1.53 \cdot 10^{-4}$	0.57
n_{oxide}		0.87	0.18	0.89	0.25
R_{pol}	kΩ.cm²	19.47	11.46	6.03	9.63
Q_{dl}	$Ss^n.cm^{-2}$	$1.61 \cdot 10^{-4}$	2.94	$1.26 \cdot 10^{-3}$	9.59
n_{dl}		0.94	1.90	0.97	3.23

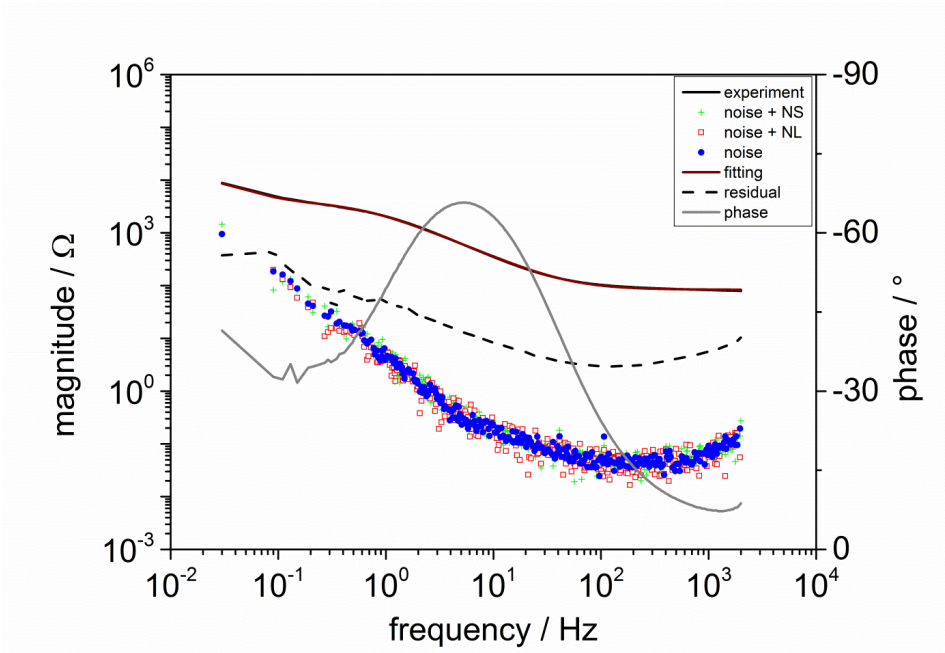

Figure 3.7 Bode plot of the system without corrosion inhibitors after 8 hours of immersion in 0.05 M NaCl with the experimental impedance and noise distortion curves and the fitted impedance and model residual curves.

In order to quantitatively describe the electrochemical behaviour of the system during the first hours of immersion in the electrolyte, the ORP-EIS data obtained for the lithium carbonate inhibited system were fitted with an alternative circuit (EEC2) (Fig. 3.5b), which has been introduced by Visser et al [15]. The extra time constant present in the EEC2 accounts for the resistive and capacitive behaviour of the porous middle layer. In this electrical circuit, R_s stands for the resistance of the electrolyte, R_{porous} and CPE_{porous} represent the contribution of the porous middle layer, R_{oxide} and CPE_{oxide} stand for the contribution of the dense inner (oxide) layer and R_{pol} and CPE_{dl} represent the charge transfer at the interface between the metal and the oxide [15]. Note that the columnar outer layer found in the hydrated aluminium oxide layer formed in the defect area [13] is not present in the proposed EEC2, since this layer is too porous and, therefore, its contribution is not distinguishable on the ORP-EIS data.

During the first hours of immersion, the lithium carbonate inhibited system does not meet the requirements of a correct EIS measurement (Fig. 3.3b). The linearity and stationarity condition are met after 2 and 6.5 hours, respectively. Since the non-stationarity contribution is dominant over the linearity contribution, the experimental data is weighted according to the *noise+non-stationarities*. This approach is illustrated for a measurement recorded 1 hour after immersion in the electrolyte (Fig. 3.8). Again, the modelling quality can be evaluated by means of the model residual. It can be seen that the model residual curve and the *noise+non-stationarities* curve are situated around the same level, meaning that the model is able to represent the experimental data within the noise distortions. The parameter values and their relative errors of the circuit elements for the lithium carbonate inhibited system after 1 hour of immersion are shown in Table 3.3. In this case, a value close to 1 is obtained for n_{porous}, nevertheless a CPE element is selected over a capacitance in EEC2, since it shows a better compatibility overall. For all the EIS data during the first 6.5 hours of immersion, similar modelling results are obtained. The model parameters are determined with uncertainty levels below or equal to 10% for R_{oxide}, Q_{oxide}, n_{porous}, n_{oxide} and n_{dl}, 20% for R_{porous}, 25% for Q_{porous} and Q_{dl} and 45% for R_{pol}.

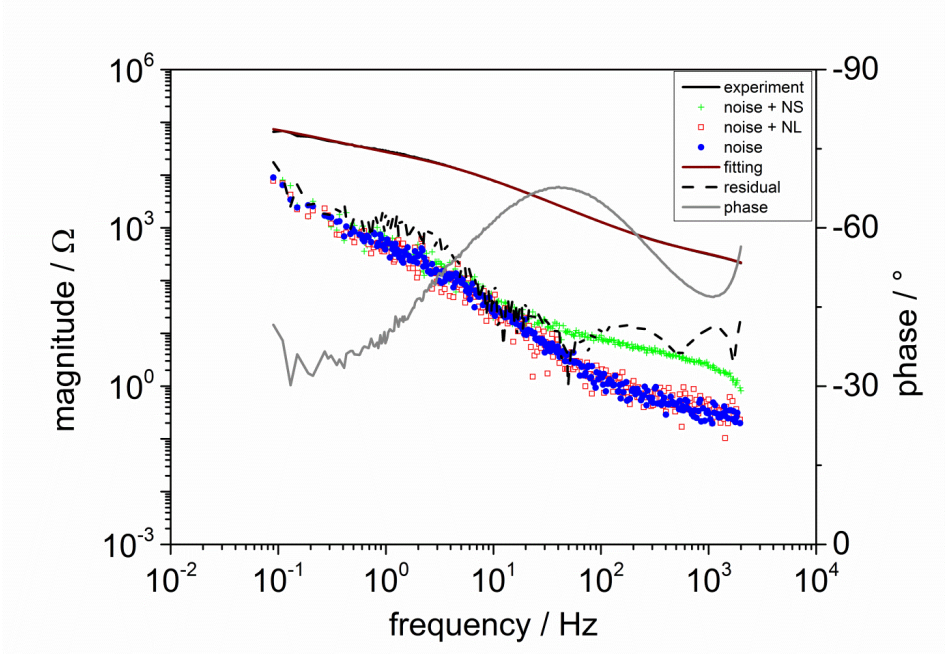

Figure 3.8 Bode plot of the lithium carbonate inhibited system after 1 hour of immersion in 0.05 M NaCl with the experimental impedance and noise distortion curves and the fitted impedance and model residual curves.

After 6.5 hours of immersion, when the requirements for a correct EIS measurement are fulfilled, a similar procedure can be followed as for the system without corrosion inhibitors. The approach is illustrated in Fig. 3.9 for the impedance after 8 hours of immersion. It can be seen that the model residual curve and the noise curve are situated around the same level, meaning that the model is able to represent the experimental data within the noise distortions. The parameter values and the relative errors on each of the circuit elements for the lithium carbonate inhibited system after 8 hours of immersion are shown in Table 3.3. For all the EIS data between 6.5 and 12 hours after immersion, similar modelling results are obtained. In any case, all model parameters are estimated with relative errors below or equal 10% for R_{oxide}, Q_{oxide}, n_{oxide}, n_{dl} and n_{porous}, 15% for R_{porous}, 25% for Q_{porous} and Q_{dl} and 45% for R_{pol}.

Table 3.3 Fitting results of the lithium carbonate inhibited system after 1 hour and 8 hours of immersion in 0.05 M NaCl, showing the parameter values and the relative errors on each of the circuit elements, respectively.

		1 hour		8 hours	
		Value	**Error (%)**	**Value**	**Error (%)**
R_s	Ω.cm²	27.89	7.43	53.49	2.18
R_{porous}	Ω.cm²	84.07	5.27	11.41	2.18
Q_{porous}	$Ss^n.cm^{-2}$	$1.26 \cdot 10^{-6}$	7.04	$2.14 \cdot 10^{-7}$	16.83
n_{porous}		1	2.55	0.99	5.63
R_{oxide}	kΩ.cm²	13.67	4.19	10.85	1.10
Q_{oxide}	$Ss^n.cm^{-2}$	$6.52 \cdot 10^{-6}$	2.19	$1.37 \cdot 10^{-5}$	1.91
n_{oxide}		0.86	0.31	0.87	0.21
R_{pol}	kΩ.cm²	35.06	16.30	28.42	7.78
Q_{dl}	$Ss^n.cm^{-2}$	$2.96 \cdot 10^{-5}$	31.00	$6.99 \cdot 10^{-5}$	4.54
n_{dl}		0.71	7.52	0.72	2.44

Before accepting the validity of the model, the estimated model parameters must be assessed to confirm that the model is physically plausible. On the one hand, the parameters values should show the differences between the systems with and without lithium carbonate. On the other hand, the time evolution of the model parameters must be physically meaningful.

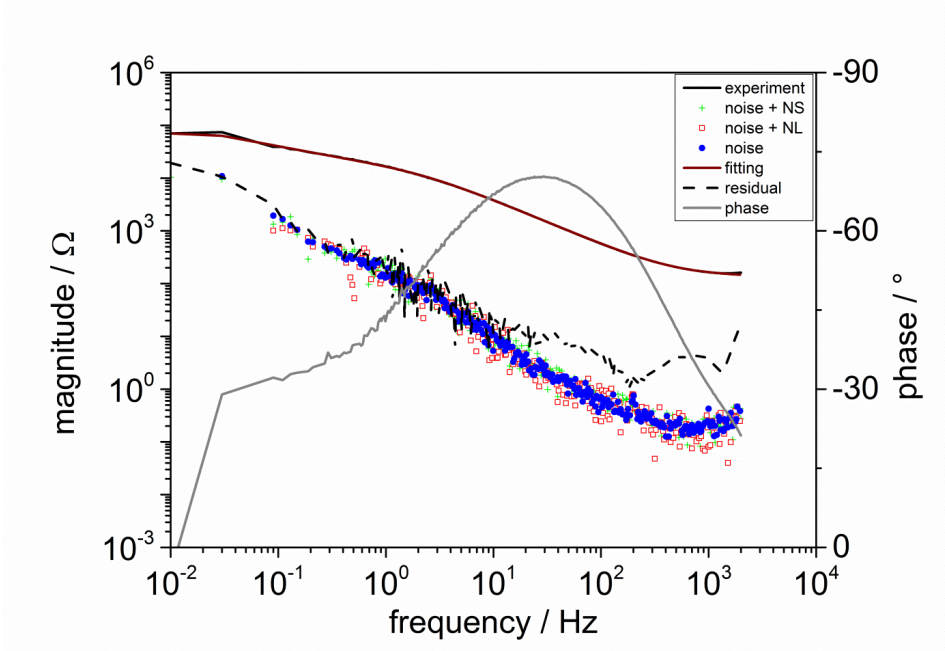

Figure 3.9 Bode plot of the lithium carbonate inhibited system after 8 hours of immersion in 0.05 M NaCl with the experimental impedance and noise distortion curves and the fitted impedance and model residual curves.

To make a useful analysis and compare the different impedance results obtained, the effective capacitance of each CPE needs to be considered. Hirschhorn et al. successfully derived a mathematical equation to estimate the effective capacitance C starting from the CPE parameters (Q and n) and the resistance R associated with the same time-constant, for a normal time-constant distribution through a surface layer [34]:

$$C = R^{\frac{(1-n)}{n}} Q^{\frac{1}{n}} \quad (2)$$

Using this approach, the effective dense oxide layer capacitance (Coxide), the double layer capacitance (Cdl) and the porous outer layer capacitance (Cporous) were calculated.

Fig. 3.10 shows the evolution of the resistance and capacitance of the oxide layer, the polarization resistance and the double-layer capacitance and the resistance and capacitance of the porous layer as a as a function of time for the system without corrosion inhibitors and the lithium carbonate inhibited system. For the system without corrosion inhibitors, the resistance and capacitance of the porous layer do not apply. The resistance of the oxide R_{oxide}

(Fig. 3.10a) is 7.82 ± 0.05 kΩ·cm² right at the start and decreases drastically in the first 6 hours after immersion, reaching a stable value of 2.16 ± 0.01 kΩ·cm². Simultaneously, the capacitance of the oxide layer C_{oxide} (Fig. 3.10b) increases from 3.60 ± 0.05 µF·cm^{-2} right at the start to a value of 137.55 ± 1.24 µF·cm^{-2} after 10 hours of immersion. The polarization resistance R_{pol} (Fig. 3.10c) rapidly decreases during the first 2 hours of immersion and stabilizes afterwards at 11.70 ± 0.23 kΩ·cm². The double layer capacitance C_{dl} (Fig. 3.10d) increases from 62.85 ± 1.67 µF·cm^{-2} right at the start to 1732.96 ± 179.86 µF·cm^{-2} after 10 hours of immersion in the electrolyte.

For the protective layer developed from the lithium carbonate leaching coating after 168 hours NSS, it can be seen that the contribution of the resistance of the porous middle layer R_{porous} (Fig. 3.10e) starts at 91.76 ± 14.76 Ω·cm² and rapidly decreases in the first couple of hours before reaching a stable value of 10.58 ± 1.04 Ω·cm² after 6.5 hours of immersion. The coupled capacitance of the porous layer C_{porous} (Fig. 3.10f) is around 1-3 µF·cm^{-2}, except for some fluctuations occurring during the first 12 hours. The resistance of the dense inner oxide layer R_{oxide} (Fig. 3.10a) is 22.43 ± 0.48 kΩ·cm² right at the start and decreases afterwards, reaching a stable value of 10.11 ± 0.31 kΩ·cm² after 2 hours and for the remaining of the measurement. Simultaneously, the capacitance of the oxide layer C_{oxide} (Fig. 3.10b) increases progressively from an initial value of 4.82 ± 0.19 µF·cm^{-2} to a value of 11.90 ± 0.16 µF·cm^{-2} after 12 hours of immersion. The polarization resistance R_{pol} (Fig. 3.10c) is 29.42 ± 13.60 kΩ·cm² for the initial stages and fluctuates around 30 to 80 kΩ·cm² for the remaining of the first 12 hours of immersion. The double layer capacitance C_{dl} (Fig. 3.10d) is 13.73 ± 3.42 µF·cm^{-2} right at the start and increases afterwards to a fluctuating value between 150 and 300 µF·cm^{-2}.

The parameter values obtained for the system without corrosion inhibitors in this work are similar to the ones obtained by Visser et al. after 4 to 8 hours of immersion in the electrolyte [15]. In the case of the system without corrosion inhibitors, values of 3.85 kΩ·cm² and 102.82 µF·cm^{-2} were obtained for the oxide resistance and capacitance, respectively, which have a good agreement with the values of 2.59 ± 0.02 to 2.10 ± 0.01 kΩ·cm² and 104.86 ± 0.92 to 132.51 ± 0.75 µF·cm^{-2} after 4 and 8 hours of immersion in this work. For the polarization resistance and double layer capacitance, 9.68 kΩ·cm² and 553.08 µF·cm^{-2} were obtained, compared to 3.78 ± 0.29 to 6.03 ± 0.58 kΩ·cm² and 628.12 ± 30.91 to 1341.72 ± 128.70 µF·cm^{-2} after 4 to 8 hours in this work.

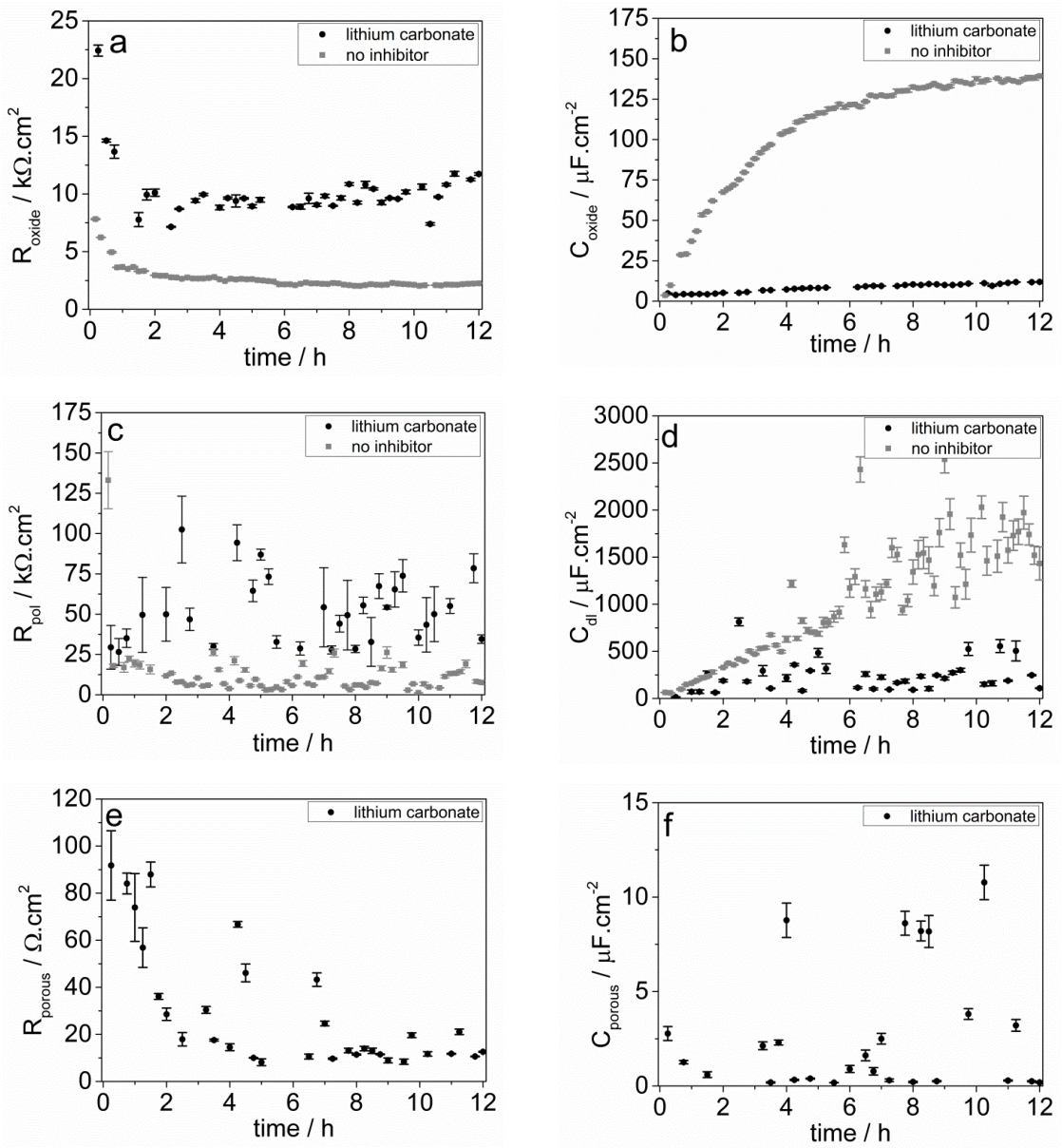

Figure 3.10 Evolution of the parameters **(a)** R_{ox}, **(b)** C_{ox}, **(c)** R_{pol}, **(d)** C_{dl}, **(e)** R_{porous} and **(f)** C_{porous} as a function of time for the system without corrosion inhibitors (▪) and the lithium carbonate inhibited system (●).

In the case of the lithium carbonate inhibited system, a similar comparison can be made. For the resistance and capacitance of the porous layer, Visser et al. obtained values of 17.00 Ω·cm² and 0.83 µF·cm^{-2} after 168 hours exposure in the NSS testing and after 4 to 8 hours of immersion in the electrolyte, compared with 14.53 ± 1.45 to 11.41 ± 0.25 Ω·cm² and a stable value of around 1 to 3 µF·cm^{-2} in this work, under the same conditions [15]. For the contribution of the oxide layer, 29.64 kΩ·cm² and 27.04 µF·cm^{-2} were obtained, compared to 8.82 ± 0.20 to 10.85 ± 0.12 kΩ·cm² and a progressive increase from 7.23 ± 0.09 up to 10.35 ± 0.20 µF·cm^{-2} after 4 to 8 hours of immersion in the electrolyte in this work. The polarization resistance and double layer capacitance were 237.43 kΩ·cm² and 46.14 µF·cm^{-2} compared to 30 to 80 kΩ·cm² and 150 to 300 µF·cm^{-2} in this study. The differences in the oxide resistance and capacitance and the polarization resistance and double layer capacitance are remarkable. Nevertheless, the evaluation of the fitting quality by means of the model residual shows that the model is able to represent the experimental data within the noise distortions. This proves that the EEC is statistically correct and that these parameter values can be considered more realistic.

It is interesting to link the resistance and the capacitance of the porous layer to the observations made in the quantitative interpretation of the ORP-EIS noise data of the lithium inhibited system. The analysis of the relative contribution of the non-stationarities shows that the system behaves non-stationary for the first 6.5 hours after immersion in the electrolyte. On the other hand, the non-stationary behaviour is predominant at the highest 2 frequency decades (IV and V), i.e., frequencies ranging from 10 Hz up to 1 kHz (Fig. 3.4b). Considering the physical behaviour of the electrochemical system and the proposed electrical circuit, the non-stationarities at high frequencies can be related to the time-varying behaviour of the porous layer. This behaviour is translated into unstable, decreasing values for the resistance of the porous layer in the first 6.5 hours. Afterwards, when the whole system, and the porous layer in particular, behaves stationary, a stable value of around 10 Ω·cm² for R_{porous} is obtained.

Regarding the parameters related to the dense oxide layer, for the system without corrosion inhibitors, the decrease in resistance and the increase in capacitance demonstrate the degradation of the native oxide layer during the first hours of immersion. A similar observation can be made for the lithium carbonate inhibited system, with a degradation of the inner dense oxide layer in the first 2 hours. This coincides with the non-stationary behaviour in the frequency region from 1 Hz to 10 Hz (decade III) (Fig. 3.4b). A stable value of around 10 kΩ·cm² is obtained for the oxide resistance of the inhibited system, more than 4 times higher than the 2.20 kΩ·cm² for the system without corrosion inhibitors. Moreover,

the oxide capacitance of the system without corrosion inhibitors increases more rapidly than the oxide capacitance of the inhibited system, which is related to the fast degradation of the native oxide layer for the system without corrosion inhibitors and the slower degradation of the dense layer formed during NSS for the inhibited system. This corresponds with the observations made in our previous work [15].

The corrosion activity is described by the low frequency time constant [35]. The polarization resistance of the lithium inhibited containing coating is more than 3 times higher, compared to the system without corrosion inhibitors. The double layer capacitance of the system without corrosion inhibitors, similar to the oxide capacitance, increases more rapidly than the inhibited system, up to values at least 5 times higher after 12 hours of immersion. This confirms the protective properties of the layer generated by the lithium leaching coating technology, in agreement with earlier observations [11, 14, 15].

The modelling residual is low compared to either the level of *noise+non-stationarities* or the noise level, dependent on the system's stability, for both the system without corrosion inhibitors and the lithium carbonate inhibited system. Moreover, the estimated parameters are physically meaningful and the proposed EEC models are physically plausible. Consequently, it is concluded that the proposed EEC models can be accepted.

3.4. Conclusions

The qualitative analysis of the ORP-EIS data of the system without corrosion inhibitors and the lithium carbonate inhibited system revealed the presence of both non-linearities and non-stationarities in the early stages after immersion in the electrolyte. For both systems, it is observed quantitatively that the presence of non-stationarities is linked to the overall instability of the electrochemical system during the first 5 and 6.5 hours, respectively. These correspond to the time needed to reach a stable degradation process of the oxide on the system without corrosion inhibitors or the multi-layered protective morphology on the lithium carbonate inhibited system. The quantification per frequency decade of the information regarding the non-stationarities of the system without corrosion inhibitors leads to the conclusion that the electrochemical processes related to the dense oxide layer, occurring in the mid-frequency region, take the longest to stabilize. In the case of the lithium carbonate inhibited system, the electrochemical processes in the porous layer, occurring in the high frequency regions prolong the system's instability.

From the monitoring of the system without corrosion inhibitors and the lithium carbonate inhibited system during the first 12 hours of immersion in 0.05 M NaCl, the parameter evolutions of the respective equivalent electrical circuit's elements are extracted. The observed trends can be explained by the evolution of the level of non-stationarities in the corresponding frequency decade(s) and they can be linked to the morphological changes happening during immersion in the electrolyte. Particularly, the non-stationary behaviour of the lithium carbonate inhibited system in the mid frequency region from 1 to 10 Hz in the first 2 hours and in the highest two frequency decades in the first 6.5 hours can be related to the unstable, decreasing values of the resistance of the oxide- and the porous layer in the first 2 and 6.5 hours, respectively. When the lithium carbonate based protective morphology becomes stable as a function of immersion time, stable parameter values are obtained for the respective EEC model elements.

This paper shows that the ORP-EIS based methodology allows us studying the behaviour of corrosion inhibitors in an alternative way. The time-dependent behaviour of electrochemical systems containing corrosion inhibitor is highlighted, proving the great value of the approach for further corrosion inhibitor research.

References

1. Lamaka, S. V., Zheludkevich, M. L., Yasakau, K. a., Montemor, M. F., & Ferreira, M. G. S. (2007). High effective organic corrosion inhibitors for 2024 aluminium alloy. *Electrochimica Acta*, *52*(25), 7231–7247.
2. Zheludkevich, M. L., Yasakau, K. a., Bastos, a. C., Karavai, O. V., & Ferreira, M. G. S. (2007). On the application of electrochemical impedance spectroscopy to study the self-healing properties of protective coatings. *Electrochemistry Communications*, *9*(10), 2622–2628.
3. van Westing, E. P. M., Ferrari, G. M., & de Wit, J. H. W. (1994). The determination of coating performance with impedance measurements—IV. Protective mechanisms of anticorrosion pigments. *Corrosion Science*, *36*(8), 1323–1346.
4. Garcia, S. J., Markley, T. a., Mol, J. M. C., & Hughes, a. E. (2013). Unravelling the corrosion inhibition mechanisms of bi-functional inhibitors by EIS and SEM–EDS. *Corrosion Science*, *69*, 346–358.
5. Balaskas, A. C., Curioni, M., & Thompson, G. E. (2015). Effectiveness of 2-mercaptobenzothiazole, 8-hydroxyquinoline and benzotriazole as corrosion inhibitors on AA 2024-T3 assessed by electrochemical methods. *Surface and Interface Analysis*, *47*(11), 1029–1039.
6. Snihirova, D., Lamaka, S. V., Taheri, P., Mol, J. M. C., & Montemor, M. F. (2016). Comparison of the synergistic effects of inhibitor mixtures tailored for enhanced corrosion protection of bare and coated AA2024-T3. *Surface and Coatings Technology*, *303*(Part B), 342–351.
7. Lopez-Garrity, O., & Frankel, G. S. (2014). Corrosion Inhibition of Aluminum Alloy 2024-T3 by Sodium Molybdate. *ECS Electrochemistry Letters*, *3*(10), C33–C35.
8. Twite, R. L., & Bierwagen, G. P. (1998). Review of alternatives to chromate for corrosion protection of aluminum aerospace alloys. *Progress in Organic Coatings*, *33*(2), 91–100.
9. Kendig, M. (2016). Corrosion Inhibition of Aluminum and Aluminum Alloys by Soluble Chromates , Chromate Coatings , and Chromate-Free Coatings Corrosion Inhibition of Aluminum and Aluminum Alloys by Soluble Chromates , Chromate Coatings , and Chromate-Free Coatings, *Corrosion, 59*(October), 379–400.
10. Forsyth, M., Seter, M., Hinton, B., Deacon, G. B., & Junk, P. (2011). New “green” corrosion inhibitors based on rare earth compounds. *Australian journal of chemistry*, *64*, 812–819.
11. Visser, P., Liu, Y., Terryn, H., & Mol, J. M. C. (2016). Lithium salts as leachable corrosion

inhibitors and potential replacement for hexavalent chromium in organic coatings for the protection of aluminum alloys. *Journal of Coatings Technology Research*, *13*(4), 557–566.

12. Visser, P., Liu, Y., Zhou, X., Hashimoto, T., Thompson, G. E., Lyon, S. B., van der Ven, L.G.J, Mol, J.M.C., Terryn, H. A. (2015). The Corrosion Protection of AA2024-T3 Aluminium Alloy by Leaching of Lithium-Containing Salts from Organic Coatings. *Faraday Discuss.*, *180*, 1–16.
13. Visser, P., Lutz, A., Mol, J. M. C., & Terryn, H. (2016). Study of the formation of a protective layer in a defect from lithium-leaching organic coatings. *Progress in Organic Coatings*, *99*, 80–90.
14. Liu, Y., Visser, P., Zhou, X., Lyon, S. B., Hashimoto, T., Curioni, M., Gholina, A. Thompson, G.E., Smyth, G., Gibbon, S.R., Graham, D., Mol, J.M.C., Terryn, H. (2016). Protective Film Formation on AA2024-T3 Aluminum Alloy by Leaching of Lithium Carbonate from an Organic Coating. *Journal of The Electrochemical Society*, *163*(3), C45–C53.
15. Visser, P., Meeusen, M., Gonzalez-Garcia, Y., Terryn, H., & Mol, J. M. C. (2017). Electrochemical Evaluation of Corrosion Inhibiting Layers Formed in a Defect from Lithium-Leaching Organic Coatings. *Journal of The Electrochemical Society*, *164*(7), C396–C406.
16. Van Ingelgem, Y., Tourwé, E., Blajiev, O., Pintelon, R., & Hubin, A. (2009). Advantages of odd random phase multisine electrochemical impedance measurements. *Electroanalysis*, *21*, 730–739.
17. Urquidi-macdonald, M., & Real, S. (1990). Applications of Kramer -Kronig Transforms in the Analysis of Electrochemical Impedance, *35*(10), 1559–1566.
18. Orazem, M., & Tribollet, B. (2008). *Electrochemical Impedance Spectroscopy*. *Wiley*.
19. Boukamp, B. A., & Ross Macdonald, J. (1994). Alternatives to Kronig-Kramers transformation and testing, and estimation of distributions. *Solid State Ionics*, *74*(1–2), 85–101.
20. Breugelmans, T., Tourwé, E., Jorcin, J. B., Alvarez-Pampliega, A., Geboes, B., Terryn, H., & Hubin, A. (2010). Odd random phase multisine EIS for organic coating analysis. *Progress in Organic Coatings*, *69*(2), 215–218.
21. Van Gheem, E., Pintelon, R., Vereecken, J., Schoukens, J., Hubin, A., Verboven, P., & Blajiev, O. (2004). Electrochemical impedance spectroscopy in the presence of non-linear distortions and non-stationary behaviour Part I: Theory and validation. *Electrochimica Acta*, *49*(26), 4753–4762.
22. Van Gheem, E., Pintelon, R., Hubin, A., Schoukens, J., Verboven, P., Blajiev, O., &

Vereecken, J. (2006). Electrochemical impedance spectroscopy in the presence of non-linear distortions and non-stationary behaviour: Part II. Application to crystallographic pitting corrosion of aluminium. *Electrochimica Acta*, *51*(8–9), 1443–1452.

23. Van Gheem, E., Vereecken, J., Schoukens, J., Pintelon, R., Guillaume, P., Verboven, P., & Pauwels, L. (2004). Instantaneous impedance measurements on aluminium using a Schroeder multisine excitation signal. *Electrochimica Acta*, *49*(17–18), 2919–2925.
24. Breugelmans, T., Lataire, J., Muselle, T., Tourwé, E., Pintelon, R., & Hubin, A. (2012). Odd random phase multisine electrochemical impedance spectroscopy to quantify a non-stationary behaviour: Theory and validation by calculating an instantaneous impedance value. *Electrochimica Acta*, *76*, 375–382.
25. Breugelmans, T., Tourwé, E., Van Ingelgem, Y., Wielant, J., Hauffman, T., Hausbrand, R., Pintelon, R., Hubin, A. (2010). Odd random phase multisine EIS as a detection method for the onset of corrosion of coated steel. *Electrochemistry Communications*, *12*(1), 2–5.
26. Hauffman, T., Van Ingelgem, Y., Breugelmans, T., Tourwé, E., Terryn, H., & Hubin, A. (2013). Dynamic, in situ study of self-assembling organic phosphonic acid monolayers from ethanolic solutions on aluminium oxides by means of odd random phase multisine electrochemical impedance spectroscopy. *Electrochimica Acta*, *106*, 342–350.
27. Hauffman, T., Breugelmans, T., Van Ingelgem, Y., Tourwé, E., Terryn, H., & Hubin, A. (2012). Measuring the adsorption of ethanol on aluminium oxides using odd random phase multisine electrochemical impedance spectroscopy. *Electrochemistry Communications*, *22*(1), 124–127.
28. Van Ingelgem, Y., Tourwé, E., Vereecken, J., & Hubin, A. (2008). Application of multisine impedance spectroscopy, FE-AES and FE-SEM to study the early stages of copper corrosion. *Electrochimica Acta*, *53*(25), 7523–7530.
29. Geboes, B., Baert, K., Hubin, A., & Breugelmans, T. (2015). Investigation of the adsorption mechanism of heterocyclic molecules on copper using potentiodynamic ORP-EIS and in-situ Ramans pectroscopy. *Electrochimica Acta*, *156*, 308–315.
30. Fernández Macía, L., Petrova, M., Hauffman, T., Muselle, T., Doneux, T., & Hubin, A. (2014). A study of the electron transfer inhibition on a charged self-assembled monolayer modified gold electrode by odd random phase multisine electrochemical impedance spectroscopy. *Electrochimica Acta*, *140*, 282–293.
31. Tzedaki, M., Verguts, S., Van Ingelgem, Y., Hammons, J. A., De Graeve, I., & Terryn, H. (2016). An ORP-EIS approach to study the gas incorporation into aluminum etch

films. *Surface and Interface Analysis*, *48*(8), 699–705.

32. Atkinson, K. (1989). *An introduction to numerical analysis* (2nd Edition). Wiley.
33. Fernández Macía, L., Petrova, M., & Hubin, A. (2015). ORP-EIS to study the time evolution of the $[Fe(CN)_6]^{3-}/[Fe(CN)_6]^{4-}$ reaction due to adsorption at the electrochemical interface. *Journal of Electroanalytical Chemistry*, *737*, 46–53.
34. Hirschorn, B., Orazem, M. E., Tribollet, B., Vivier, V., Frateur, I., & Musiani, M. (2010). Determination of effective capacitance and film thickness from constant-phase-element parameters. *Electrochimica Acta*, *55*(21), 6218–6227.
35. Zheludkevich, M. L., Yasakau, K. A., Poznyak, S. K., & Ferreira, M. G. S. (2005). Triazole and thiazole derivatives as corrosion inhibitors for AA2024 aluminium alloy. *Corrosion Science*, *47*(12), 3368–3383.

Chapter 4

A complementary electrochemical approach for time-resolved evaluation of corrosion inhibitor performance

This chapter is published as a scientific paper:
M. Meeusen, L. Zardet, A. M. Homborg, M. Lekka, F. Andreatta, L. Fedrizzi, B. Boelen, H. Terryn and J.M.C. Mol (2019). A Complementary Electrochemical Approach for Time-Resolved Evaluation of Corrosion Inhibitor Performance. *Journal of The Electrochemical Society, 166 (11)*. C1-C13.

Abstract

In this paper, different macroscopic electrochemical techniques are applied to study the corrosion inhibitor efficiency, protection mechanism and stability of a calcium aluminium polyphosphate silicate hydrate inhibitor on hot-dip galvanized steel in the time-domain. Potentiodynamic polarization (PP) measurements are applied to study the anodic and cathodic mechanistic behaviour as well as inhibitor efficiencies at discrete and single times of exposure. Open circuit potential (OCP) with superimposed linear polarization resistance (LPR) measurements are applied as a faster, non-invasive alternative to PP, characterizing the overall performance of the system in terms of the polarization resistance. Electrochemical impedance spectroscopy (EIS) measurements are applied to detail both the overall performance of the system as well as the corrosion inhibition mechanism related to the electrochemical system's physicochemical representation over time. Electrochemical noise (EN) measurement are used to evaluate the inhibition efficiency as a function of exposure time, represented by the electrochemical noise resistance. Odd random phase electrochemical impedance spectroscopy (ORP-EIS) is selected as the electrochemical tool to study the system's instability, by evaluation of the non-linearities and non-stationarities over time. The non-stationarities present in the inhibitor-containing electrochemical system are shown to cause the overall instability of the system and should be taken into account when interpreting results from the different techniques over time.

4.1. Introduction

Corrosion protection by the application of inhibitor doped organic coatings or the addition of inhibiting species to aqueous corrosive solutions is amongst the most common means of corrosion control strategies for metal applications in aggressive environments. While the use of hexavalent chromium (Cr(VI)) based corrosion inhibitive chemistries has been common practice for many decades, strict international health and safety legislation including the Registration, Evaluation, Authorisation and Restriction of Chemicals (REACH) regulation of the European Union adopted in 2007, aims to create a new legal framework for the use of hazardous chemical substances. Multiple Cr(VI) containing compounds, added as active corrosion inhibitors in many polymer formulations because of their exceptional performance, have been or are prone to be phased out in the near future even for demanding applications because of their toxic and carcinogenic nature [1]. The replacement of these Cr(VI) based inhibitors by eco-friendly, Cr(VI)-free inhibitors is challenging, since there is a significant performance 'gap' between them [2]. Different alternatives to the hexavalent chromium technology have been studied, including rare-earth-, vanadate- and lithium- based inhibitors but are not universal and experience some technical constraints, such as upscaling and cost adjustments, to date [3].

These corrosion protective substances or mixtures, added in low concentration, prevent or minimize the corrosion rate of a variety of metal substrates. Apart from their chemical nature, they can also be classified according to their working principle as anodic, cathodic or mixed type corrosion inhibitors [4][5]. Anodic inhibitors typically form or facilitate the formation of a protective oxide film on the metal matrix and consequently shift the corrosion potential into the passive range. Cathodic inhibitors either slow down the cathodic reactions themselves or form precipitates on cathodic areas, reducing the diffusion of electrolyte, oxygen and water to the surface. Mixed corrosion inhibitors impact both the anodic and cathodic reactions. In all cases, the presence of corrosion inhibitors changes the overall electrochemistry and reduces the corrosion reaction kinetics over time [4][5][6].

Up to now, multiple studies applying a variety of electrochemical characterization techniques exist to study Cr(VI)-free corrosion inhibitors and investigate their performance for a given metallic substrate. However, few works are dedicated to the comparison between stationary and non-stationary techniques to study electrochemical systems [7].

Potentiodynamic polarization (PP) experiments describe the kinetic behaviour of an inhibitor-containing electrochemical system by decoupling the anodic and cathodic

reactions on the surface under investigation. Zin, Pokhmurs'kyi et al. studied the synergistic effect of phosphate and calcium-containing pigments on the corrosion resistance of galvanized steel with PP to distinguish between anodic, cathodic or mixed control at discrete immersion times [8][9]. Deflorian et al. used PP measurements to study the anodic and cathodic corrosion mechanism separately for the corrosion protection performance of primers containing polyphosphate-based ion-exchange pigments for galvanized steel [10]. Kartsonakis et al. screened six possible corrosion inhibitors for hot-dip galvanized steel with PP experiments and differentiated between anodic and cathodic inhibitors in terms of anodic and cathodic current density and by a shift in the open circuit potential (OCP) [11]. Hernandez-Alvarado et al. studied a chromate-free organic inhibitor for galvanized steel with PP to identify the oxidation and reduction reactions and the related increase and decrease in corrosion current density [12].

The polarization resistance method or Stern-Geary method is a well-established technique for the determination of corrosion rates [13]. Through linear polarization resistance (LPR) measurements using a small amplitude excitation potential and measuring the current density response, the polarization resistance (R_p) can be calculated from the slope of the potential versus current density slope around the corrosion potential (E_{corr}). Subsequently, the corrosion current density and the corrosion rate can be determined through the Stern-Geary coefficient (B) [13][14][15]. Moreover, LPR measurements could be applied as such to determine the corrosion protective properties of inhibitor-containing systems over time. Kartsonakis et al. applied the LPR technique for the characterization of different corrosion inhibitors for hot-dip galvanized steel after 168 h to compare their inhibition performance [11]. Hernadez-Alvarado et al. used the R_p method to evaluate the protective properties of a chromate-free organic inhibitor for galvanized steel at discrete times over a period of 140 days. These observations were coupled to the protective mechanism through anodic and cathodic polarization measurements [12][16]. However, complications may occur regarding the potential scan rate as well as with non-linear and non-stationary behaviour of the system under investigation since this method de facto assumes linear and time-invariant electrochemical behaviour [13][15].

Electrochemical impedance spectroscopy (EIS) has manifested itself as a powerful technique to screen and study the corrosion protective properties of corrosion inhibitors over time both qualitatively and quantitatively. The former refers to the comparison of the magnitude of the impedance modulus at low frequencies over time [17]. The latter corresponds to the fitting of the impedance data to a physicochemical sound equivalent electrical circuit so that the individual contributions to the overall system's performance can be quantified [8][9][18].

However, since corrosion processes are intrinsically non-linear and non-stationary [19], trustworthy EIS measurements can only be carried out if it is proven that the inhibitor-containing electrochemical system is linear and time-invariant within the timeframe of the measurement [20]. A number of possible solutions have been proposed lately. Application of the Kramers-Kronig (K-K) transforms provide verification criteria with respect to the linearity and stationary conditions. Nevertheless it has been illustrated that the conformity with the condition of time-invariance is difficult to deal with [21][22][23]. Generally, in other works, EIS measurements are only performed after stabilization of the OCP with a small amplitude of the excitation signal, supposing the respective conditions to be fulfilled. Hamlaoui et al. waited for 30 minutes prior to performing an EIS measurement, using an signal amplitude of 10 mV when monitoring the corrosion of galvanized coatings and presuming linearity and stationarity during measuring [24]. Kartsonakis et al. studied the corrosion protective mechanisms of inhibitors for hot-dip galvanized steel with a signal amplitude of 10 mV root mean square (RMS) but first allowing the system to stabilize for one hour [11]. Deflorian et al. studied cerium oxides as corrosion inhibitors for galvanized steel using EIS with a signal amplitude of 5 mV starting from one hour after immersion [12]. Consequently the initial, rapidly evolving stages of corrosion inhibitor-containing electrochemical processes prior to the first EIS measurement cannot be described adequately [25].

Electrochemical noise (EN) measurements have proven to be a suitable technique for in-depth corrosion analysis. When two identical working electrodes are connected through a zero resistance ammeter (ZRA) and with a potentiometer to a reference electrode, one can differentiate between different types of corrosion processes. Moreover, through alternative transient analysis methods, non-stationary electrochemical processes can be described [26]. Homborg et al. successfully identified localized corrosion of stainless steel, corrosion inhibition on AA2024-T3 by Ce ions and microbiologically influenced corrosion of carbon steel using EN [27][28][29].

Odd random phase electrochemical impedance spectroscopy (ORP-EIS) is a multisine EIS technique providing information about the linearity and time-invariance of electrochemical systems. Here, the system is excited with a multisine signal over the entire frequency range instead of exciting the electrochemical system at each subsequent frequency. This periodic broadband signal comprises harmonically related sine waves whereof only the odd harmonics are excited and one out of three consecutive harmonics is randomly omitted [30]. The linearity and time-invariant information is then obtained through a dedicated data analysis procedure. The concept of ORP-EIS has already been demonstrated to be a

successful tool to study non-linear and particularly non-stationary electrochemical systems. Fernández Macía et al. studied the electron transfer inhibition on a charged self-assembled monolayer modified gold electrode and the time-varying characteristics of the electron transfer of the ferri/ferrocyanide reaction on gold [31][32]. Alvarez-Pampliega et al. investigated the initial non-stationary corrosion process of aluminium rich metal coated steel [33]. Hauffmann et al. used ORP-EIS to study the growth of self-assembled monolayers on aluminium oxides in-situ, which is essentially non-stationary [34][35]. By the detection of non-linearities and especially non-stationarities, the onset of corrosion on coated steel was studied by Breugelmans et al. [36]. Recently Ji et al. studied the corrosion behaviour of hot dip galvanized steel wires in sodium chloride solution. The initial, non-stationary corrosion behaviour was linked with the microstructural properties of the steel wires [37]. In earlier work we already highlighted the time-dependent behaviour of inhibitor-containing electrochemical systems. The presence of non-stationarities in a certain frequency range was linked to the trends in the evolution of the equivalent electrical circuit (EEC) parameters and the unstable behaviour of the electrochemical processes could be related to the associated morphological changes [25].

Beyond the scope of the present study, the macroscopic study of corrosion inhibitors is often coupled to dedicated surface analysis measurements or alternatively, the study of corrosion inhibitors is approached from a local electrochemical point of view.

In this paper, different macroscopic electrochemical techniques are applied to study corrosion inhibitor efficiency, protection mechanism and stability of a calcium aluminium polyphosphate silicate hydrate inhibitor on hot-dip galvanized steel in the time-domain. While the search for optimized inhibitor performance in itself was out of scope of this work, a phosphate based inhibitor was chosen as the corrosion inhibitor of study as in its basics and chemistry it represents an industrially and commonly applied inhibitor class. PP is used to determine the inhibitor working principle and efficiency at a single time of exposure. The application of repetitious LPR measurements superimposed on a continuous OCP measurement is used as a non-invasive alternative to measure the corrosion inhibitor performance over time. EIS is applied to study also the working mechanism of the corrosion inhibitor over time. EN measurements are applied to identify the corrosion inhibition efficiency as a function of exposure time, represented by the electrochemical noise resistance. ORP-EIS is used to quantify the stability of the corrosion inhibitor over time. Initially, the mechanistic, efficiency and stability information obtained from the different techniques is discussed separately. Finally, a comparison between the information obtained with the different electrochemical techniques is made in the time-domain, in order to

evaluate the complementarity of the macroscopic electrochemical techniques used in this study.

4.2. Experimental details

4.2.1. Materials and sample preparation

Hot-dip galvanized steel was obtained from Tata Steel, IJmuiden The Netherlands, with an average coating mass of 275 $g \cdot m^{-2}$ and nominal composition of the steel substrate and galvanized coating as listed in Table 4.1. The galvanized steel samples were cut to 30mm by 50mm, with a circular exposed area of 2.01 cm^2 for PP, LPR, EIS and ORP-EIS and 0.28 cm^2 for EN measurements. However, all results are surface area corrected. The samples were then alkaline cleaned according to ASTM D 6386– 99: the samples were cleaned with acetone for 5 minutes in the ultrasonic bath. Then, the samples were immersed in a 1 M NaOH solution, adjusted to pH 12 with H_3PO_4, for 30 seconds. Finally, the samples were rinsed with distilled water and dried.

Table 4.1 Nominal composition of the hot-dip galvanized steel substrate and the galvanized coating.

steel substrate (ppm)	**C**	**Mn**	**Si**	**Al**	**N**	**P**	**S**	**V**	**Ti**	**Cu**	**Sn**
	440	2120	120	460	27	70	70	10	20	150	20
	Cr	**Ni**	**Mo**	**Ca**							
	150	210	20	33							
coating (wt%)	**Al**	**Fe**	**Mg**	**Zn**							
	0.36	0.25	0	rest							

Heucophos®CAPP, a calcium aluminium polyphosphate silicate hydrate provided by Heubach, Langelsheim Germany, was used as a zinc-free phosphate corrosion inhibitor for hot-dip galvanized steel [38]. The reference solution used for all measurements was 0.05 M NaCl, relevant for building construction steel applications. Moreover, this concentration is preferred for future local electrochemical research. Based on this, a 0.5 mM solution of the corrosion inhibitor was prepared.

X-ray Fluorescence (XRF) analysis was carried out to determine the molar mass of the corrosion inhibitor and to make the correct corrosion inhibitor solution. The measurements on the pressed powders were performed with a Panalytical Axios Max WD-XRF spectrometer and the data evaluation was done with SuperQ5.0i/Omnian software. XRF analysis on Heucophos®CAPP revealed the presence of silica (34.46 wt%), phosphorous pentoxide (29.40 wt%), calcium oxide (25.89 wt%) and alumina (8.83 wt%) as main components.

4.2.2. Potentiodynamic Polarization

A typical three electrode set-up was used for the PP experiments with an Ag/AgCl 3 M KCl reference electrode, a graphite bar as the counter electrode and the hot-dip galvanized steel as the working electrode.

PP curves after 1.5 hours, after stabilization of the OCP, and after 24 hours were acquired by measuring the anodic and cathodic branch separately, using different hot-dip galvanized steel samples and for at least three times per system with or without corrosion inhibitor. The cathodic branch was measured starting from +30 mV to -500 mV relative to the OCP and the anodic branch was measured from -30 mV to +500 mV relative to the OCP ensuring a small overlap between both branches around the OCP. The scan rate applied was 1 mV/s and a measurement point was taken every 0.2 s. The Tafel extrapolation procedure has been applied to determine the corrosion potential (Ecorr) and the corrosion current density (icorr). The Ecorr value was then compared versus the OCP value to evaluate the quality of the extrapolation and the icorr value was used to calculate the inhibitor efficiency η (%). All results presented in this work are rounded according to the two-digits rule: the standard deviation is rounded to two significant digits, and the mean is then matched accordingly to the decimal places of the standard deviation [39][40].

4.2.3. Open Circuit Potential with superimposed Linear Polarization Resistance

A typical three electrode set-up was used for the OCP with superimposed LPR experiments with an Ag/AgCl 3 M KCl reference electrode, a graphite bar as the counter electrode and the hot-dip galvanized steel as the working electrode.

The OCP has been monitored for 168 hours, while performing a superimposed LPR measurement every hour with an amplitude of ± 5 mV relative to the OCP at a scan rate of 0.1667 mV/s on at least three samples per system with or without corrosion inhibitor. The Rp was calculated from the slope from the potential versus current graph at the corrosion potential Ecorr [41].

4.2.4. Electrochemical Impedance Spectroscopy

A typical three electrode set-up, placed in a Faraday cage, was used for the electrochemical experiments with an Ag/AgCl 3 M KCl reference electrode, a stainless steel grid as the counter electrode and hot-dip galvanized steel as the working electrode with an area of 2.01 cm^2.

The EIS measurements on at least three samples per system with or without corrosion inhibitor were performed with a Biologic VMP-300 multichannel potentiostat in a frequency range from 10-2 Hz to 105 Hz, with 7 points per decade. The amplitude of the excitation signal was set to 10 mV, relative to the OCP. Measurements were performed every 30 minutes, while the OCP was monitored in between, for a total duration of 168 hours. The impedance data were fitted with different equivalent electrical circuits using Zview from Scribner Associates Inc.

4.2.5. Electrochemical noise

A conventional three electrode set-up was used for the EN experiments with two identical hot-dip galvanized steel working electrodes and an Ag/AgCl 3 M KCl reference electrode, under open-circuit conditions. A well-defined area of 0.28 cm^2 of each working electrode was exposed to the electrolyte. The electrochemical cells were placed in a Faraday cage to avoid electromagnetic disturbance from external sources. Potential and current signals were recorded using a Compactstat from Ivium Technologies working as potentiometer and ZRA on at least three samples per system with or without corrosion inhibitor. The sampling frequency was set to 20 Hz. A low-pass filter of 10 Hz, which is the Nyquist frequency at this sampling rate, was applied during data recording. The minimum and maximum ranges of the ZRA were automatically determined during the measurements, depending on the dynamic range of the electrochemical current noise signal locally, with a lower limit of 1 nA and an

upper limit of 100 µA. The range of the potentiometer was set at 40 mV with the removal of the initial DC drift component. The data were processed using Matlab from Mathworks [28][42][43].

4.2.6. Odd Random Phase Electrochemical Impedance Spectroscopy

A typical three electrode set-up was used for the electrochemical experiments with an Ag/AgCl 3 M KCl reference electrode, a stainless steel grid as the counter electrode and the hot-dip galvanized steel sample as the working electrode. The set-up was placed in a Faraday cage. Measurements were recorded immediately after immersion in both the reference and corrosion inhibitor solution and continued for 24 hours. In both cases, a measurement was taken every 15 minutes. The measurements on each system, with or without corrosion inhibitors, was repeated at least once for consistency.

The ORP-EIS measurements were performed with a MATLAB controlled set-up comprising of a Bio-Logic SP-200 potentiostat and a National Instruments PCI-6110 DAQ card. The frequency range was from 10-2 Hz to 2·103 Hz. The amplitude of the excitation signal was set to 3 mV (2.12 mV root mean square (RMS)) in the case of hot-dip galvanized steel without corrosion inhibitor and 5 mV (3.54 mV RMS) in the case of hot dip galvanized steel with corrosion inhibitor, applied relative to the OCP, to have a good signal-to-noise ratio while keeping the non-linearities confined. The MATLAB software to build the odd random phase multisine excitation signal, record the impedance measurements and perform the modelling was developed at the Vrije Universiteit Brussel. A more detailed description of this technique can be found elsewhere [20][44].

4.3. Results and discussion

4.3.1. Potentiodynamic polarization

PP measurements were performed to obtain information about the corrosion inhibitor's working mechanism and efficiency. In Figure 4.1a, the PP curves for hot-dip galvanized steel with and without corrosion inhibitor after 1.5 hours and 24 hours are presented. The system

with corrosion inhibitor after 1.5 hours shows lower cathodic current densities as compared to the system without corrosion inhibitor after 1.5 hours, but only marginal anodic inhibition. After 24 hours, the system with corrosion inhibitor demonstrates similar behaviour, while the system without inhibitors shows a significant increase in cathodic current density. These observations suggest a cathodic inhibition behaviour, in agreement with an earlier study of calcium-aluminium-polyphosposilicahydrate pigments for the protection of galvanized steel by Deflorian et al. [10].

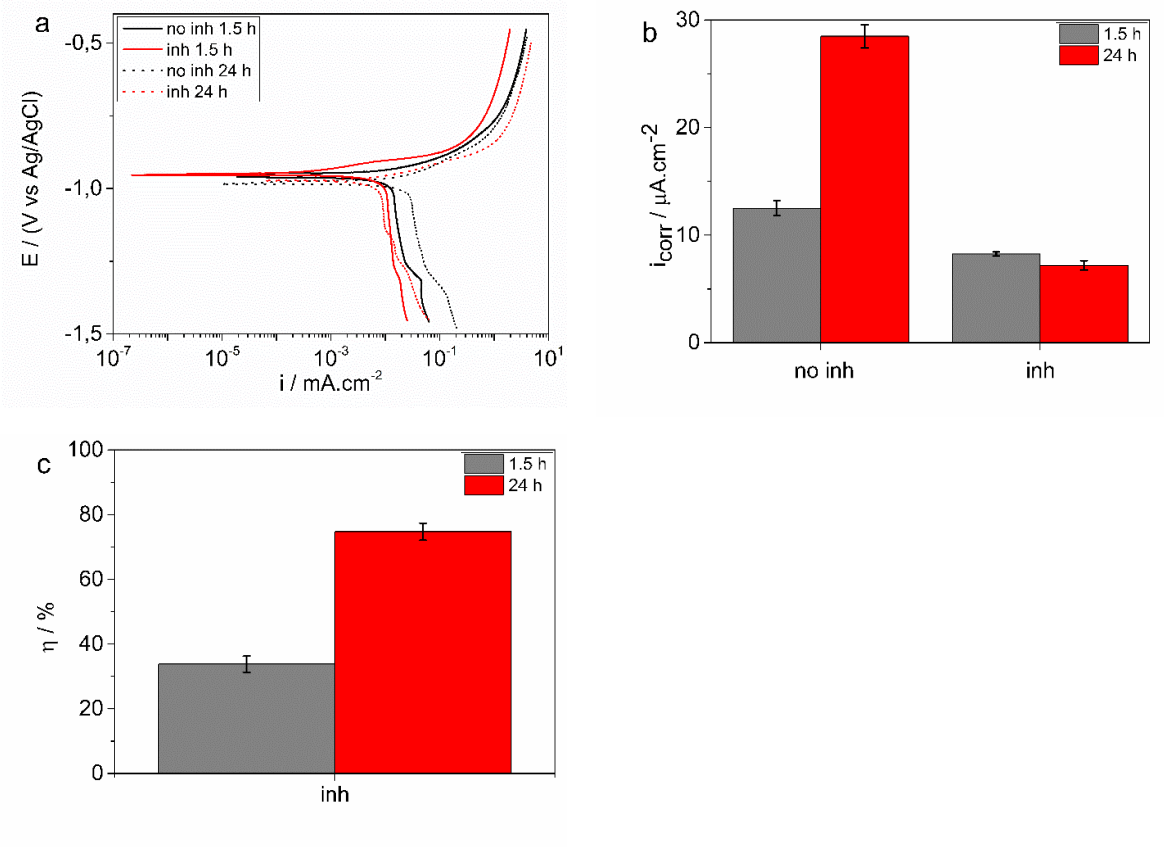

Figure 4.1 Potentiodynamic polarization diagram **(a)**, corrosion current density (i_{corr}) **(b)** and corrosion inhibitor efficiency (η) **(c)** of hot-dip galvanized steel without (0.05 M NaCl) and with corrosion inhibitor (0.5 mM Heucophos® CAPP) after 1.5 h and 24 h.

In Figure 4.1b, the corrosion current density, obtained through Tafel extrapolation [45], after 1.5 hours and 24 hours is plotted for the hot-dip galvanized steel with and without corrosion

inhibitor. In the case of the reference solution, the corrosion current density increased from 12.50 ± 0.71 µA cm-2 after 1.5 hours to 28.5 ± 1.1 µA cm-2 after 24 hours. The ± values represent the standard deviation on each measurement. In the case of the corrosion inhibitor containing solution, icorr decreased from 8.28 ± 0.20 µA cm-2 after 1.5 hours to 7.20 ± 0.43 µA cm-2 after 24 hours. This shows the active corrosion process of the hot-dip galvanized steel without corrosion inhibitor and the effective corrosion inhibition of the hot-dip galvanized steel with 0.5 mM of corrosion inhibitor.

In order to assess the effectiveness of corrosion inhibitor, the corrosion inhibitor efficiency (η) is calculated from the corrosion current density of the inhibited system (icorr(inh)) and the reference (icorr) according to [46]:

$$\eta\,(\%) = \frac{i_{corr} - i_{corr(inh)}}{i_{corr}}\; x\; 100 \qquad (1)$$

In Figure 4.1c, the corrosion inhibitor efficiency is plotted after 1.5 hours and 24 hours. The corrosion inhibitor efficiency approximately doubles from 33.8 ± 2.5 % to 74.7 ± 2.7 % after 1.5 hours and 24 hours, respectively. However, this increase in efficiency can be attributed primarily to the relatively large increase (+128 %) of the corrosion current density of the reference system rather than the minor decrease (-13 %) of the corrosion current density of the inhibited system.

It can be concluded that PP measurements can provide detailed mechanistic information in terms of the anodic and cathodic stationary behaviour at discrete times of immersion. However, obtaining time-resolved information on inhibitor performance and efficiency is time intensive.

4.3.2. Open Circuit Potential with superimposed Linear Polarization Resistance

In order to characterize the performance of the system in the first 168 hours after immersion with and without the presence of corrosion inhibitors, continuous OCP measurements with coupled LPR measurements every hour were carried out. From the slope of the potential versus current plot for every hour, the Rp can be calculated and as such monitored every hour.

Figure 4.2 shows the Rp values and their standard deviation of the hot-dip galvanized steel with and without corrosion inhibitor over time. It can be seen that in the case of the reference solution, the Rp is 1.65 ± 0.14 kΩ cm² after 1 hour, decreasing rapidly in the first 10 hours to 0.99 ± 0.12 kΩ cm² and eventually continuing to decrease slowly to 0.61 ± 0.11 kΩ cm² after 168 hours of immersion. In the case of hot-dip galvanized steel with corrosion inhibitor, the Rp is 1.51 ± 0.48 kΩ cm² at the start and decreases gradually in the first 8 hours to 1.274 ± 0.064 kΩ cm². Afterwards a gradual increase is noticeable to 1.56 ± 0.19 kΩ cm² after 168 hours, which is more than two times higher compared to the reference solution.

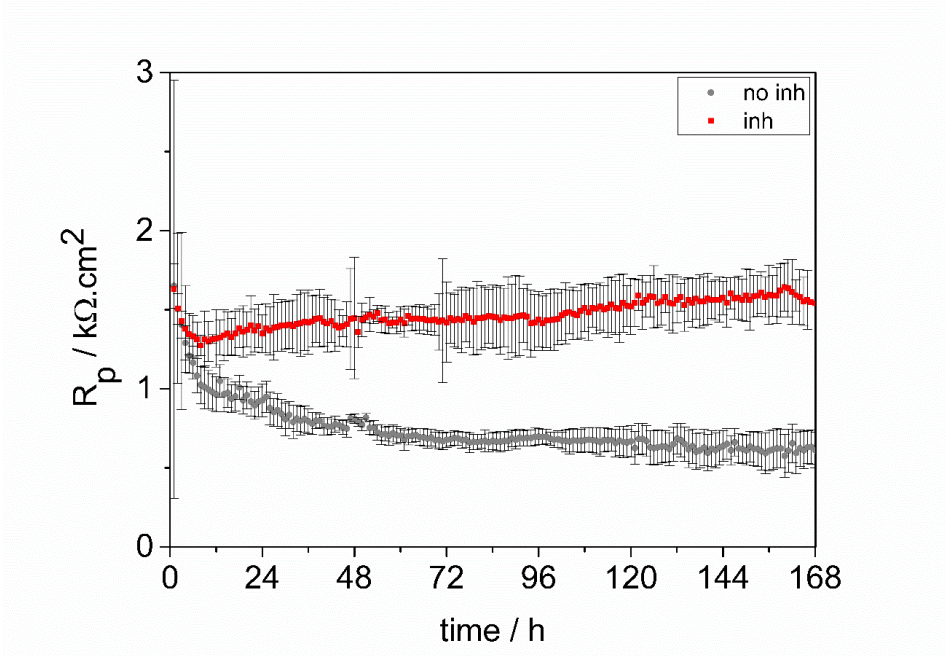

Figure 4.2 Polarization resistance (R_p) results and their standard deviation obtained from linear polarization resistance measurements of hot-dip galvanized steel without (0.05 M NaCl) and with corrosion inhibitor (0.5 mM Heucophos® CAPP) for 168 h.

The Rp value for the sample without corrosion inhibitor after 1 hour is in good agreement with the value of 2.049 kΩ cm² obtained by Kartsonakis et al. after 1 hour of immersion in 0.05 M NaCl [11].

In order to be able to compare these LPR results with the results obtained through PP measurements earlier, the icorr is calculated from the Rp and the anodic and cathodic slopes of the Tafel plot (βa and βc, respectively) according to the Stern-Geary equation [13]:

$$i_{corr} = \frac{\beta_a \cdot \beta_c}{2.3\,(\beta_a + \beta_c)\,R_p} \quad (2)$$

For comparison, an LPR value after 1.5 hours is calculated as the average from the Rp values after 1 and 2 hours, respectively. The necessary parameters for the calculation of icorr are summarized in Table 4.2. It can be seen that the resulting icorr values are 15.1 ± 1.1 µA cm² and 46.8 ± 5.5 µA cm² for the hot-dip galvanized steel without corrosion inhibitors and 10.2 ± 5.8 µA cm² and 16.9 ± 1.5 µA cm² for the hot-dip galvanized steel with 0.5 mM of corrosion inhibitor in 0.05 M NaCl, after 1.5 hours and 24 hours respectively.

Table 4.2 Tafel Parameters from PP and R_p from LPR for the determination of i_{corr} using Stern-Geary.

	time	**R_p** (kΩ cm²)	**std. dev.** (kΩ cm²)	**β_a** (V/dec)	**β_c** (V/dec)	**i_{corr}** (µA cm^{-2})	**std. dev.** (µA cm^{-2})
no inh	1.5 h	1.58	0.12	0.059	0.084	15.1	1.1
	24 h	0.93	0.11	0.11	1.2	46.8	5.5
inh	1.5 h	1.57	0.90	0.045	0.21	10.2	5.8
	24 h	1.35	0.12	0.079	0.16	16.9	1.5

Comparison of these icorr values with the previously obtained icorr values through PP measurement reveals that there is a good agreement between the values after 1.5 hours for both the system without and with corrosion inhibitor, although the standard deviation on the latter is considerable. In the case of the results after 24 hours, a remarkable difference can be observed in both cases. However, it is important to remark that for the determination of icorr from LPR using Stern-Geary, values determined from the Tafel extrapolation need to be used, making an independent comparison impossible.

It has been shown that the application of OCP with superimposed LPR measurements with a small amplitude of the excitation signal every hour allows multiple measurements on the same sample over time to be performed. Consequently, they present a faster, non-invasive alternative to the PP technique, although, any mechanistic information about the cathodic and anodic behaviour is lost.

4.3.3. Electrochemical Impedance Spectroscopy

The electrochemical characteristics of the hot-dip galvanized steel with and without corrosion inhibitor were evaluated with EIS. Figure 4.3 shows the Bode plots of the different systems every day up to 1 week after immersion. The Bode plots of the hot-dip galvanized steel without corrosion inhibitor (Fig. 4.3a) show a remarkable decrease in the impedance modulus of the middle frequency (103-100 Hz) and a gradual decrease in the low frequency (100-10-1 Hz) region over time. The associated phase plot clearly shows two time-constants, one in the middle frequency region and one in the lower frequency region. The former is associated with corrosion activity, related to the effect of the ionic double layer capacitance [47][48]. The latter is related to the diffusion of the zinc oxidation products to the bulk solution or to oxygen reduction [11][48][49][50]. Associated with the decrease in impedance modulus in mid- and low-frequency regions is a decrease and shift of the phase angle of the first time-constant towards lower frequencies and a decrease of the phase angle of the second time-constant. This can be related to the decreased corrosion resistance of the reference system.

The Bode plots of the hot-dip galvanized steel with corrosion inhibitor (Fig. 4.3b) show an initial decrease in the magnitude of the impedance modulus at 10 mHz during the first day of immersion. Afterwards the magnitude of the impedance modulus increases again over time. The Bode phase plot reveals again two time-constants. The first time-constant, in the mid-frequency region, decreases slightly with time, but shifts to higher frequencies, revealing the occurrence of corrosion protective action on the surface. The second time-constant, in the low-frequency region, increases over the course of 168 hours, indicating an increased corrosion protection [17][51].

To evaluate the consistency between the results obtained from different electrochemical techniques, the Rp values of the EIS measurements are calculated. For the LPR measurements, the Rp values were directly available, while for the EIS measurements the Rp values can be determined from the real component of the impedance at 100 kHz and 10 mHz according to [52]:

$$R_p = Z'(0) - Z'(\infty) \tag{3}$$

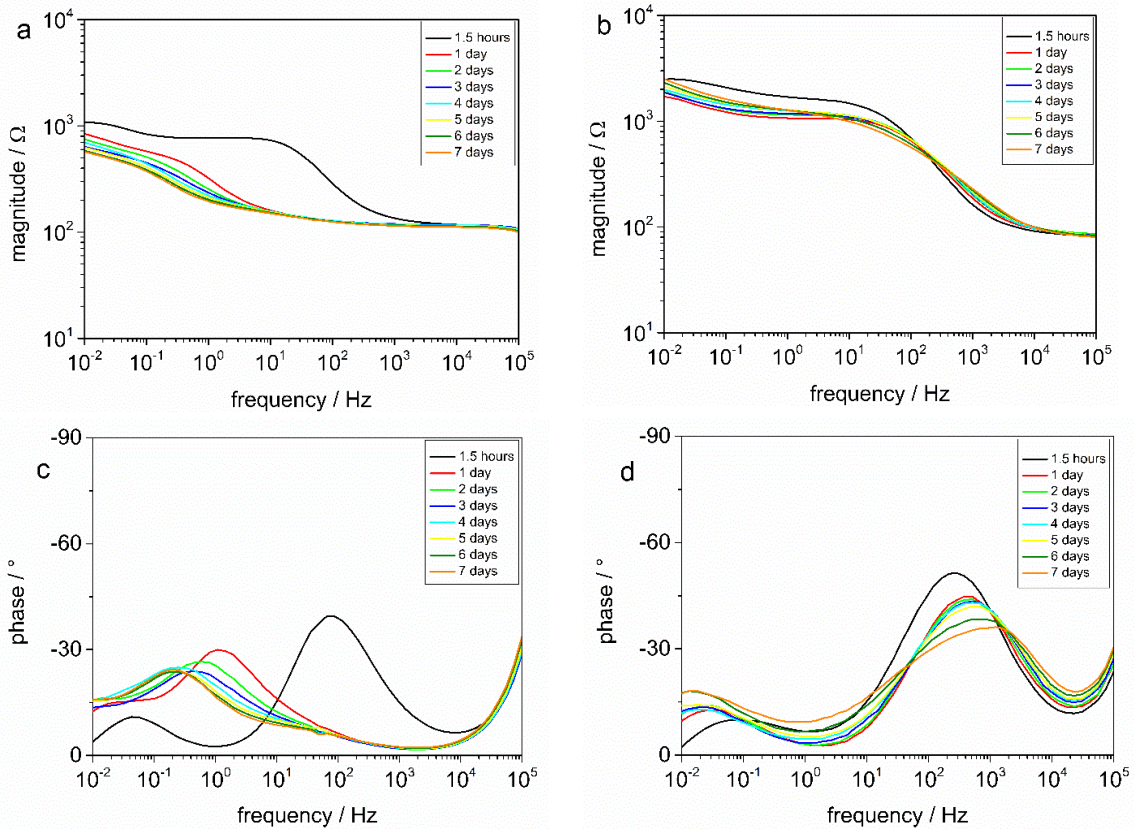

Figure 4.3 EIS bode plots for hot-dip galvanized steel **(a,c)** without corrosion inhibitor (0.05 M NaCl) and **(b,d)** with corrosion inhibitor (0.5 mM Heucophos® CAPP) every 24 h for 168 h.

Figure 4.4 shows the evolution of the Rp with their standard deviation obtained from EIS measurements for the system with and without corrosion inhibitor as a function of immersion time. It can be seen that, for the system without corrosion inhibitors, the Rp is 1.87 ± 0.31 kΩ cm² after 1 hour and decreases strongly in the initial hours after immersion. After 10 hours, a Rp value of 0.75 ± 0.13 kΩ cm² is reached. Subsequently, the Rp decreases more slowly, reaching a value of 0.475 ± 0.041 kΩ cm² after 168 hours.

The Rp of hot-dip galvanized steel with corrosion inhibitor is 2.85 ± 0.42 kΩ cm² after 2 hours of immersion and decreases rapidly in the first 12 hours after immersion, reaching a value of 1.71 ± 0.16 kΩ cm². Afterwards, the Rp value starts increasing gradually with time for the

remaining duration of the measurement. After 168 hours of immersion, the Rp value has reached a value of 2.43 ± 0.47 kΩ cm².

The Rp values of the hot-dip galvanized steel without corrosion inhibitor in this work are similar to the results obtained by Kartsonakis et al. [11]. Rp values of 0.77, 0.63 and 0.86 kΩ cm² were obtained after 3 h, 72 h and 168 h in 0.05 M NaCl, while values of 0.969 ± 0.011, 0.524 ± 0.012 and 0.475 ± 0.041 kΩ cm² were obtained in this work. A comparison with the Rp values obtained from LPR measurements will be made at a later stage.

It has been demonstrated that EIS measurements provide both qualitative and quantitative information about the performance of the electrochemical system over time. Compared to PP and OCP with superimposed LPR measurements, EIS provides also frequency-resolved information about the corrosion inhibition mechanism, related to the presence of different time-constants, while assumingly working in the stationary regime of the electrochemical process.

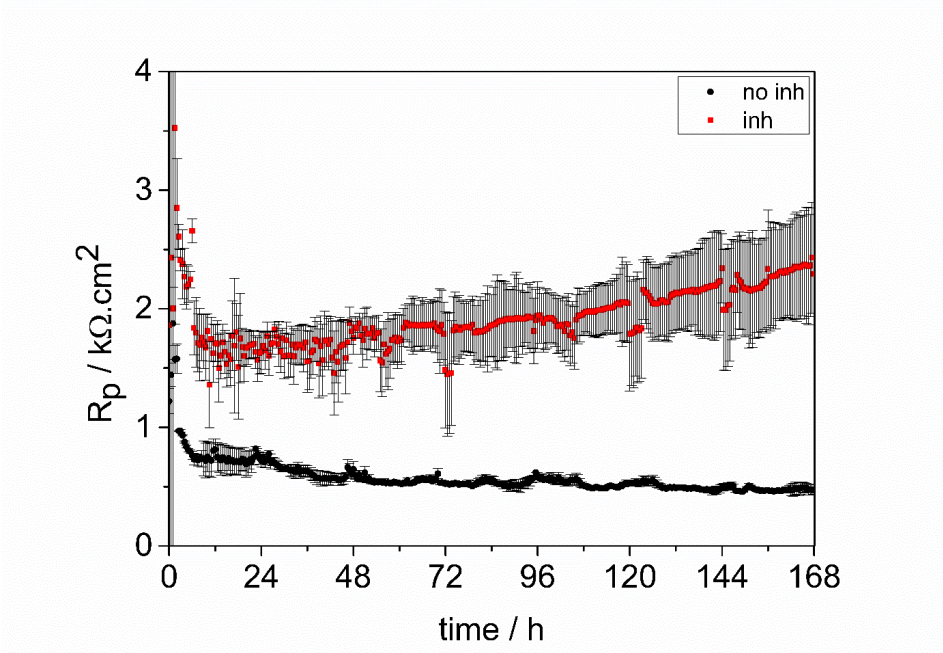

Figure 4.4 Polarization resistance (R_p) results and their standard deviation obtained from electrochemical impedance spectroscopy measurements of hot-dip galvanized steel without (0.05 M NaCl) and with corrosion inhibitor (0.5 mM Heucophos® CAPP) for 168 h.

4.3.4. Electrochemical noise measurements

EN measurements were carried out continuously for 24 hours after immersing the hot-dip galvanized steel in the electrolyte with or without corrosion inhibitor. In order to make a useful comparison with other stationary and non-stationary electrochemical techniques, the electrochemical potential (EPN) and current noise (ECN) are divided into windows of 1 hour. For each of these windows the DC drift component is removed through a discrete wavelet transform (DWT) procedure [42]. The noise resistance (Rn) is then calculated by dividing the standard deviation of the EPN by the standard deviation of the ECN according to [53]:

$$R_n = \frac{std\ (EPN)}{std\ (ECN)} \tag{4}$$

Afterwards, the Rn is normalized by the area of the working electrode, 0.28 cm² in this case. [54] This electrochemical quantity is selected because of its equivalence to the polarization resistance Rp [55]. In Figure 4.5, the Rn of the hot-dip galvanized steel with and without corrosion inhibitor in the first 24 hours after immersion is presented. The time indicated corresponds to the starting time of each respective window. It can be seen that the Rn and its standard deviation is 8.3 ± 4.3 kΩ cm² and 3.68 ± 0.53 kΩ cm² right after immersion for the system without and with corrosion inhibitors, respectively. The Rn of the hot-dip galvanized steel without corrosion inhibitors after 2 hours of immersion is 2.18 ± 0.47 kΩ cm² and remains just at around 2 kΩ cm² for the rest of the measurement. In the case of the hot-dip galvanized steel with corrosion inhibitor, the Rn increases gradually towards 5.5 ± 1.1 kΩ cm² after 10 hours of immersion before decreasing again to reach a value of 2.45 ± 0.56 kΩ cm² after 24 hours of immersion, comparable to what is obtained for the system without corrosion inhibitor.

It can be concluded that EN measurements can quantitatively describe the electrochemical system in terms of the Rn, averaged over a specific time frame. Additionally, EN measurements are able to present non-stationary information, while the previous techniques assumingly work in a stationary regime.

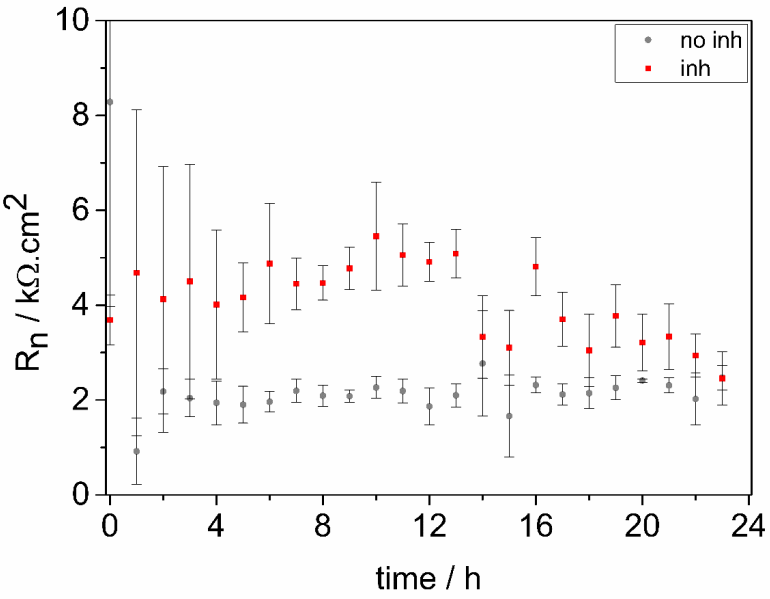

Figure 4.5 Noise resistance (R_n) results and their standard deviation obtained from electrochemical noise measurements of hot-dip galvanized steel without (0.05 M NaCl) and with corrosion inhibitor (0.5 mM Heucophos® CAPP) in the first 24 h after immersion.

4.3.5. Odd Random Phase electrochemical impedance spectroscopy measurements

4.3.5.1. Qualitative interpretation of ORP-EIS noise distortions

In order to examine the evolution of the system towards a 'stable' electrochemical system, i.e. meeting the three requirements needed for a valid EIS spectrum [20], both hot-dip galvanized steel with and without corrosion inhibitor were intensively monitored (a measurement was performed every 15 minutes) for 24 hours after immersion in the electrolyte. In Figure 4.6, the ORP-EIS results of the hot-dip galvanized steel after 15 min, 1 h, 2 h, 5 h, 8 h and 10 h in 0.05 M NaCl are presented. The black line and the grey line represent the magnitude of the impedance modulus, labelled as 'experiment', and the phase angle, respectively. The characteristics of the ORP-EIS data are presented by the curves

representing the noise, the noise plus the non-linearities (NL) and the noise plus the non-stationarities (NS). The ORP-EIS data interpretation can be described in the following way: in order to have a fully linear system, the noise curve and the noise + non-linearities curve have to overlap, indicated by an equal amount of points above and under the noise curve; in order to have a fully time-invariant system, the noise and noise + non-stationarities curve have to overlap [25][31].

For the hot-dip galvanized steel after 15 min in the reference electrolyte (Fig. 4.6a), neither the noise + non-linearities nor the noise + non-stationarities overlaps the noise curve. This indicates the presence of non-linearities and non-stationarities in the system. After 1 hour of immersion (Fig. 4.6b), the noise + non-linearities curve overlaps with the noise curve, suggesting the system has evolved towards a linear system. Nevertheless, the noise + non-stationarities curve does not overlap with the noise curve in the middle and higher frequency regions (100 – 103 Hz), meaning that the overall system is still behaving in a non-stationary way because the electrochemical processes with characteristic time-constants corresponding to the middle and high frequency regions are still 'unstable'. After 2 hours of immersion (Fig. 4.6c), the noise + non-stationarities curve overlaps the noise curve in the low frequency (10-2 – 100 Hz) and high frequency (102 – 2·103 Hz) regions indicating that the electrochemical processes with corresponding time-constants are behaving stable. However, the noise + non-stationarities curve is not overlapping the noise curve in the middle frequency region (100 – 102 Hz). After 5 hours of immersion (Fig. 4.6d), the noise + non-stationarities curve approaches the noise curve in the middle frequency region, almost fulfilling the condition of time-invariance. After 8 hours of immersion (Fig. 4.6e), the noise + non-stationarities curve also overlaps the middle frequency region from 101 – 102 Hz, but in the middle frequency region from 100 – 100 Hz the noise + non-stationarities curve is not completely overlapping the noise curve yet. After 10 hours of immersion (Fig. 4.6f) the noise + non-stationarities curve overlaps completely with the noise curve and the system is behaving fully linearly and stationary.

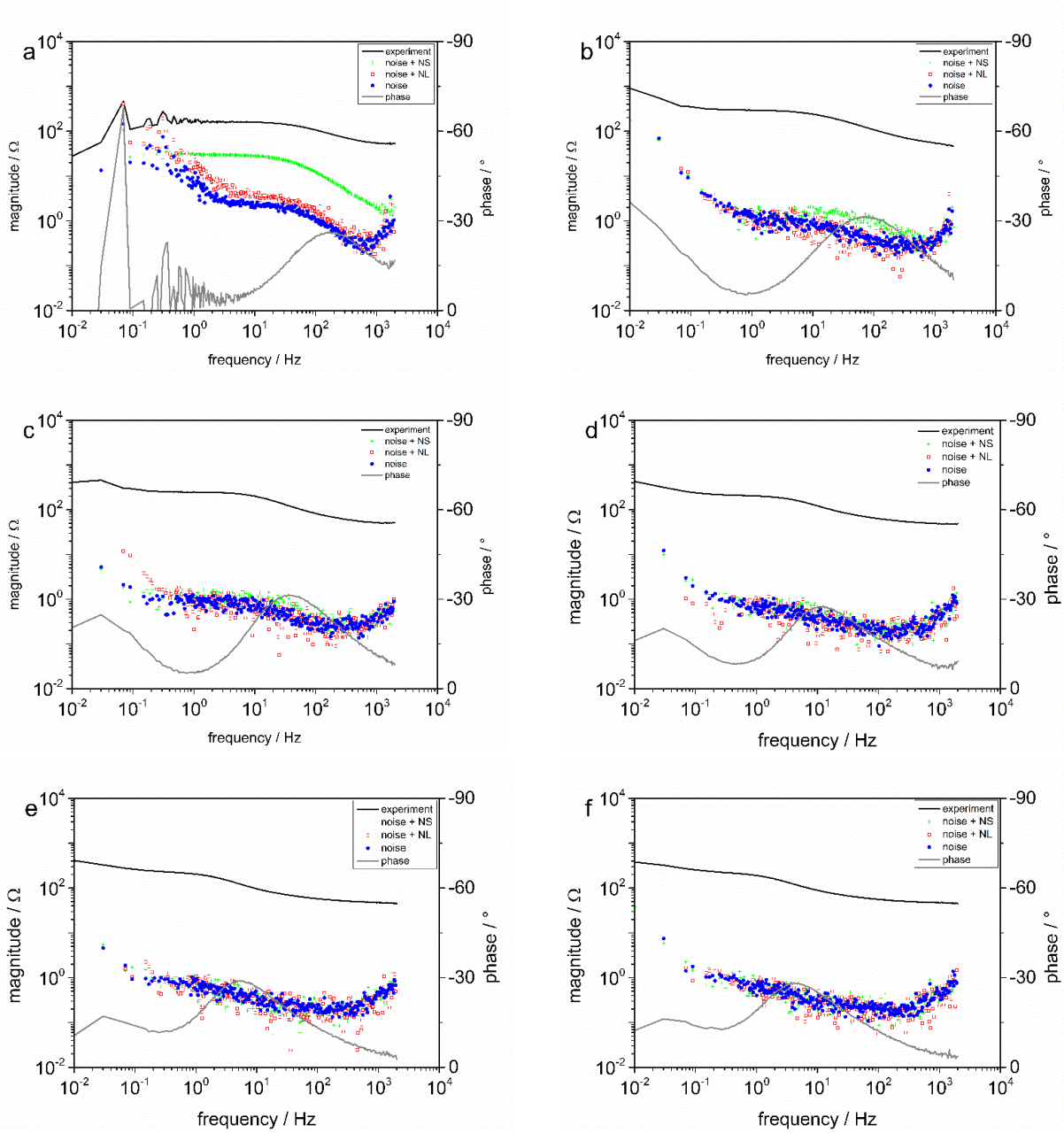

Figure 4.6 Bode plots of hot-dip galvanized steel without corrosion inhibitor after 15 min **(a)**, 1 h **(b)**, 2 h **(c)**, 5 h **(d)**, 8 h **(e)** and 10 h **(f)** in 0.05 M NaCl with the experimental impedance and noise distortion curves.

Comparison of the situation after 1.5 hours from EIS (Fig. 4.3a and Fig. 4.3c) with the situation after 1 hour and 2 hours from ORP-EIS (Fig. 4.6b and Fig. 4.6c) shows good agreement in the phase angle plots in terms of the number of time-constants and the shape and position of the respective time-constants. The same goes for the magnitude of the impedance modulus plots apart from the low-frequency behavior, however, difficult to observe because of the log-log scale. This can be explained as follow: any discrepancies between the values from point to point observed from EIS and ORP-EIS in the magnitude of the impedance modulus need to be interpreted taking into account the contribution of the noise, the non-linearities and non-stationarities on these points [25]. The contribution of these noise distortions are correcting for any non-linear and non-stationary behavior. In this case, only the contribution of the noise and the non-stationarities has to be taken into account since it has been shown that the system without corrosion inhibitor behaves in a non-stationary way at these times.

In Figure 4.7, the Bode plots of hot-dip galvanized steel with corrosion inhibitor are presented. After 15 minutes of immersion in the electrolyte (Fig. 4.7a), neither the noise + non-linearities curve nor the noise + non-stationarities curve completely overlaps the noise curve, indicating that the system did not reach the linearity and stationarity condition yet. After 1 hour of immersion, the noise + non-linearities curve overlaps the noise curve in the high frequency region and starts overlapping the noise curve in the middle and low frequency region. The noise + non-stationarities curve does not overlap the noise curve. Overall the system is still behaving in a non-linear and non-stationary way. After 2 hours of immersion (Fig. 4.7c), the noise + non-linearities completely overlaps the noise curve, indicating that the system has fulfilled the linearity condition. At the same time, the noise + non-stationarities curve starts approaching the noise curve in the high frequency (102 – 2·103 Hz) region but not yet in the low frequency (10-2 – 100 Hz) and middle frequency (100 – 102 Hz) regions. After 3 hours of immersion (Fig. 4.7d), the noise + non-stationarities further approaches the noise curve over the entire frequency range, almost fulfilling the stationarity condition. After 5 hours of immersion (Fig. 4.7e), the noise + non-stationarities completely overlaps the noise curve in the low frequency (10-2 – 100 Hz) and high frequency (102 – 2·103 Hz) regions, indicating that the electrochemical processes with characteristic time-constants corresponding to the low and high frequency region are stable and that, equivalently, the electrochemical processes with characteristic time-constants corresponding to the middle frequency region are 'unstable' and cause the overall system's instability. After 6.5 hours of immersion (Fig. 4.7f), both the noise + non-linearities curve and the noise + non-stationarities curve overlap the noise curve, meaning that the system behaves in a fully linear and stationary way.

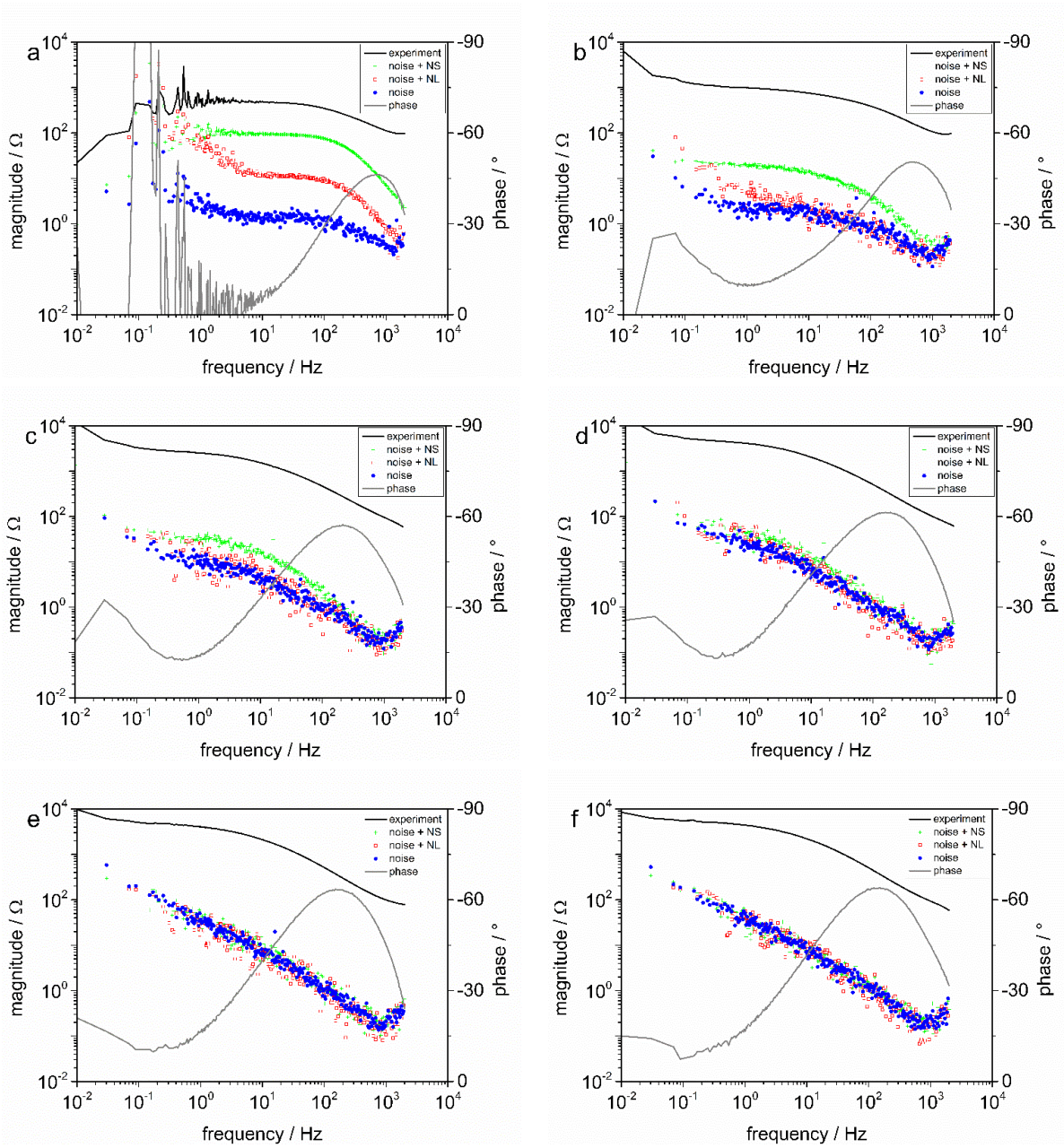

Figure 4.7 Bode plots of hot-dip galvanized steel with 0.5 mM Heucophos® CAPP corrosion inhibitor after 15 min **(a)**, 1 h **(b)**, 2 h **(c)**, 3 h **(d)**, 5 h **(e)** and 6.5 h **(f)** with the experimental impedance and noise distortion curves.

Similarly to the system without corrosion inhibitor, a comparison between the results from EIS after 1.5 hours (Fig. 4.3b and Fig. 4.3d) and ORP-EIS after 1 hour and 2 hours (Fig. 4.7b and Fig. 4.7c) can be made for the system with corrosion inhibitor. Here again, the phase angle plots show good agreement in terms of the number of time-constants and the shape and position of these time-constants and apart from the low frequency region, also the magnitude of the bode impedance plots show good agreement. These discrepancies can again be explained by the presence of non-stationarities.

This qualitative interpretation signifies that for the system without and with corrosion inhibitor, it takes 10 hours and 6.5 hours respectively, to reach a stationary behavior and to fulfil the time-invariance condition. These periods of time correspond to the duration to reach a stable electrochemical process and designate the time the system needs to stabilize enabling a reliable EIS measurement to be obtained. The frequency dependent non-stationary behavior requires further investigation in terms of a quantitative interpretation of the non-linear and non-stationary noise distortions.

4.3.5.2 Quantitative interpretation of ORP-EIS noise data

The qualitative interpretation of the ORP-EIS noise distortions data for the hot-dip galvanized steel with and without corrosion inhibitor presents an idea of the 'stabilization time' the respective system requires to meet the requirements of linearity and time-invariance. However, in order to draw a parallel between the morphological changes, the stability of electrochemical processes and the parameter evolution of the electrochemical parameters describing the electrochemical processes, the ORP-EIS information concerning the noise, non-linearities and non-stationarities present in the system is quantified [25].

By numerical integration through interpolation over the frequency domain using the trapezoidal rule, and subtraction of the noise curve from the noise + non-linearities curve and noise + non-stationarities curve, the individual contributions of the noise, non-linearities and non-stationarities were calculated [56]. Expressing this information relative to the magnitude of the impedance modulus (N/|Z|; NL/|Z|; NS/|Z|), also quantified by a numerical integration through interpolation, yields the relative contribution of the noise, non-stationarities and non-linearities as a function of immersion time. In Figure 4.8, the curves representing the relative contribution of the noise, non-linearities and non-stationarities as

a function of immersion time are presented for hot-dip galvanized steel with and without corrosion inhibitor.

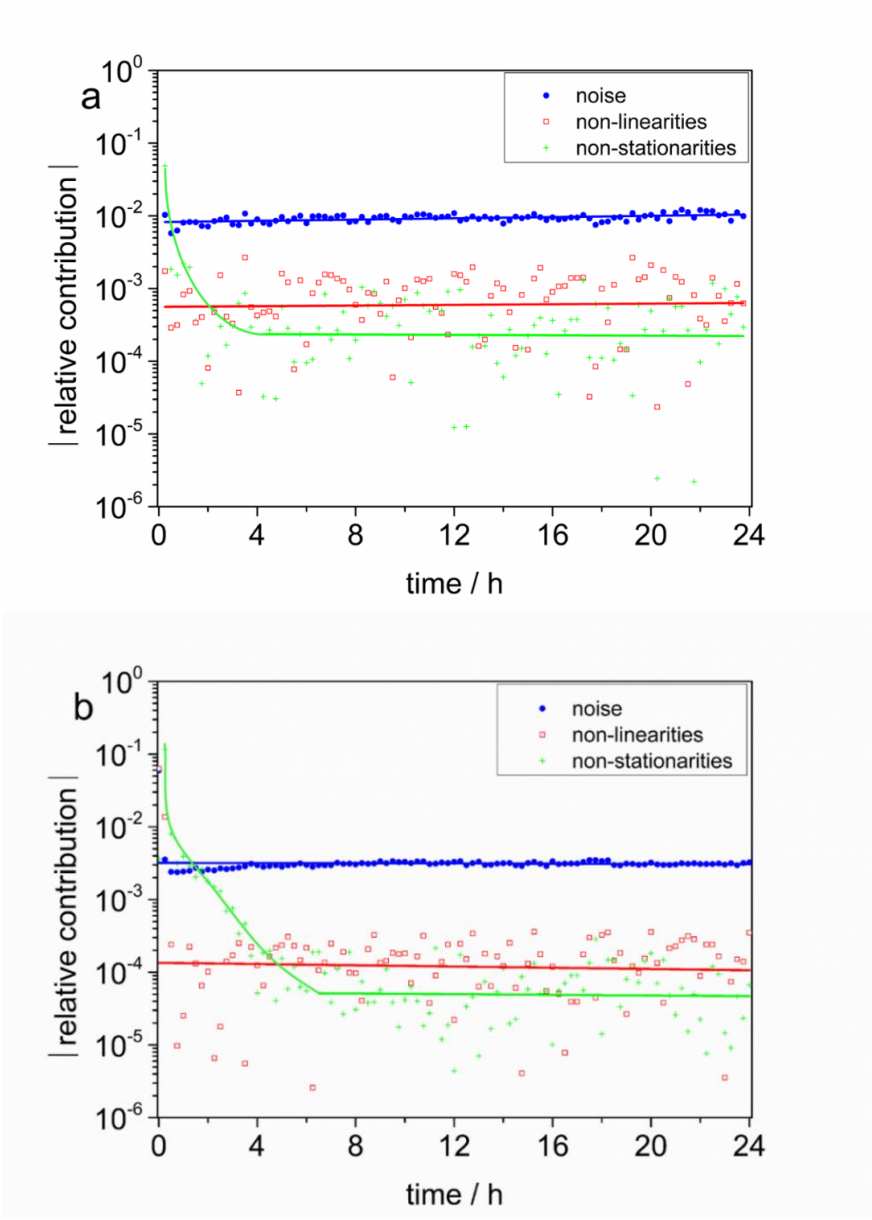

Figure 4.8 Evolution of the contribution of the noise, non-linearities and non-stationarities relative to the impedance modulus for hot-dip galvanized steel **(a)** without corrosion inhibitor (0.05 M NaCl) and **(b)** with corrosion inhibitor (0.5 mM Heucophos® CAPP) for the first 24 h of immersion, respectively. The blue, red and green line represent the trend line of the noise, non-linearities and non-stationarities, respectively.

For the hot-dip galvanized steel without corrosion inhibitors (Fig. 4.8a), it can be noticed that the non-stationarities have the highest relative contribution of the three right at the start after immersion in the electrolyte, with a relative contribution only more than one order of magnitude lower than the magnitude of the impedance modulus, corresponding to 4.89 %. The contribution of the noise is two orders of magnitude lower compared to the magnitude of the impedance modulus, corresponding to 1.03 %, and the contribution of the non-linearities more than two orders, accounting for only 0.17 %.

In the following hours, the contribution of the non-stationarities decreases over time. The relative contribution of the noise and the non-linearities remains equal over the course of the measurement. The contribution of the non-stationarities decreases strongly in the first hour, reaching a relative contribution of 3·10-4 or less (Fig. 4.8a). Afterwards, the relative contribution of the non-stationarities keeps decreasing and after 2 h, the contribution reaches a stable value of approximately 2·10-4. This contribution remains stable for the rest of the measurement time.

It needs to be noted that this does not correspond completely with what was observed during the qualitative interpretation at longer times where a non-stationary behaviour in the mid frequency regions was observed for 8 up to 10 hours. For that reason, and to examine the contribution of the different electrochemical processes to the overall system instability, the data regarding the non-stationarities was also quantified per frequency decade [25]. Therefore, the impedance data were divided into 6 frequency decades. The first frequency decade, ranging from 10 mHz to 100 mHz, and the last frequency decade, ranging from 1kHz to 10 kHz, were not taken into account because the former only contains three data points and the latter comprises only data of one tenth of the frequency decade. The relative contributions (NS/|Z|) are calculated for each frequency decade and presented in Figure 4.9.

It can be observed that the contribution of the non-stationarities (Fig. 4.9a) decreases for every frequency decade with time. For the lowest and highest frequency decades (II and V), ranging from 10-1 Hz to 100 Hz and from 102 Hz to 103 Hz, respectively, the contribution decreases more rapidly and stabilizes after 2 hours. For the middle frequency decades (III and IV), ranging from 100 Hz to 101 Hz and from 101 Hz to 102 Hz, respectively ,the contribution decreases more slowly and stabilizes only after 10 hours and 8 hours, respectively. Therefore the system needs to be considered as a non-stationary system for the first 10 hours.

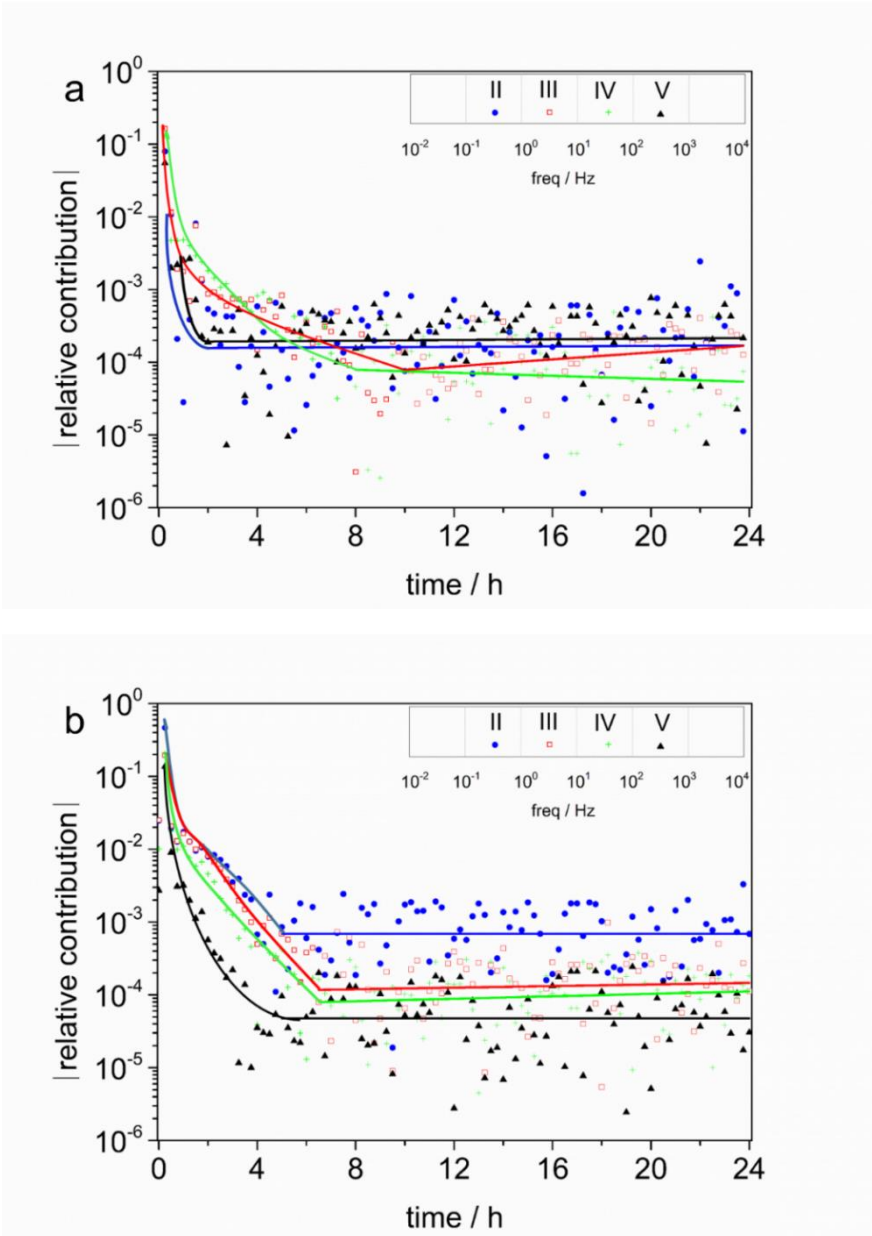

Figure 4.9 Evolution of the relative contribution of the non-stationarities for the different frequency decades for hot-dip galvanized steel **(a)** without corrosion inhibitor (0.05 M NaCl) and **(b)** with corrosion inhibitor (0.5 mM Heucophos® CAPP) for the first 24 h of immersion, respectively. The blue, red, green and black lines represent the trend line of the non-stationarities in the respective frequency decades.

It needs to be remarked that the non-stationarities observed in the qualitative interpretation were not reflected in the overall quantitative interpretation but only in the quantitative interpretation per decade. Consequently, when studying the evolution of an electrochemical system, and in particular the stabilization of different electrochemical processes with different characteristic time-constants, it is important to consider the quantitative interpretation per frequency decade.

For the hot-dip galvanized steel with corrosion inhibitor, it can be observed from the quantitative interpretation (Fig. 4.8b) that the relative contribution of the noise and non-linearities are the highest right after the start of immersion, only 1 order of magnitude lower compared to the magnitude of the impedance modulus, corresponding to 6.02 % and 6.30 %, respectively. All three contributions decrease over time. The relative contribution of the noise decreases to 3·10-3 after 30 minutes of immersion and remains stable for the rest of the measurement. The contribution of the non-linearities decreases rapidly in the first 30 minutes and reaches a value of 3·10-4 or less which remains the same for the rest of the measurement. The contribution of the non-stationarities decreases more gradually. After 1 hour of immersion, the relative contribution is around 4·10-3, after 2 hours around 2·10-3 and after 3 hours around 8·10-4. Only after 6.5 hours, the relative contribution of the non-stationarities stabilizes around 2·10-4 or less, indicating a fully stationary electrochemical system.

Similarly to the hot-dip galvanized steel without corrosion inhibitor, the same quantification per decade was carried out for the system with corrosion inhibitor. From the quantification of the non-stationarities per decade (Fig. 4.9b), it can be seen that the contribution of the non-stationarities decreases with time for all frequency decades.

The relative contribution the non-stationarities of the lowest (II) and highest (V) frequency decades decrease more rapidly and reach a stable value after 5 hours. The relative contribution of the non-stationarities of the middle frequency (III and IV) region decrease more slowly and stabilize after 6.5 hours of immersion. This trend is in good agreement with what was observed earlier in a qualitative and quantitative way, with a higher non-stationary behaviour in the mid frequency region. This indicates that the electrochemical processes with characteristic time-constants corresponding to the mid frequency region take the longest time to stabilize and dominate the overall instability of the electrochemical system.

Here it can be concluded that the qualitative behaviour of the non-stationarities is reflected in both the overall quantitative interpretation and the quantitative interpretation per decade. Moreover, it can be concluded that ORP-EIS measurements are able to detect and

quantify stationary and non-stationary behaviour of electrochemical processes and consequently describe the stability of an electrochemical system over time.

4.3.6. Overview of the electrochemical results after 1.5 hours and 24 hours

The objective of this work was to compare the results obtained from different macroscopic electrochemical techniques. Before discussing the overall behaviour over time, we can discuss the results obtained after 1.5 hours and 24 hours, since a PP measurement was only performed at these two times. For comparison reasons, a LPR value after 1.5 hours is calculated as the average from the polarization resistance values after 1 and 2 hours, respectively, and the noise resistance of the noise measurements between 1 hour and 2 hours is selected. In Figure 4.10, the Rp obtained from LPR, EIS and EN measurements after 1.5 hours and 24 hours is presented, as well as the absolute errors in the respective resistances.

It can be seen that for the hot-dip galvanized steel after 1.5 hours (Fig. 4.10a), the Rp values obtained from LPR, EIS and EN measurements are 1.58 ± 0.12 kΩ cm², 1.57 ± 0.12 kΩ cm² and 0.92 ± 0.70 kΩ cm², respectively. For the hot-dip galvanized steel with corrosion inhibitor after 1.5 hours, the Rp values are 1.57 ± 0.90 kΩ cm², 3.5 ± 1.7 kΩ cm² and 4.7 ± 3.4 kΩ cm², respectively.

For the hot-dip galvanized steel after 24 hours (Fig. 4.10b), the Rp values obtained from LPR, EIS and EN measurements are 0.93 ± 0.11 kΩ cm², 0.720 ± 0.053 kΩ cm² and 2.47 ± 0.26 kΩ cm², respectively. In the case of hot-dip galvanized steel with corrosion inhibitor, the Rp values are 1.35 ± 0.12 kΩ cm², 1.63 ± 0.18 kΩ cm² and 2.45 ± 0.56 kΩ cm², respectively.

First of all, it needs to be remarked that the errors on the EN measurements are significantly high, especially for the measurements after 1.5 hours. For the other two electrochemical techniques, all errors are below 15 %, except for the Rp values obtained from LPR and EIS measurements after 1.5 hours, which are 57 % and 47 % respectively. It has been observed that the results after 1.5 hours suffer from non-stationary behaviour, causing an overall unstable electrochemical system after 1.5 hours, as observed from the ORP-EIS experiments. This is reflected in unstable Rp values after relatively short immersion times. For the LPR and EIS technique, which assume stationarity during measurement, this is evident. For the EN technique, which measures non-stationarity behaviour, the DWT procedure applied for DC drift removal suffers from the presence of non-stationarities. Despite the high effectiveness

of this procedure, the effect of the non-stationarities is never eliminated completely, causing the spread of the first EN measurements. Also the uncertainty related to electrode asymmetry when performing an EN measurement is worth mentioning, since this is not applicable for an LPR or EIS measurement and could led to misinterpretation of the EN data. This has already led to the conclusion that EIS provides a better estimate of the impedance than EN does [54].

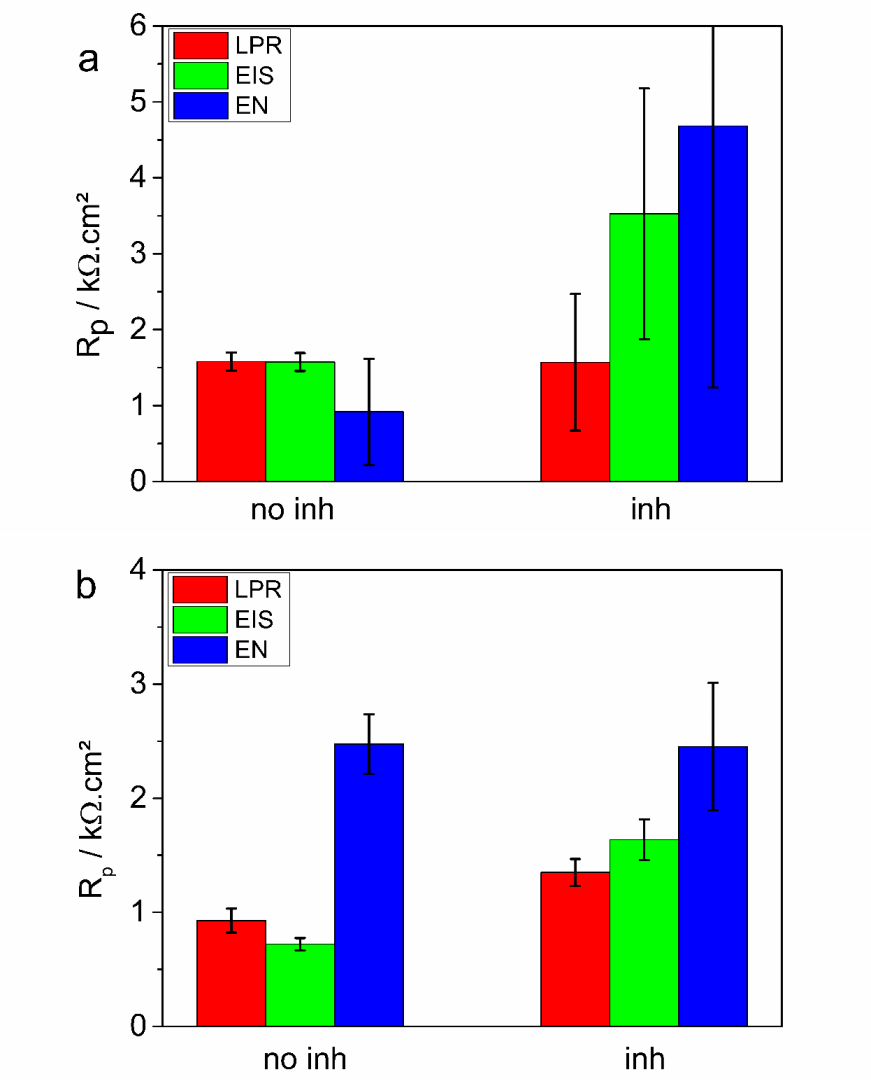

Figure 4.10 Overview of the results obtained through linear polarization resistance (LPR), electrochemical impedance spectroscopy (EIS) and electrochemical noise (EN) measurements for hot-dip galvanized steel without (0.05 M NaCl) and with corrosion inhibitor (0.5 mM Heucophos® CAPP) after **(a)** 1.5 h and **(b)** 24 h.

In general, the results obtained through LPR and EIS are more in line with each other than with the EN measurement results after similar immersion times. When interpreting the results obtained after 1.5 hours, it is important to consider that both the systems with and without corrosion inhibitor were still behaving in a non-stationary fashion. As a result, the basic conditions necessary for successful application of the EIS technique are not fulfilled, which is reflected in the large scatter of values.

In the case of EN measurements and the calculation of the noise resistance as a function of time, it needs to be remarked that the system is not polarized and as such the spontaneous corrosion process is measured. Any non-stationarity behaviour in the corrosion process will manifest itself as DC drift in the EN signal, which has a large influence on the determination of standard deviation and, as a result, on the noise resistance. Consequently, the accuracy of the calculated noise resistance relies heavily on the effectiveness of the applied DC drift removal procedure. Although this is interesting from a scientific point of view, the different nature of the EN technique as compared to the active electrochemical techniques investigated in this paper makes comparison with the Rp values from the other techniques rather difficult.

4.3.7. Overview of the electrochemical results over time

In Figure 4.11, the Rp values of the hot-dip galvanized steel with and without corrosion inhibitor obtained through LPR, EIS and EN measurements, together with the relative contribution of the non-stationarities from the ORP-EIS measurements over the course of 24 hours, are presented. The deviation of the Rp obtained from EN measurements compared with the other electrochemical techniques was already discussed in the previous paragraph.

It can be seen that for the hot-dip galvanized steel without corrosion inhibitor (Fig. 4.11a) the Rp values obtained from LPR and EIS measurements, measured every hour and every 30 minutes, respectively, show a similar trend over the course of the measurement. After 1 hour, the Rp values obtained from LPR and EIS are 1.65 ± 0.14 kΩ cm² and 1.87 ± 0.31 kΩ cm², respectively. Both decrease strongly in the first 10 hours, reaching a Rp value of 0.99 ± 0.12 kΩ cm² for the LPR and 0.75 ± 0.13 kΩ cm² for the EIS measurement, respectively.

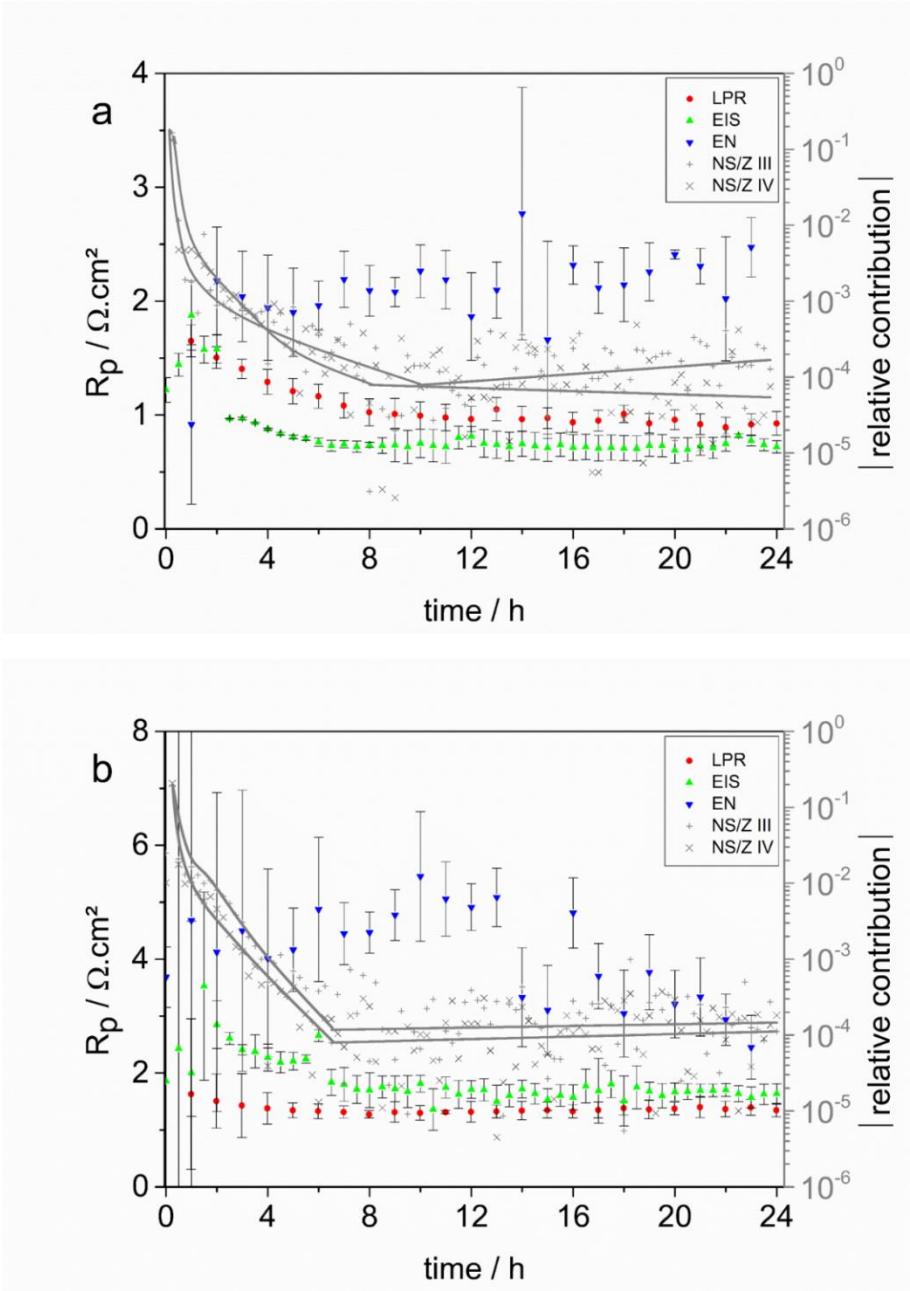

Figure 4.11 Overview of the results obtained through linear polarization resistance (LPR), electrochemical impedance spectroscopy (EIS), electrochemical noise (EN) and odd random phase electrochemical impedance spectroscopy (ORP-EIS) measurements for hot-dip galvanized steel **(a)** without corrosion inhibitor (0.05 M NaCl) and **(b)** with corrosion inhibitor (0.5 mM Heucophos® CAPP) for 24 h.

Afterwards, the Rp values remain stable. This time corresponds to the time needed until the system is fully stationary and can be considered as 'stable', as indicated by the grey lines representing the relative contribution of the non-stationarities of frequency decade III and IV. In the quantitative interpretation per decade, it has been observed that the electrochemical processes with characteristic time-constants corresponding to these frequency decades were the last to stabilize and cause the overall system instability during the first 10 hours after immersion.

After 10 hours, the electrochemical system is 'stable', since the relative contribution of the non-stationarities are minimal and remain stable for the rest of the measurement. This is reflected in the stable Rp values in the same timeframe.

In Figure 4.11b, the Rp of the hot-dip galvanized steel with corrosion inhibitor obtained through LPR, EIS and EN measurements, together with the relative contribution of the non-stationarities from the ORP-EIS measurements over the course of 24 hours, are presented.

Initially the system is behaving in a non-stationary fashion, as observed from the high relative contribution of the non-stationarities in the mid frequency (III and IV) ranges. This is reflected in the unstable Rp values obtained from EIS experiments and the high absolute errors on the Rp values obtained from both EIS and LPR experiments initially. After 2 hours of immersion, the fluctuations in the Rp values from EIS disappear, reaching a value of 2.85 ± 0.42 kΩ cm². At the same time, the Rp value from LPR reaches a value of 1.50 ± 0.47 kΩ cm². In the following hours the Rp value follow a similar trend and decrease towards a stable value of 1.32 ± 0.12 kΩ cm² in the case of LPR measurements and 1.84 ± 0.23 kΩ cm² in the case of EIS measurements after 6.5 hours of immersion. At the same time, the relative contribution of the non-stationarities in the mid frequency regions reaches a minimum, almost four order of magnitude lower compared to the magnitude of the impedance modulus. At this moment, the electrochemical system with corrosion inhibitor is behaving fully stationary. At a later stage, the electrochemical system is considered stable, reflected in stable values of Rp from both LPR and EIS measurements.

4.4. Conclusions

Comparison of the characteristic information obtained from the electrochemical techniques applied in this work makes it possible to position the electrochemical techniques in the time-domain. A distinction between three different characteristic factors of time can be made.

Firstly the measurement time, i.e. the time to perform the electrochemical measurement. Secondly the possibility to provide time-resolved information, i.e. electrochemical information in the time domain. Thirdly the possibility to provide frequency-resolved information and consequently differentiation between different electrochemical processes with different characteristic time-constants.

PP measurements provide mechanistic information of the anodic and cathodic stationary behaviour of an inhibited electrochemical system after specific periods of immersion, basically a snapshot in time. These measurements, taking approximately 10 minutes for the evaluation of a potential range of [-30,+500] or [+30,-500] mV versus the OCP at a scan rate of 1 mV/s, are time intensive if also time-resolved information on inhibitor performance is of interest.

The approach of applying LPR experiments every hour superimposed on a continuous OCP measurement provides a non-invasive and faster alternative to the PP technique, due to the small amplitude of the excitation signal (± 5 mV versus the OCP). This provides the possibility to characterize the electrochemical system in terms of the Rp over time. However, no frequency-resolved information can be obtained. Compared to the PP measurements, any mechanistic information is lost.

EIS measurements can both characterize the overall performance of the electrochemical system over time as well as provide details about the corrosion inhibition mechanism and the related time-constants. However, the presence of non-linearities and non-stationarities may cause problems in the interpretation of EIS data since fulfilment of the linearity and stationarity is assumed de facto by applying only an excitation signal with a small amplitude in the stationary regime of the electrochemical process.

Characterization of the electrochemical system through EN measurements provides non-stationarity information about the electrochemical system over time. Conversion of this information into the calculation of the Rn provides semi-quantitative information about the inhibition of the electrochemical system averaged over a certain time frame but is unsuccessful in quantitatively describing the electrochemical system at specific discrete times of exposure.

ORP-EIS measurements were applied to provide information about the time-invariance (stationarity) of inhibitor containing electrochemical processes over time. The differences in polarization resistance obtained from the other techniques after 1.5 hours of immersion can be attributed to the presence of non-stationarities and a consequently ‘unstable’ electrochemical system. In terms of stability it needs to be remarked that the addition of

corrosion inhibitors in the electrolyte stabilizes the electrochemical interface as compared to the system without corrosion inhibitors.

Comparison of all results revealed that there is a relation between the Rp values from LPR and EIS on the one hand and the relative contribution of the non-stationarities from ORP-EIS on the other hand. The presence of non-stationarities in the initial stages after immersion and the related unstable behaviour of the electrochemical processes is linked to the fluctuations and the scatter in the Rp values from LPR and EIS measurements. When the non-stationarities disappear, and the system can be considered as a stable electrochemical system, also the Rp values become stable as a function of time. However, no agreement was found with the polarization resistance values obtained from EN measurements.

References

1. Baghni, I. M., Lyon, S. B., & Ding, B. (2004). The effect of strontium and chromate ions on the inhibition of zinc. *Surface and Coatings Technology*, *185*(2–3), 194–198.
2. Sinko, J. (2001). Challenges of chromate inhibitor pigments replacement in organic coatings. *Progress in Organic Coatings*, *42*, 267–282.
3. Gharbi, O., Thomas, S., Smith, C., & Birbilis, N. (2018). Chromate replacement : what does the future hold ?. *Materials Degradation, 12*, 23–25.
4. Brett, C., & Brett, A. M. . (1993). *Electrochemistry Principles, Methods and Applications*. *Oxford university press* (Vol. 1).
5. Revie, R. W. (2008). *Corrosion and Corrosion control an introduction to corrosion science and engineering*.
6. Twite, R. L., & Bierwagen, G. P. (1998). Review of alternatives to chromate for corrosion protection of aluminum aerospace alloys, *Progress in organic coatings, 33*, 91–100.
7. Frankel, G. S. (2015). Electrochemical Techniques in Corrosion : Status , Limitations, *Journal of testing and evaluation, 42*, 1-22.
8. Pokhmurs'kyi, V. I., Zin', I. M., Layon, S. B., & Bilyi, L. M. (2003). Synergistic effect of phosphate and calcium-containing pigments on the corrosion resistance of galvanized steel. *Materials Science*, *39*(2), 153–160.
9. Zin, I. M., Lyon, S. B., & Pokhmurskii, V. I. (2003). Corrosion control of galvanized steel using a phosphate/calcium ion inhibitor mixture. *Corrosion Science*, *45*(4), 777–788.
10. Deflorian, F., Felhosi, I., Rossi, S., Fedrizzi, L., & Bonora, P. L. (2002). Performance of primers containing polyphosphate-based ion-exchange pigments for the protection of galvanised steel. *Macromolecular Symposia*, *187*, 87–96.
11. Kartsonakis, I. A., Stanciu, S. G., Matei, A. A., Hristu, R., Karantonis, A., & Charitidis, C. A. (2016). A comparative study of corrosion inhibitors on hot-dip galvanized steel. *Corrosion Science*, *112*, 289–307.
12. Hernandez-Alvarado, L. A., Hernandez, L. S., Miranda, J. M., & Dominguez, O. (2009). The protection of galvanised steel using a chromate-free organic inhibitor. *Anti-Corrosion Methods and Materials*, *56*(2), 114–120.
13. Badea, G. E., Caraban, A., Sebesan, M., Cret, P., & Setel A. (2010). Polarisation Measurements Used for Corrosion Rates Determination. *Journal of Sustenable Energy*, *1*(1), 1–4.
14. ASTM G59-97. (2014). Standard Test Method for Conducting Potentiodynamic Polarization Resistance Measurements. *ASTM*, 1-4.
15. Mansfeld, F. (2009). Fundamental aspects of the polarization resistance technique-the

early days. *Journal of Solid State Electrochemistry*, *13*(4), 515–520.

16. Hernandez-Alvarado, L. A., Hernandez, L. S., & Rodriguez-Reyna, S. L. (2012). Evaluation of corrosion behavior of galvanized steel treated with conventional conversion coatings and a chromate-free organic inhibitor. *International Journal of Corrosion*, 1–12.
17. van Westing, E. P. M., Ferrari, G. M., & de Wit, J. H. W. (1994). The determination of coating performance with impedance measurements-IV. Protective mechanisms of anticorrosion pigments. *Corrosion Science*, *36*(8), 1323–1346.
18. Zin, I. M., Howard, R. L., Badger, S. J., Scantlebury, J. D., & Lyon, S. B. (1998). The mode of action of chromate inhibitor in epoxy primer on galvanized steel, *Progress in Organic Coatings, 33*, 203–210.
19. Arundell, M., Anil, B., Yeoman, M. S., Parker, K. H., & Hare, D. O. Õ. (2004). Hilbert transform of voltammetric data, *Electrochemistry communications, 6*, 366–372.
20. Van Ingelgem, Y., Tourwé, E., Blajiev, O., Pintelon, R., & Hubin, A. (2009). Advantages of odd random phase multisine electrochemical impedance measurements. *Electroanalysis*, *21*(6), 730–739.
21. Macdonald, D. D. (1985). Application of Kramers-Kronig Transforms in the Analysis of Electrochemical Systems. *Journal of The Electrochemical Society*, *132*(10), 2316.
22. Boukamp, B. A., & Ross Macdonald, J. (1994). Alternatives to Kronig-Kramers transformation and testing, and estimation of distributions. *Solid State Ionics*, *74*(1–2), 85–101.
23. Boukamp, B. A. (1993). Practical Application of the Kramers-Kronig Transformation on Impedance Measurements in Solid-State Electrochemistry. *Solid State Ionics*, *62*(1–2), 131–141.
24. Hamlaoui, Y., Pedraza, F., & Tifouti, L. (2008). Corrosion monitoring of galvanised coatings through electrochemical impedance spectroscopy, *Corrosion Science, 50*, 1558–1566.
25. Meeusen, M., Visser, P., Fernández Macía, L., Hubin, A., Terryn, H., & Mol, J. M. C. (2018). The use of odd random phase electrochemical impedance spectroscopy to study lithium-based corrosion inhibition by active protective coatings. *Electrochimica Acta*, *278*, 363–373.
26. Cottis, R. A., Homborg, A. M., & Mol, J. M. C. (2016). The relationship between spectral and wavelet techniques for noise analysis. *Electrochimica Acta*, *202*, 277–287.
27. Homborg, A. M., Tinga, T., Zhang, X., Van Westing, E. P. M., Oonincx, P. J., Ferrari, G. M., … Mol, J. M. C. (2013). Transient analysis through Hilbert spectra of electrochemical noise signals for the identification of localized corrosion of stainless

steel. *Electrochimica Acta*, *104*, 84–93.

28. Homborg, A. M., Van Westing, E. P. M., Tinga, T., Ferrari, G. M., Zhang, X., De Wit, J. H. W., & Mol, J. M. C. (2014). Application of transient analysis using Hilbert spectra of electrochemical noise to the identification of corrosion inhibition. *Electrochimica Acta*, *116*, 355–365.
29. Homborg, A. M., Leon Morales, C. F., Tinga, T., De Wit, J. H. W., & Mol, J. M. C. (2014). Detection of microbiologically influenced corrosion by electrochemical noise transients. *Electrochimica Acta*, *136*, 223–232.
30. Breugelmans, T., Tourwé, E., Jorcin, J. B., Alvarez-Pampliega, A., Geboes, B., Terryn, H., & Hubin, A. (2010). Odd random phase multisine EIS for organic coating analysis. *Progress in Organic Coatings*, *69*(2), 215–218.
31. Fernández Macía, L., Petrova, M., Hauffman, T., Muselle, T., Doneux, T., & Hubin, A. (2014). A study of the electron transfer inhibition on a charged self-assembled monolayer modified gold electrode by odd random phase multisine electrochemical impedance spectroscopy. *Electrochimica Acta*, *140*, 266–274.
32. Fernández Macía, L., Petrova, M., & Hubin, A. (2015). ORP-EIS to study the time evolution of the $[Fe(CN)_6]^{3-}/[Fe(CN)_6]^{4-}$ reaction due to adsorption at the electrochemical interface. *Journal of Electroanalytical Chemistry*, *737*, 46–53.
33. Alvarez-Pampliega, A., Hauffman, T., Petrova, M., Breugelmans, T., Muselle, T., Van Den Bergh, K., De Strycker, J., Terryn, H., Hubin, A. (2014). Corrosion study on Al-rich metal-coated steel by odd random phase multisine electrochemical impedance spectroscopy. *Electrochimica Acta*, *124*, 165–175.
34. Hauffman, T., Breugelmans, T., Van Ingelgem, Y., Tourwé, E., Terryn, H., & Hubin, A. (2012). Measuring the adsorption of ethanol on aluminium oxides using odd random phase multisine electrochemical impedance spectroscopy. *Electrochemistry Communications*, *22*(1), 124–127.
35. Hauffman, T., Van Ingelgem, Y., Breugelmans, T., Tourwé, E., Terryn, H., & Hubin, A. (2013). Dynamic, in situ study of self-assembling organic phosphonic acid monolayers from ethanolic solutions on aluminium oxides by means of odd random phase multisine electrochemical impedance spectroscopy. *Electrochimica Acta*, *106*, 342–350.
36. Breugelmans, T., Tourwé, E., Van Ingelgem, Y., Wielant, J., Hauffman, T., Hausbrand, R., Pintelon, R., Hubin, A. (2010). Odd random phase multisine EIS as a detection method for the onset of corrosion of coated steel. *Electrochemistry Communications*, *12*(1), 2–5.
37. Ji, G., Macía, L. F., Allaert, B., Hubin, A., & Terryn, H. (2018). Odd Random Phase

Electrochemical Impedance Spectroscopy to Study the Corrosion Behavior of Hot Dip Zn and Zn-Alloy Coated Steel Wires in Sodium Chloride Solution. *Journal of The Electrochemical Society*, *165*(5), C246–C257.

38. Przywecka, K., Grzmil, B., Kowalczyk, K., & Sreńscek-Nazzal, J. (2018). Studies on preparation of phosphate pigments for application in composite protective coatings. *Progress in Organic Coatings*, *119*, 44–49.
39. Cole, T. J. (1984). Too many digits : the presentation of numerical data, *Arch Dis Child,* 100. 608-609.
40. Kordi, R. (2011). Sports Medicine Update, *Scandinavian Journal of Medicine and Science in Sports, 21*. 867–868.
41. ASTM. (1999). ASTM G3-89 Standard Practice for Conventions Applicable to Electrochemical Measurements in Corrosion Testing, ASTM, *89*, 1–10.
42. Homborg, A. M., Tinga, T., Zhang, X., Van Westing, E. P. M., Oonincx, P. J., De Wit, J. H. W., & Mol, J. M. C. (2012). Time-frequency methods for trend removal in electrochemical noise data. *Electrochimica Acta*, *70*, 199–209.
43. Homborg, A. M., Cottis, R. A., & Mol, J. M. C. (2016). An integrated approach in the time, frequency and time-frequency domain for the identification of corrosion using electrochemical noise. *Electrochimica Acta*, *222*, 627–640.
44. Van Gheem, E., Pintelon, R., Vereecken, J., Schoukens, J., Hubin, A., Verboven, P., & Blajiev, O. (2004). Electrochemical impedance spectroscopy in the presence of non-linear distortions and non-stationary behaviour Part I: Theory and validation. *Electrochimica Acta*, *49*(26), 4753–4762.
45. Buchanan, R. A., & Stansbury, E. E. (2012). *Handbook of Environmental Degradation of Materials*.
46. Ismail, K. M. (2007). Evaluation of cysteine as environmentally friendly corrosion inhibitor for copper in neutral and acidic chloride solutions. *Electrochimica Acta*, *52*(28), 7811–7819.
47. Mouanga, M., & Berçot, P. (2010). Comparison of corrosion behaviour of zinc in NaCl and in NaOH solutions; Part II: Electrochemical analyses. *Corrosion Science*, *52*(12), 3993–4000.
48. Barranco, V., Feliu, S., & Feliu, S. (2004). EIS study of the corrosion behaviour of zinc-based coatings on steel in quiescent 3% NaCl solution. Part 1: Directly exposed coatings. *Corrosion Science*, *46*(9), 2203–2220.
49. Deslouis, C. (1989). The kinetics of zinc dissolution in aerated sodium sulphate solutions. A measurement of the corrosion rate by impedance techniques. *Corrosion Science*, *29*(1), 13–30.

50. Da Silva, P. S. G., Costa, A. N. C., Mattos, O. R., Correia, A. N., & De Lima-Neto, P. (2006). Evaluation of the corrosion behavior of galvannealed steel in chloride aqueous solution and in tropical marine environment. *Journal of Applied Electrochemistry*, *36*(3), 375–383.
51. Zheludkevich, M. L., Yasakau, K. A., Bastos, A. C., Karavai, O. V., & Ferreira, M. G. S. (2007). On the application of electrochemical impedance spectroscopy to study the self-healing properties of protective coatings. *Electrochemistry Communications*, *9*(10), 2622–2628.
52. Macdonald, J. R., & Barsoukov, E. (2005). *Impedance Spectroscopy Theory , Experiment , and Applications*. *Wiley intersience* (Vol. 125). Wiley-Interscience.
53. Dong, Z., Guo, X., Zheng, J., & Xu, L. (2001). Calculation of noise resistance by use of the discrete wavelets transform. *Electrochemistry Communications*, *3*(10), 561–565.
54. Cottis, R. A. (2001). Interpretation of Electrochemical Noise Data, *Corrosion*, *57*(3), 265–285.
55. Chen, J.F., Bogaerts, W. F. (1995). The Physical meaning of noise resistance. *Corrosion Science*, *37*(11), 1839–1842.
56. Atkinson, K. E., & Wiley, J. (1978). *An introduction to numerical analysis, Second Edition*.

Chapter 5

The effect of time evolution and timing of the electrochemical data recording of corrosion inhibitor protection of hot-dip galvanized steel

This chapter is based on a submitted scientific paper:
M. Meeusen, L. Zardet, A. M. Homborg, M. Lekka, F. Andreatta, L. Fedrizzi, B. Boelen, H. Terryn and J.M.C. Mol (2019). The effect of time evolution and timing of the electrochemical data recording of corrosion inhibitors of hot-dip galvanized steel.

Abstract

In previous work, the importance of taking the time-domain into account when studying corrosion inhibitor-containing electrochemical systems was highlighted. In this work, odd random phase electrochemical impedance spectroscopy (ORP-EIS) is applied as the electrochemical tool to study the time-effect by the evaluation of the non-stationarities per frequency decade over time for the screening of different silica- and phosphate- based corrosion inhibitors for hot-dip galvanized steel and possible corrosion inhibitor synergism. This serves as the basis for the interpretation of the results obtained from different macroscopic electrochemical techniques such as potentiodynamic polarization (PP), open circuit potential (OCP) with superimposed linear polarization resistance (LPR), electrochemical impedance spectroscopy (EIS) and electrochemical noise (EN) measurements. Finally, these results are compared with a high-throughput corrosion screening method. The analysis of the time-domain shows that all systems have a system-specific 'stabilization' time which affects the interpretation of the results obtained from the macroscopic electrochemical techniques. Furthermore, these results indicate that all corrosion inhibitors tested exhibit corrosion protective action and that the combination of both silica-based corrosion inhibitors show synergistic action on hot-dip galvanized steel.

5.1. Introduction

In quest for eco-friendly corrosion inhibition of metals, the replacement of chromate corrosion inhibitors is of particular interest nowadays [1]. Rare-earth based corrosion inhibitors, vanadium compounds, lithium-based corrosion inhibitors, silica-based corrosion inhibitors and phosphate-based corrosion inhibitors present examples of categories of promising alternatives for a variety of metal substrates [1][2]. In addition, it has been stated that the replacement of chromate corrosion inhibitors will require synergistic combinations of protective chemistries, which, to date, need to be identified and characterized mainly experimentally [3].

Silicates are known to form complex colloidal structures in aqueous solutions with characteristic physicochemical properties [4]. As such, the protective properties depend highly on the pH and the salt concentration in the solution [4]. Calcium-exchanged silica or calcium ion exchange silica is a basic pigment with a high specific surface area releasing in an efficient and controlled way its inhibitive species that undergo an exchange reaction with aggressive ions (e.g. H^+ and Cl^-), reducing their availability, and leaching calcium ions at the same time. These calcium ions, together with the polysilicate ions, inhibit corrosion by the formation of protective layers on the metallic surface [5][6].

Zinc phosphates are a widely used alternative to chromates but unfortunately have inadequate inhibition performance, related to their low solubility [7][8][9]. This led to the use of second and third generation, 'modified', phosphate-based inhibitors through the modification of the cationic constituent as well as the anionic part [7][9][10]. These substances exhibit superior anticorrosion behaviour compared to zinc phosphate [7]. Polyphosphates are known to be cathodic corrosion inhibitors which require the presence of oxygen for effective functioning [4]. Modified zinc phosphate pigments, such as zinc aluminium molybdenum orthophosphate hydrate and zinc calcium strontium aluminium orthophosphate silicate hydrate, were found to have superior corrosion protective properties compared to conventional zinc phosphate pigments [2][7]. Furthermore, it has been shown that the combination of silicates and polyphosphates provides a synergistic effect on carbon steel [4].

These systems have been studied extensively with different electrochemical and surface analysis techniques. In our previous paper, we developed a strategy for the study of corrosion inhibitor-containing systems in the time-domain [11]. It was shown that an elaborated approach combining different electrochemical techniques is strictly necessary for a detailed evaluation of the behaviour of corrosion inhibitors in the time-domain.

Potentiodynamic polarization (PP) measurements provide mechanistic information on the cathodic and anodic stationary behaviour at discrete moments in time. Open circuit potential (OCP) measurements with superimposed linear polarization resistance (LPR) measurements are a faster and non-invasive alternative providing time-resolved information in terms of the polarization resistance (R_p) over immersion time in an inhibitor-containing aqueous solution. However, any mechanistic information is lost and frequency-resolved information cannot be obtained. Electrochemical impedance spectroscopy (EIS) measurements can, on top of providing overall performance information of an inhibitor-containing electrochemical system over time, also provide information about the corrosion inhibitive mechanism in the frequency domain. Nevertheless, only stationary information is obtained since time-invariance is assumed de facto in the technique execution and analysis. Electrochemical noise (EN) measurements, however, can provide non-stationary information in terms of the instantaneous electrochemical current noise (ECN) and electrochemical potential noise (EPN) over time but are insufficient in quantitatively describing the system at specific discrete times of exposure in terms of the noise resistance (R_n). The application of odd random phase electrochemical impedance spectroscopy (ORP-EIS) measurements is strictly necessary to study the time-invariance behaviour of corrosion inhibitor-containing electrochemical systems and evaluate the trustworthiness of the quantitative results obtained from the previously discussed electrochemical techniques. The presence of non-stationarities in the initial stages after immersion is translated in unstable R_p values with significant standard deviation obtained from LPR and EIS. As soon as the corrosion inhibitor-containing system reaches a stationary state, also the R_p values become stable as a function of time. In this paper, this methodology is now applied to study the protection performance of different silica- and phosphate- based corrosion inhibitors and corrosion inhibitor synergy for hot-dip galvanized steel and compared with a high-throughput corrosion screening technique.

5.2. Experimental details

5.2.1 Materials and sample preparation

Hot-dip galvanized steel samples were obtained from Tata Steel, IJmuiden The Netherlands, with an average coating mass of 275 g·m^{-2} and a nominal composition of the steel substrate and the galvanized coating as presented in Table 5.1. For all electrochemical techniques, except the high-throughput corrosion testing, the hot-dip galvanized steel samples were

then cut to 50 by 30 mm. On these samples, a circular exposed area of 2.01 cm² is used for PP, LPR, EIS and ORP-EIS and of 0.28 cm² for EN measurements. All results presented are surface area corrected. The hot-dip galvanized steel samples were then alkaline cleaned according to ASTM D 6386-99 [12]. Firstly, the samples are cleaned with acetone in the ultrasonic bath for 5 minutes. Secondly, the samples are immersed in a 1 M NaOH solution, adjusted to pH 12 with H3PO4, for 30 seconds. Finally, the samples are rinsed with distilled water and dried.

Table 5.1 Nominal composition of the hot-dip galvanized steel substrate and the galvanized coating.

steel substrate (ppm)	**C**	**Mn**	**Si**	**Al**	**N**	**P**	**S**	**V**	**Ti**	**Cu**	**Sn**
	440	2120	120	460	27	70	70	10	20	150	20
	Cr	**Ni**	**Mo**	**Ca**							
	150	210	20	33							
coating (wt%)	**Al**	**Fe**	**Mg**	**Zn**							
	0.36	0.25	0	rest							

5 Commercially available corrosion inhibitors were selected to perform this study. The first corrosion inhibitor, Novinox®ACE110, is a new generation of modified silica as an alternative to strontium chromate and acquired from SNCZ anticorrosion. The second one, Novinox®XCA02, a calcium exchanged silica, is also acquired from SNCZ anticorrosion. The third corrosion inhibitor, Halox®SW-111, is a strontium phosphosilicate from ICL performance products. The fourth and fifth corrosion inhibitor, Heucophos®CAPP and Zinc Phosphate ZP10, respectively, are a calcium aluminium polyphosphate silicate hydrate and a zinc orthophosphate hydrate provided by Heubach. A 0.05 M NaCl solution was used as a reference for all measurements, relevant for building and construction steel applications. Furthermore, this salt concentration is preferred for future local electrochemical experiments. Based on this reference solution, different corrosion inhibitor-containing solutions were prepared.

X-ray Fluorescence (XRF) analysis was carried out to determine the molar mass of the corrosion inhibitors to make corrosion inhibitor solutions with different molarity and to identify the characteristic elements present in the corrosion inhibitor powders. The measurements on the pressed powders were performed with a Panalytical Axios Max WD-XRF spectrometer and the data evaluation was done with SuperQ5.0i/Omnian software. The main composition of the tested corrosion inhibitors as analysed by XRF is presented in Table

5.2. XRF analysis on corrosion inhibitor 1 (Novinox®ACE110) revealed mainly silica (88.42 wt%) and phosphorous pentoxide (P2O5, 7.12 wt%). Inhibitor 2 (Novinox®XCA02) comprises next to silica (94.06 wt%) also calcium oxide (CaO, 5.40 wt%). Inhibitor 3 (Halox®SW-111) consists primarily of silica (43.74 wt%), calcium oxide (36.08 wt%) and phosphorous pentoxide (12.49 wt%). Inhibitor 4 (Heucophos®CAPP) incorporated silica (34.46 wt%), phosphorous pentoxide (29.40 wt%), calcium oxide (25.89 wt%) and alumina (Al2O3, 8.83 wt%) as main components. Inhibitor 5 Zinc (Zinc Phosphate ZP 10) is made up of mainly zinc oxide (ZnO, 60.66 wt%) and phosphorous pentoxide (38.58 wt%) with small traces of silicon (as silica) as characteristic element present.

Table 5.2 Main composition of the 5 commercially available corrosion inhibitors tested as determined by XRF.

Inh #	**Tradename**	**Chemical name**	**SiO_2 (wt%)**	**P_2O_5 (wt%)**	**CaO (wt%)**	**Al_2O_3 (wt%)**	**ZnO (wt%)**	**Other (w%)**
1	Novinox®ACE110	Modified silica	88.42	7.12				4.46
2	Novinox®XCA02	Calcium exchanged silica	94.06		5.40			0.54
3	Halox®SW-111	Strontium phosphosilicate	43.74	12.49	36.08			7.69
4	Heucophos®CAPP	Calcium aluminum polyphosphate silicate hydrate	34.46	29.40	25.89	8.83		1.42
5	Zinc Phosphate ZP10	Zinc orthophosphate hydrate		38.58			60.66	0.76

5.2.2 Odd-random phase electrochemical impedance spectroscopy

A typical three electrode set-up, consisting of a Ag/AgCl 3 M KCl reference electrode, a stainless steel grid as the counter electrode and the hot-dip galvanized steel sample as the working electrode, placed in a Faraday cage, was used for the ORP-EIS experiments. Measurements were recorded immediately after immersion in solution with and without corrosion inhibitors every 15 minutes for 24 hours. For each system, without or with corrosion inhibitors, the measurement was at least repeated once for reproducibility reasons.

The ORP-EIS experiments were performed with a Matlab controlled set-up consisting of a SP-200 potentiostat from Bio-Logic Science Instruments and a National Instruments PCI-6110 DAQ card. The frequency range was set from 10-2 Hz to 2·103 Hz. The amplitude of the excitation signal was set to 3 mV (2.12 mV root mean square (RMS)) in the case of the hot-dip galvanized steel without corrosion inhibitors and 5 mV (3.54 mV RMS) in the case of hot-dip galvanized steel with corrosion inhibitors, versus the OCP, in order to have a good signal-to-noise ratio and keeping the non-linearities confined meanwhile. The Matlab software to build the odd random phase multisine excitation signal and record the measurements was developed at the Vrije Universiteit Brussel. An in-depth description of this technique can be found elsewhere [13][14].

In order to take the time-effect into account and study the evolution of each respective system towards a 'stable' electrochemical system, i.e. fulfilling the causality, linearity and stationarity condition, hot-dip galvanized steel was intensively monitored with ORP-EIS for 24 hours after immersion in each of the corrosion inhibitor-containing solutions. ORP-EIS measurements on hot-dip galvanized steel without corrosion inhibitor were carried out as a reference. Each electrochemical system is discussed separately. In our previous work, we have shown that it is necessary to quantify the ORP-EIS data per frequency decade in order to precisely study the evolution of a corrosion-inhibitor containing system towards stability and correlate this to the (in)stability of different electrochemical processes with different characteristic time-constants [11]. The rigorous approach how the quantitative interpretation per frequency decade was obtained from the qualitative and overall quantitative information can be found in Appendix A.

The impedance data, ranging from 10-2 Hz to 2·103 Hz, is first divided into 6 frequency decades. Nevertheless, the highest (103 - 2·103 Hz) and lowest (10-2 – 10-1 Hz) frequency decade are not taken into account during interpretation because the former only comprises one tenth of a frequency decade and the latter only contains three data points. The

information is then quantified by a numerical integration through interpolation procedure using the trapezoidal rule and subtracting the noise curve form the noise + nonlinearities and noise + non-stationarities curve, respectively. The resulting individual contributions of the noise, non-linearities and non-stationarities per frequency are then expressed relative to the magnitude of the impedance modulus, which is also quantified through a numerical integration [15].

5.2.3 Potentiodynamic polarization

A typical three electrode set-up, consisting of an Ag/AgCl 3 M KCl reference electrode, a stainless steel grit as the counter electrode and the hot-dip galvanized steel as the working electrode was used for the PP measurements.

PP curves were acquired after 1.5 hours, after stabilization of the OCP, and after 24 hours by measuring the cathodic and anodic branch separately on different hot-dip galvanized steel samples and for at least three times per system without or with corrosion inhibitor. The cathodic and anodic branch were measured from +30 mV to -500 mV and -30 mV to +500 mV relative to the OCP, respectively, ensuring a small overlap between both branches around the OCP. A scan rate of 1 mV/s was applied and a measurement point was taken every 0.2 s. The corrosion potential (Ecorr) and the corrosion current density (icorr) were determined using the Tafel extrapolation procedure. The former was then compared versus the OCP value to evaluate the quality of the extrapolation. The latter was used to calculate the inhibitor efficiency η (%) and the polarization resistance Rp (kΩ cm^2) later on. Throughout this work, all results are rounded according to the two-digits rule: the standard deviation is rounded to two significant digits first, and the mean is then rounded to the same number of decimal places as the standard deviation [16][17].

5.2.4 Open Circuit Potential with superimposed Linear Polarization Resistance

A typical three electrode set-up, consisting of an Ag/AgCl 3 M KCl reference electrode, a stainless steel grid as the counter electrode and the hot-dip galvanized steel as the working electrode were used for the OCP with superimposed LPR experiments.

The OCP is monitored continuously for 168 hours, while on top performing a superimposed LPR measurements every hour with an amplitude of ± 5 mV versus the OCP with a scan rate of 0.1667 mV/s on at least three samples without or with corrosion inhibitor. The Rp was calculated from the slope from the potential versus current graph at the corrosion potential (Ecorr) as described in ASTM G3-89 [18]. Based on this, and using the anodic and cathodic Tafel slopes (βa and βc) obtained from PP experiments, the corrosion current density (icorr) was calculated [19].

5.2.5 Electrochemical Impedance Spectroscopy

A typical three electrode set-up, consisting of a Ag/AgCl 3 M KCl reference electrode, a stainless steel grid as the counter electrode an the hot-dip galvanized steel as the working electrode, place in a Faraday cage, was used for the EIS experiments.

The EIS measurements were performed with a VMP-300 multichannel potentiostat from Bio-Logic Science Instruments in a frequency range from 105 Hz to 10-2 Hz, with 7 points per decade on at least three samples per system without or with corrosion inhibitors. The amplitude of the excitation signal was set to 10 mV versus the OCP. An EIS measurement was carried out every 30 minutes, for a total duration of 168 hours.

5.2.6 Electrochemical Noise

A conventional three electrode set-up with two identical hot-dip galvanized steel working electrodes placed on equal distance on either side of a Ag/AgCl 3 M KCl reference electrode, under open-circuit conditions, was used for the EN experiments. To avoid electromagnetic disturbance form external source, the electrochemical set-up was placed in a Faraday cage.

EPN and ECN signals were recorded with a Compactstat potentiostat from Ivium Technologies working as potentiometer and zero resistance ammeter (ZRA) on at least three samples per system without or with corrosion inhibitor. The sampling frequency was set to 20 Hz and a low-pass filter of 10 Hz, the Nyquist frequency at this sampling rate, was applied during data recording. The measurement range of the potentiometer was set at 40 mV after removal of the initial DC drift component. The minimum and maximum ranges of the ZRA were automatically selected during the experiments, depending on the dynamic range of the ECN signal locally, with a lower limit of 1 nA and an upper limit of 100 µA. The data were processed using Matlab from Mathworks [20][21][22].

5.2.7 High-Throughput corrosion testing

The same procedure that was previously developed and demonstrated for aluminium alloy 2024-T3 was applied for hot-dip galvanized steel [23]. Hot-dip galvanized steel sheet was cut into lengths of 100 mm x 75 mm and placed into the experimental setup with a grid of 8 x 11 holes of 6 mm diameter. In this setup, the hot-dip galvanized steel could be exposed to 11 different solutions which could each be applied 8 times. The exposure time for the experiment was either 5 or 24 hours. Afterwards, the exposed hot-dip galvanized steel plate was removed from the setup, washed with deionized water and left to dry for 12 hours in a desiccator containing self-indicating silica gel at room temperature before imaging. Two images were taken in different lighting conditions: one diffuse box image to enhance white coloured corrosion products and one side lighting image to enhance black coloured corrosion products. These images are then processed with Adobe Photoshop, generating a final image from the side lighting image and the diffuse box image and a masked image. These two images are then processed by analysing the average brightness of the pixels in the corrosion circle compared to the average brightness of the background pixels and ranked from 0 to 100 and later on scaled from 0 to 10, i.e. the corrosion value, describing the degree of corrosion attack.

Since the corrosion products of hot-dip galvanized steel have different colour characteristics compared to the corrosion products of aluminium alloys, the analysis procedure developed for AA2024-T3 cannot be used as such [23]. Therefore measurements with different concentrations of sodium chloride, ranging from 0.000005 wt% NaCl to 0.5 wt% NaCl, with demineralized water (as a non-corrosive electrolyte) and without solution (unexposed sample) have been carried out to calibrate the procedure for hot-dip galvanized steel products after 5 and 24 hours.

5.3. Results and discussion

5.3.1. Odd-random phase EIS

The relative contribution of the noise, non-linearities and non-stationarities per frequency decade as a function of immersion time is shown in Figure 5.1.

5.3.1.1 Hot-dip galvanized steel without corrosion inhibitors

From the quantitative interpretation per decade for the system without corrosion inhibitors (Fig. 5.1a), it can be observed that the contribution of the non-stationarities for all frequency decades decreases with time, although the decrease for the highest and lowest frequency decades (V and II) is more rapidly as compared to the middle frequency decades (IV and III). The former stabilize after 2 hours while the latter stabilize only after 8 and 10 hours. Consequently the system needs to be considered as non-stationary in the first 10 hours after immersion.

5.3.1.2 Hot-dip galvanized steel with corrosion inhibitor 1

From the quantitative analysis per frequency decade (Fig. 5.1b), it can be seen that the contribution of the higher frequency decades decreases more rapidly than the contribution of the middle and lower frequency decades, i.e. frequency decade V reaches a stable value after 7 hours, while frequency decades IV and III only reach a stable value after 10 and 11 hours and decade II only after 12 hours. This implicates that the electrochemical processes with characteristic time-constants corresponding to the middle and lower frequency region cause the overall system instability, meaning that the corrosion inhibitor protective action and the corrosion activity are causing the instability in the case of inhibitor 1.

5.3.1.3 Hot-dip galvanized steel with corrosion inhibitor 2

From the quantitative interpretation per frequency decade (Fig. 5.1c) for the system containing corrosion inhibitor 2, it can be seen that all frequency decades decrease rapidly with time, reaching a stable value after 2, 4 and 6 hours in the case of the high frequency decade (V), middle frequency decades (IV and III) and low frequency decades (II), respectively. This implies that the electrochemical processes related to the corrosion inhibitor protective action stabilize before the corrosion activity, i.e. the charge transfer reaction, stabilizes.

5.3.1.4 Hot-dip galvanized steel with corrosion inhibitor 3

From this quantitative interpretation per frequency decade (Fig. 5.1d), it can be observed that the highest frequency decade (V) stabilizes first, after 4 hours. The middle frequency decades (IV and III) and the lowest frequency decade (II) all stabilize after 10 hours. This indicates that the corrosion inhibitor protective action and the corrosion activity, with characteristic time-constants corresponding to the middle and low frequency region, respectively, prolong the overall system's instability but stabilize after the same time. It can be remarked that the first stabilization plateau, visible in the overall quantitative interpretation, corresponds to the stabilization of the higher frequency decades and the corresponding electrochemical processes.

5.3.1.5 Hot-dip galvanized steel with corrosion inhibitor 4

From the quantitative interpretation per frequency decade (Fig. 5.1e), it can be seen that the contribution of the highest and lowest frequency decade decrease more rapidly, reaching a stable value after 5 hours, compared to the relative contribution of the middle frequency decades, reaching a stable value after 6.5 hours. This indicates that for the system with corrosion inhibitor 4, the corrosion inhibitor protective action causes the overall system's instability since these frequency decades correspond to the time-constants describing those electrochemical processes. Compared to the system without corrosion inhibitors, it can be concluded that the presence of corrosion inhibitor 4 effectively stabilizes the surface of the hot-dip galvanized steel.

5.3.1.6 Hot-dip galvanized steel with corrosion inhibitor 5

The quantitative analysis per frequency decade of the system containing corrosion inhibitor 5 shows a remarkable difference in stabilization time of the different frequency decades (Fig. 5.1f). The highest and lowest frequency decades (V and II) stabilize first, after 6 hours and 8 hours, respectively. At the same time, the middle frequency decades (IV and III) reach a stabilization plateau more than three orders of magnitude lower compared to the magnitude of the impedance modulus. Nevertheless, after 12 hours, the non-stationarities of the middle frequency regions decrease further to eventually more than three orders of magnitude lower than the magnitude of the impedance modulus after 16 hours. It can be concluded that corrosion inhibitor 5 is ineffective in stabilizing the interface, indicated by the presence of non-stationarities in the middle frequency region accounting for this.

5.3.1.7 Hot-dip galvanized steel with corrosion inhibitor 1+2

Since this research also aimed to study synergistic combinations between corrosion inhibitors, different combinations out of the working corrosion inhibitors were tested for possible corrosion inhibitor synergism. One of the tested corrosion inhibitor combinations, is the system consisting of a combination of inhibitor 1 and 2 (both 0.5 mM).

It can be seen from the quantitative interpretation per decade (Fig. 5.1g) that here the lowest frequency decade (II) stabilizes first after 1 hour. The highest (V) and middle (IV and III) frequency decades stabilize together after 7 hours, indicating that the electrochemical processes with characteristic time-constants corresponding to theses frequencies, i.e. the corrosion inhibitor protective action, stabilize after 7 hours.

In general, it can be concluded that the system without corrosion inhibitors is behaving non-stationary during the first 10 hours after immersion, with the electrochemical processes with characteristic time-constants corresponding to the middle frequency region, i.e. the corrosion activity, prolonging the system's instability. For the system with the silica-based corrosion inhibitors, i.e. corrosion inhibitor 1 and corrosion inhibitor 2, the non-stationarities in the low-frequency region dominate the overall system's instability for 12 hours and 6 hours, respectively. The combination of corrosion inhibitor 1 and 2 effectively stabilizes the electrochemical interface after 7 hours, where the corrosion inhibitor protective action prolongs the system instability, related to the middle frequency region. For the phosphate-based corrosion inhibitors, i.e. corrosion inhibitors 3, 4 and 5, the electrochemical processes with time-constants related to the middle frequency region dominate the system's instability and eventually stabilize after 10 hours, 6.5 hours and 16 hours, respectively. These 'stabilization times' are important to consider when interpreting the electrochemical data obtained from conventional, well-established electrochemical techniques in the subsequent paragraphs.

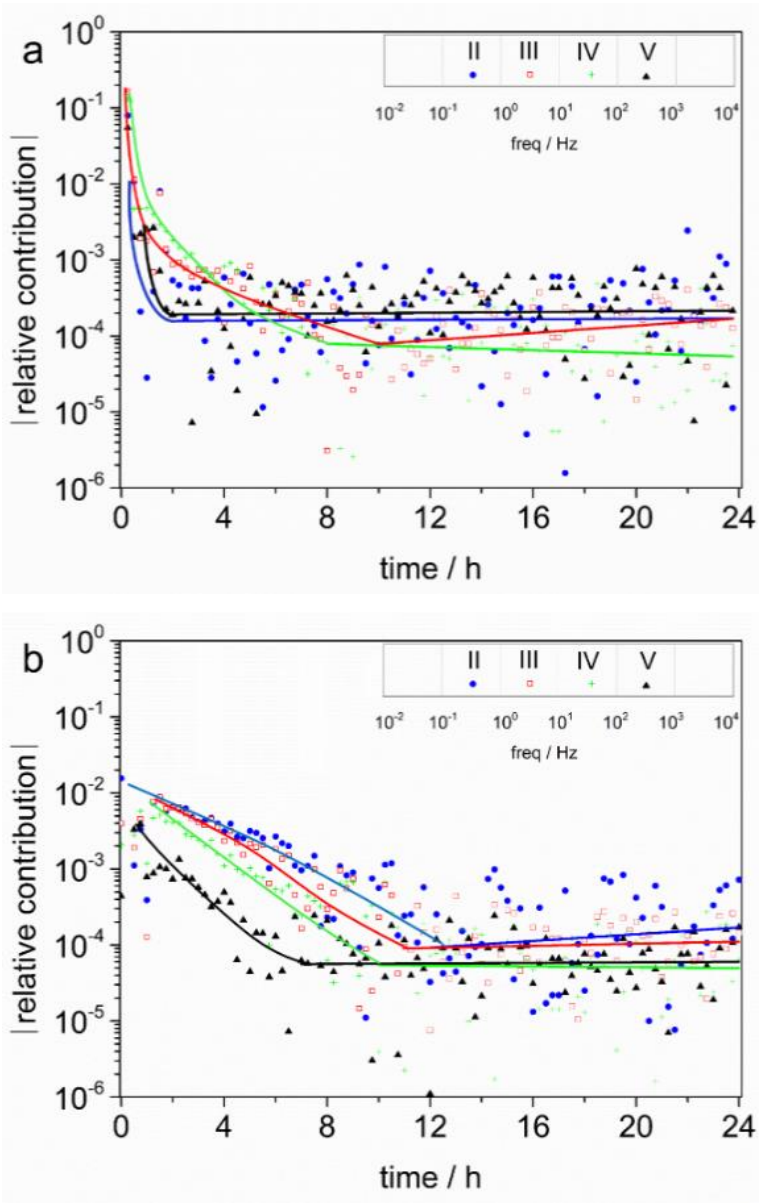

Figure 5.1 Evolution of the relative contribution of the non-stationarities for the different frequency decades for hot-dip galvanized steel without corrosion inhibitor (0.05 M NaCl) **(a)**, with Inhibitor 1 (0.5 mM Novinox®ACE110) **(b)**, inhibitor 2 (0.5 mM Novinox®XCA02) **(c)**, inhibitor 3 (0.1 mM Halox®SW-111) **(d)**, inhibitor 4 (0.5 mM Heucophos®CAPP) **(e)**, inhibitor 5 (0.02 mM Zinc Phosphate ZP10) **(f)** and inhibitor 1+2 (both 0.5 mM) **(g)** for the first 24 h of immersion, respectively. The blue, red, green and black lines represent the trend line of the non-stationarities in the respective frequency decades.

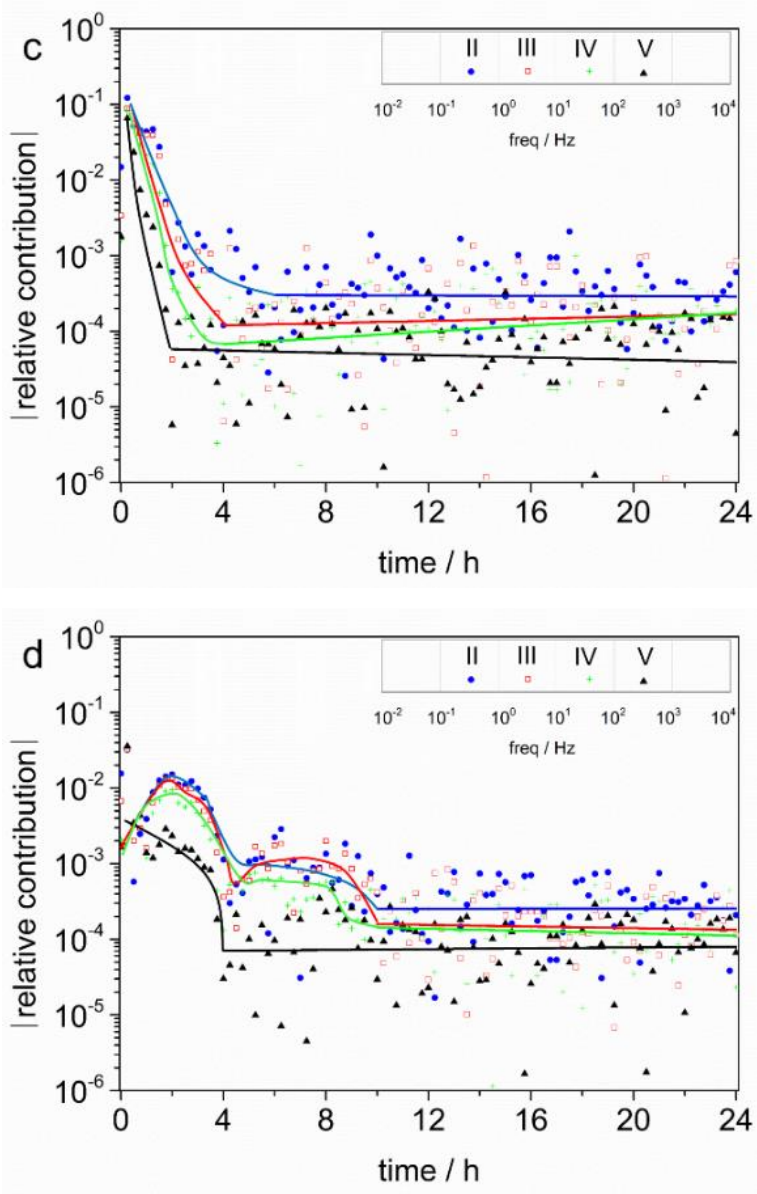

Figure 5.1 (continued)

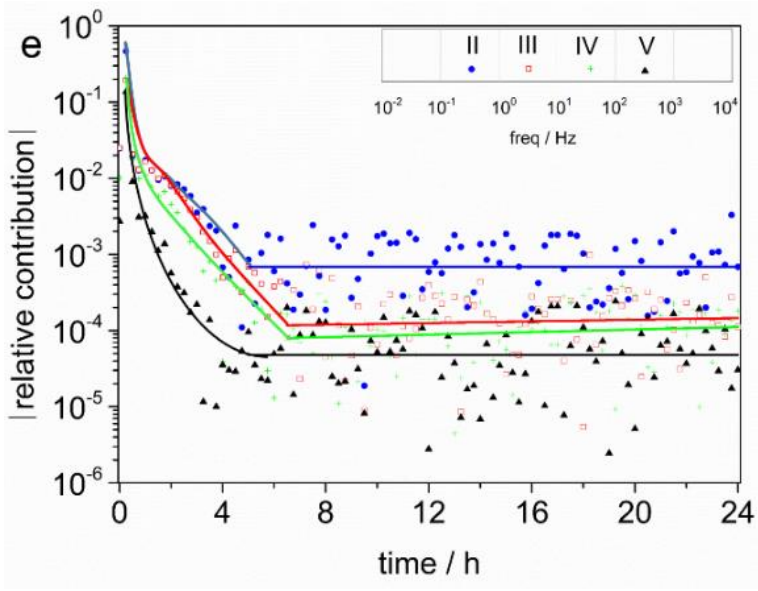

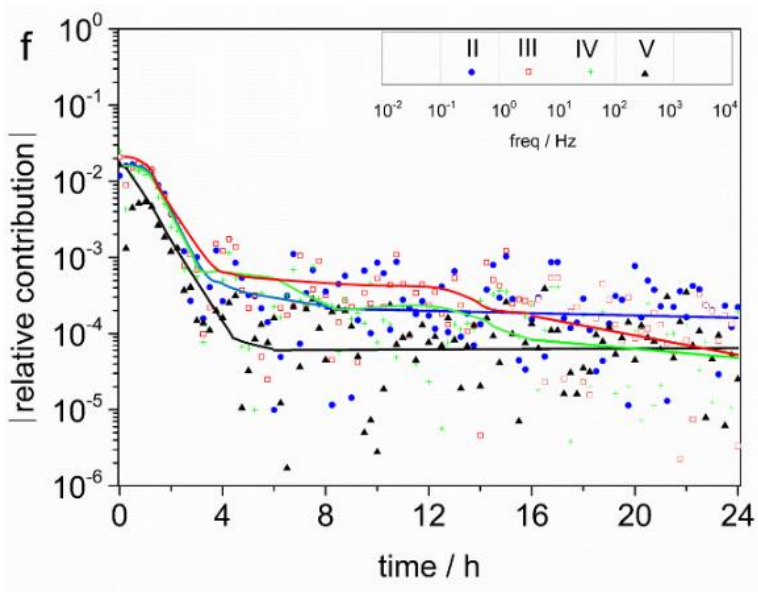

Figure 5.1 (continued)

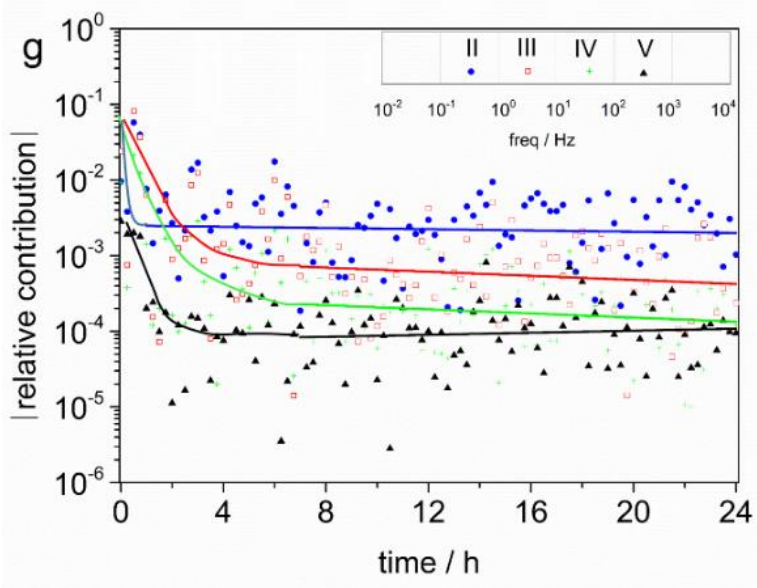

Figure 5.1 (continued)

5.3.2. Potentiodynamic polarization

Potentiodynamic polarization measurements represent a first well-established conventional electrochemical technique to retrieve information about the working principle and the optimal dosage of corrosion inhibitors. Therefore, the corrosion inhibitor concentration is varied from one measurement to another. The variety of concentrations that is measured depended on the solubility of the respective corrosion inhibitor powders in the 0.05 M NaCl reference solution. Three different concentrations were used for the highly soluble corrosion inhibitors (1, 2 and 4), i.e. 1 mM, 0.5mM and 0.1 mM, while for inhibitor 3 the concentrations were 0.1 mM and 0.02 mM and for inhibitor 5 only 0.02 mM was used.

In Figure 5.2, the PP curves for hot-dip galvanized steel with and without corrosion inhibitors after 1.5 hours and 24 hours are presented. The system with corrosion inhibitor 1 (Novinox®ACE110) after 1.5 hours shows lower cathodic current densities for all tested concentrations as compared to the system without corrosion inhibitors after 1.5 hours, but only marginal anodic inhibition (Fig. 5.2a). The highest concentration tested, i.e. 1 mM, proves to reduce the corrosion current density the most. After 24 hours, the corrosion

current density demonstrates similar behaviour for a 0.5 mM corrosion inhibitor concentration, with only a slight increase in corrosion current density. On the contrary, the system without corrosion inhibitors shows a significant increase in cathodic corrosion current density.

The system with corrosion inhibitor 2 (Novinox®XCA02) behaves similarly to the system with corrosion inhibitor 1, with the highest concentration being the most effective (Fig. 5.2b). However, after 24 hours, the corrosion current density shows a remarkable increase for a 0.5 mM inhibitor concentration.

For the system with corrosion inhibitor 3 (Halox®SW-111), only 2 concentrations were tested, due to the lower solubility of the corrosion inhibitor compared to corrosion inhibitors 1 and 2. For both concentrations, i.e. 0.1 mM and 0.02 mM, lower cathodic current densities are noted after 1.5 hours, compared to the system without corrosion inhibitors after 1.5 hours (Fig. 5.2c). However, no difference is observed between both concentrations. After 24 hours, the system with 0.1 mM corrosion inhibitors shows similar behaviour to the system after 1.5 hours for the same concentration.

In the case of the system with corrosion inhibitor 4 (Heucophos®CAPP), the lowest concentration, i.e. 0.1 mM has proven to reduce the cathodic current density the most after 1.5 hours, compared to the system without corrosion inhibitors after 1.5 hours (Fig. 5.2d). After 24 hours, the system with corrosion inhibitor demonstrates similar behaviour, while a significant increase in cathodic current density is observed in the case of the system without corrosion inhibitor.

The system with corrosion inhibitor 5 (Zinc Phosphate ZP10) was only tested at a single concentration, i.e. 0.02 mM, due to its low solubility in the 0.05 M NaCl reference solution. After 1.5 hours, the system shows a significant decrease in cathodic current density compared to the system without corrosion inhibitors after 1.5 hours (Fig. 5.2e). Nevertheless, the effect is only temporarily since the cathodic current density after 24 hours increased again towards similar values as for the system without corrosion inhibitor. The system with corrosion inhibitors 1 and 2 (Fig. 5.2f) shows a significant decrease in cathodic current density both after 1.5 hours and 24 hours, respectively, compared to the system without corrosion inhibitors.

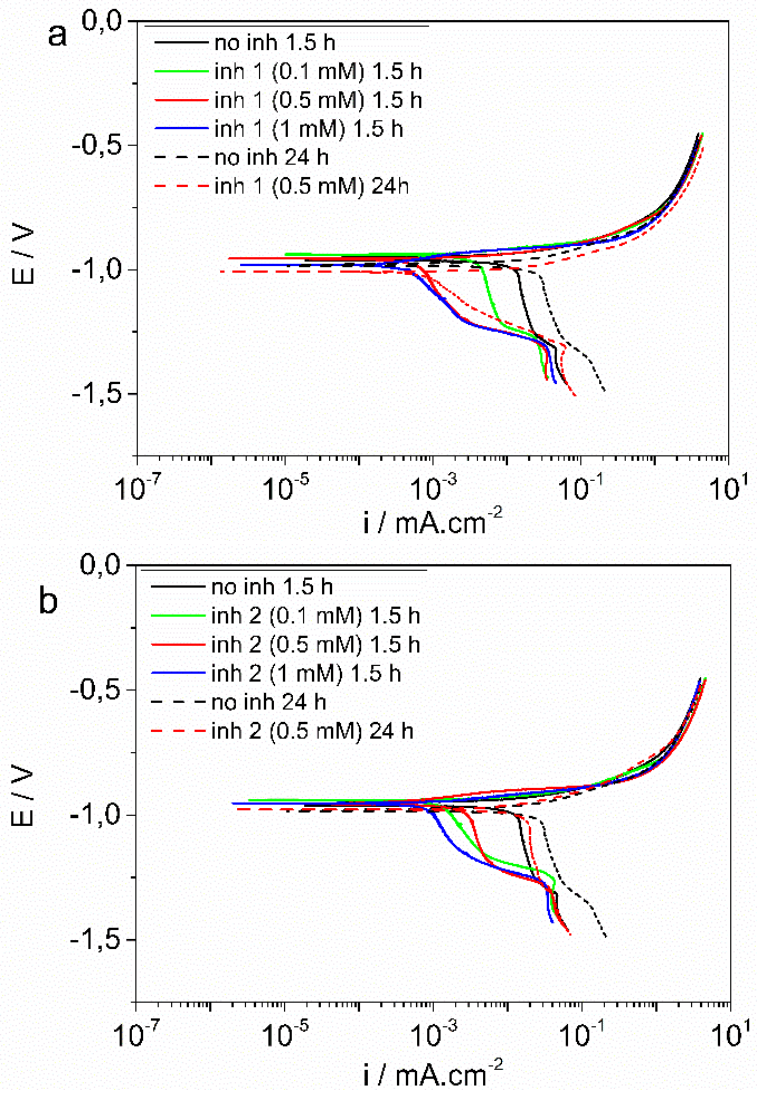

Figure 5.2 Potentiodynamic polarization diagram of hot-dip galvanized steel with and without corrosion inhibitors after 1.5 h and 24 h. Inhibitor 1 (Novinox®ACE110) **(a)**; inhibitor 2 (Novinox®XCA02) **(b)**; inhibitor 3 (Halox®SW-111) **(c)**; inhibitor 4 (Heucophos®CAPP) **(d)**; inhibitor 5 (Zinc Phosphate ZP10) **(e)**; inhibitor 1+2 **(f)**.

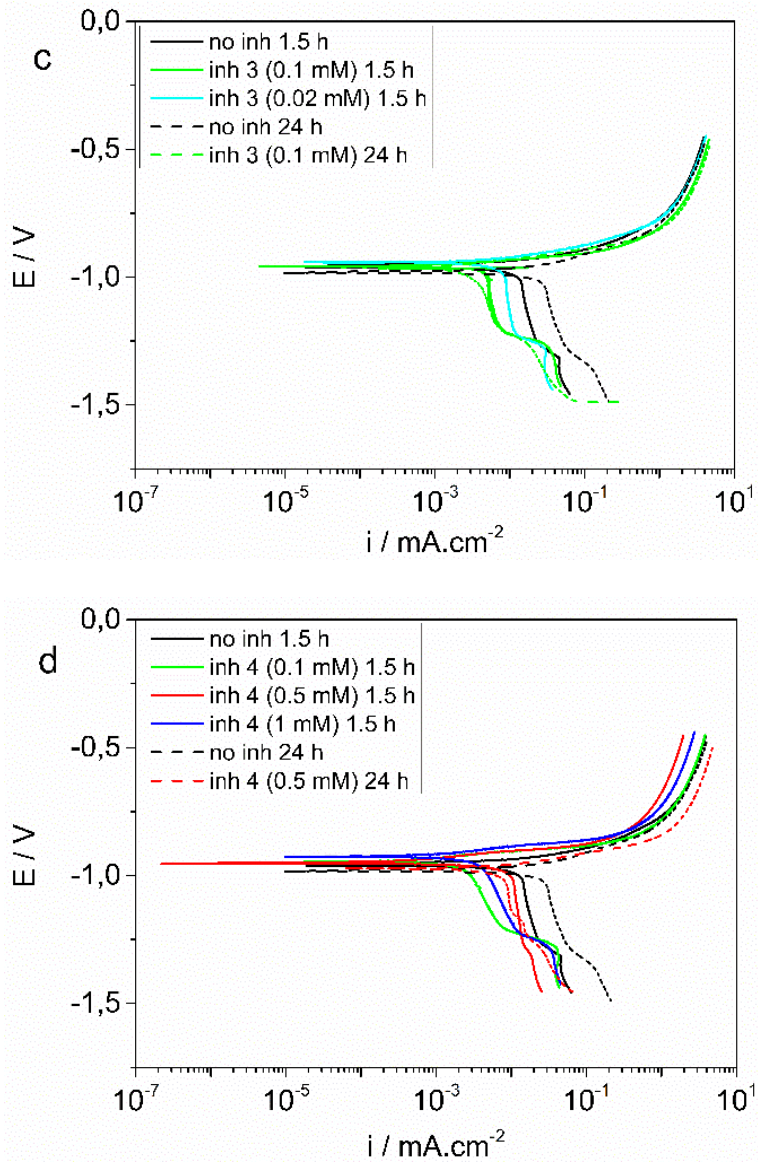

Figure 5.2 (continued)

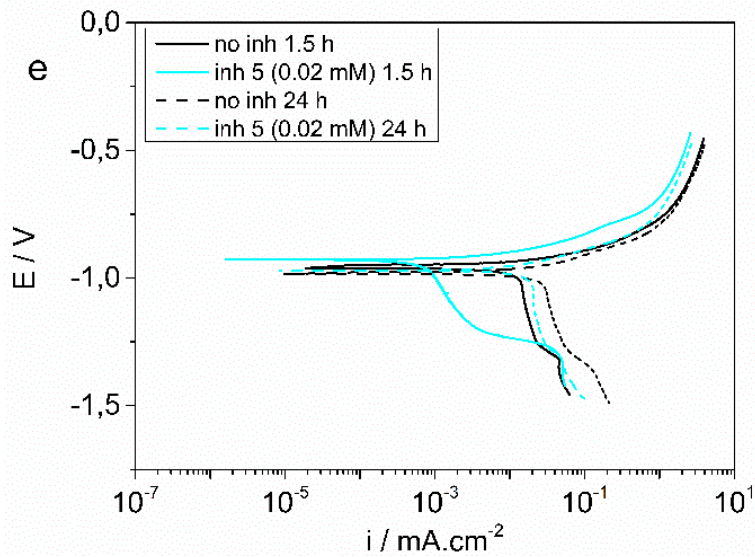

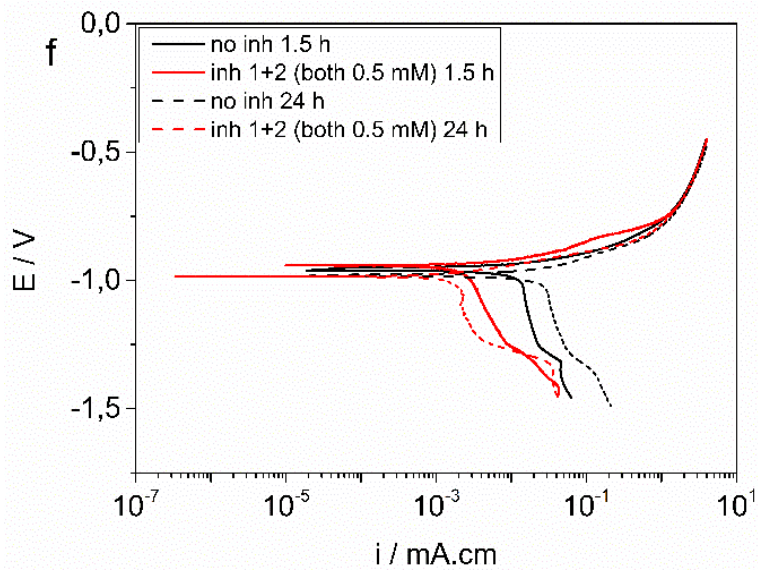

Figure 5.2 (continued)

In order to make a quantitative comparison between the corrosion inhibitors both over time and as a function of inhibitor concentration, the qualitative observations were translated into corrosion current densities, obtained through Tafel extrapolation [24] and corrosion inhibitor efficiencies (Fig. 5.3). In Figure 5.3a, the corrosion current density (i_{corr}) is shown for the system with and without corrosion inhibitors at different working concentrations after 1.5 hours. In the case of the system without corrosion inhibitors, i_{corr} is 12.50 ± 0.71 µA cm^{-2}. The ± values represent the standard deviation on each measurement. For all corrosion inhibitors and all concentrations, i_{corr} is reduced significantly. For the system with corrosion inhibitor 1 (Novinox®ACE110), i_{corr} decreases to 0.413 ± 0.048 µA cm^{-2}, 0.66 ± 0.38 µA cm^{-2} and 4.21 ± 0.32 µA cm^{-2} in the case of a 1 mM, 0.5 mM and 0.1 mM corrosion inhibitor concentration. i_{corr} for corrosion inhibitor 2 (Novinox®XCA02) decreases to 0.92 ± 0.28 µA cm^{-2}, 2.49 ± 0.42 µA cm^{-2} and 1.29 ± 0.24 µA cm^{-2} for a 1 mM, 0.5 mM and 0.1 mM corrosion inhibitor solution, respectively. Corrosion inhibitor 3 (Halox®SW-111) shows comparable i_{corr} values of 4.00 ± 0.64 µA cm^{-2} and 5.1 ± 1.5 µA cm^{-2} at 0.1 mM and 0.02 mM, respectively. In the case of corrosion inhibitor 4 (Heucophos®CAPP), i_{corr} is reduced to 3.70 ± 0.61 µA cm^{-2}, 8.28 ± 0.20 µA cm^{-2} and 2.45 ± 0.22 µA cm^{-2} for a 1mM, 0.5 mM and 0.1 mM inhibitor solution. In the case of inhibitor 5 (Zinc Phosphate ZP10), where only one concentration was used, i_{corr} was reduced to 0.74 ± 0.32 µA cm^{-2}, compared to the system without corrosion inhibitors after 1.5 hours. The synergistic combination of corrosion inhibitor 1 and 2 reduces i_{corr} to 2.28 ± 0.33 µA cm^{-2}. However, it needs to be taken into account that all corrosion inhibitor containing systems are still behaving 'unstable', dominated by the presence of non-stationarities, as pointed out by the quantitative analysis per frequency decade of the ORP-EIS data. Consequently, the corrosion current density values presented here should be interpreted as a snapshot in time in the non-stationary regime and should only be compared against each other rather than looking at their exact values.

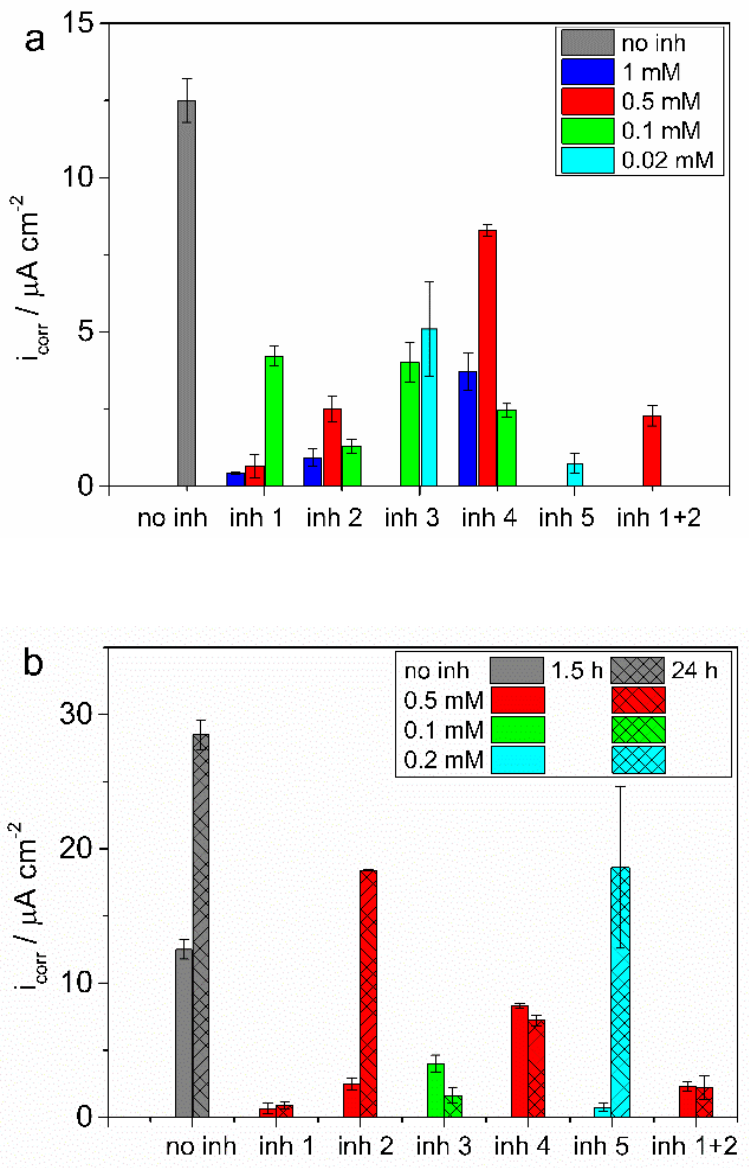

Figure 5.3 Corrosion current density a.f.o. concentration **(a)**, corrosion current density a.f.o. immersion time **(b)** and corrosion inhibitor efficiency (η) **(c)** of hot-dip galvanized steel with and without corrosion inhibitors after 1.5 h and 24 h. Inhibitor 1 (Novinox®ACE110); inhibitor 2 (Novinox®XCA02); inhibitor 3 (Halox®SW-111); inhibitor 4 (Heucophos®CAPP); inhibitor 5 (Zinc Phosphate ZP10).

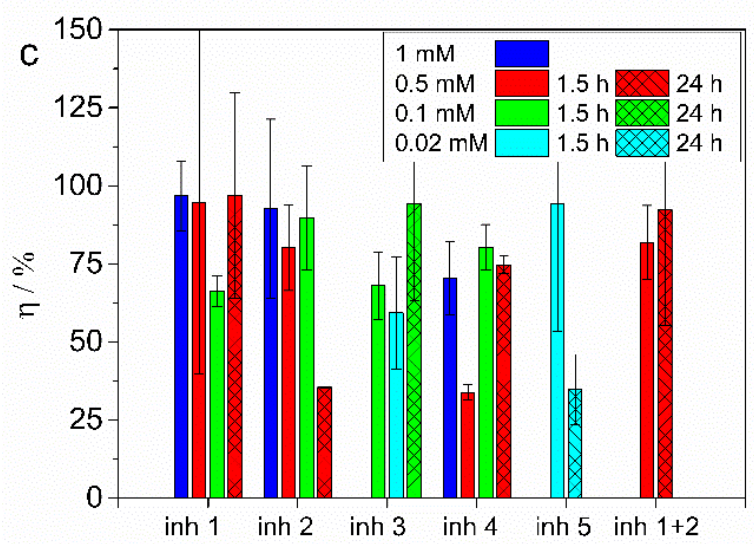

Figure 5.3 (continued)

From the quantitative interpretation per frequency decade of the ORP-EIS data, it has been observed that both the system without and with corrosion inhibitors are behaving 'stable' after 24 hours. Therefore the corrosion current densities obtained after 24 hours are basically a snapshot in the stationary regime of the respective electrochemical system generating more precise values. Figure 5.3b shows the evolution of the corrosion current density after 1.5 hours and 24 hours, respectively. In the case of the reference solution, i_{corr} increases from 12.50 ± 0.71 µA cm^{-2} after 1.5 hours to 28.5 ± 1.1 µA cm^{-2} after 24 hours. In the case of corrosion inhibitors 1, 2 and 5, a similar observation is made, with an increase in i_{corr} over time: i_{corr} of a 0.5 mM solution of inhibitor 1, of inhibitor 2 and of a 0.02 mM solution of inhibitor 5 increased from 0.66 ± 0.38 µA cm^{-2}, 2.49 ± 0.42 µA cm^{-2} and 0.74 ± 0.32 µA cm^{-2} after 1.5 hours to 0.87 ± 0.30 µA cm^{-2}, 18.39 ± 0.036 µA cm^{-2} and 18.6 ± 6.0 µA cm^{-2} after 24 hours, respectively. However, the increase in i_{corr} of corrosion inhibitor 1 should be placed in perspective since its increase is small and remains negligible compared to the system without corrosion inhibitors after 24 hours. In the case of corrosion inhibitors 3, 4 and the combination of 1 and 2, i_{corr} decreases as a function of time, showing an improved corrosion protection at longer immersion times. I_{corr} decreases from 4.00 ± 0.64 µA cm^{-2}, 8.28 ± 0.20 µA cm^{-2} and 2.28 ± 0.33 µA cm^{-2} after 1.5 hours to 1.63 ± 0.54 µA cm^{-2}, 7.20 ± 0.43 µA cm^{-2} and 2.20 ± 0.88 µA cm^{-2} after 24 hours in the case of corrosion inhibitor 3, 4 and 1+2, respectively. It can be concluded that all corrosion inhibitor shown an immediate corrosion protection, but that only corrosion inhibitors 1, 3, 4 and the synergistic combination of

corrosion inhibitor 1 and 2 are capable of effectively protecting the hot-dip galvanized steel after 24 hours.

To evaluate the effectiveness of the corrosion inhibitors, the corrosion inhibitor efficiency (η) is calculated from the corrosion current density of the inhibited system ($i_{cor(inh)}$) and the reference system (i_{corr}) presented above according to [25]:

$$\eta\ (\%) = \frac{i_{corr} - i_{corr(inh)}}{i_{corr}}\ x\ 100 \qquad (1)$$

In Figure 5.3c, the corrosion inhibitor efficiency is presented after 1.5 hours and 24 hours at various concentrations. In the case of corrosion inhibitor 1, the inhibitor efficiencies vary from 97 ± 11 %, 95 ± 55 % and 66.3 ± 5.0 % in the case of a 1 mM, 0.5 mM and 0.1 mM inhibitor solution. Over time, the efficiency of the 0.5 mM inhibitor solution remains equal. For corrosion inhibitor 2, the inhibitor efficiencies amount 93 ± 29 %, 80 ± 14 % and 90 ± 17 % for a 1 mM, 0.5 mM and 0.1 mM solution. Over time, the inhibitor efficiency decreases drastically towards 35.432 ± 0.069 % after 24 hours. The system with corrosion inhibitor 3 with 0.1 mM and 0.02 mM inhibitor solutions presents inhibitor efficiencies of 68 ± 11 % and 59 ± 18 %, respectively. After 24 hours, the corrosion inhibitor efficiency has increased to 94 ± 31 %. In the case of corrosion inhibitor 4, the inhibitor efficiencies are 70 ± 12 %, 33.8 ± 2.5 % and 80.4 ± 7.2 % for a 1 mM, 0.5 mM and 0.1 mM inhibitor solution, respectively. Over time, the efficiency of the 0.5 mM solution has increased to 74.7 ± 2.7 %. For corrosion inhibitor 5, measured only at 0.02 mM, the inhibitor efficiency decreased from 94 ± 10 % after 1.5 hours to 35 ± 11 % after 24 hours. Finally, the system consisting of a 0.5 mM solution of corrosion inhibitor 1 and a 0.5 mM solution of corrosion inhibitor 2 shows an increase in inhibitor efficiency from 82 ± 12 % after 1.5 hours to 92 ± 37 % after 24 hours.

In the case of inhibitor 1, it needs to be noted that although the corrosion current density increased over time, the inhibitor efficiency increased. This is due to the difference in corrosion current density of the system without corrosion inhibitors after 1.5 hours and 24 hours, which increased by 128 %. Therefore, only a small decrease or even increase in corrosion current density of the corrosion inhibitor containing system could lead to an efficiency increase and an associated misinterpretation. This indicates that all results have to be placed in the right perspective.

It can be concluded that that all corrosion inhibitor-containing systems, as well as the combination of corrosion inhibitor 1 and 2 showed lower cathodic current densities compared to the system without corrosion inhibitors and only marginal anodic inhibition, indicating cathodic type corrosion inhibitors. Corrosion inhibitor 1 and corrosion inhibitor 3

experience a positive effect of concentration, i.e. an increased inhibitor concentration reduces i_{corr}. For corrosion inhibitor 2 and 4, the highest (1 mM) and lowest (0.1 mM) concentrations tested reduce i_{corr} the most. For the systems containing corrosion inhibitors 5 and the combination of corrosion inhibitor 1 and 2, only one concentration was tested, which effectively reduced i_{corr}. Over time, when comparing the results after 24 hours and 1.5 hours, only in the case of corrosion inhibitors 3 and 4 i_{corr} is reduced while for corrosion inhibitors 2 and 5, i_{corr} has increased significantly, similarly to the situation without corrosion inhibitors. For corrosion inhibitors 1 and the combination of corrosion inhibitors 1 and 2, comparable i_{corr} are observed. This is all reflected in the corrosion inhibitor efficiencies. These differences in i_{corr} at discrete times in the corrosion inhibitive solutions stress again the importance of studying the electrochemical behaviour of each system as a function of immersion time.

At this point, it has been decided to continue with the 0.5 mM concentrations for corrosion inhibitors 1, 2, 4 and the combination of 1 and 2 and a 0.1 mM and 0.02 mM concentration for corrosion inhibitor 3 and 5, respectively. The former has been chosen to allow a comparison between corrosion inhibitors 1 and 2 on one hand and the combination of corrosion inhibitors 1 and 2 on the other hand. The latter is selected because of efficiency and solubility reasons.

5.3.3 Open Circuit Potential with superimposed Linear Polarization Resistance

In the previous section, discrete electrochemical information about the corrosion inhibitor-containing system was gathered by means of potentiodynamic polarization experiments. In order to assess continuous, time-resolved information about the performance of the system over longer times after immersion with and without the presence of corrosion inhibitors, continuous OCP measurements with superimposed LPR measurements every hour were carried out for 168 hours. From the slope of the potential versus current plot for every hour, the Rp can be calculated and as such monitored every hour.

Figure 5.4 shows the Rp values and their standard deviation of the hot-dip galvanized steel with and without corrosion inhibitors over time, presented separately for the phosphate- (Fig. 5.4a-b) and silica- based (Fig. 5.4c-d) corrosion inhibitors. It can be seen that for the hot-dip galvanized steel without corrosion inhibitors (Fig. 5.4a), the Rp is 1.65 ± 0.14 kΩ cm² for the first measurement after 1 hour, but decreases rapidly in the first 10 hours to 0.99 ±

0.12 kΩ cm². Note also the relatively high absolute error on the Rp values in the first 10 hours. This, together with the unstable Rp values during the initial 10 hours after immersion can be explained by the presence of the non-stationarities for the same duration and a consequently 'unstable' system which is directly reflected here. Eventually the Rp values continue to decrease to 0.61 ± 0.11 kΩ cm² after 168 hours of immersion.

In the case of hot-dip galvanized steel with corrosion inhibitor 3 (Fig. 5.4a-b), the Rp is 3.82 ± 0.17 kΩ cm² at the start and decreases strongly towards 1.62 ± 0.16 kΩ cm² after 10 hours followed by a more gradual decrease to 1.19 ± 0.22 kΩ cm² after 31 hours of immersion. The transition from the strong to the more gradual decrease corresponds to the stabilization time of the system as previously observed by the quantitative interpretation per frequency decade of the OPR-EIS data. Following this gradual decrease, a gradual increase is visible to 1.40 ± 0.21 kΩ cm² after 100 hours and eventually 1.61 ± 0.28 kΩ cm² after 168 hours of immersion, which is almost three times higher as compared to the hot-dip galvanized steel without corrosion inhibitor. For corrosion inhibitor 4 (Fig. 5.4a-b), the Rp is 1.51 ± 0.48 kΩ cm² at the start and decreases to 1.31 ± 0.11 kΩ cm² after 7 hours at the same time the contribution of the non-linearities stabilizes and the system can be considered fully stable. Similar to corrosion inhibitor 3, a gradual increase is apparent afterwards to 1.56 ± 0.19 kΩ cm² after 168 hours, also almost three times higher as compared to the system without corrosion inhibitor. The Rp of hot-dip galvanized steel with corrosion inhibitor 5 (Fig. 5.4a-b) amounts 22.8 ± 5.7 kΩ cm² after 1 hour, more than 10 times higher as compared to the system without corrosion inhibitors, indicating imminent protective action. However, the Rp decreases initially strongly to 4.12 ± 0.95 kΩ cm² after 16 hours and afterwards more gradually over the course of the measurement to 1.64 ± 0.42 kΩ cm² after 168 hours, comparable to what was observed for corrosion inhibitors 3 and 4. Yet again, the initial strong decrease in the first 16 hours with corresponding unstable Rp values with high absolute error could be related to the 'unstable' behaviour of the electrochemical system at these times as shown by the ORP-EIS interpretation per frequency decade.

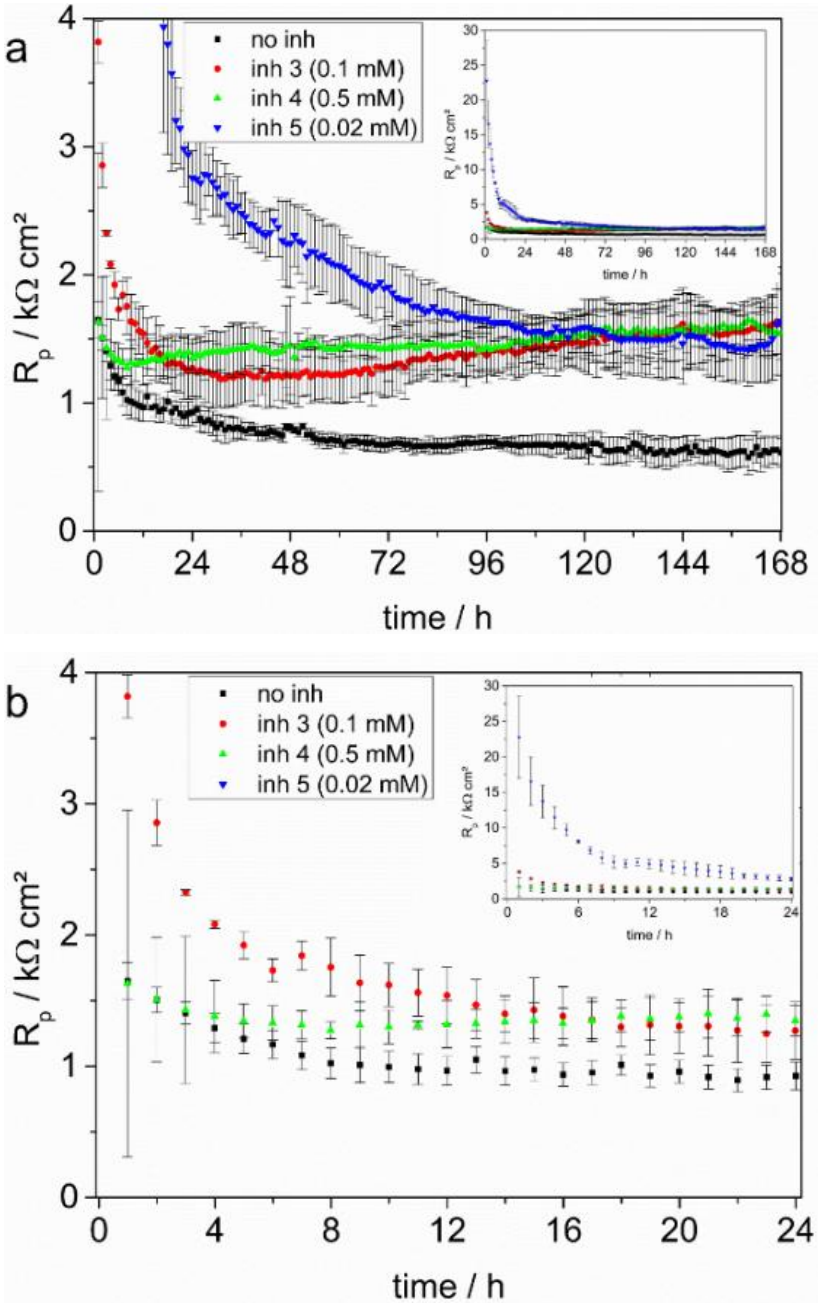

Figure 5.4 Polarization resistance (R_p) results and their standard deviation obtained from linear polarization resistance measurements of hot-dip galvanized steel without corrosion inhibitor (0.05 M NaCl), with inhibitor 3 (0.1 mM Halox SW111), inhibitor 4 (0.5 mM Heucophos Capp) and inhibitor 5 (0.02 mM Zinc Phosphate ZP10) **(a)** and **(b)** and with inhibitor 1 (0.5 mM Novinox ACE110), inhibitor 2 (0.5 mM Novinox XCA02) and inhibitor 1+2 (both 0.5 mM) **(c)** and **(d)** for 168 h.

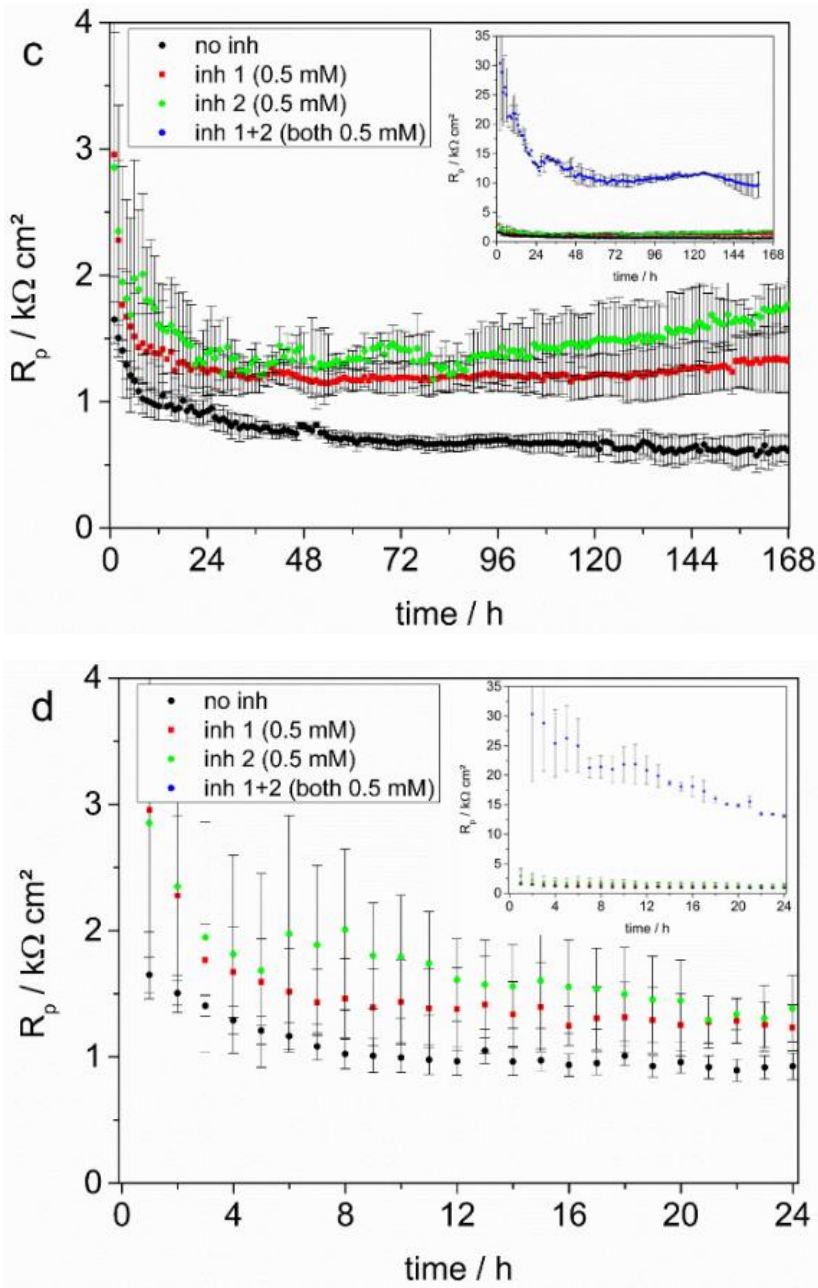

Figure 5.4 (continued)

For the system with corrosion inhibitors 1, 2 and the combination of corrosion inhibitors 1 and 2 a similar observation can be made. For corrosion inhibitors 1 and 2 (Fig. 5.4c-d), the R_ps are 2.95 ± 0.97 kΩ cm² and 2.85 ± 1.39 kΩ cm² respectively, right at the start. Both decrease initially strongly to 1.38 ± 0.33 kΩ cm² and 1.98 ± 0.94 kΩ cm² in the first 12 and 6 hours after immersion and more gradually in the following hours to eventually 1.15 ± 0.10 kΩ cm² after 54 hours and 1.212 ± 0.057 kΩ cm² after 37 hours, respectively. Afterwards a gradual increase to 1.32 ± 0.25 kΩ cm² and 1.67 ± 0.30 kΩ cm² after 168 hours is noticeable for the hot-dip galvanized steel with corrosion inhibitor 1 and 2, respectively. The behaviour of the hot-dip galvanized steel with equal combination of corrosion inhibitor 1 and 2 (Fig. 5.4c-d) is furthermore remarkable. The R_p is 30 ± 11 kΩ cm² right at the start, more than 15 times higher than the system without corrosion inhibitors. Afterwards the R_p decreases initially strongly to 21.3 ± 1.7 kΩ cm² after 7 hours and eventually more gradually to 9.88 ± 0.52 kΩ cm² after 68 hours and remains approximately constant for the rest of the measurement, reaching an R_p of 9.8 ± 2.2 kΩ cm² after 168 hours. Here again, the quantitative interpretation of the ORP-EIS data per frequency decade indicated that the systems with corrosion inhibitor 1, 2 and the combination of 1 and 2 behave non-stationary during the initial 12, 6 and 7 hours, respectively, which is reflected in the unstable values with relatively high absolute error in these timeframes and depicts the uncertainty on the results acquainted there.

Similarly to our previous paper, a comparison can be made between the results obtained from LPR and the results obtained from PP previously in terms of the i_{corr} [11]. Starting from the R_p from LPR after 1.5 hours, calculated as the average from the respective values after 1 and 2 hours, and 24 hours, and the anodic and cathodic slopes of the Tafel plot (β_a and β_c, respectively), i_{corr} can be calculated according to the Stern-Geary equation [26]:

$$i_{corr} = \frac{\beta_a \cdot \beta_c}{2.3\,(\beta_a + \beta_c)\,R_p} \quad (2)$$

These parameters and the resulting i_{corr} values are summarized in Table 5.3.

Comparison of these values with the previously obtained values from PP show that there is in general no agreement between the values obtained through both techniques, not only for results after 1.5 hours, when all systems are still behaving 'unstable', but also after 24 hours when all systems are behaving fully 'stable'. Only for the system without corrosion inhibitor and the system with corrosion inhibitor 5 an agreement is found in both the trend and the i_{corr} values over time. It can be seen that the resulting i_{corr} values for the system without corrosion inhibitors are 15.1 ± 1.1 µA cm^{-2} and 46.8 ± 5.5 µA cm^{-2} obtained from LPR compared to 12.50 ± 0.71 µA cm^{-2} and 28.5 ± 1.1 µA cm^{-2} obtained from PP after 1.5 hours

and 24 hours respectively. For the system containing corrosion inhibitor 5, the resulting i_{corr} values are 0.72 ± 0.17 µA cm^{-2} and 15.0 ± 1.1 µA cm^{-2} from LPR, compared to 0.74 ± 0.32 µA cm^{-2} and 18.6 ± 6.0 µA cm^{-2} from PP after 1.5 hours and 24 hours. Nevertheless, a complete independent comparison is impossible, since kinetic parameters from the Tafel extrapolation need to be used to calculate i_{corr} from R_p obtained through LPR measurements.

Table 5.3 Tafel Parameters from PP and R_p from LPR for the determination of i_{corr} using Stern-Geary.

	time	**R_p** (kΩ cm^2)	**std. dev.** (kΩ cm^2)	**β_a** (V/dec)	**β_c** (V/dec)	**i_{corr}** (µA cm^{-2})	**std. dev.** (µA cm^{-2})
no inh	1.5 h	1.58	0.12	0.059	0.084	15.1	1.1
	24 h	0.93	0.11	0.109	1.208	46.8	5.5
Inh 1	1.5 h	2.62	0.80	0.038	0.410	5.8	1.8
	24 h	1.23	0.18	0.036	0.211	10.8	1.6
Inh 2	1.5 h	2.6	1.2	0.054	0.893	8.5	3.9
	24 h	1.39	0.26	0.098	3.192	29.7	5.5
Inh 3	1.5 h	3.34	0.17	0.026	0.949	3.32	0.17
	24 h	1.27	0.22	0.042	0.158	11.3	1.9
Inh 4	1.5 h	1.57	0.90	0.045	0.206	10.2	5.8
	24 h	1.35	0.12	0.079	0.158	16.9	1.5
Inh 5	1.5 h	19.7	4.6	0.035	0.453	0.72	0.17
	24 h	2.76	0.21	0.099	2.574	15.0	1.1
Inh 1+2	1.5 h	38	17	0.040	0.545	0.42	0.19
	24 h	13.10	0.23	0.055	15.419	1.802	0.031

It can be concluded that corrosion inhibitor 5 provides immediate corrosion protection significantly higher than corrosion inhibitor 3 and corrosion inhibitor 4. Over the course of the measurement, the R_p of corrosion inhibitor 5 decreases gradually while for corrosion inhibitors 3 and 4, the R_p increases gradually. Eventually, after 168 hours, an R_p of around 1.60 kΩ cm^2 is observed for all three inhibitors almost three times higher than the 0.61 kΩ cm^2 observed for the system without corrosion inhibitor. In the case of corrosion inhibitor 1

and 2, a similar trend is observed with an initial decrease in R_p during the first 2 days and eventually a gradual increase to values two to three times higher as compared to the system without corrosion inhibitor. The LPR results for the system with both corrosion inhibitor 1 and corrosion inhibitor 2 indicate that a synergistic effect is observed. After 168 hours, an R_p of 9.8 ± 2.2 kΩ cm², which is more than three times higher than the sum of the R_ps of corrosion inhibitor 1 and corrosion inhibitor 2, 1.32 ± 0.25 kΩ cm² and 1.67 ± 0 30 kΩ.cm², respectively. Moreover, it needs to be remarked that in the beginning, for both the system without corrosion inhibitors and the systems with corrosion inhibitors, an evolution in terms of an increase or decrease in R_p is observed, while at a certain moment, all systems show stable R_p values. However, the point in time where this transition occurs is different from system to system and is related to the 'stability' of the electrochemical system as studied by the quantitative interpretation per frequency decade of the ORP-EIS data.

5.3.4 Electrochemical Impedance Spectroscopy (EIS)

EIS was used to provide not only time-resolved information but also frequency-resolved information on the electrochemical characteristics of hot-dip galvanized steel with and without corrosion inhibitors over time. Since a correct and trustworthy EIS measurement requires the fulfilment of the causality, linearity and stationarity condition, the quantitative interpretation of the ORP-EIS data serves as the basis for the EIS data interpretation providing an electrochemical 'stability' criterion [13].

Figure 5.5 shows the bode plots of the different systems every day up to 1 week after immersion. In the case of the hot-dip galvanized steel without corrosion inhibitors (Fig. 5.5a), the Bode plots show a remarkable decrease in the impedance modulus of the middle frequency region (10^3-10^0 Hz) and a gradual decrease in the low frequency region (10^0-10^{-1}) with time. In the associated phase plots, two time-constants can be distinguished, one in the middle frequency region and one in the lower frequency region. These can be associated with the corrosion activity, related to the effect of the ionic double layer capacitance and the diffusion of the zinc oxidation products to the bulk solution or oxygen reduction [27][28][29][30][31]. Connected to the decrease in impedance modulus in the middle and low frequency regions is a decline and shift of the phase angle of the first time-constant towards lower frequencies and a decline of the phase angle of the second time-constant. This can be associated to a decreased corrosion resistance of the system without corrosion inhibitors.

The Bode plots of hot-dip galvanized steel with corrosion inhibitor 1 (Novinox®ACE110) (Fig. 5.5b) shows a gradual decrease in the impedance modulus of the middle frequency region in the first three days, which stabilizes afterwards, before decreasing again after six days. Connected is an initial decrease in impedance modulus of the low frequency region which stabilizes after three days and eventually increases again towards the end of the measurement. The Bode phase plot reveals again two time-constants. The first time-constant, in the middle frequency region, gradually decreases with time. The second time-constant, in the low frequency region, increases slightly with time from day 2 to day 7.

The Bode plots of corrosion inhibitor 2 (Novinox XCA02) (Figure 5.5c) show an initial slightly higher impedance modulus, compared to the system without corrosion inhibitor. Nevertheless, the magnitude of the impedance modulus decreases fast over the first days, in the middle frequency region as well as in the low frequency region, reaching a stable value after three days. From the associated Bode phase plots, showing again two time-constants, it can be observed that there are is initially a large time-constant in the mid-frequency region and a smaller time constant in the low-frequency region. Upon immersion, the mid-frequency region time-constant decreases and shifts to lower frequencies, while the low frequency time constant slightly increases and shifts to lower frequencies. This can be explained in terms of active corrosion occurring during the first days and stabilization of the corrosion destructive processes.

The Bode plots of corrosion inhibitor 3 (Halox®SW-111) (Fig. 5.5d) reveal that the impedance modulus in the middle frequency as well as the low frequency region decreases heavily in the first days and increases again in the final days of the measurement. This is coupled to the behaviour of the phase angle in the associated phase plots where the first middle frequency dominates by decreasing initially but eventually increasing and shifting towards higher frequency, indicating the occurrence of corrosion protective action on the surface. At the same time, the low-frequency time-constant increases slightly over the course of 168 hours.

The Bode plots of corrosion inhibitor 4 (Heucophos®CAPP) (Fig. 5.5e) show an initial decrease in the magnitude of the impedance modulus at 10 mHz during the first day of immersion but afterwards the magnitude of the impedance modulus increases again over time. The Bode phase plot shows again two time constants. The first time-constant, present in the mid-frequency region, decreases slightly over time, but shifts to higher frequencies at the same time, unveiling the appearance of corrosion protective action on the surface. The second time constant, present in the low-frequency region, increases over the course of 168 hours, designating an increased corrosion resistance [32][33].

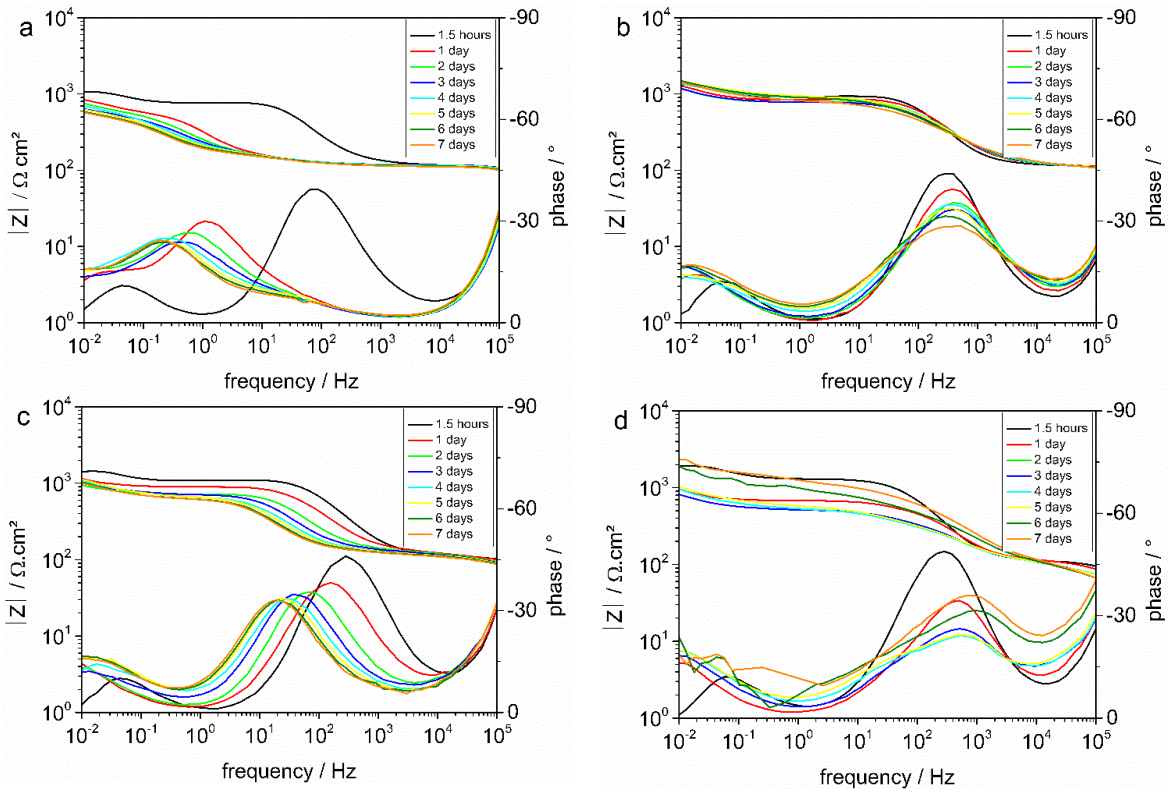

Figure 5.5 EIS bode plots for hot-dip galvanized steel with and without corrosion inhibitors every 24 h for 168 h. Without corrosion inhibitor (0.05 M NaCl) **(a)** Inhibitor 1 (0.5 mM Novinox ACE110) **(b)**; inhibitor 2 (0.5 mM Novinox XCA02) **(c)**; inhibitor 3 (0.1 mM Halox SW111) **(d)**; inhibitor 4 (0.5 mM Heucophos Capp) **(e)**; inhibitor 5 (0.02 mM Zinc Phosphate ZP10) **(f)**; inhibitor 1+2 (both 0.5 mM) **(g)**.

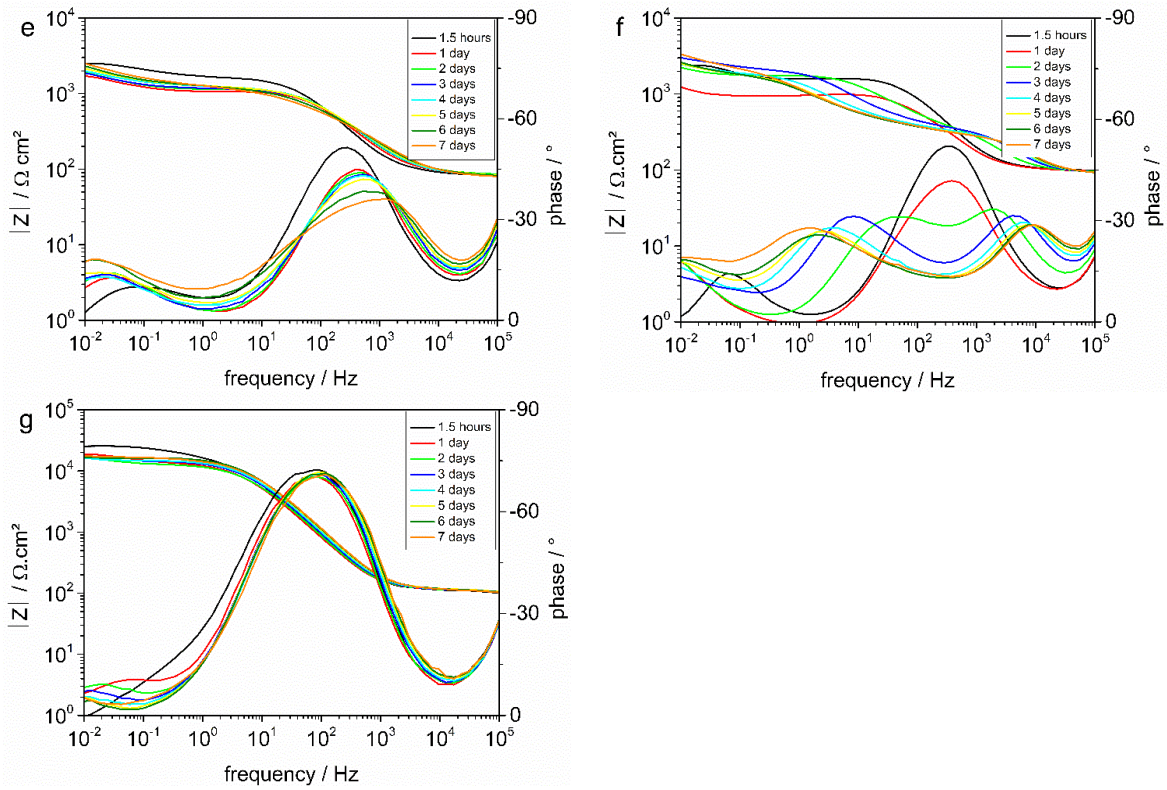

Figure 5.5 (continued)

The Bode plots of corrosion inhibitor 5 (Zinc Phosphate ZP10) (Fig. 5.5f) indicate that the magnitude of the impedance modulus is approximately three times higher, compared to the magnitude of the impedance modulus of the system without corrosion inhibitors. However, the impedance modulus decreases heavily during the first day, both in the middle frequency region and in the lower frequency region. Afterwards, the magnitude of the of the impedance modulus increases again, not only in the low frequency region but also in the higher frequency region (10^4-10^3 Hz). The Bode phase plot reveals the presence of two time-constants initially, one in the middle frequency region and one in the low frequency region. However, the mid-frequency time-constant broadens over time and eventually, after 2 days, two time-constants can be differentiated here. Additionally to the time-constant in the low-frequency region (10^0-10^{-1}) and mid-frequency region (10^3-10^0 Hz), a third time-constant appears in the higher frequency region (10^4-10^3 Hz). The low-frequency time-constant increases over time, while the mid-frequency time-constant decreases and shifts to lower

frequencies. The high frequency time-constant shifts to higher frequencies however over the course of 168 hours, indicating increased corrosion protection over time.

In the case of synergistic combination of corrosion inhibitor 1 and corrosion inhibitor 2 (Fig. 5.5g), the Bode plots show a magnitude of the impedance modulus at 10 mHz more than one order of magnitude higher compared to the system without corrosion inhibitors. Over time, the magnitude of the impedance modulus at minimum frequency decreases slowly and stabilizes after 48 hours, but remains substantially higher. Compared to phase plots with corrosion inhibitor 1 and corrosion inhibitor 2, again two time-constants are observed here. Both undergo only little change over the course of the measurement, with the mid-frequency region decreasing and shifting to higher frequencies.

In order to evaluate the consistency between the results obtained from the different macroscopic electrochemical techniques, the R_p values of the EIS measurements are calculated from the real component of the impedance at maximum and minimum frequency, i.e. 100 kHz and 10 mHz, according to [34]:

$$R_p = Z'(0) - Z'(\infty) \quad (3)$$

Figure 5.6 displays the evolution of the R_p with their standard deviation obtained from EIS measurements for the system with and without corrosion inhibitors over time, shown separately for the phosphate- (Fig. 5.6a-b) and silica- based (Fig. 5.6c-d) corrosion inhibitors. For the system without corrosion inhibitors (Fig. 5.6a-b), the R_p is 1.87 ± 0.31 kΩ cm² after 1 hour of immersion and decreases strongly in the initial hours. An R_p value of 0.75 ± 0.13 kΩ cm² is reached after 10 hours of immersion. This time corresponds to the 'stabilization' time of the electrochemical system, i.e. the time to reach a linear and stationary system. In the following hours, the R_p decreases more slowly, reaching a value of 0.475 ± 0.041 kΩ cm² after 168 hours.

In the case of corrosion inhibitor 3 (Fig. 5.6a-b), the R_p is 2.06 ± 0.32 kΩ cm² after 1 hour, comparable to the system without corrosion inhibitor after the same time. Nevertheless, the R_p decreases strongly initially and eventually more slowly, reaching a value of 1.51 ± 0.18 kΩ cm² and 1.21 ± 0.35 kΩ cm² after 10 and 24 hours of immersion, respectively. The transition from the strong decrease with unstable values to a more gradual decrease corresponds yet again to the moment in time the system reaches a 'stable' state. Afterwards, a gradual increase in R_p is noticeable towards a value of 1.89 ± 0.41 kΩ cm² after 168 hours. The system with corrosion inhibitor 4 (Fig. 5.6a-b) shows an R_p value of 2.85 ± 0.42 kΩ cm² after 2 hours, which decreases rapidly in the first hours after immersion, reaching a value of 1.84 ± 0.23 kΩ cm² after 6.5 hours, corresponding to the point in time where the system behaves

'stable'. Next, its value starts to increase gradually again to a value of 2.43 ± 0.47 kΩ cm² after 168 hours of immersion. For the system with corrosion inhibitor 5 (Fig. 5.6a-b), the R_p value at the start is substantially higher as compared to the system without corrosion inhibitors, but in addition the decrease in the initial stages after immersion is more rapid. After 16 hours, an R_p of 2.15 ± 0.93 kΩ cm² is observed, compared to 0.75 ± 0.13 kΩ cm² for the system without corrosion inhibitors. After 24 hours, the R_p is 1.98 ± 0.81 kΩ cm², which fluctuates and increases slightly to 2.47 ± 0.78 kΩ cm² after 168 hours.

It can be seen that the system with corrosion inhibitor 1 behaves similarly to the system with corrosion inhibitor 2 (Fig. 5.6c-d). Their R_ps are 1.806 ± 0.072 kΩ cm² and 2.01 ± 0.21 kΩ cm² after 1 hour of immersion and decrease strongly in the first hours after immersion to 1.263 ± 0.094 kΩ cm² and 1.55 ± 0.15 kΩ cm², respectively after 12 and 6 hours of immersion . Afterwards the R_p remains approximately equal with time, reaching a value of 1.278 ± 0.049 kΩ cm² and 1.08 ± 0.16 kΩ cm² after 168 hours. At all times, the R_ps are well above the R_p of the hot-dip galvanized steel without corrosion inhibitor. The system with equal combination of corrosion inhibitor 1 and corrosion inhibitor 2 (Fig. 5.6c-d) shows an initial R_p of 35 ± 27 kΩ cm² after 1 hour of immersion which decreases strongly in the first 7 hours after immersion to 24 ± 12 kΩ cm². From this point on, the R_p values become more stable with lower absolute error, corresponding to the stabilization of the electrochemical system after 7 hours. Afterwards, the R_p values decrease gradually over the course of the measurement. Nevertheless, the system consisting of equal amounts of corrosion inhibitor 1 and corrosion inhibitor 2 shows superior behaviour compared to both the system with corrosion inhibitor 1, corrosion inhibitor 2 and the system without corrosion inhibitors. After 10 hours of immersion, the R_p is 22.1 ± 9.0 kΩ cm², compared to 1.321 ± 0.087 kΩ cm², 1.46 ± 0.28 kΩ cm² and 0.75 ± 0.13 kΩ cm² in the case of the system with corrosion inhibitor 1, corrosion inhibitor 2 and the system without corrosion inhibitors, respectively. Afterwards the R_p decreases strongly, reaching an approximately stable value of 14.2 ± 2.5 kΩ cm² and 14.0 ± 5.0 kΩ cm² after 48 hours and 168 hours respectively.

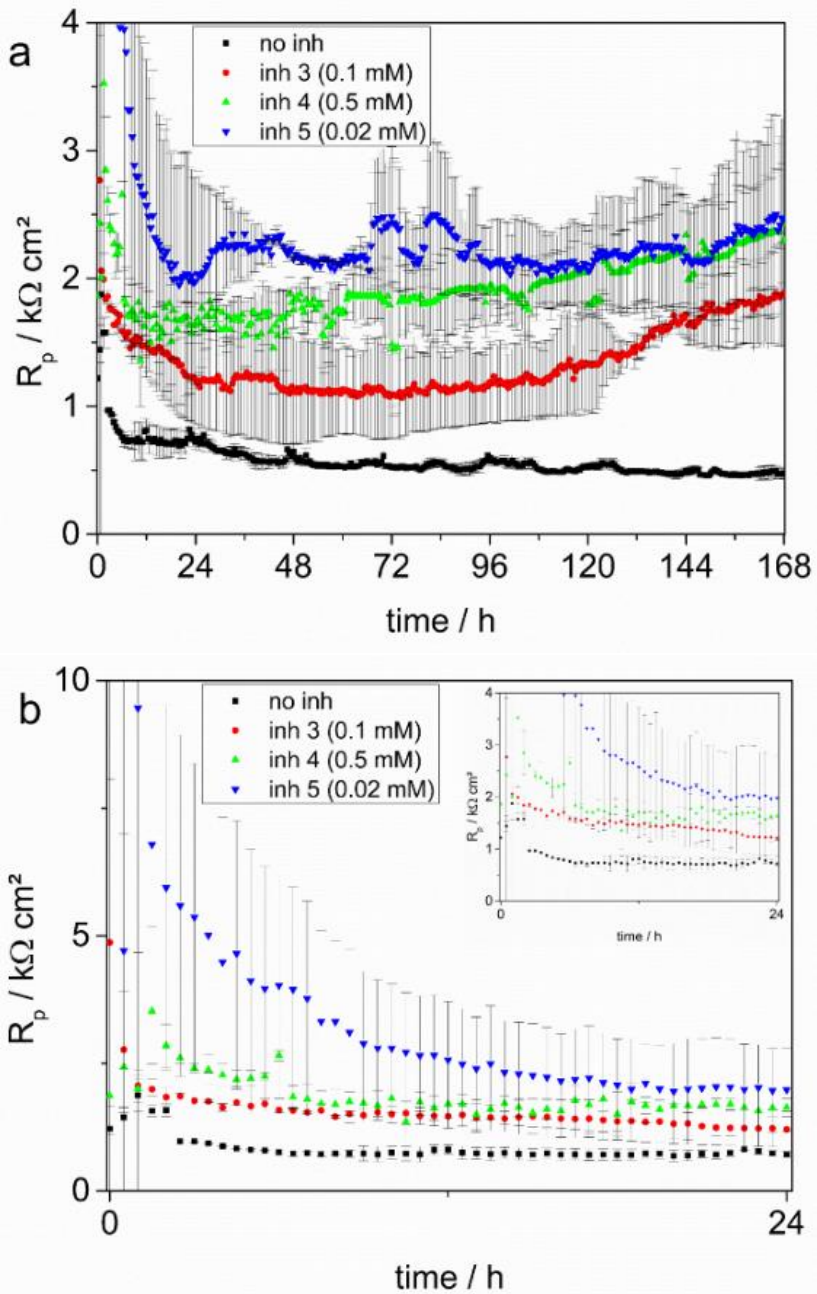

Figure 5.6 Polarization resistance (R_p) results and their standard deviation obtained from electrochemical impedance spectroscopy measurements of hot-dip galvanized steel without corrosion inhibitor (0.05 M NaCl), with inhibitor 3 (0.1 mM Halox SW111), inhibitor 4 (0.5 mM Heucophos Capp) and inhibitor 5 (0.02 mM Zinc Phosphate ZP10) **(a)** and with inhibitor 1 (0.5 mM Novinox ACE110), inhibitor 2 (0.5 mM Novinox XCA02) and inhibitor 1+2 (both 0.5 mM) **(b)** for 168 h.

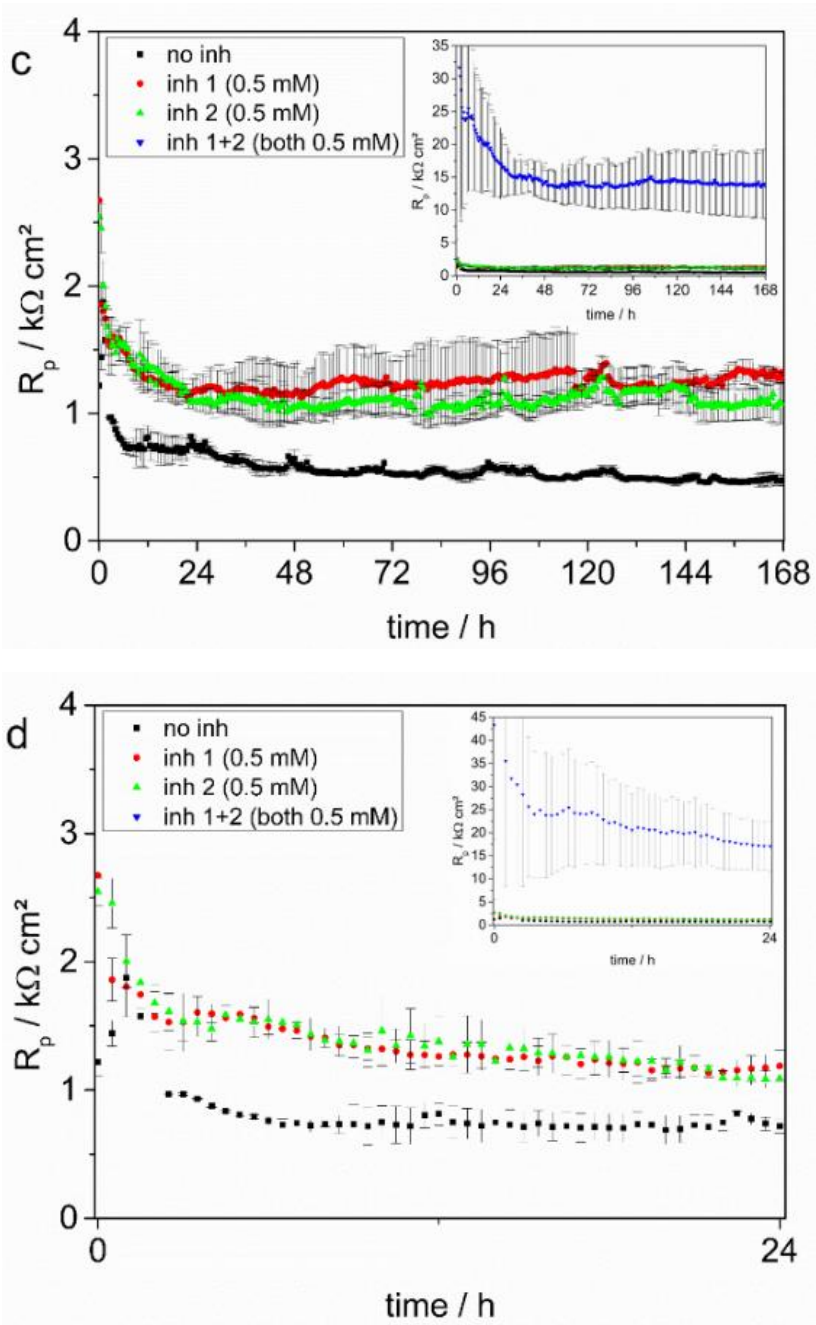

Figure 5.6 (continued)

It can be concluded for corrosion inhibitors 3, 4 and 5 that immediate corrosion protection is observed, indicated by the increase in R_p right at the start after immersion as compared to the system without corrosion inhibitors. During the first 24 hours the R_p decreases strongly. Afterwards, the R_p gradually increases again towards 2 kΩ cm², approximately 4 times higher compared to the 0.50 kΩ cm² observed for the system without corrosion inhibitors. Corrosion inhibitors 1 and 2 show a similar trend with an initial decrease and eventually a gradual increase towards 168 hours. At that stage, the polarization resistance is more than two times higher as compared to the system without corrosion inhibitors. The system with both corrosion inhibitor 1 and corrosion inhibitor 2 behaves superior to its individual constituents and reaches an R_p of 14.0 ± 5.0 kΩ cm² after 168 hours, more than 5 times higher than the sum of its constituents, 1.278 ± 0.049 kΩ cm² and 1.08 ± 0.16 kΩ cm², respectively. Based on these observations it may be concluded that there definitely exists a synergistic combination of corrosion inhibitor 1 and corrosion inhibitor 2.

Yet again, a similar observation can be made regarding the evolution of the R_p values over time, similar to the R_p values obtained from LPR measurements. In the beginning, a decrease and/or increase is noticeable but after a certain time, a stable R_p value is obtained for the remaining of the measurement, related to the stabilization times observed from the ORP-EIS quantitative interpretation per frequency decade.

5.3.5. Electrochemical noise

EN measurements were applied as a non-stationary analysis technique, compared to the previously applied stationary electrochemical techniques and were performed continuously for 24 hours after immersion of the hot-dip galvanized steel in the solution with or without corrosion inhibitor. To make a comparison with the other electrochemical techniques in this work, the EPN and ECN data are divided into windows of 1 hour. Through a discrete wavelet transform (DWT) procedure, the DC drift component for each of the time windows is removed [21]. The noise resistance (R_n) can then be calculated by dividing the standard deviation of the EPN by the standard deviation of the ECN according to [35]:

$$R_n = \frac{std\ (EPN)}{std\ (ECN)} \quad (4)$$

This R_n is then normalized by the area of the working electrode, which is 0.28 cm² for EN measurements. It has been chosen to use this electrochemical parameter because of its correspondence with the polarization resistance R_p [36]. Figure 5.7 shows the R_n values and

their standard deviation of the hot-dip galvanized steel with and without corrosion inhibitors in the first 24 hours after immersion, shown separately for the phosphate- (Fig. 5.7a) and silica- based (Fig. 5.7b) corrosion inhibitors. It should be noted that the indicated times correspond to the starting times of the respective windows. For the system without corrosion inhibitors (Fig. 5.7a), it can be seen that the R_n is 8.3 ± 4.3 kΩ cm² at the start and decreases towards of value of around 2 kΩ cm² after 2 hours and for the remaining of the measurement. In the case of hot-dip galvanized steel with corrosion inhibitor 3, the R_n is 11.9 ± 9.4 kΩ cm² at the start and decreases gradually to 2.46 ± 0.17 kΩ cm² after 11 hours of immersion. Afterwards, the R_n remains around 2.50 kΩ cm² for the remaining of the measurement, slightly higher to the 2 kΩ cm² observed for the hot-dip galvanized steel without corrosion inhibitor. For the system with corrosion inhibitor 4, the R_n is 3.69 ± 0.53 kΩ cm² at the start and increases gradually to 5.5 ± 1.1 kΩ cm² after 10 hours of immersion. Afterwards, the R_n decreases again to reach a value of 2.45 ± 0.56 kΩ cm² after 24 hours, comparable to what was observed for the hot-dip galvanized steel without corrosion inhibitors. In the case of the hot-dip galvanized steel exposed to the solution containing corrosion inhibitor 5, the R_n at the start amounts 13.2 ± 6.0 kΩ cm² but decreases rapidly towards 2.3 ± 1.6 kΩ cm² after 4 hours of immersion, comparable to the system without corrosion inhibitors. Afterwards, R_n increases again over time to a maximum of 4.6 ± 1.6 kΩ cm² after 14 hours of immersion before decreasing again to 3.1 ± 1.4 kΩ cm² after 24 hours. Although a higher value is always obtained compared to the situation without corrosion inhibitor present, no stable R_n value is obtained.

A similar observation can be made for the systems containing corrosion inhibitor 1, corrosion inhibitor 2 and the synergistic combination of corrosion inhibitor 1 and 2. It can be seen that (Fig. 5.7b) there is no effect of corrosion inhibitor 2 on R_n, with similar values as for the hot-dip galvanized steel without corrosion inhibitors. For the system with corrosion inhibitor 1 however, a noticeable increase is visible after 1 hour of immersion: R_n increases to 20.78 ± 0.93 kΩ cm². In the following stages, R_n decreases to 2.05 ± 0.23 kΩ cm² after 18 hours, before gradually increasing again to 4.114 ± 0.055 kΩ cm² after 24 hours. In the case of the hot-dip galvanized steel with both corrosion inhibitor 1 and corrosion inhibitor 2, it can be seen that the R_n is stable throughout the measurement with an average value of 10.2 ± 1.4 kΩ cm², which clearly states the synergistic effect of the two corrosion inhibitors after 5 hours up to 24 hours after immersion. In the first 4 hours after immersion, the R_n of the hot-dip galvanized steel with corrosion inhibitor 1 exceeds the R_n of the combination of inhibitor 1 and 2.

It has to be remarked that the EN technique provides non-stationary information about the electrochemical system and is therefore not directly affected by the 'stabilization' time and non-stationary behaviour, as determined from the quantitative interpretation per frequency decade from the ORP-EIS data. Nevertheless, the relatively high absolute errors on the first R_n values are due to the non-stationary behaviour which affects the DWT procedure used for DC drift removal [11].

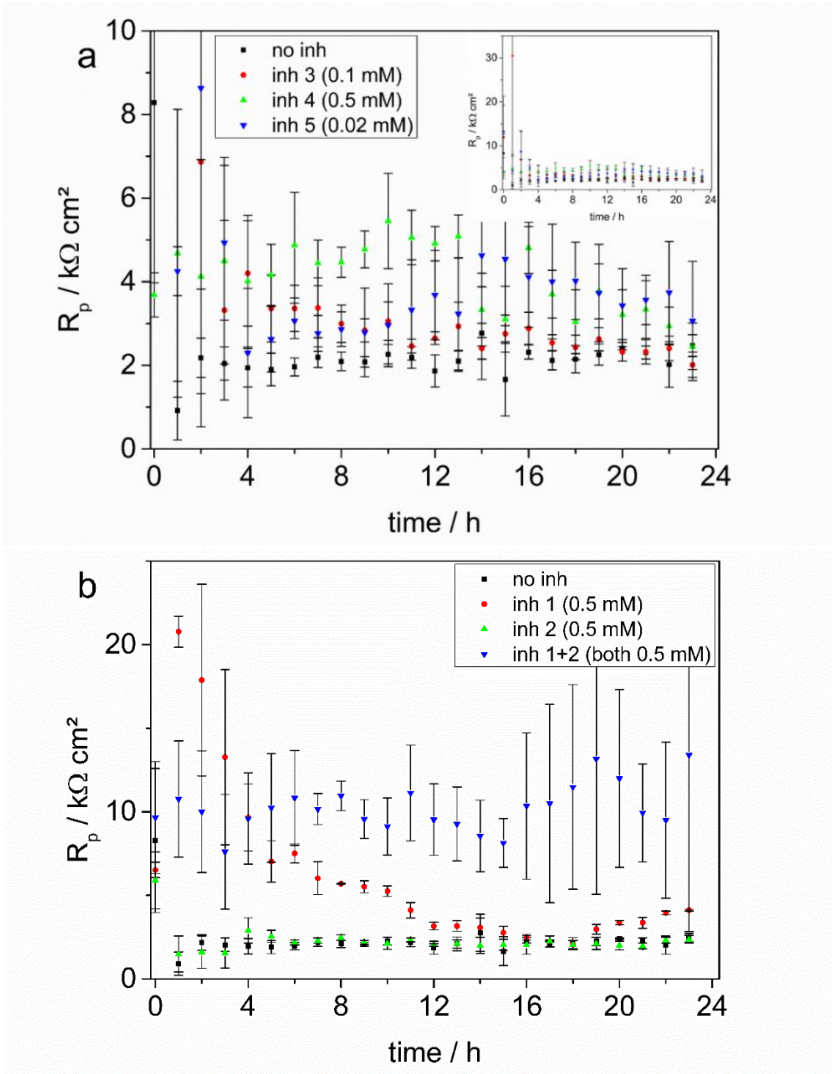

Figure 5.7 Noise resistance (R_n) results and their standard deviation obtained from electrochemical noise measurements of hot-dip galvanized steel without corrosion inhibitor (0.05 mM NaCl), with inhibitor 3 (0.1 mM Halox SW111), inhibitor 4 (0.5 mM Heucophos Capp) and inhibitor 5 (0.02 mM Zinc Phosphate ZP10) **(a)** and with inhibitor 1 (0.5 mM Novinox ACE110), inhibitor 2 (0.5 mM Novinox XCA02) and inhibitor 1+2 (both 0.5 mM) **(b)** in the first 24 h after immersion.

It can be concluded that in the case of the phosphate-based corrosion inhibitors (inhibitors 3, 4 and 5), fluctuations in noise resistance are observed over the course of the measurement. After 24 hours, the noise resistance reaches a value only slightly higher compared to the hot-dip galvanized steel without corrosion inhibitors. In the case of the silica-based corrosion inhibitors (inhibitors 1 and 2), corrosion inhibitor 1 only increases the noise resistance in the initial stages after immersion and corrosion inhibitor 2 has a comparable noise resistance to the system without corrosion inhibitors. In the case of both corrosion inhibitor 1 and 2, a remarkable increase in the noise resistance is observed for the entire measurement, approximately 5 times higher than for the case without corrosion inhibitors.

5.3.6. Comparison of different corrosion inhibitors with different electrochemical techniques in the time-domain.

In the previous paragraphs, different macroscopic electrochemical techniques were applied to study the protective action of different corrosion inhibitors for hot-dip galvanized steel and their results were interpreted according to the stability of the respective electrochemical systems as determined from the quantitative interpretation per frequency decade from ORP-EIS data. In this paragraph, all results obtained from the different macroscopic electrochemical techniques are presented together with the evolution of the relative contribution of the non-stationarities per frequency decade over time.

In order to study the impact of the 'stabilization' time on the results of the respective electrochemical techniques in practice, two characteristic times have been selected: one well before the stabilization time and one well after the stabilization time for each respective system. Taking into account the discrete times in which a PP experiment was performed, 1.5 hours and 24 hours were selected. It needs to be noted that in the case of the LPR technique, where a measurement was performed at discrete times every hour, a LPR value after 1.5 hours is obtained from the average of the Rp values after 1 hour and 2 hours, respectively. In the case of the EN technique, where measurements with a duration of 1 hour were performed, the EN values after 1.5 hour are taken from the Rn values from the measurements that started after 1 hour of immersion and the EN values after 24 hours are taken from the measurements starting after 23 hours and ending after 24 hours. It has been previously discussed that these Rn values are selected because of their equivalence to the polarization resistance [36]. In Figure 5.8, the Rps obtained from LPR, EIS and EN measurements after 1.5 hours and 24 hours are presented with the related absolute errors

on the resistance values. Tables 5.4 and 5.5 present an overview of the respective values and their absolute errors after 1.5 hours and 24 hours, respectively.

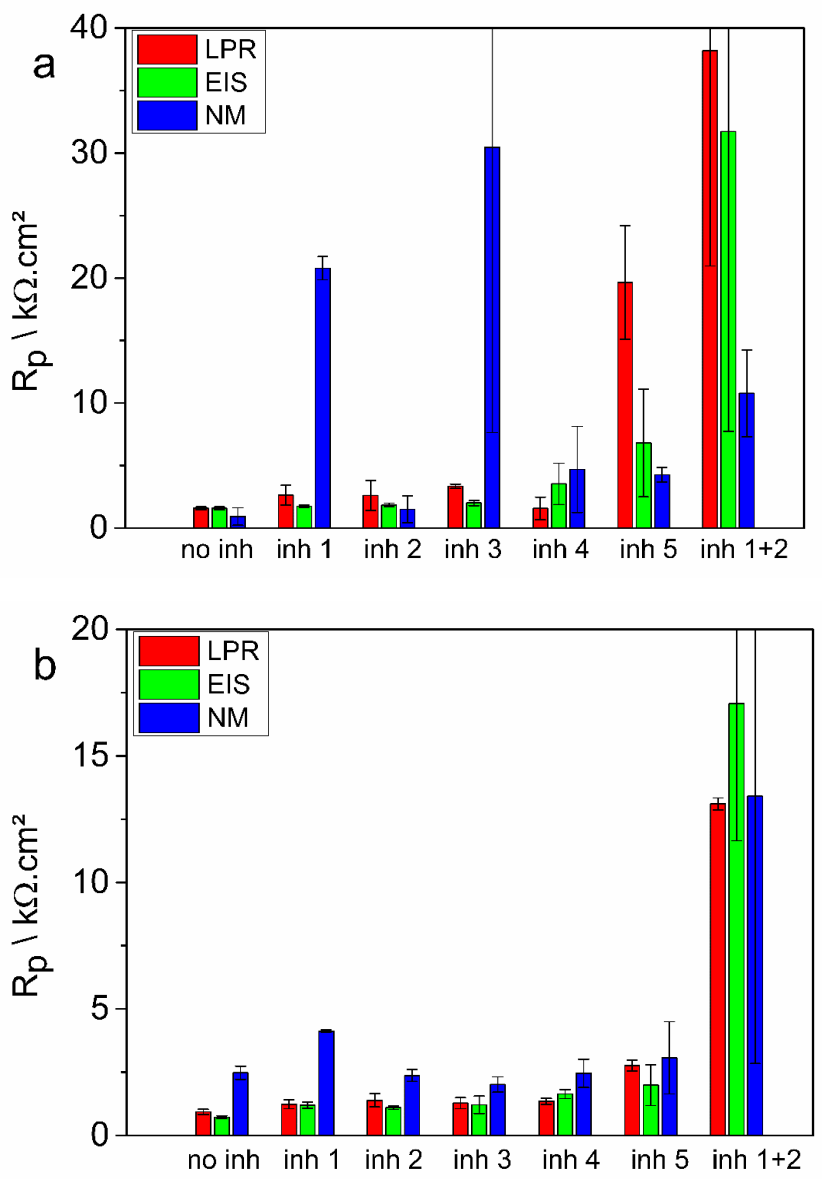

Figure 5.8 Overview of the results obtained through linear polarization resistance (LPR), electrochemical impedance spectroscopy (EIS) and electrochemical noise (EN) measurements for hot-dip galvanized steel with and without corrosion inhibitor after 1.5 h **(a)** and **(b)** 24 h. Inhibitor 1 (Novinox®ACE110); inhibitor 2 (Novinox®XCA02); inhibitor 3 (Halox®SW-111); inhibitor 4 (Heucophos®CAPP); inhibitor 5 (Zinc Phosphate ZP10).

From the results after 1.5 hours (Fig. 5.8a and Table 5.4), it can be seen that the system containing corrosion inhibitor 5 and the system containing corrosion inhibitor 1+2 have an increased Rp, compared for the system without corrosion inhibitor and other corrosion inhibitor containing systems. Nevertheless, all corrosion inhibitor containing systems have an increased Rp compared to the system without corrosion inhibitor. After 24 hours, however, only the system containing the combination of corrosion inhibitor 1 and 2 has a higher Rp. It needs to be remarked that, as mentioned before, when interpreting the results after 1.5 hours (Fig. 5.8a and Table 5.4), the system without corrosion inhibitors as well as the systems with corrosion inhibitors suffer from non-stationary behaviour. This causes the overall system's instability as observed from ORP-EIS measurements. Consequently, the errors on the Rps after 1.5 hours are significantly high, especially the errors on the EN measurements due to the DWT procedure used for DC drift removal [11]. However, it is also possible that EN measurements show these instabilities by significantly high standard deviations and consequently untrustworthy Rn values. After 24 hours, when the system is stable, good agreement between LPR, EIS and EN is observed, with low standard deviations on the Rn values. This indicates that EN measurements could be an indicator of non-stationary behaviour when the respective standard deviations are taken into account.

The R_p for the system containing both corrosion inhibitor 1 and 2 after 24 hours (Fig. 5.8b and Table 5.5) is 13.10 ± 0.23 kΩ cm² and 17.1 ± 5.43 kΩ cm² obtained from LPR and EIS, respectively. For the system containing corrosion inhibitor 1, a R_p of 1.23 ± 0.18 kΩ cm² and 1.19 ± 0.12 kΩ cm² is obtained from LPR and EIS measurements and for the system containing corrosion inhibitor 2, a similar R_p, of 1.39 ± 0.26 kΩ cm² and 1.091 ± 0.067 kΩ cm², is obtained. For both techniques, the R_p of the inhibitor combination is more than 4 times higher than for the sum of the individual corrosion inhibitors. This signifies that the system containing both inhibitors is a synergistic combination of these inhibitors.

For the results after 24 hours (Fig. 5.8b and Table 5.5) all systems are behaving time-invariant resulting in more stable R_p values with lower absolute error. Yet again, it can be confirmed here that the R_p values obtained from LPR and EIS measurements are in good agreement for most of the measurements apart from the measurements containing corrosion inhibitor 5 after 1.5 hours. Therefore the systems will be evaluated from now on based mainly on the R_p values obtained from LPR and EIS measurements.

Table 5.4 R_p values with their absolute error obtained from LPR and EIS measurements and R_n values obtained from EN measurments after 1.5 hours.

	LPR		EIS		EN	
	value (kΩ.cm²)	abs. error (kΩ.cm²)	value (kΩ.cm²)	abs. error (kΩ.cm²)	value (kΩ.cm²)	abs. error (kΩ.cm²)
no inh	1.58	0.12	1.57	0.12	0.92	0.70
inh 1	2.62	0.80	1.74	0.10	20.78	0.93
inh 2	2.60	1.20	1.84	0.14	1.49	1.08
inh 3	3.34	0.17	1.99	0.20	30.47	22.83
inh 4	1.57	0.90	3.53	1.65	4.68	3.44
inh 5	19.65	4.55	6.79	4.30	4.25	0.59
inh 1+2	38.19	17.23	31.71	24.00	10.77	3.47

Table 5.5 R_p values with their absolute error obtained from LPR and EIS measurements and R_n values obtained from EN measurments after 24 hours.

	LPR		EIS		EN	
	value (kΩ.cm²)	abs. error (kΩ.cm²)	value (kΩ.cm²)	abs. error (kΩ.cm²)	value (kΩ.cm²)	abs. error (kΩ.cm²)
no inh	0.93	0.11	0.72	0.05	2.47	0.26
inh 1	1.23	0.18	1.19	0.12	4.11	0.06
inh 2	1.39	0.26	1.09	0.07	2.37	0.23
inh 3	1.27	0.22	1.21	0.35	2.01	0.30
inh 4	1.35	0.12	1.63	0.18	2.45	0.56
inh 5	2.76	0.21	1.98	0.81	3.06	1.43
inh 1+2	13.10	0.23	17.07	5.43	13.41	10.57

In our previous work, it has been observed that there is a correlation between the stability of electrochemical processes, obtained from ORP-EIS, and the stability of the Rp values obtained from LPR and EIS measurements whereas a substantial difference with the results from EN is observed in the first 24 hours after immersion [11]. In this paragraph, the same interpretation is done for the systems discussed here serving as the deciding tool for the trustworthiness of the electrochemical values and of the related effectiveness of the respective corrosion inhibitors. In Figure 5.9, the Rp values of the hot-dip galvanized steel without corrosion inhibitors and with corrosion inhibitor 3, 4 and 5 (the phosphate- based corrosion inhibitors) obtained through LPR, EIS and EN measurements and coupled to the relative contribution of the non-stationarities of the ORP-EIS measurements for the first 24 hours after immersion. In Figure 5.10, the same comparison is made similarly for corrosion inhibitor 1, 2 and the combination of 1 and 2 (the silica- based corrosion inhibitors).

For the hot-dip galvanized steel without corrosion inhibitors (Fig. 5.9a), the Rp values obtained from LPR and EIS follow a similar trend over the course of the measurement: both decrease strongly in the first 10 hours, reaching a stable value of 0.99 ± 0.12 kΩ cm² for the LPR measurement and 0.75 ± 0.13 kΩ cm² for the EIS measurement, respectively. This time window corresponds to the time the relative contribution of the non-stationarities in frequency decades IV and III needs to become stable. Since these frequency decades were the last to stabilize, as discussed during the ORP-EIS interpretation, these present a fully time-invariant and consequently 'stable' electrochemical system from this point on.

In the case of the hot-dip galvanized steel with corrosion inhibitor 3 (Fig. 5.9b), three distinct regions in time are observed. In the first hours after immersion, the Rps obtained through LPR and EIS measurements are substantially different and decrease strongly towards 2.083 ± 0.030 kΩ cm² and 1.638 ± 0.073 kΩ cm² after 4 hours, respectively. At the same time, the relative contribution of the non-stationarities in frequency decades IV, III and II decreases strongly and stabilizes after 4 hours. In the following hours, their contribution remains initially at the same level, before decreasing towards a stable value after 10 hours. This is reflected in fluctuations in the Rp values from LPR mainly and stabilization of the Rp obtained from LPR and EIS after 10 hours. At this time, the respective Rp values are 1.62 ± 0.16 kΩ cm² and 1.51 ± 0.18 kΩ cm², respectively. After 10 hours, the system is fully stationary, reflected in stable values of the respective Rp values.

The system containing corrosion inhibitor 4 (Fig. 5.9c) initially behaves non-stationary, reflected in the high relative contribution of the non-stationarities in the middle frequency region (decades IV and III). This is translated in unstable Rp values obtained from LPR and EIS initially. Afterwards, the relative contribution of the non-stationarities in the middle frequency region decreases towards a stable value after 6.5 hours of immersion. At the same time, the Rp values from LPR and EIS decrease gradually towards 1.32 ± 0.12 kΩ cm² and 1.84 ± 0.23 kΩ cm² after 6.5 hours, respectively. Afterwards, when the system is behaving fully stationary, due to the stabilization of the electrochemical processes with characteristic time-constants corresponding to the mid frequency region, stable values of Rp from both techniques are obtained.

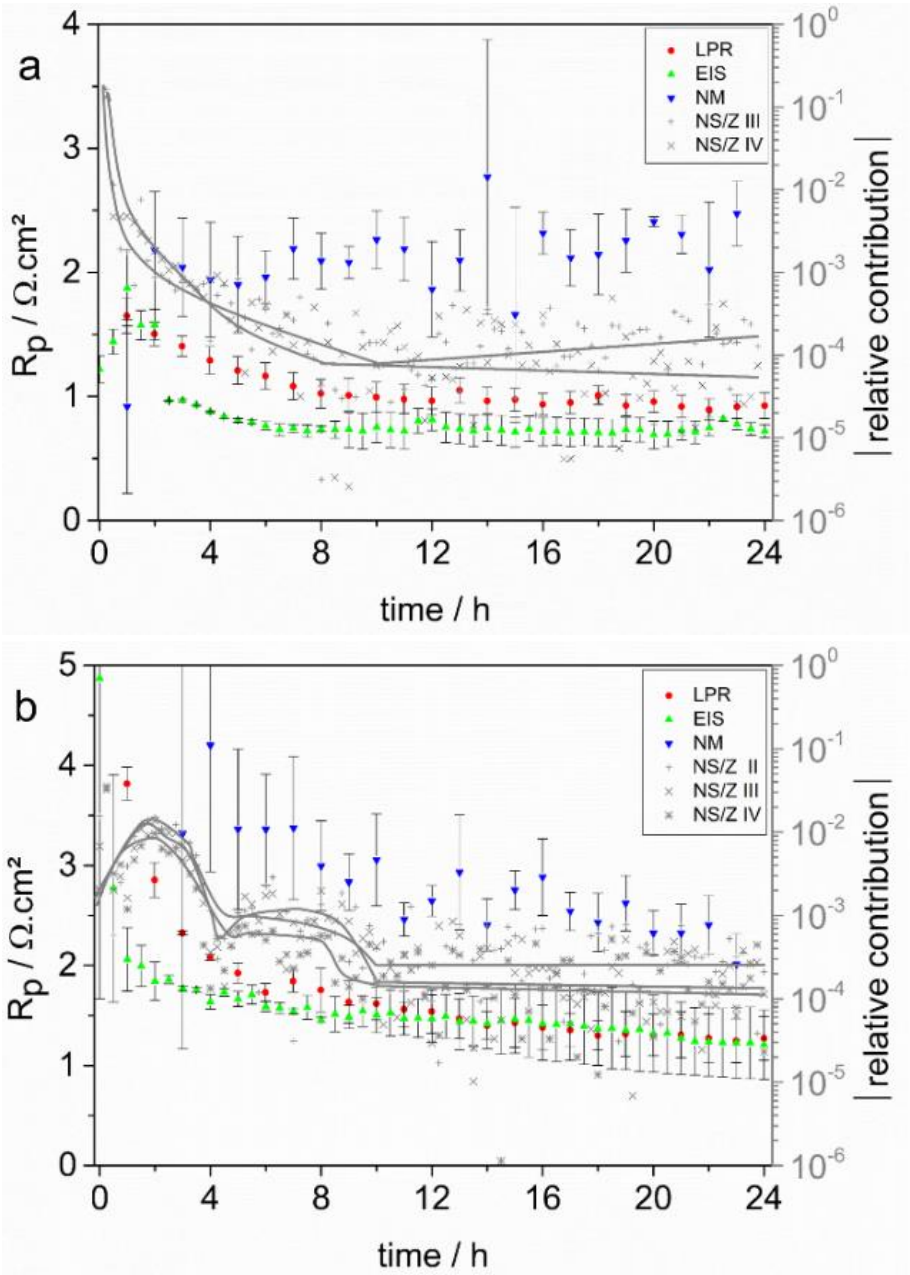

Figure 5.9 Overview of the results obtained through linear polarization resistance (LPR), electrochemical impedance spectroscopy (EIS), electrochemical noise (EN) and odd-random-phase electrochemical impedance spectroscopy (ORP-EIS) measurements for hot-dip galvanized steel with and without corrosion inhibitor for 24 h. Without corrosion inhibitors (0.05 mM NaCl) **(a)**, corrosion inhibitor 3 (0.1 mM Halox®SW-111) **(b)**, corrosion inhibitor 4 (0.5 mM Heucophos®CAPP) **(c)** and corrosion inhibitor 5 (0.02 mM Zinc Phosphate ZP10) **(d)**.

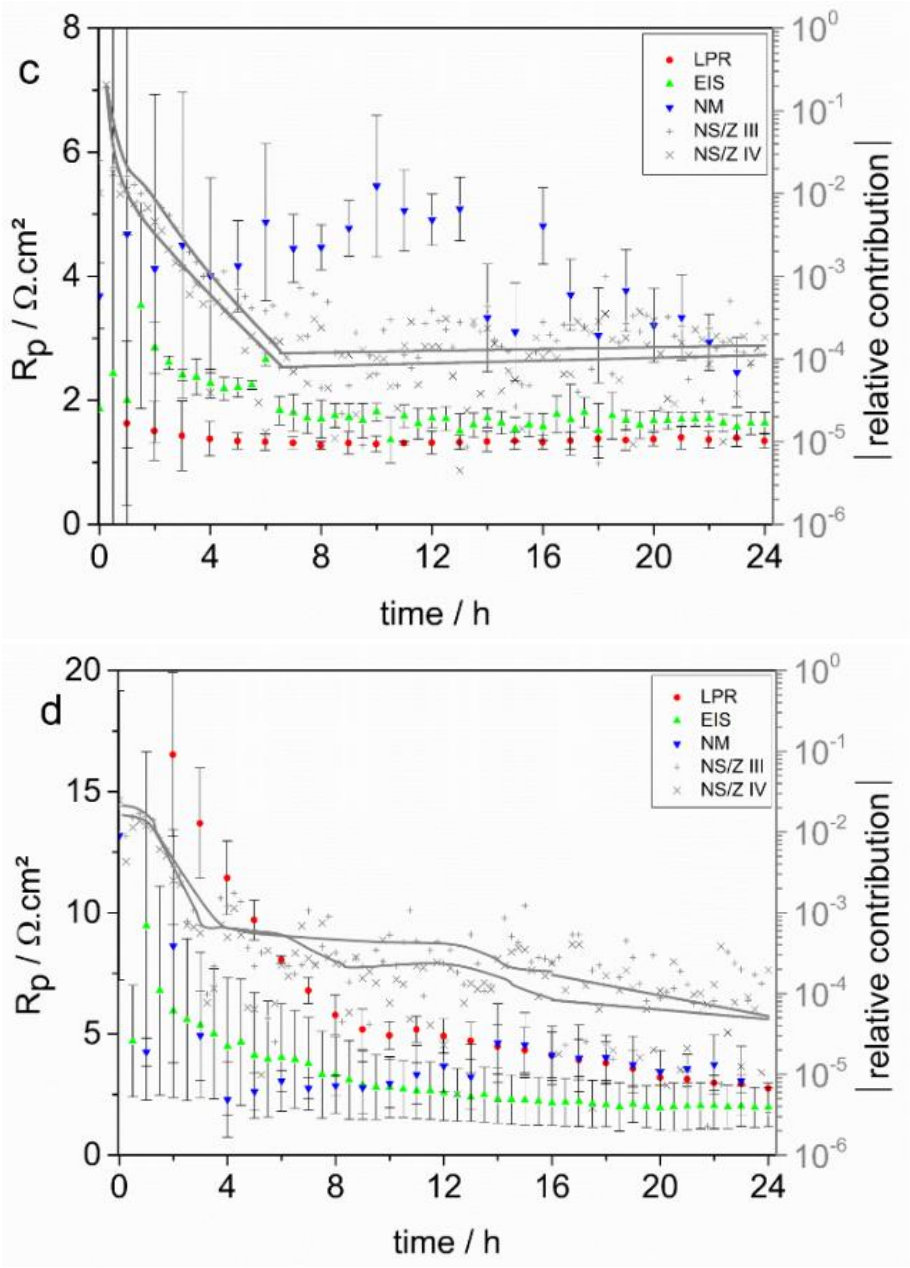

Figure 5.9 (continued)

For the hot-dip galvanized steel with corrosion inhibitor 5 (Fig. 5.9d), the R_p values obtained from LPR and EIS decrease gradually as a function of time towards a value of 4.12 ± 0.95 kΩ cm² and 2.15 ± 0.93 kΩ cm² after 16 hours of immersion. This time corresponds to the time

needed to stabilize, over different plateaus, the electrochemical processes with time-constants corresponding to the middle frequency decades (IV and III). Afterwards, the R_p value obtained from EIS remains stable for the remaining course of the measurement. The R_p value obtained from LPR decreases slightly, but compared to its initial evolution, this slight decrease is negligible.

For the system containing corrosion inhibitor 1 (Fig. 5.10a), it can be seen that the relative contribution of the non-stationarities in the middle frequency decades (III and II) dominates the instability of the system. Only after 11 and 12 hours, respectively, their contribution becomes stable and the system can be considered as time-invariant. This is reflected in the behaviour of the R_p values from LPR and EIS. Only after 12 hours, an R_p value of 1.38 ± 0.33 kΩ cm² and 1.263 ± 0.094 kΩ cm² is obtained from LPR and EIS measurements, respectively.

For the system containing corrosion inhibitor 2 (Fig. 5.10b), the 'instability' of the overall electrochemical system is governed by the electrochemical processes with time-constants corresponding to the lower frequency region (decade II) since the relative contribution of the non-stationarities in this frequency decade stabilizes later compared to the middle and higher frequency region. In this case, this is only reflected in the behaviour of the R_p obtained from EIS measurements, which stabilizes at 1.55 ± 0.15 kΩ cm² after 6 hours of immersion and not in the behaviour of the R_p from LPR measurements, which fluctuates at later stages over the course of the measurement.

The R_p of the hot-dip galvanized steel with the combination of corrosion inhibitor 1 and 2 obtained from LPR and EIS measurements (Fig. 5.10c) decreases rapidly to 28.8 ± 8.1 kΩ cm² and 26 ± 15 kΩ cm² after 3 hours of immersion and 21.3 ± 1.7 kΩ cm² and 24 ± 12 kΩ cm² after 7 hours of immersion. Afterwards both values tend to stabilize and decrease only slightly over the course of the measurement. A similar trend is observed in the relative contribution of the non-stationarities in the middle (IV and III) and higher frequency (V) decades which stabilize after 7 hours respectively.

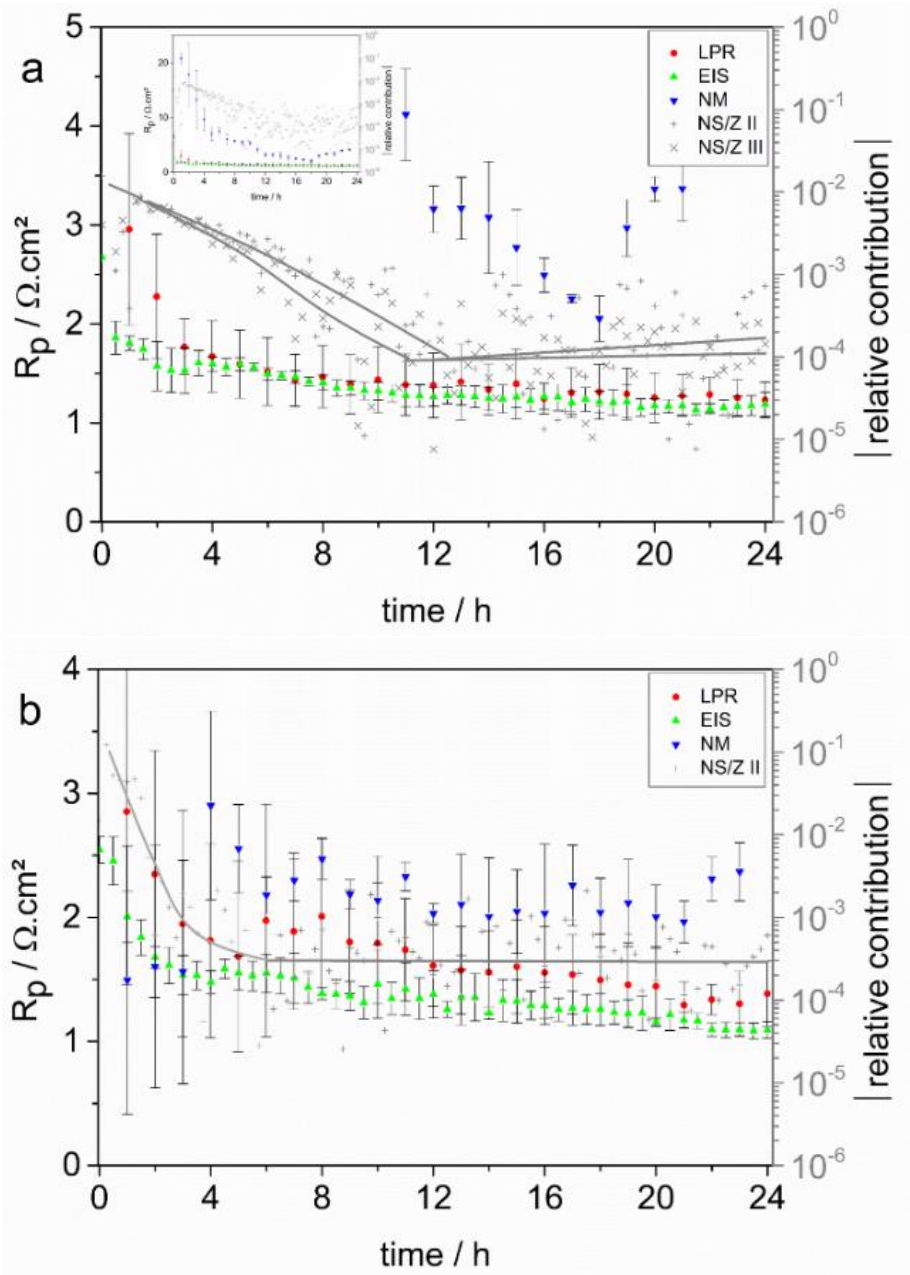

Figure 5.10 Overview of the results obtained through linear polarization resistance (LPR), electrochemical impedance spectroscopy (EIS), electrochemical noise (EN) and odd-random-phase electrochemical impedance spectroscopy (ORP-EIS) measurements for hot-dip galvanized steel with corrosion inhibitor 1 (0.5 mM Novinox®ACE110) **(a)**, corrosion inhibitor 2 (0.5 mM Novinox®XCA02) **(b)** and corrosion inhibitor 1+2 (both 0.5 mM) **(c)** for 24 h.

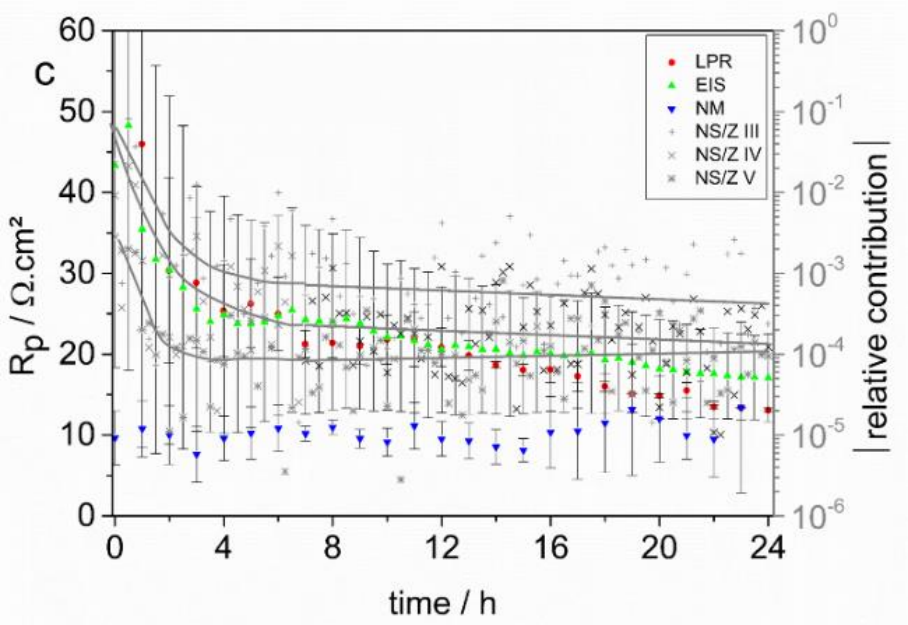

Figure 5.10 (continued)

It can be concluded that it is difficult to compare the electrochemical results obtained with different electrochemical techniques after 1.5 hours since the system without corrosion inhibitors as well as the systems with corrosion inhibitors is behaving non-stationary. This is reflected in significantly high errors on the respective R_p values at this stage. After 24 hours, when the systems are behaving fully time-invariant, the errors on R_p become smaller. The combination of both inhibitor 1 and 2 is definitely a synergistic combination, based on the comparison between the R_p values from LPR and EIS on the one hand and the values of the individual components on the other hand. In general, before the characteristic stabilization of each respective electrochemical system, when the system is behaving in a non-stationary way, non-stable R_p values from LPR and EIS are obtained. After the characteristic stabilization time, the system behaves in a fully stationary way and stable R_p values from LPR and EIS are obtained for the remaining of the experiment.

5.3.7. High-throughput corrosion testing

Up to now, different macroscopic electrochemical techniques have been applied for the screening of corrosion inhibitors and corrosion inhibitor synergy for hot-dip galvanized steel. Another potential strategy for the screening of corrosion inhibitors could be the application of a high-throughput method. Therefore, the aim of is this paragraph is to compare the previously discussed macroscopic electrochemical results with the results from a high-throughput corrosion inhibitor testing procedure previously developed for AA2024-T3 [23].

From the high-throughput corrosion testing measurements after 5 hours (Table 5.6), it can be seen that for 0.5 wt% NaCl a corrosion value of 2 is obtained, for a 0.05 wt% NaCl a corrosion value of 5 and for all other concentrations, from $5 \cdot 10^{-3}$ wt% to $5 \cdot 10^{-6}$ wt% NaCl, a corrosion value of 6. For the demineralized water and the measurement without solution (representing situations where we suspect no visible corrosion), corrosion values of 6 and 5 are obtained. This indicates that for decreasing concentrations of NaCl up to zero amount of NaCl, the corrosion values increase, reaching a maximum of value 6. From the high-throughput measurements after 24 hours (Table 5.7), it can be seen that for both a 0.1 M NaCl and a 0.05 M NaCl solution, a corrosion value of 4 is obtained. In case of the demineralized water and the measurement without solution, corrosion values of 9 and 8 are obtained. This indicates that after 24 hours, a maximum corrosion value of 9 can be reached, for situations where no visible corrosion is expected. This indicates that for the high-throughput corrosion testing for hot-dip galvanized steel, the corrosion number is inversely proportional with the amount of corrosion. As such, the results for the hot-dip galvanized steel in combination with different corrosion inhibitors can be interpreted.

It can be seen that after 5 hours of immersion (Table 5.6), a corrosion value of 5 to 6 is obtained for corrosion inhibitors 1, 2 and 4 (all 0.5 mM). These values correspond to the values obtained for lower concentrations of NaCl, demineralized water and the measurement without solution, indication a relatively low amount of corrosion.

After 24 hours of high-throughput corrosion testing (Table 5.7), the corrosion values of inhibitor 1 and inhibitor 2 remained 6 and 7, respectively, while the corrosion value of inhibitor 4 decreased to 3. This indicates that inhibitor 1 and 2 (both 0.5 mM in 0.05 M NaCl) show less severe corrosion attack, compared to both the same and the double NaCl concentration without inhibitor. On the other hand, inhibitor 4 shows more corrosion compared to the situation without inhibitor. This indicates that corrosion inhibitors 1, 2 and 4 are providing immediate corrosion protection, but that only corrosion inhibitor 1 and 2 are providing corrosion protection over a time span of 24 hours. For corrosion inhibitor 3 (0.1

mM in 0.05 M NaCl) and inhibitor 5 (0.02 mM in 0.05 M NaCl), corrosion values of 4 and 3 are obtained, respectively, similarly to the situation without corrosion inhibitor.

Table 5.6 Corrosion values from the 5 h high-throughput corrosion testing

	5 h	
Solution	Corrosion value	Std. dev.
0.5% NaCl	2	2.7
0.05% NaCl	5	2.3
0.005% NaCl	6	2.4
0.0005% NaCl	6	2.0
0.00005% NaCl	6	1.4
0.000005% NaCl	6	1.4
demineralized water	6	0.9
empty	5	0.1
inhibitor 1 (0.5 mM)	5	1.6
inhibitor 2 (0.5 mM)	5	1.6
inhibitor 4 (0.5 mM)	6	1.1

Table 5.7 Corrosion values from the 24 h high-throughput corrosion testing

	24 h	
Solution	Corrosion value	Std dev.
0.1 M NaCl	4	0.8
0.05 M NaCl	4	0.1
demineralized water	9	1.5
empty	8	1.5
inhibitor 1 (0.5 mM)	6	1.7
inhibitor 2 (0.5 mM)	7	1.6
inhibitor 3 (0.1 mM)	4	0.9
inhibitor 4 (0.5 mM)	3	1.2
inhibitor 5 (0.02 mM)	3	0.2

It can be concluded that the results for corrosion inhibitor 1 and corrosion inhibitor 2 after 5 and 24 hours and the results for corrosion inhibitor 4 after 5 hours are in line with what was obtained from the macroscopic electrochemical techniques, whereas the results for corrosion inhibitor 3, 4 and 5 after 24 hour are not. The rapid, high-throughput corrosion testing technique provides only a rough indication of the corrosion inhibitors and their effectiveness for further electrochemical investigation. The differences between the results after 5 hours and 24 hours (for example corrosion inhibitor 4) highlight the importance of the electrochemistry in the time-domain and indicate that further (macroscopic) electrochemical investigation is strictly necessary.

5.4. Conclusions

In this work, different macroscopic electrochemical techniques were applied for the screening of silica- and phosphate- based corrosion inhibitors and corrosion inhibitor synergy for the protection of hot-dip galvanized steel, taking into account the electrochemical time-domain studied by ORP-EIS.

Quantitative interpretation of the ORP-EIS data per frequency decade indicated that for each electrochemical system with and without corrosion inhibitors, a certain period of time is required before the system behaves in a stationary way. Prior to this system-dependent stabilization time, the system behaves in a non-stationary fashion, while afterwards, the system can be considered as a fully stationary system. This effect has an unneglectable impact on the interpretation of the electrochemical results. Initially, the polarization resistance (Rp) or noise resistance (Rn) values obtained from potentiodynamic polarization (PP), linear polarization resistance (LPR), electrochemical impedance spectroscopy (EIS) and electrochemical noise (EN) measurements are generally 'unstable' and suffer from relatively high absolute error. This is due to either the application of a stationary technique in the non-stationary regime or the influence of the non-stationary behaviour on the data treatment procedure. After the period of stabilization, the values are more stable with lower absolute error.

The quantitative interpretation per frequency decade of ORP-EIS data indicated that for the phosphate- as well as the silica-based corrosion inhibitors, the non-stationarities are dominating the system's 'instability'. Some corrosion inhibitors effectively stabilize the electrochemical interface while other prolong the electrochemical stability. Nevertheless, the combination of both silica-based corrosion inhibitors stabilizes the electrochemical interface to the largest extent.

PP measurements revealed that all corrosion inhibitors are behaving as cathodic corrosion inhibitors, effectively reducing the cathodic current densities. Studying the influence of concentration showed no particular trend for neither the silica based nor the phosphate based corrosion inhibitors.

The hourly application of LPR measurements revealed that both the phosphate- and silica-based corrosion inhibitors provide immediate corrosion protection as well as protection over the course of the measurement. After 168 hours, the polarization resistance is approximately two to three times higher compared to the situation without corrosion inhibitors. However, the combination of both silica-based inhibitors exhibits a synergistic

effect with an Rp value approximately three times higher than the sum of its constituents and approximately 15 times higher than the case without corrosion inhibitors after 168 hours.

Characterization by EIS revealed the presence of corrosion inhibitor protective action in the middle frequency region, having a positive effect on the overall performance of the corrosion inhibitor-containing electrochemical systems. The phosphate- and silica-based corrosion inhibitors exhibit an increase in polarization resistance of respectively 4 and 2 times higher as compared to the system without corrosion inhibitor. Yet again, it has been observed that the combination of both silica-based corrosion inhibitors has a synergistic effect with an increase in polarization resistance of more than 5 times as compared to the sum of the values of the individual components.

EN measurements on the phosphate-based corrosion inhibitors revealed no effective corrosion protection over the course of 24 hours compared to the system without corrosion inhibitors. For the silica-based corrosion inhibitors, the synergistic action is yet again confirmed.

When comparing the results obtained from different macroscopic electrochemical techniques, the 'stability' of the system in terms of the presence of non-stationarities should be taken into account. As such, the results after 1.5 hours are less significant. However, the results after 24 hours confirm the synergistic effect by combining both silica-based corrosion inhibitors. The comparison in the first 24 hours, taking into account the relative contribution of the non-stationarities, shows that the evaluation with LPR and EIS provides similar results based on the polarization resistance. However, LPR only describes the overall performance over time while EIS also details the corrosion protective mechanisms.

Comparison of the results obtained from the electrochemical techniques with the results obtained from a high throughput corrosion testing procedure highlights the importance of the electrochemistry in the time-domain and the necessity of detailed (macroscopic) electrochemical analysis.

In terms of corrosion inhibition performance, the combination of both silica-based corrosion inhibitors (inhibitor 1 and inhibitor 2) presents a system with high polarization resistance and fast 'stabilization' of the electrochemical interface as compared to the values of the individual components and the system without corrosion inhibitors.

References

1. Gharbi, O., Thomas, S., Smith, C., & Birbilis, N. (2018). Chromate replacement: what does the future hold? *npj Materials Degradation*, *2*(1), 12.
2. Umoren, S. A., & Solomon, M. M. (2016). Synergistic corrosion inhibition effect of metal cations and mixtures of organic compounds: A Review. *Journal of Environmental Chemical Engineering*, *5*(1), 246–273.
3. Taylor, S. R., & Chambers, B. D. (2008). Identification and characterization of nonchromate corrosion inhibitor synergies using high-throughput methods. *Corrosion*, *64*(3), 255–270.
4. Ebrahimi, M., Shahrabi, T., & Hosseini, M. G. (2004). Determination of suitable corrosion inhibitor formulation for a potable water supply. *Anti-Corrosion Methods and Materials*, *51*(6), 399–405.
5. Romagnoli, R., Deyá, M. C., & Del Amo, B. (2003). The mechanism of the anticorrosive action of calcium-exchanged silica. *Surface Coatings International Part B: Coatings Transactions*, *86*(2), 135–141.
6. Granizo, N., Martín, M. I., López, F. A., Vega, J. M., De La Fuente, D., & Morcillo, M. (2011). Chemical and structural changes of calcium ion exchange silica pigment in 0.5M NaCl and 0.5M Na2SO4 solutions. *Afinidad*, *68*(556), 439–446.
7. Naderi, R., Arman, S. Y., & Fouladvand, S. (2014). Investigation on the inhibition synergism of new generations of phosphate-based anticorrosion pigments. *Dyes and Pigments*, *105*, 23–33.
8. M. Mahdavian, M. M. A. (2005). Evaluation of zinc phosphate and zinc chromate effectiveness via AC and DC methods. *Progress in Organic Coatings, 53(3)*, 191–194.
9. Askari, F., Ghasemi, E., Ramezanzadeh, B., & Mahdavian, M. (2016). Synthesis and characterization of the fourth generation of zinc phosphate pigment in the presence of benzotriazole. *Dyes and Pigments, 124*, 18–26.
10. Bethencourt, M., Botana, F. J., Marcos, M., Osuna, R. M., & Sánchez-amaya, J. M. (2003). Inhibitor properties of " green " pigments for paints, *Progress in Organic Coatings, 46,* 280-287.
11. Meeusen, M., Zardet, L., Homborg, A. M., Lekka, M., Andreatta, F., Fedrizzi, L., Boelen, B., Terryn, H., Mol, J.M.C. (2019). Complementary Electrochemical Approach for Time-Resolved Evaluation of Corrosion Inhibitor Performance. *J. Electrochem. Soc.*, *166*(11), 3220–3232.
12. ASTM D 6386. (2005). Standard Practice for Preparation of Zinc (Hot-Dip Galvanized) Coated Iron and Steel Product and Hardware Surfaces for Painting. *Annual Book of*

ASTM Standards, *02*(Reapproved), 1–12.

13. Van Ingelgem, Y., Tourwé, E., Blajiev, O., Pintelon, R., & Hubin, A. (2009). Advantages of odd random phase multisine electrochemical impedance measurements. *Electroanalysis*, *21*(6), 730–739.
14. Van Gheem, E., Pintelon, R., Vereecken, J., Schoukens, J., Hubin, A., Verboven, P., & Blajiev, O. (2004). Electrochemical impedance spectroscopy in the presence of non-linear distortions and non-stationary behaviour Part I: Theory and validation. *Electrochimica Acta*, *49*(26), 4753–4762.
15. Atkinson, K. E., & Wiley, J. (1978). *An introduction to numerical analysis, second edition*.
16. Cole, T. J. (1984). Too many digits : the presentation of numerical data. *Arch. Dis. Child., 100,* 608.
17. Kordi, R. (2011). Sports Medicine Update, *Scandinavian Journal of Medicine and Science in Sports, 21,* 867–868.
18. ASTM. (1999). ASTM G3-89 Standard Practice for Conventions Applicable to Electrochemical Measurements in Corrosion Testing, *89*(Reapproved), 1–10.
19. Mansfeld, F. (2009). Fundamental aspects of the polarization resistance technique-the early days. *Journal of Solid State Electrochemistry*, *13*(4), 515–520.
20. Homborg, A. M., Van Westing, E. P. M., Tinga, T., Ferrari, G. M., Zhang, X., De Wit, J. H. W., & Mol, J. M. C. (2014). Application of transient analysis using Hilbert spectra of electrochemical noise to the identification of corrosion inhibition. *Electrochimica Acta*, *116*, 355–365.
21. Homborg, A. M., Tinga, T., Zhang, X., Van Westing, E. P. M., Oonincx, P. J., De Wit, J. H. W., & Mol, J. M. C. (2012). Time-frequency methods for trend removal in electrochemical noise data. *Electrochimica Acta*, *70*, 199–209.
22. Homborg, A. M., Cottis, R. A., & Mol, J. M. C. (2016). An integrated approach in the time, frequency and time-frequency domain for the identification of corrosion using electrochemical noise. *Electrochimica Acta*, *222*, 627–640.
23. White, P. a., Smith, G. B., Harvey, T. G., Corrigan, P. a., Glenn, M. a., Lau, D., Hardin, S.G., Mardel, J., Markley, T.A., Muster, T.H., Sherman, N., Garcia, S.J., Mol, J.M.C., Hughes, A.E. (2012). A new high-throughput method for corrosion testing. *Corrosion Science*, *58*, 327–331.
24. Buchanan, R. A., & Stansbury, E. E. (2012). *Handbook of Environmental Degradation of Materials*.
25. Ismail, K. M. (2007). Evaluation of cysteine as environmentally friendly corrosion inhibitor for copper in neutral and acidic chloride solutions. *Electrochimica Acta*, *52*(28), 7811–7819.

26. Badea G E, Caraban A, Sebesan M, Cret P, & Setel A. (2010). Polarisation Measurements Used for Corrosion Rates Determination. *Journal of Sustenable Energy*, *1*(1), 1–4.
27. Kartsonakis, I. A., Stanciu, S. G., Matei, A. A., Hristu, R., Karantonis, A., & Charitidis, C. A. (2016). A comparative study of corrosion inhibitors on hot-dip galvanized steel. *Corrosion Science*, *112*, 289–307.
28. Mouanga, M., & Berçot, P. (2010). Comparison of corrosion behaviour of zinc in NaCl and in NaOH solutions; Part II: Electrochemical analyses. *Corrosion Science*, *52*(12), 3993–4000.
29. Barranco, V., Feliu, S., & Feliu, S. (2004). EIS study of the corrosion behaviour of zinc-based coatings on steel in quiescent 3% NaCl solution. Part 1: Directly exposed coatings. *Corrosion Science*, *46*(9), 2203–2220.
30. Deslouis, C., Duprat, M., & Tournillon, C. (1989). The kinetics of zinc dissolution in aerated sodium sulphate solutions. A measurement of the corrosion rate by impedance techniques. *Corrosion Science*, *29*(1), 13–30.
31. Da Silva, P. S. G., Costa, A. N. C., Mattos, O. R., Correia, A. N., & De Lima-Neto, P. (2006). Evaluation of the corrosion behavior of galvannealed steel in chloride aqueous solution and in tropical marine environment. *Journal of Applied Electrochemistry*, *36*(3), 375–383.
32. van Westing, E. P. M., Ferrari, G. M., & de Wit, J. H. W. (1994). The determination of coating performance with impedance measurements-IV. Protective mechanisms of anticorrosion pigments. *Corrosion Science*, *36*(8), 1323–1346.
33. Zheludkevich, M. L., Yasakau, K. A., Bastos, A. C., Karavai, O. V., & Ferreira, M. G. S. (2007). On the application of electrochemical impedance spectroscopy to study the self-healing properties of protective coatings. *Electrochemistry Communications*, *9*(10), 2622–2628.
34. Macdonald, J. R., & Barsoukov, E. (2005). *Impedance Spectroscopy Theory , Experiment , and Applications*. *Wiley intersience* (Vol. 125). Wiley-Interscience.
35. Dong, Z., Guo, X., Zheng, J., & Xu, L. (2001). Calculation of noise resistance by use of the discrete wavelets transform. *Electrochemistry Communications*, *3*(10), 561–565.
36. Chen, J.F., Bogaerts, W. F. (1995). The Physical meaning of noise resistance. *Corrosion Science*, *37*(11), 1839–1842.

Chapter 6

Conclusions and recommendations

6.1. Introduction

Corrosion inhibitor research has been performed for decades, including dedicated electrochemical research and surface analysis. A variety of electrochemical and surface analysis techniques have been developed and applied over the years for the investigation of corrosion inhibitor-containing electrochemical systems in particular. In practice, usually a combination of a couple of conventional electrochemical and surface analysis techniques is used in such a way that both mechanistic information as well as the corrosion protective performance can be studied. Among these conventional techniques are potentiodynamic polarization (PP), electrochemical impedance spectroscopy (EIS) as electrochemical techniques and scanning electron microscopy with energy dispersive X-ray spectroscopy (SEM-EDX) and Fourier transform infrared spectroscopy (FTIR) as surface analysis techniques.

However, one important aspect that is usually overlooked is the time-effect, describing how the electrochemical system behaves and how the electrochemical stability is altered over time. This is of huge importance when studying rapidly evolving electrochemical systems and when information about the initial and developing corrosion protective properties and the underlying corrosion (inhibition) mechanism is required. This PhD work questions the widely used classical approach followed in corrosion inhibitor research. We developed a methodology that takes into account also the time-effect when studying an electrochemical system for mechanistic and protective performance information.

This methodology consists in the use of odd random phase electrochemical impedance spectroscopy (ORP-EIS) as the electrochemical tool to study the stability/instability of corrosion inhibitor containing electrochemical systems by evaluation of the non-linearities and non-stationarities over time. This allows us to position the electrochemical behaviour obtained through the application of conventional electrochemical techniques such as PP and EIS in the time-domain and couple the electrochemistry as a function of time with the stationary or non-stationary regime of the corrosion inhibitor. Since PP and EIS present both stationary information, whether or not frequency resolved, without any assurance about linearity, two less conventional electrochemical techniques for the evaluation of corrosion inhibitor- containing electrochemical systems were brought into play.

First of all, the application of a continuous open circuit potential (OCP) measurement with superimposed linear polarization resistance (LPR) measurement every hour presents a faster and less disturbing alternative allowing to characterize the electrochemical system in terms of the polarization resistance (R_p).

Secondly, electrochemical noise (EN) measurements provide a non-stationary alternative to the previously mentioned techniques without perturbation of the electrochemical system. Conversion of the information regarding the current and potential noise into the noise resistance (R_n) provides a macroscopic quantity readily to compare with the R_p.

The work in this thesis focussed on the study of corrosion inhibitor-containing systems on metallic substrates, i.e. lithium-based corrosion inhibitor technology for AA2024-T3 and silica- and phosphate- based corrosion inhibitors for the corrosion protection of hot-dip galvanized steel, respectively. Lithium-based corrosion inhibitor technology was selected because of the previously obtained knowledge about the physical system and its chemical and electrochemical behaviour over time. The recent findings with EIS required further in depth electrochemical analysis, especially in the initial stages after immersion in the electrolyte when the system is rapidly evolving. For this purpose, ORP-EIS was selected as the electrochemical tool. The study of the corrosion protection of hot-dip galvanized steel by different commercially available silica- and phosphate- based corrosion inhibitors and the search for possible corrosion inhibitor synergy was the initial goal of this PhD work. The outcome of the study on lithium- based corrosion inhibitors in the initial stages after immersion and the use of ORP-EIS highlighted the importance of taking into account the time- effect and dictated the methodology followed in the remaining work. Focus was placed initially on the methodology/strategy to study these systems and later on the intrinsic behaviour of the respective systems.

6.2. Li-based corrosion inhibitors for the protection of AA2024-T3

The combination of surface analysis and electrochemical evaluation in the defect of Li-leaching organic coatings on an aluminium alloy AA2024-T3 substrate lead to the discovery of the presence of a three-layered corrosion protective structure with distinct characteristic properties upon neutral salt spray (NSS) exposure (Chapter 2) (Fig. 6.1a).

Surface analysis, by means of scanning electron microscopy (SEM), revealed the existence of a dense (oxide) barrier layer at the aluminium interface, a porous middle layer and a columnar outer layer (Fig. 6.1b).

Electrochemical evaluation, by means of EIS, showed the build-up of the electrochemical properties of the lithium-leaching coatings as a function of NSS exposure time and compared

them to a non-inhibited reference. The inhibited samples showed an increase in the impedance values in the middle and low frequency region, characteristic for the formation of an oxide layer and an increased corrosion resistance, respectively, and the appearance of an extra time constant, characteristic for the porous middle layer, compared to the non-inhibited samples.

Fitting the EIS data with equivalent electric circuits (EECs) allowed linking the physical properties of the protective layer, obtained from SEM analysis, with the development of the electrochemical characteristics in the defect. An EEC consisting of three time-constants, accounting for the porous middle layer, the dense (oxide) barrier layer and the corrosion activity at the metal/oxide interface, could successfully describe the ongoing electrochemical processes (Fig. 6.1c).

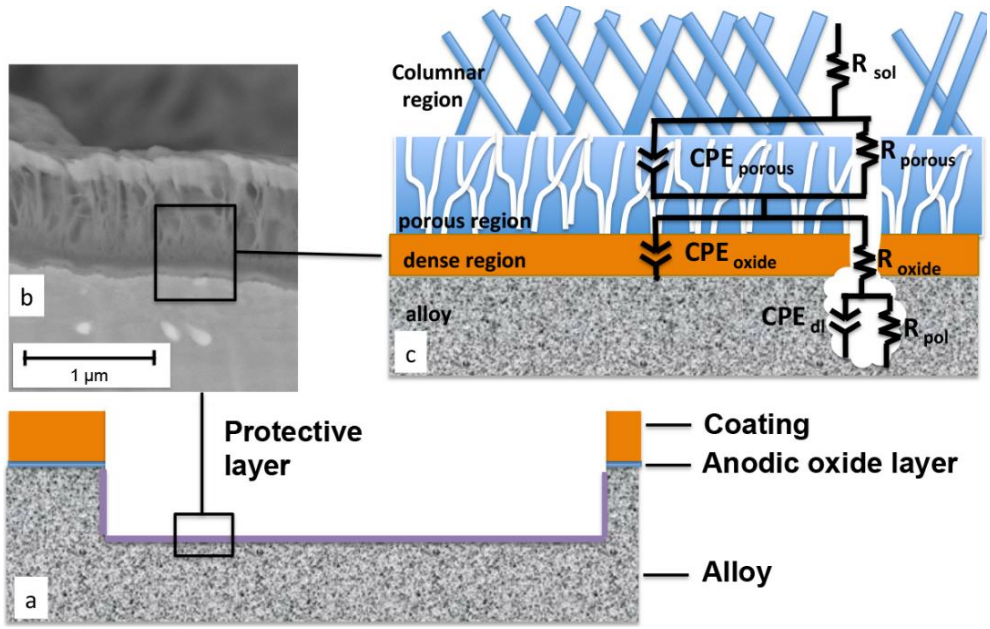

Figure 6.1 Schematic representation of the fitted equivalent circuit based on the physical properties of the protective layer generated in the defect from lithium-leaching organic coatings **(a)** the defect area with protective layer, **(b)** the physical coating morphology and **(c)** schematic representation of EC in protective layer.

6.3. ORP-EIS as electrochemical tool to study the initial stages of inhibitor-containing electrochemical systems

Electrochemical evaluation of the lithium-leaching organic coatings on aluminium alloy 2024-T3 by means of EIS and fitting of this data allowed to quantitatively link the electrochemical properties with the physical model of the layer in the scribed area as observed by SEM. However, since corrosion processes are initially de facto non-linear and non-stationary electrochemical processes, these phenomena can only be described adequately with EIS if it has been proven that the system is behaving in a linear and stationary way within the measurement time. Because of its possibility to examine the non-linearities and non-stationarities present, odd random phase electrochemical impedance spectroscopy (ORP-EIS) has been selected as the electrochemical tool to study the corrosion protective properties as a function of immersion time.

Qualitative analysis of the ORP-EIS data provides an estimation of the stabilization time an electrochemical system needs and a reliable EIS measurement can be obtained. Moreover, it has been observed that the presence of non-stationarities dominate and prolong the system's instability. Dedicated overall quantitative analysis and quantitative analysis per frequency decade allowed linking the presence of non-stationarities in certain frequency ranges to the stable/unstable behaviour of different electrochemical processes since electrochemical processes with different characteristic time-constants are well-distinguished in the frequency spectrum.

Intensively monitoring of both the system with and without lithium-based protective technology in the initial stages after immersion in the electrolyte and modelling of the ORP-EIS data with EECs revealed a relation between the trends in the parameter evolution of the respective circuit elements and the (un)stable behaviour of the morphological changes taking places during these initial moments.

6.4. The importance of the time-effect when studying corrosion inhibitor-containing electrochemical systems

The evaluation of lithium-leaching organic coatings on aluminium alloy AA2024-T3 in a defect already highlighted the importance of taking the time-effect into account when studying inhibitor containing electrochemical systems over time. This has led to a

comparison between different macroscopic electrochemical techniques to study a phosphate-based corrosion inhibitor on hot-dip galvanized steel and position them in the time-domain. Here it is important to consider three characteristic factors of time:

the measurement time, i.e. the time to perform the electrochemical measurement;

the ability to provide time-resolved information, i.e. electrochemical information in the time domain;

the ability to provide frequency-resolved information, i.e. electrochemical information in the frequency domain, indicating that differentiation between different electrochemical processes is possible;

Potentiodynamic polarization (PP) measurements were applied to study the mechanistic behaviour and inhibitor efficiency at discrete and specific periods of exposure and were found to be time intensive if time-resolved information must be obtained while providing only stationary mechanistic behaviour about the inhibited electrochemical system.

Open circuit potential (OCP) with superimposed linear polarization resistance (LPR) measurements were employed as a faster, non-invasive alternative and could characterize the system's overall performance in terms of the polarization resistance over time. However, any information about the mechanistic behaviour is lost and no frequency-resolved information could be obtained.

Electrochemical impedance spectroscopy (EIS) measurements were utilised to describe not only the overall system's performance but also the corrosion inhibitive mechanism over time linked to system's physicochemical representation by providing frequency-resolved information about its time-constants. Nevertheless, the EIS technique suffers from non-linearity and non-stationarity issues in the initial times after immersion before electrochemical stabilization.

Electrochemical noise (EN) measurements were applied to study the inhibition efficiency over time and are capable to provide non-stationary information over time and semi-quantitative information, in terms of the noise resistance, averaged over a specific time window but are incapable to quantitatively describe the system with a macroscopic quantity at discrete times of exposure.

Odd random phase electrochemical impedance spectroscopy (ORP-EIS) was selected as the electrochemical tool to study the electrochemical system's evolution towards stability, described by the behaviour of the non-linearities and non-stationarities over time. On the

one hand this could explain the unstable, fluctuating results with high relative error before stabilization has been reached. On the other hand the stabilization of the system could be linked to the stable results in terms of the polarization resistance obtained from LPR and EIS measurements (Figure 6.2).

Moreover, it has been shown that the non-stationarities present in the inhibitor containing electrochemical system dominate the overall system's instability and should therefore be taken into account when interpreting results from different electrochemical techniques over time.

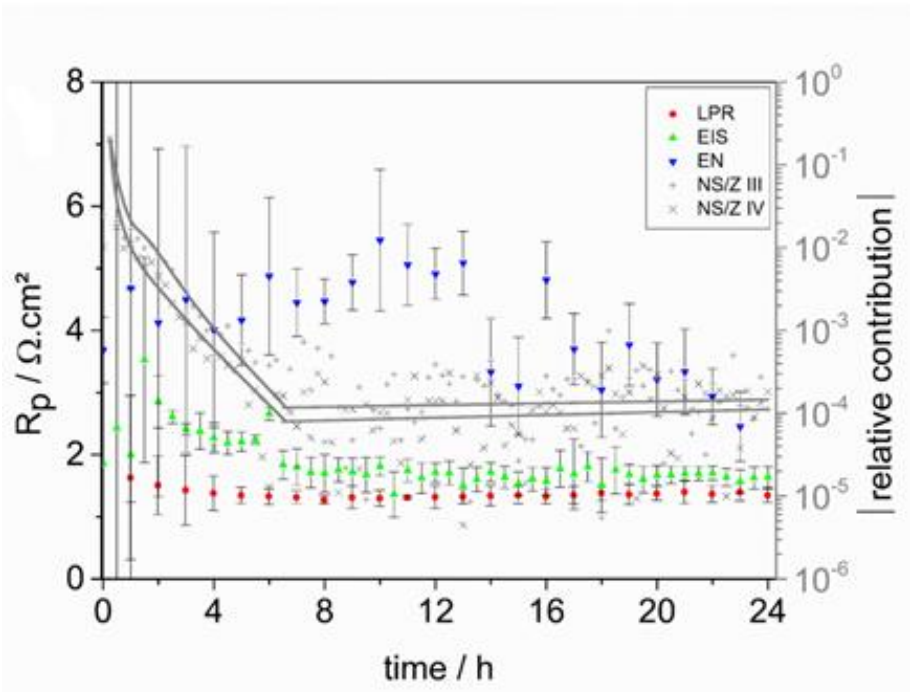

Figure 6.2 Overview of the results obtained through linear polarization resistance (LPR), electrochemical impedance spectroscopy (EIS), electrochemical noise (EN) and odd random phase electrochemical impedance spectroscopy (ORP-EIS) measurements for hot-dip galvanized steel with corrosion inhibitor (0.5 mM Heucophos® CAPP) for 24 h.

6.5. Performance of silica- and phosphate- based corrosion inhibitors for hot-dip galvanized steel

The findings related to the importance of the time-effect were then put into practice when studying a number of silica- and phosphate- based corrosion inhibitors and possible corrosion inhibitor synergy for hot-dip galvanized steel. A specific methodology was followed for the interpretation of the electrochemical data obtained by different macroscopic electrochemical techniques. Firstly, ORP-EIS measurements were applied to study the time evolution of the different corrosion inhibitor-containing electrochemical systems. The quantitative interpretation per frequency decade served as the evaluation criteria for the 'stability', i.e. the linearity and stationarity (time-invariance), of the respective systems and as the interpretation tool for the results from the macroscopic techniques applied. It has been observed that the presence of non-stationarities dominate the instability of the corrosion inhibitor-containing systems in the first 6 up to 12 hours after immersion. Consequently it cannot be generalized that any corrosion inhibitor effectively stabilizes an electrochemical interface.

Potentiodynamic polarization (PP) measurements after 1.5 hours and 24 hours indicated dominant cathodic behaviour for all inhibitors whereas the results after 1.5 hours suffer from unstable behaviour, reflected in the relatively high absolute errors, and should therefore only be used in a qualitative way.

The application of a continuous open circuit potential (OCP) with superimposed linear polarization resistance (LPR) measurement and of electrochemical impedance spectroscopy (EIS) measurements revealed that both the silica- and phosphate-based corrosion inhibitors provide both immediate as well as long-term corrosion protection while the former also account for a remarkable synergistic effect when combining them. The presence of the non-stationarities in the early stages and the related instability of the respective systems is reflected in the unstable values of the polarization resistance (Rp) with relatively high absolute error and depicts the untrustworthiness of the values at these instances.

Electrochemical noise (EN) measurements yet again confirmed the synergistic action of both silica-based corrosion inhibitors. Although the presence of non-stationarities has no influence on the results obtained from EN, the technique remains incapable in describing the electrochemical system with a macroscopic quantity at discrete times of exposure.

6.6. Overall conclusions

The importance of the time-effect was highlighted similarly on two completely different electrochemical systems. It can be concluded that corrosion inhibitor-containing electrochemical systems are initially unstable electrochemical systems but evolve however towards a stable electrochemical system within the first couple of hours after immersion typically and are therefore interesting to study during the early evolving stages of corrosion inhibition. This requires macroscopic electrochemical techniques that can acquire the correct information in these initial times after immersion. Since most of the conventional electrochemical techniques such as potentiodynamic polarization (PP) and electrochemical impedance spectroscopy (EIS) measurement or the newly introduced continuous open circuit potential (OCP) measurement with superimposed linear polarization resistance (LPR) measurement require at least one stabilization criterion, i.e. either linearity and/or time-invariance, the results obtained from these techniques have to be placed in the right perspective. This suggested a study of the evolution towards a stable electrochemical system, wherefore odd random phase electrochemical impedance spectroscopy was selected as the appropriate electrochemical tool. The evolution of the non-linearities and in particular the non-stationarities served as the stabilization criterion, i.e. as soon as the non-stationarities have reached their minimum, stable value, the system can be considered. This is reflected in stable values with low relative error obtained from the respective macroscopic electrochemical techniques. On the other hand, before stabilization, the values obtained from the respective techniques were unstable and suffered from a high relative error, indicating they should be interpreted with extra care. A possible solution to overcome this would consist in not only using the ORP-EIS data as a stabilization criterion but also by modelling the data with the appropriate equivalent electrical circuit (EEC) and correction for the unstable behaviour by attributing the correct weight to the data points. Nevertheless, modelling of ORP-EIS data is rather difficult and time-intensive but provides a reliable system identification tool with correct experimental data and a verification criteria during modelling.

An overall conclusion can be made about the intrinsic behaviour of the lithium-leaching coatings on aluminium alloy AA2024-T3 in a defect and silica- and phosphate-based corrosion inhibitors for the corrosion protection of hot-dip galvanized steel, respectively. The former showed an increased corrosion protection after 168 hours of NSS provided by a characteristic three-layered protective structure, compared to a reference system without lithium-based inhibiting species present. The latter showed an improved corrosion protective performance over the course of 168 hours, compared to hot-dip galvanized steel

without corrosion inhibitors, for both the silica- and phosphate-based inhibitor containing electrochemical systems as well as the synergistic system containing both silica-based corrosion inhibitors. It can be said that both systems effectively inhibit the respective corrosion reactions.

6.7. Reflections and recommendations

Although the results presented in this work provide a methodological approach to study corrosion inhibitor- containing electrochemical systems over time, there are definitely some interesting challenges ahead which will improve the strategy to be followed.

Firstly, all results throughout this work are coming from corrosion inhibitors in solution experiments. A transition to corrosion inhibitors placed into coatings would be definitely a challenge, since there is no guaranteed correlation between the behaviour of corrosion inhibitors in solutions and coatings. Definition of a well-understood model coatings system and a reproducible coating application procedure is strictly necessary to focus on the intrinsic behaviour of the electrochemical techniques and the corrosion inhibitors' behaviour in coatings.

Secondly, the macroscopic electrochemical results could be coupled to surface analysis in order to substantiate the proposed corrosion mechanism and corrosion inhibitor protective action mechanisms in terms of corrosion product characterization and protective layer formation characterization, respectively. Ex-situ spectroscopic methods such as scanning electron microscopy coupled to energy dispersive X-ray spectroscopy (SEM-EDX), glow discharge optical emission spectroscopy (GDOES) and Fourier transform infrared spectroscopy (FTIR) have been applied at certain stages of this work but were unusable due to the changes that were made in the sample preparation procedure of the hot-dip galvanized steel substrate in order to remove the superficial aluminium. However, a dedicated in-situ spectroscopic analysis coupled to the macroscopic electrochemical techniques is suggested over the previously mentioned ex-situ spectroscopic analysis. This would allow to monitor the surface morphological changes and surface chemistry as well as the electrochemical behaviour as a function of time. This could be performed by means of attenuated total reflection Fourier transform infrared spectroscopy (ATR-FTIR) coupled to odd random phase electrochemical impedance spectroscopy. In this framework, the work of Sven Pletincx and Laura-Lynn Fockaert on in-situ ATR-FTIR coupled with ORP-EIS for the investigation of coating/metal interactions could serve as the starting point for the

application on inhibitor systems [1][2][3]. Investing on this coupled in-situ spectroscopic/macroscopic electrochemical analysis methodology would be an efficient strategy to investigate corrosion inhibitor-containing electrochemical systems over time.

References

1. Pletincx, S., Fockaert, L. I., Meeusen, M., Mol, J. M. C., Terryn, H., Hauffman, T. (2018). In Situ Methanol Adsorption on Aluminum Oxide Monitored by a Combined ORP-EIS and ATR-FTIR Kretschmann Setup. *J. Phys. Chem. C, 122(38)*, 21963-21973.
2. Pletincx, S. (2019). Probing the formation and degradation of chemical interactions from model molecule / metal oxide to buried polymer / metal oxide interfaces. *npj Materials Degradation, 3(23)*, 1-12.
3. Pletincx, S., Abrahami, S., Mol, J.M.C., Hauffman, T., Terryn, H. (2018). Advanced (In Situ) Surface Analysis of Organic Coating / Metal Oxide Interactions for Corrosion Protection of Passivated Metals, *Encyclopedia of Interfacial Engineering in Reference Module in Chemistry, Molecular Sciences and Chemical Engineering,* 1–17.

Appendix A

From qualitative ORP-EIS data to quantitative information per frequency decade

This section aims to describe the rigorous approach followed to interpret the ORP-EIS data and obtain the quantitative interpretation per frequency decade presented in the manuscript from the qualitative interpretation and overall quantitative interpretation.

Firstly, the qualitative ORP-EIS data is discussed at characteristic times (Figures A1 to A7) with attention for the behaviour of the non-linearities and non-stationarities over time, presenting an idea of the 'stabilization time' the system needs to fulfil the linearity and stationarity condition. Secondly, the data regarding the noise distortions is quantified to discuss the evolution of the system towards a linear and time-invariant system previously described more quantitatively and draw a parallel between the stability of electrochemical processes, the morphological changes and the parameter evolution of the electrochemical parameters describing the electrochemical processes [1]. The information is quantified by a numerical integration through interpolation procedure using the trapezoidal rule and subtracting the noise curve form the *noise + nonlinearities* and *noise + non-stationarities* curve, respectively. The resulting individual contributions of the noise, non-linearities and non-stationarities are then expressed relative to the magnitude of the impedance modulus, which is quantified also quantified through a numerical integration through interpolation procedure [2]. The relative contribution of the noise, non-linearities and non-stationarities over time is presented in Figure A8. Finally, the information regarding the non-stationarities is further quantified per frequency decade, to examine which electrochemical processes with characteristic time-constants corresponding to a certain frequency decade can be coupled to the system's (in)stability [3]. The same numerical integration through interpolation procedure using the trapezoidal rule has been applied, after dividing the impedance data into 6 frequency decades. Nevertheless, the highest (10^3 - $2 \cdot 10^3$ Hz) and lowest (10^{-2} – 10^{-1} Hz) frequency decade are not taken into account during interpretation because the former only comprises one tenth of a frequency decade and the latter only contains three data points, making application of the interpolation procedure inaccurate. The relative contribution of the noise, non-linearities and non-stationarities per frequency decade as a function of immersion time is shown in Figure A9.

1. Hot-dip galvanized steel without corrosion inhibitors

In Figure A1, the ORP-EIS data of hot-dip galvanized steel without corrosion inhibitors after 30 min, 1 h, 5 h and 10 h are presented. The magnitude of the impedance modulus and the phase angle are represented by the black line and the grey line, respectively. The characteristics of the ORP-EIS technique, i.e. the curves representing the noise, the noise plus the non-linearities and the noise plus the non-stationarities, are represented by the blue, red and green points, respectively. It has been shown that, in order to have a fully linear system, the noise curve and the noise + non-linearities curve have to overlap and in order to have a fully time-invariant system, the noise curve and the noise + non-stationarities curve have to overlap [1][4]. For the hot-dip galvanized steel after 30 min in the electrolyte (Fig. A1a), it can be seen that the noise + non-linearities overlaps with the noise curve in the mid- and high- frequency region but not in the low-frequency region and that the noise + non-linearities does not overlap with the noise curve. This signifies the presence of both non-linearities and non-stationarities in the electrochemical system. After 1 hour of immersion (Fig. A1b), the noise + non-linearities curve completely overlaps with the noise curve, indicating a linear system's behaviour. However, the noise + non-stationarities curve does not overlap with the noise curve in the frequency range from 1 Hz to 1 kHz, indicating that the overall system is still behaving non-stationary. This means that the electrochemical processes with characteristic time-constants corresponding to these frequencies, i.e. the corrosion activity related to the effect of the ionic double layer capacitance (paragraph 3.4), are still 'unstable'. After 5 hours of immersion (Fig. A1c), the condition of time-invariance is nearly fulfilled, indicated by the approach of the noise + non-stationarities curve towards the noise curve. After 10 hours of immersion (Fig. A1d), the system is behaving fully linearly and stationary since the noise + non-stationarities also completely overlaps the noise curve at this stage.

For the hot-dip galvanized steel without corrosion inhibitors (Fig. A8a), it can be observed that the non-stationarities are predominant right at the start, with a relative contribution only more than one order of magnitude lower compared to the magnitude of the impedance modulus, accounting for 4.89 %. The contribution of the noise and the non-linearities is two (or more) orders of magnitude lower, corresponding to 1.03 % and 0.17 %, respectively. In the successive hours, their contribution remains equal while the contribution of the non-stationarities decreases strongly in the beginning, reaching a relative contribution of 2·10-4 after 2 h, which remains stable over the course of the measurement. It needs to be remarked that this time does not correspond which what was observed during the qualitative interpretation, with the presence of non-stationarities for up to 10 hours.

From the quantitative interpretation per decade for the system without corrosion inhibitors (Fig. A9a), it can be observed that the contribution of the non-stationarities for all frequency decades decreases with time, although the decrease for the highest and lowest frequency decades (V and II) is more rapidly compared to the middle frequency decades (IV and III). The former stabilize after 2 hours while the latter stabilizes only after 8 and 10 hours, respectively. Consequently the system needs to be considered as non-stationary in the first 10 hours after immersion.

2. Hot-dip galvanized steel with corrosion inhibitor 1

Figure A2 shows the ORP-EIS results of hot-dip galvanized steel with 0.5 mM of corrosion inhibitor 1 after 30 min, 2 h, 8.5 h and 12 h, respectively. After 30 min (Fig A2a), it can be seen that the noise + non-linearities curve overlaps the noise curve, indicating linear behaviour, but that the noise + non-stationarities curve does not overlap the noise curve over almost the entire frequency range. After 2 h (Fig. A2b), the noise + non-linearities curve overlaps with the noise curve, indicating a fully linear system. The noise + non-stationarities overlaps with the noise curve in the high frequency region (102 – 2·103 Hz) but not yet in the middle and low frequency region. After 8.5 h of immersion (Fig. A2c), the noise + non-stationarities overlaps with the noise curve in the low frequency (10-2 – 100 Hz) and high frequency region, but not completely yet in the middle frequency (100 – 102) region, designated by the number of green points above the blue points. After 12 hours of immersion (Fig. A2d), the system is behaving fully time-invariant since the noise + non-stationarities curve overlaps with the noise curve over the entire frequency range.

From the quantitative analysis of the system containing corrosion inhibitor 1 (Fig. A8b), it can be seen that all three contributions are only one order of magnitude lower relative to the magnitude of the impedance modulus right at the start. However the noise and non-linearities decrease rapidly and reach a stable value after 30 minutes. The overall contribution of the non-stationarities decreases more slowly and reaches a sable value only after 9 hours, four orders of magnitude lower compared to the magnitude of the impedance modulus.

From the quantitative analysis per frequency decade (Fig. A9b), it can be seen that the contribution of the higher frequency decades decreases more rapidly than the contribution of the middle and lower frequency decades, i.e. frequency decade V reaches a stable value after 7 hours, while frequency decades IV and III only reach a stable value after 10 and 11 hours and decade II only after 12 hours, respectively. This implicates that the electrochemical processes with characteristic time-constants corresponding to the middle

and lower frequency region cause the overall system instability, meaning that the corrosion inhibitor protective action and the corrosion activity are causing the instability in the case of inhibitor 1.

3. Hot-dip galvanized steel with corrosion inhibitor 2

Figure A3 shows the ORP-EIS data of hot-dip galvanized steel with 0.5 mM of corrosion inhibitor 2 after 30 min, 1 h, 3 h and 6 h. For the system after 30 min (Fig. X3a), it can be seen that neither the noise + non-linearities curve nor the noise + non-stationarities overlaps with the noise curve. After 1 hour of immersion (Fig. A3b), a similar situation is presented, although all curves start overlapping in the high frequency region. After 3 h of immersion (Fig. A3c), the noise + non-linearities curve overlaps the noise curve. From the noise + non-stationarities curve and the noise curve in the frequency range from 10-1 Hz to 101 Hz, it can be seen that the system is still behaving non-stationary, because of number of green points above the blue points at these frequencies. The ORP-EIS data after 6 h (Fig. A3d) presents a fully linear and time-invariant electrochemical system.

It can be observed from the quantitative interpretation (Fig. A8c) that the relative contribution of the noise, non-linearities and non-stationarities decreases rapidly in the initial stages after immersion, reaching a stable value after 30 min, 1.5 hours and 3 hours respectively. It is apparent that the addition of corrosion inhibitor 2 effectively stabilizes the electrochemical interface, compared to the system without corrosion inhibitor (Fig. A8a) or the system with corrosion inhibitor 1 (Fig. A8b).

From the quantitative interpretation per frequency decade (Fig. A9c) for the system containing corrosion inhibitor 2, it can be seen that all frequency decades decrease rapidly with time, reaching a stable value after 2, 4 and 6 hours in the case of the high frequency decade (V), middle frequency decades (IV and III) and low frequency decades (II), respectively. This implies that the electrochemical processes related to the corrosion inhibitor protective action stabilize before the corrosion activity, i.e. the charge transfer reaction, stabilizes.

4. Hot-dip galvanized steel with corrosion inhibitor 3

Figure A4 shows the ORP-EIS data of the system containing 0.1 mM of corrosion inhibitor 5 after 30 min, 3 h, 6 h and 10 h, respectively. It can be observed that after 30 min (Fig. A4a), the system is behaving linearly, due to the overlap between the noise + non-linearities curve and the noise curve but not yet stationary, since the noise + non-stationarities does not overlap with the noise curve at this stage yet. Although the noise + non-stationarities curve

is approaching the noise curve in the high frequency region, the system is still behaving non-stationary after 3 h of immersion (Fig. A4b). After 6 h of immersion (Fig. A4c), the noise + non-stationarities curve is overlapping with the noise curve for almost the entire frequency range, apart for the frequencies around 1 Hz. The situation after 10 h of immersion (Fig. A4d) presents a fully linear and time-invariant system.

The quantitative interpretation of the system containing corrosion inhibitor 3 (Fig. A8d) reveals that the noise and non-linearities stabilize first, after 15 min and 30 min, respectively. The trend in the relative contribution of the non-stationarities is remarkable. Initially, its contribution decreases to a stable contribution after 30 min of approximately 3·10-3 relative to the magnitude of the impedance modulus. However, after 3 to 4 hours, its contribution decreases again and reaches a lower, stable value of approximately 4 orders of magnitude lower compared to the magnitude of the impedance modulus. A detailed quantitative interpretation per frequency decade imposes itself.

From this quantitative interpretation per frequency decade (Fig. A9d), it can be observed that the highest frequency decade (V) stabilizes first, after 4 hours. The middle frequency decades (IV and III) and the lowest frequency decade (II) all stabilize after 10 hours. This indicates that the corrosion inhibitor protective action and the corrosion activity, with characteristic time-constants corresponding to the middle and low frequency region, respectively, prolong the overall system's instability but stabilize after the same time. It can be remarked that the first stabilization plateau, visible in the overall quantitative interpretation, corresponds to the stabilization of the higher frequency decades and the corresponding electrochemical processes.

5. Hot-dip galvanized steel with corrosion inhibitor 4

Figure A5 shows the ORP-EIS data of hot-dip galvanized steel with 0.5 mM of corrosion inhibitor 4 after 30 min, 2 h, 5 h and 6.5 h in the electrolyte. It can be seen that after 30 min of immersion in the electrolyte (Fig. A5a), neither the noise + non-linearities curve nor the noise + non-stationarities curve completely overlaps the noise curve, indicating that the system has not met the linearity or time-invariance condition at this stage. After 2 h (Fig. A5b), the noise + non-linearities curve and the noise curve completely overlap, indication that the system is behaving fully linear. Similarly, the noise + non-stationarities curve approaches the noise curve at the high frequency region (102 – 2·103 Hz) but not yet in the low frequency (10-2 – 100 Hz) and middle frequency (100 – 102) regions. After 5 h (Fig. A5c), the noise + non-stationarities curve overlaps with the noise curve in the low frequency and high frequency region but not yet in the middle frequency region. This indicates that the

electrochemical processes with characteristic time-constants corresponding to the middle frequency region, i.e. related to the corrosion protective action of the inhibitor on the surface, are 'unstable'. After 6.5 h (Fig. A5d) the system behaves fully linearly and stationary, indicated by the complete overlap of the noise + non-linearities curve and noise + non-stationarities curve with the noise curve.

From the quantitative interpretation (Fig. A8e), it can be observed that the relative contribution of both the noise and non-linearities is predominant right at the start after immersion in the inhibitor 4 containing solution, only one order of magnitude lower compared to the magnitude of the impedance modulus. However, these contribution decreases more rapidly compared to the relative contribution of the non-stationarities and stabilize after 30 min of immersion. In contrast, the relative contribution of the non-stationarities decreases more gradually and stabilizes around 2·10-4 after 6.5 hours, indication a fully time-invariant system at this stage. This corresponds to what was observed earlier during the qualitative interpretation.

From the quantitative interpretation per frequency decade (Fig. A9e), it can be seen that the contribution of the highest and lowest frequency decade decrease more rapidly, reaching a stable value after 5 hours, compared to the relative contribution of the middle frequency decades, reaching a stable value after 6.5 hours. This indicates that for the system with corrosion inhibitor 4, the corrosion inhibitor protective action related action causes the overall system's instability since these frequency decades correspond to the time-constants describing those electrochemical processes. Compared to the system without corrosion inhibitors, it can be concluded that the presence of corrosion inhibitor 4 effectively stabilizes the surface of the hot-dip galvanized steel.

6. Hot-dip galvanized steel with corrosion inhibitor 5

The ORP-EIS data of hot-dip galvanized steel 30 min, 4 h, 7.5 h and 16 h after immersion in a 0.02 mM solution of corrosion inhibitor 5 are presented in Figure A6. After 30 min (Fig. A6a) a non-linear (in the lower frequency range) and non-stationary (over the entire frequency range) is observed. After 4 h (Fig. A6b) the system is fully linear, since the noise + non-linearities curve overlaps noise + non-stationarities overlaps with the noise curve. Nevertheless, the system is still non-stationary because of the presence of non-stationarities in the middle frequency region (100 – 102 Hz). The system after 7.5 h (Fig. A6c) presents a similar situation. Eventually, after 16 h (Fig. A6d) of immersion, the system is behaving fully linear and stationary.

From the quantitative interpretation of the system containing corrosion inhibitor 5 (Fig. A8f), it can be seen that the relative contribution of the noise and non-linearities is stable directly from the start after immersion. The relative contribution of the non-stationarities, initially only more than 1 order of magnitude lower than the magnitude of the impedance modulus, decreases rapidly in the first hours and reaches a stable relative contribution of approximately 4 order of magnitude lower after 6 hours eventually.

The quantitative analysis per frequency decade of the system containing corrosion inhibitor 5 shows a remarkable difference is stabilization time of the different frequency decades (Fig. A9f). The highest and lowest frequency decades (V and II) stabilize first, after 6 hours and 8 hours, respectively. At the same time, the middle frequency decades (IV and III) reach a stabilization plateau more than three orders of magnitude lower compared to the magnitude of the impedance modulus. Nevertheless, after 12 hours, the non-stationarities of the middle frequency regions decrease further to eventually more than three orders of magnitude lower than the magnitude of the impedance modulus. It can be concluded that corrosion inhibitor 5 is ineffective in stabilizing the interface, related to the presence of non-stationarities in the middle frequency region accounting for this.

7. Hot-dip galvanized steel with corrosion inhibitor 1+2

The ORP-EIS data of the hot-dip galvanized steel with 0.5 mM of both corrosion inhibitor 1 and corrosion inhibitor 2 after 30 min, 3 h, 6 h and 7 h is shown in Figure A7. It can be observed that after 30 min of immersion (Fig. A7a), neither the noise + non-linearities curve nor the noise + non-stationarities curve overlaps with the noise curve. After 3 h (Fig. A7b), the noise + non-linearities curve overlaps the noise curve, signifying linear behaviour. The noise + non-stationarities curve only overlaps the noise curve in the low frequency and high frequency region, but not in the middle frequency region. This indicates again that the electrochemical processes with characteristic time-constants related to these frequencies, in this case the corrosion protective action of the corrosion inhibitors, are still unstable and cause the overall instability of the system. Figure A7c, after 6 hours of immersion represents a similar situation. After 7 h of immersion (Fig. A7d), the system has reached a fully linear and time-invariant situation.

The quantitative interpretation of the system containing both corrosion inhibitor 1 and corrosion inhibitor 2 (Fig. A8g) shows that the relative contribution of the noise is stable right from the start, the relative contribution of the non-linearities stabilize after 1 hour and the non-stationarities after 4 hours, respectively.

It can be seen from the quantitative interpretation per decade (Fig. A9g) that here the lowest frequency decade (II) stabilizes first after 1 hour. The highest (V) and middle (IV and III) frequency decades stabilize together after 7 hours, indicating that the electrochemical processes with characteristic time-constants corresponding to theses frequencies, i.e. the corrosion inhibitor protective action, stabilize after 7 hours.

References

1. Meeusen, M., Visser, P., Fernández Macía, L., Hubin, A., Terryn, H., & Mol, J. M. C. (2018). The use of odd random phase electrochemical impedance spectroscopy to study lithium-based corrosion inhibition by active protective coatings. *Electrochimica Acta*, *278*, 363–373.
2. Atkinson, K. E., & Wiley, J. (1978). *AN INTRODUCTION TO NUMERICAL ANALYSIS Second Edition*.
3. Meeusen, M., Zardet, L., Homborg, A. M., Lekka, M., Boelen, B., Terryn, H., … Fedrizzi, L. (2019). Complementary Electrochemical Approach for Time-Resolved Evaluation of Corrosion Inhibitor Performance. *J. Electrochem. Soc.*, *166*(11), 3220–3232.
4. Fernández Macía, L., Petrova, M., Hauffman, T., Muselle, T., Doneux, T., & Hubin, A. (2014). A study of the electron transfer inhibition on a charged self-assembled monolayer modified gold electrode by odd random phase multisine electrochemical impedance spectroscopy. *Electrochimica Acta*, *140*, 266–274.

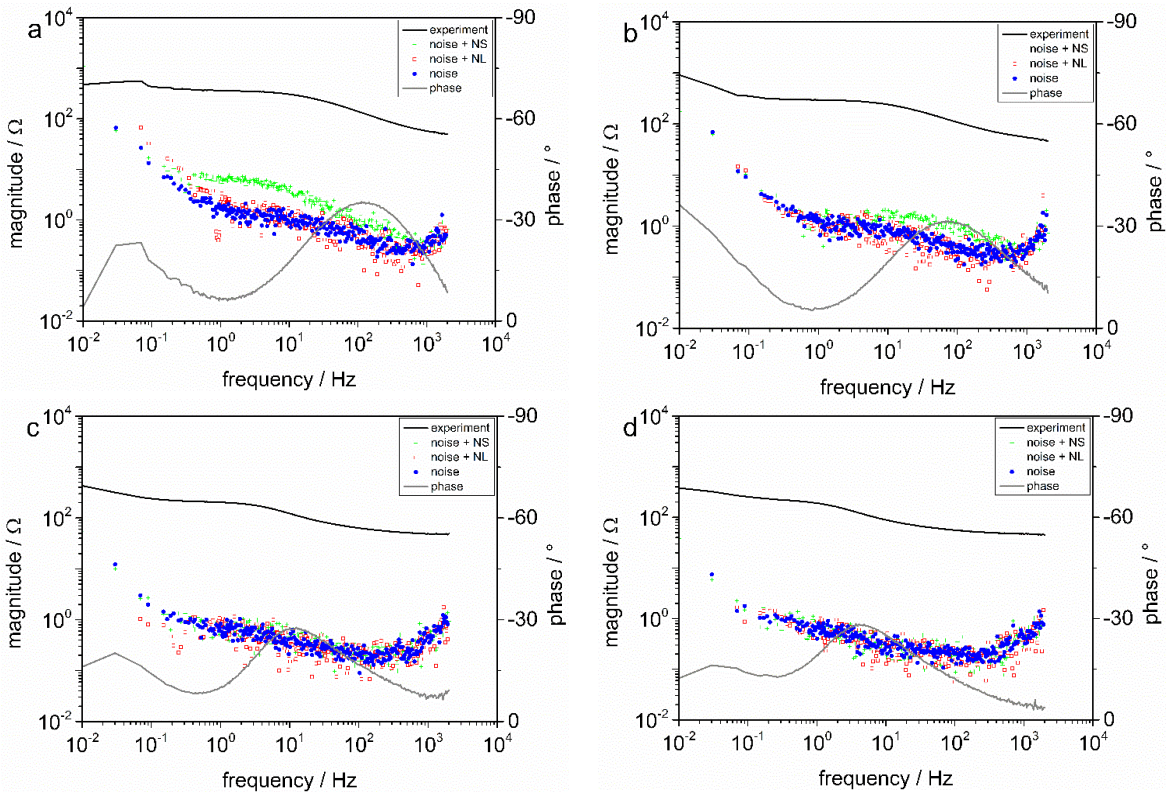

Figure A1 Bode plots of hot-dip galvanized steel without corrosion inhibitors after 30 min **(a)**, 1 h **(b)**, 5 h **(c)** and 10 h **(d)** in 0.05 M NaCl with the experimental impedance and noise distortion curves.

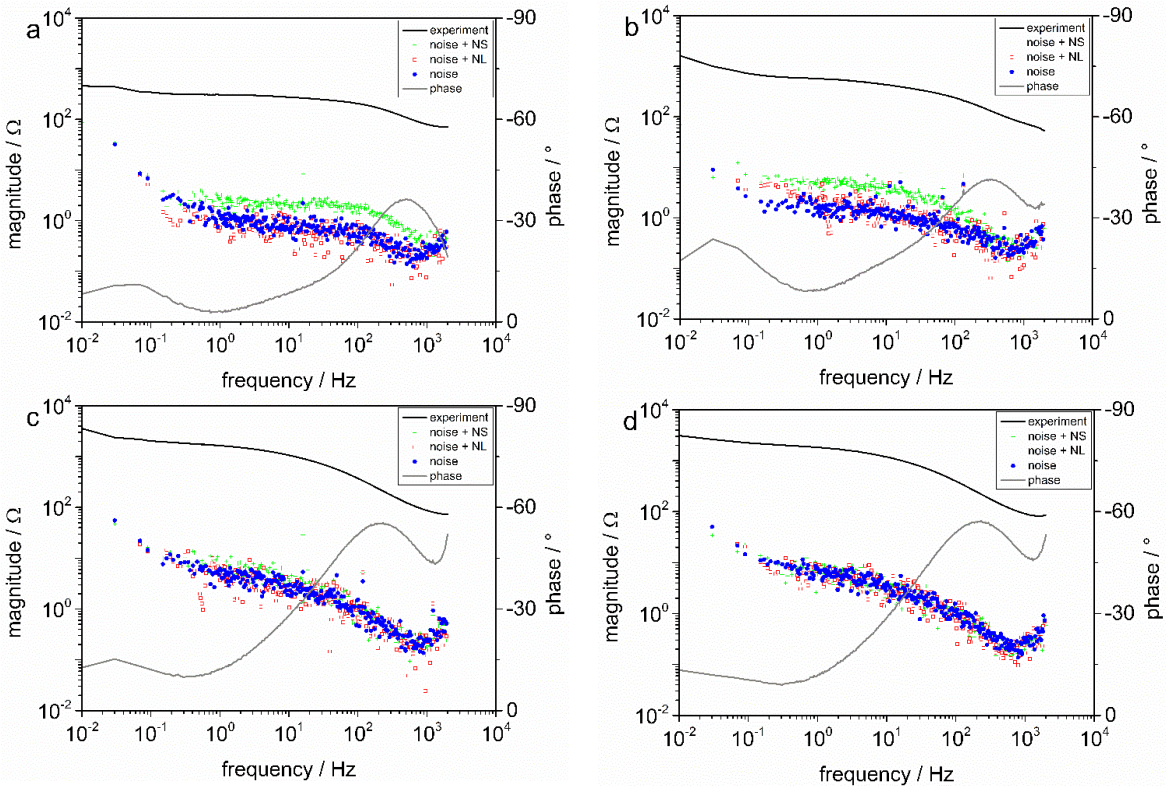

Figure A2 Bode plots of hot-dip galvanized steel with 0.5 mM corrosion inhibitor 1 (Novinox®ACE110) after 30 min **(a)**, 2 h **(b)**, 8.5 h **(c)** and 12 h **(d)** with the experimental impedance and noise distortion curves.

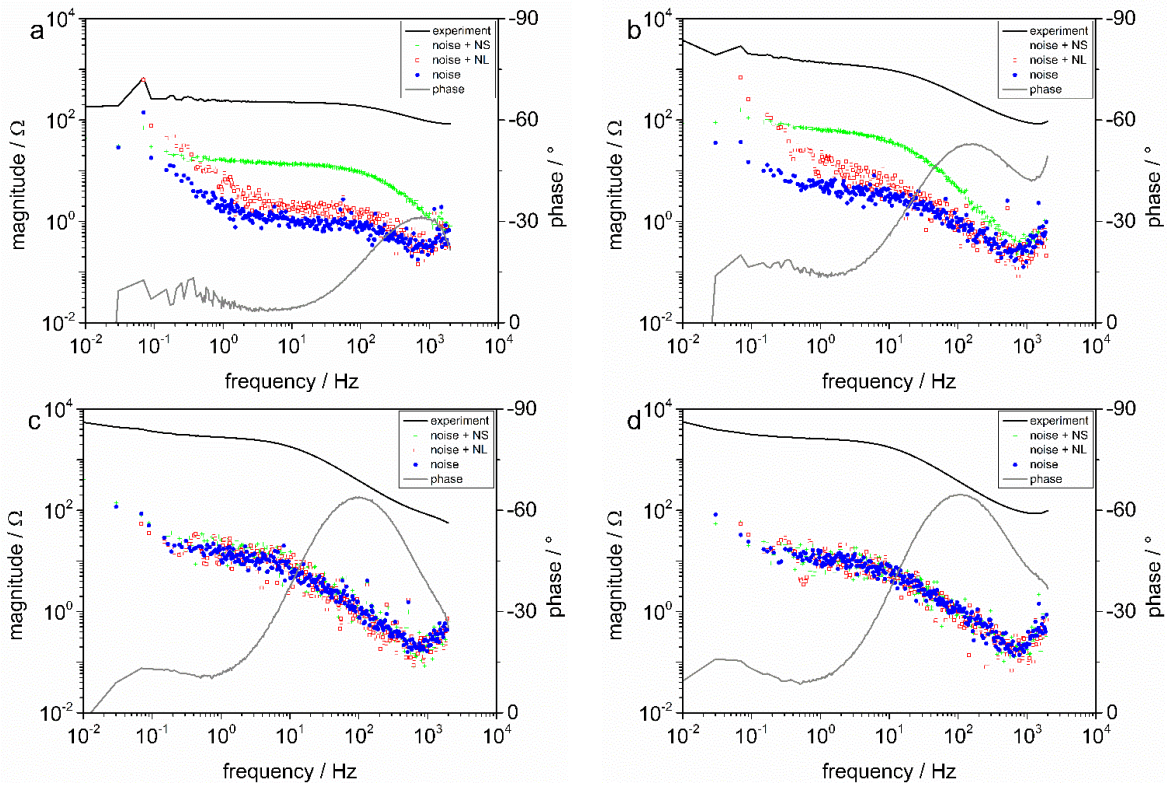

Figure A3 Bode plots of hot-dip galvanized steel with 0.5 mM corrosion inhibitor 2 (Novinox®XCA02) after 30 min **(a)**, 1 h **(b)**, 3 h **(c)** and 6 h **(d)** with the experimental impedance and noise distortion curves.

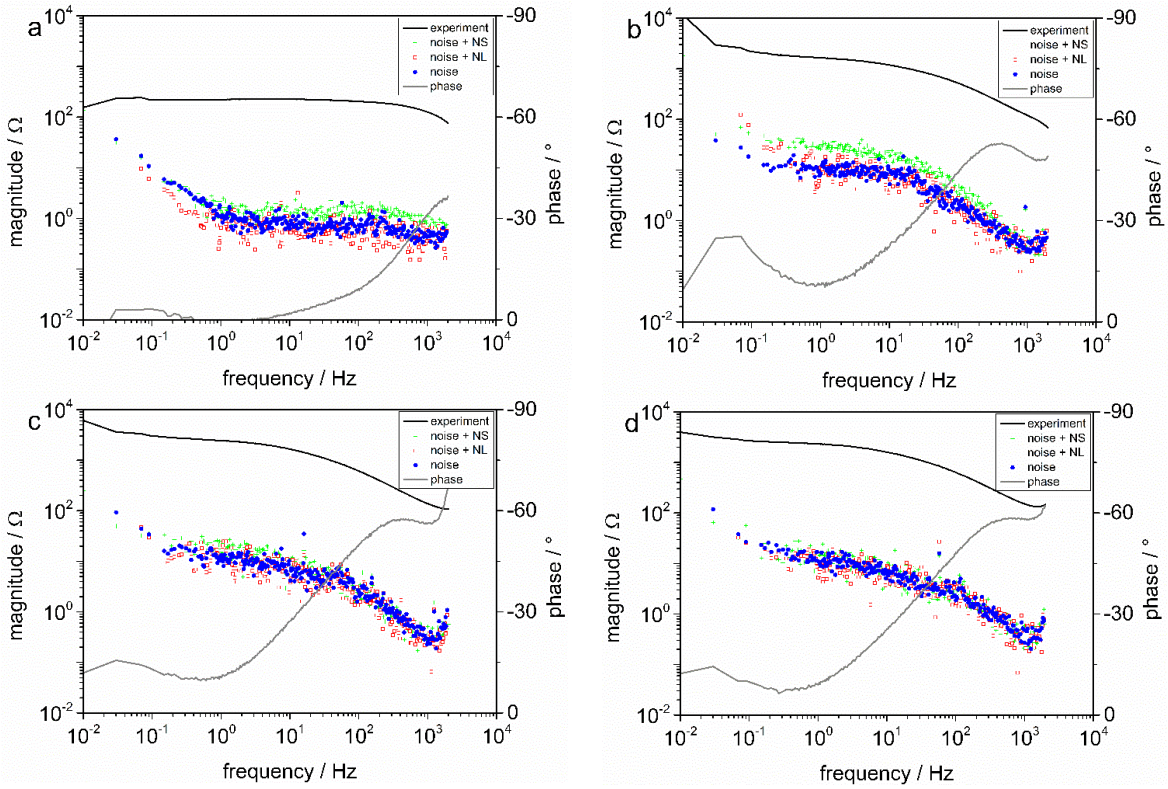

Figure A4 Bode plots of hot-dip galvanized steel with 0.1 mM corrosion inhibitor 3 (Halox®SW-111) after 30 min **(a)**, 3 h **(b)**, 6 h **(c)** and 10 h **(d)** with the experimental impedance and noise distortion curves.

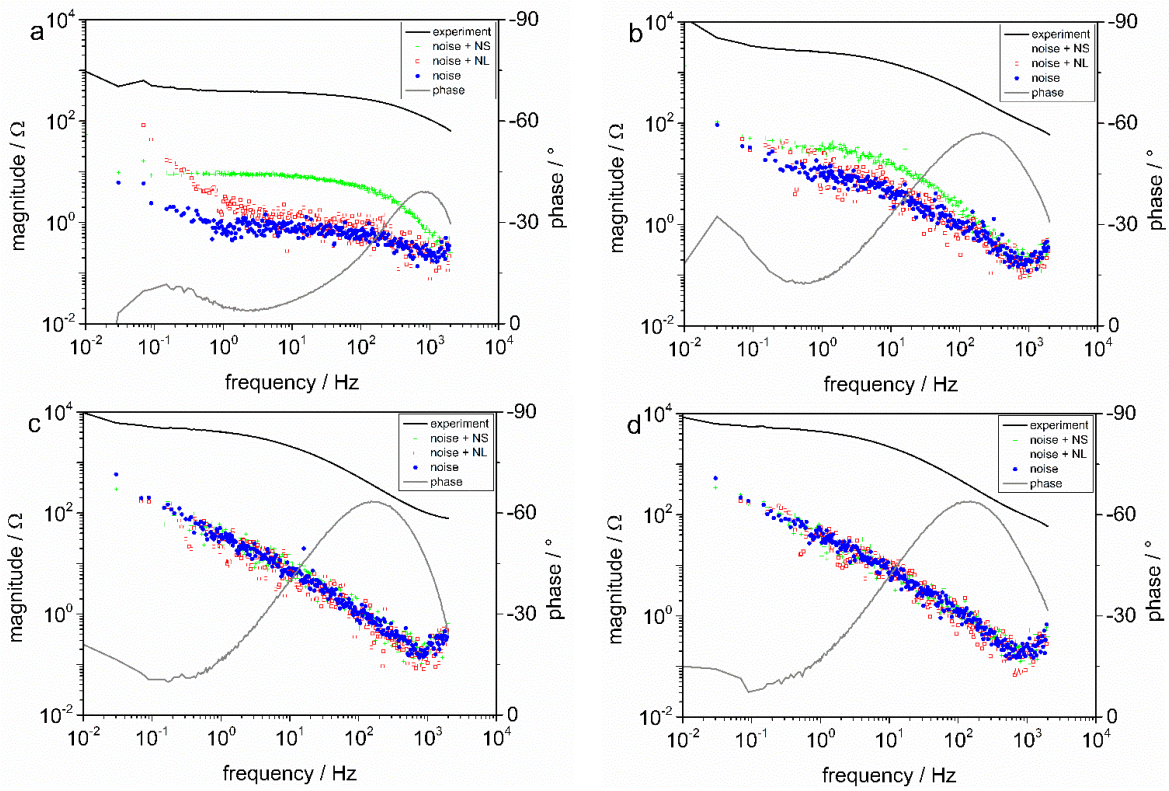

Figure A5 Bode plots of hot-dip galvanized steel with 0.5 mM corrosion inhibitor 4 (Heucophos®CAPP) after 30 min **(a)**, 2 h **(b)**, 5 h **(c)** and 6.5 h **(d)** with the experimental impedance and noise distortion curves.

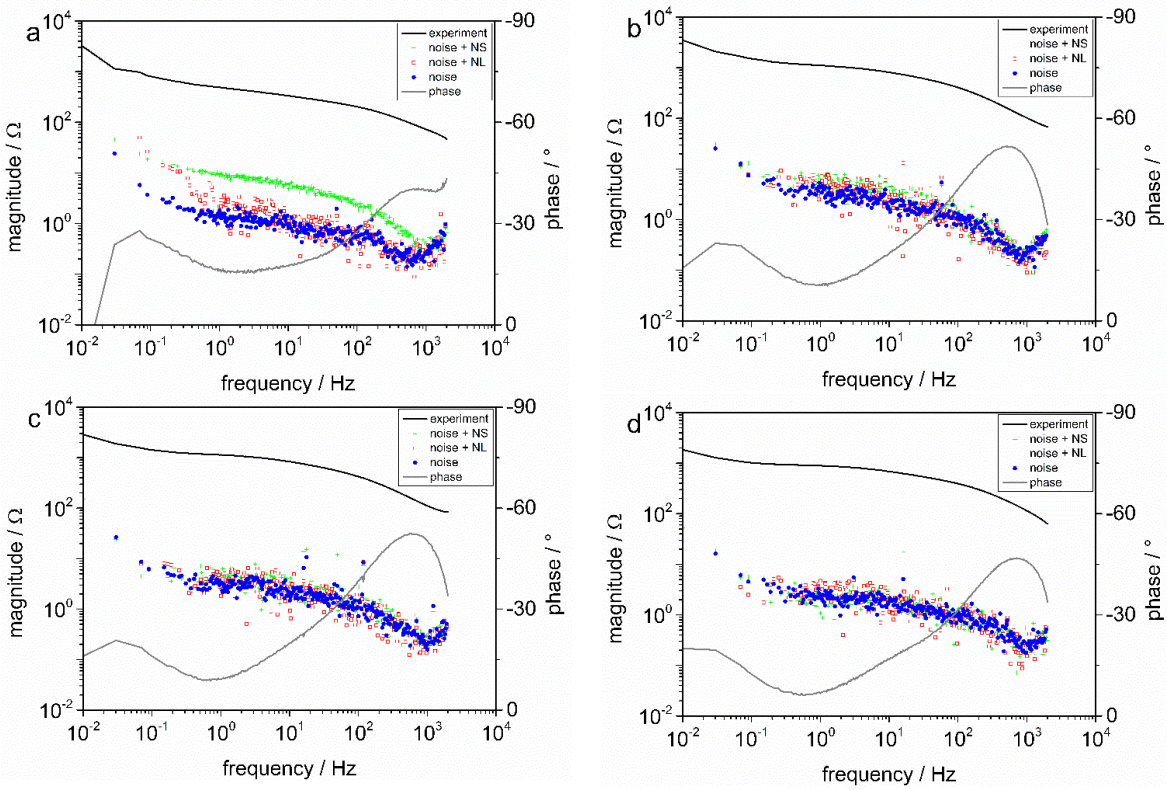

Figure A6 Bode plots of hot-dip galvanized steel with 0.02 mM corrosion inhibitor 5 (Zinc Phosphate ZP10) after 30 min **(a)**, 4 h **(b)**, 7.5 h **(c)** and 16 h **(d)** with the experimental impedance and noise distortion curves.

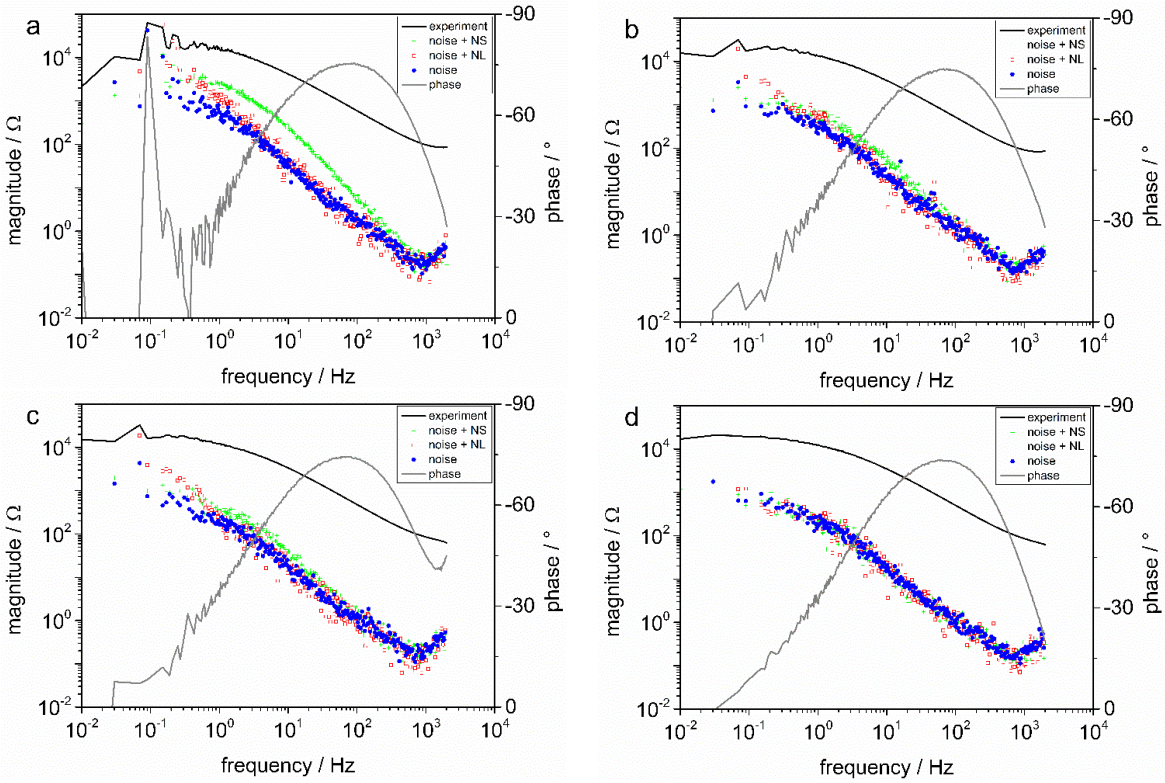

Figure A7 Bode plots of hot-dip galvanized steel with 0.5 mM of both corrosion inhibitor 1 (Novinox®ACE110) and corrosion inhibitor 2 (Novinox®XCA02) after 30 min **(a)**, 3 h **(b)**, 6 h **(c)** and 7 h **(d)** with the experimental impedance and noise distortion curves.

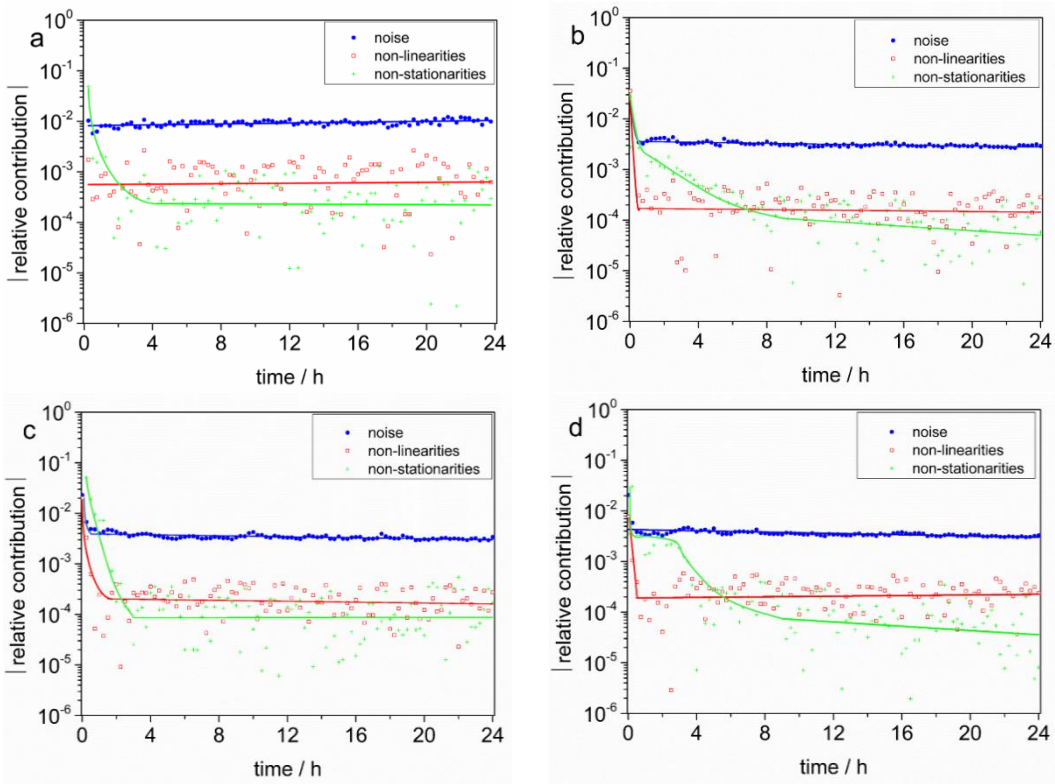

Figure A8 Evolution of the contribution of the noise, non-linearities and non-stationarities relative to the impedance modulus for hot-dip galvanized steel without corrosion inhibitor **(a)**, with Inhibitor 1 (Novinox®ACE110) **(b)**, inhibitor 2 (Novinox®XCA02) **(c)**, inhibitor 3 (Halox®SW-111) **(d)**, inhibitor 4 (Heucophos®CAPP) **(e)**, inhibitor 5 (Zinc Phosphate ZP10) **(f)** and inhibitor 1+2 **(g)**. The blue, red and green line represent the trend line of the noise, non-linearities and non-stationarities, respectively.

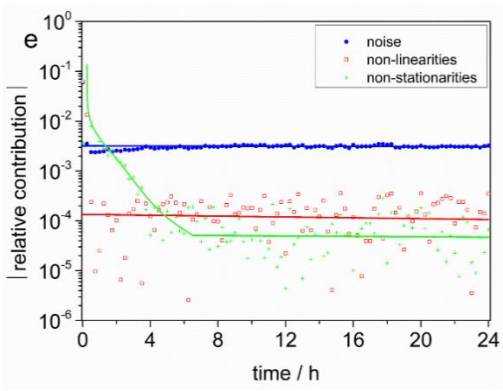

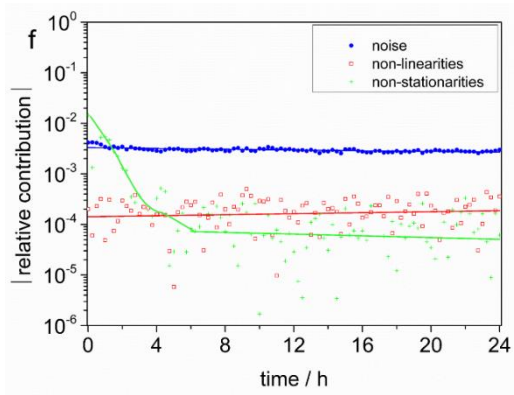

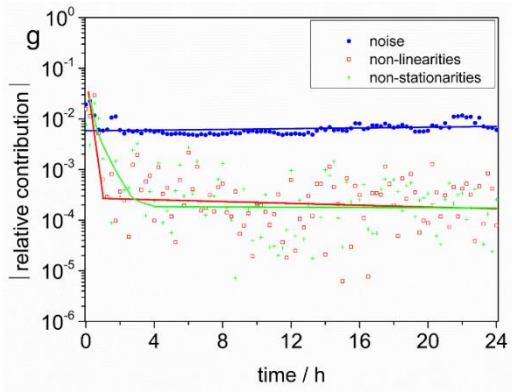

Figure A8 (continued)

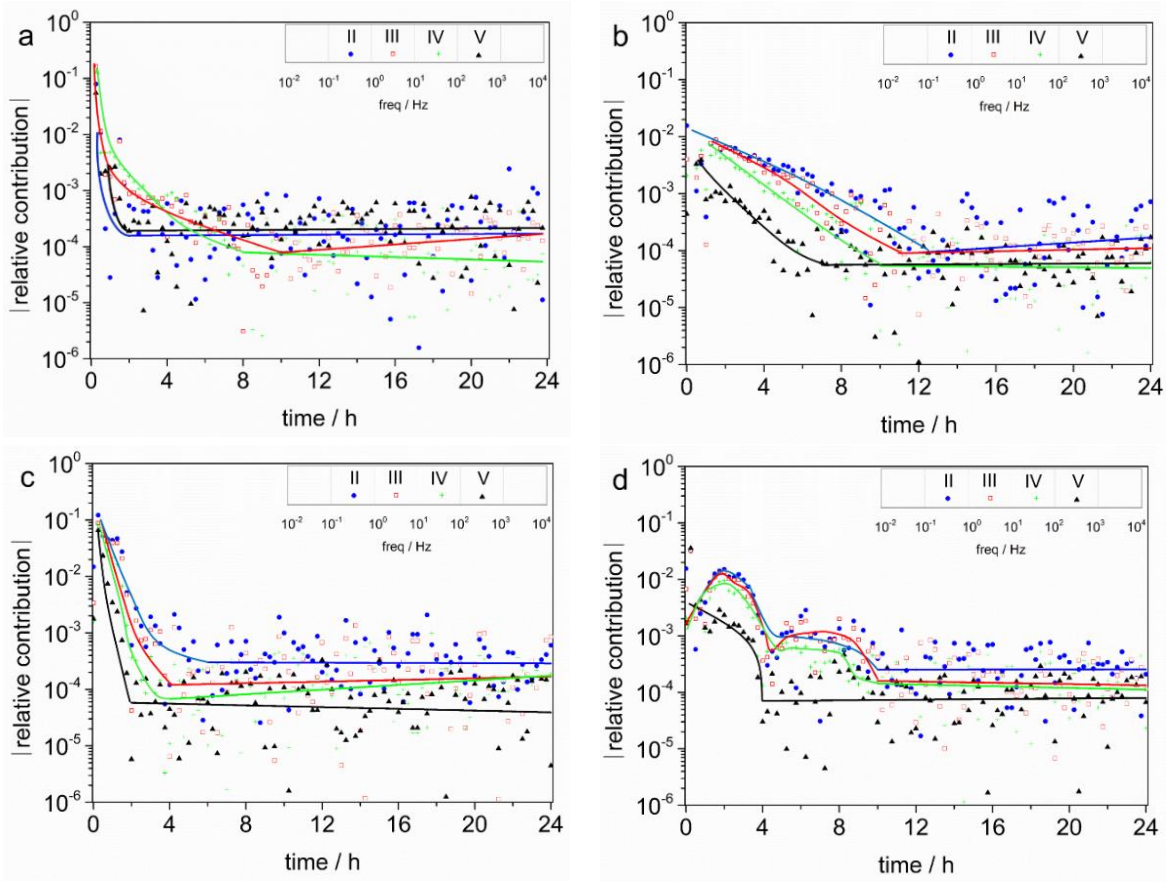

Figure A9 Evolution of the relative contribution of the non-stationarities for the different frequency decades for hot-dip galvanized steel without corrosion inhibitor **(a)**, with Inhibitor 1 (Novinox®ACE110) **(b)**, inhibitor 2 (Novinox®XCA02) **(c)**, inhibitor 3 (Halox®SW-111) **(d)**, inhibitor 4 (Heucophos®CAPP) **(e)**, inhibitor 5 (Zinc Phosphate ZP10) **(f)** and inhibitor 1+2 **(g)** for the first 24 h of immersion, respectively. The blue, red, green and black lines represent the trend line of the non-stationarities in the respective frequency decades.

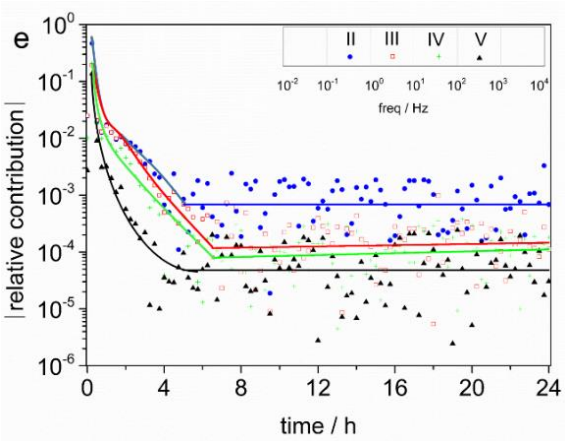

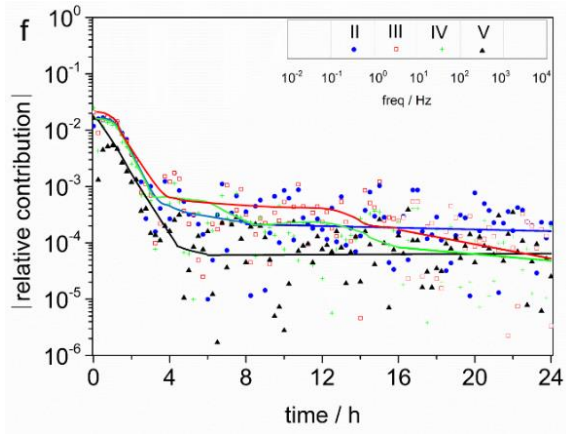

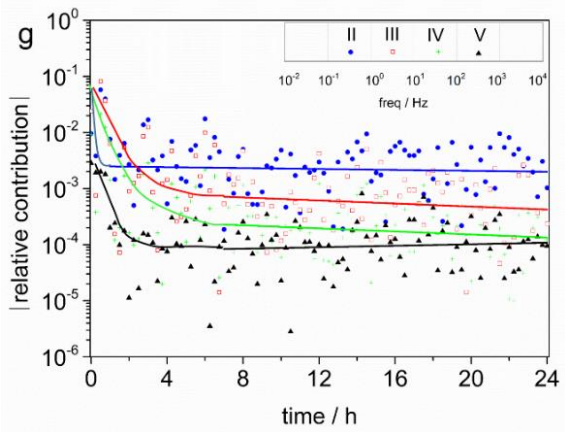

Figure A9 (continued)

Acknowledgements

During the first semester of the academic year 2014-2015, when I was finishing the last courses and writing the thesis of my masters, I was highly doubting what would be the next step: going to the industry, going to the consultancy-world or something completely else. Starting an academic career was never even considered as a real option. At that time, Herman informed me that there was a PhD position open in Delft with a similar topic as the subject of my master thesis which I enjoyed a lot. At that moment I realised that this PhD opportunity was actually what I wanted. Look where we are now.

Herman and Arjan, your impact during my PhD work cannot be underestimated, while giving me the freedom to choose my own direction. When I had a research question you were there to help me, when I needed assistance from outside you pointed me in the right direction. Also, when I was postponing the first, second, third or fourth draft version of a new paper or manuscript, you were there to give me a well-deserved kick up the arse. I think the power of VUB and TUD working together has once again been proven.

I would like to thank especially Shoshan, Joost, Laura-Lynn and Agnieszka for the warm welcome they gave me when arriving in Delft and helping me starting up my research. Thanks also to Yaiza and Peyman, for the interesting discussions regarding our research topics. I would also like to thank all the new faces that came into our group in the past years for adding new, positive energy and enhancing the group knowledge: Ali, Aytac, Mirsajiad, Ursa, Sven, Bala, Emina, Marta and Prakash. Special thanks to Saskia for all the help with the administrative part which, as you know, often frustrated me a lot. Maxine, thanks for the help with corrosion inhibitor research for your master thesis project. Soheil and Benham, we started off as colleagues but now I can refer to you as real friends.

I would also like to thank the entire SURF team for taking care of me during the first 8 months of my PhD and in particular Chiara and Thibault for the help with the ORP-EIS. Thanks also to Lorenzo, Berk and Sven for all the fun during and after work, the dinner parties and the enjoyable conferences we went on together.

Over the years I worked together with a lot of people from different groups and universities resulting in a number of co-authored papers. Therefore I would like to thank Peter (TUD/Akzo Nobel) for the collaboration regarding the lithium corrosion inhibitor technology; Lucia and Annick (VUB) for their feedback regarding the multisine impedance measurements; Axel (Netherlands Defence Academy) for the fruitful implementation of noise measurements in my research which I believe we will continue in the future; Luca, Francesco and Lorenzo (University of Udine) for the excellent work in Delft and the

continuation in Udine on the corrosion inhibitors for hot-dip galvanized steel; and Berend (TATA steel) for the resources, the company tours and industrial input over the entire duration of the PhD.

Starting a life in another country definitely brought challenges to the table. I'm well aware that I got a head start thanks to Cleo and Laura for selecting me as their first ever male roommate to live in their house with special features, thanks to Leo and the boys of 'de paardenmarkt 1' and thanks to Joost for introducing me into his football team and the after work "borrel" culture. Over the years, Joost, you have helped me with so many things, not only related to work and I hope I can do the same for you now and I wish you all the best finishing your PhD.

I would also like to express my gratitude towards my two paranymphs: Timo and Maarten. Timo, I guess you are my oldest childhood friend and together we discovered already so many things. I was honestly afraid that your move to the UK would affect our friendship but luckily it hasn't. You have always been the first one to joke about doing a PhD, the related office hours and the enormous amount of holidays. I was hoping that after four years that would finally come to an end, but I guess the continuation of my academic career in terms of a PostDoc isn't making it any better for the future. Maarten, from the moment I lured myself in the football team as a goalkeeper, you were there to welcome me with open arms. Although my goalkeeping skills were questionable, I could stay as a field player. I soon realized we shared not only the same interests and passions but also similar approaches and opinions about life. When you asked me to join last notice to Dekmantel festival, everything took off rapidly. From then on, I really felt home in the Netherlands and things only went better. I keep on looking forward to our monthly visiting schedule. Having you both here by my side means a lot to me 🖐🖐🖐.

To my father Danny and my mother Annik, thank you for all the opportunities you have given me and all the support in pursuing my own dreams in life. For 28 years already you have my back and although I didn't always express my appreciation, I will try to improve that. To my sister Ellis and my brothers Dries and Floris, I would like to say thank you for all the support and bringing us as brothers and sisters more together during the last years. I'm so happy that all of you found a direction you really like and are also really good at and I hope you can fulfil your long term dreams and expectations.

I would like to thank all my friends that were there for me to help me clearing my head after work, during the weekend or during the numerous holidays we went on together. Seppe, when we became lab partners more than 10 years ago, I never expected it to grow in such

an intensive friendship over the years, discovering together everything what possibly can be discovered. It's going to be hard to find new things but I'm sure that won't be a problem. A special thanks goes to the 'Komen fretten crew' for the multiple rounds of dinner parties organized; the 'Argentinaaaa crew', the 'Brazil topteam', 'Team ColOmbia', 'Team Iran', the 'From Russia with Love crew', the different skiteams and the 'Lowlandsvikings' for the awesome holidays with unbelievable memories; the Junction-, Voodoo- and Selectors- crew for the joyful weekends; an honourable mention goes to 'the 5 sweeties'; and last but not least, the 'Dekmantel crew' for the yearly growing combination of BE and NL people with a shared love for music and 'gezelligheid'.

Louise, without you this PhD would never have been finished. For many it will sound like a sentence of empty, cheap words, but it's actually true (you can ask her the story). The laughter when you tried to explain the topic of my PhD quickly turned into a proud smile when I realised how important it was for you to understand what I was actually doing all the time. If it was allowed to let you present the Layman's talk, I would definitely go for it. Not only you listened to all my problems and frustrations regarding my PhD but you also taught me how to solve them. It intrigues me how motivated and persistent you are in everything you do in your personal life as well as your working career in which I will always support you as your biggest fan. I think we found a perfect balance between our common lives and our separate lives. I think most of your friends became also friends of mine and vice versa while we are still getting to know new people around us. We took a lot of challenges together already, but there are many more to come, to which I'm looking so much forward to. They say the fastest point from point A to point B is a straight line, but with you I prefer anything else than that. You are definitely one of the strongest persons I know, not only physically. At this moment, I prefer to keep some things for later since I guess more opportunities will present itself in the future to express how much I love you...

PS. Tine (Koffie bij Tine) is thanked for the beautiful design of the cover, bookmark and invitation.

List of publications

Journal Articles

Visser, P., Meeusen, M., Gonzalez-Garcia, Y., Terryn, H., Mol, J.M.C. (2017). Electrochemical evaluation of corrosion inhibiting layers formed in a defect from lithium-leaching organic coatings. *Journal of the electrochemical society,* 164, 396-406.

Meeusen, M., Visser, P., Fernandez Macia, L., Hubin, A., Terryn, H., Mol, J.M.C. (2018). The use of odd random phase electrochemical impedance spectroscopy to study lithium-based corrosion inhibition by active protective coatings. *Electrochimica Acta, 278,* 363–373.

Pletincx, S., Fockaert, L.L.I, Meeusen, M., Mol, J.M.C, Terryn, H., Hauffman, T. (2018). In Situ Methanol adsorption on aluminium oxide monitored by a combined ORP-EIS and ATR-FTIR Kretchmann setup. *The journal of physical chemistry,* 122, 21963-21973

Meeusen, M., Zardet, L., Homborg, A.M., Lekka, M., Andreatta, F., Fedrizzi, L., Boelen, B., Terryn, H., Mol, J.M.C. (2019). A complementary electrochemical approach for time-resolved evaluation of corrosion inhibitor performance. *Journal of the Electrochemical Society, 166 (11)*, C3220-C3232.

Meeusen, M., Zardet, L., Homborg, A.M., Lekka, M., Andreatta, F., Fedrizzi, L., Boelen, B., Terryn, H., Mol, J.M.C. (2020). The effect of time evolution and timing of the electrochemical data recording of corrosion inhibitor protection of hot-dip galvanized steel. *Corrosion Science* (submitted).

Taheri, P., Milosev, I., Meeusen, M., Kapun, B., White, P., Kokalj, A., Mol, J.M.C. (2020). On the importance of time-resolved electrochemical evaluation in corrosion inhibitor screening studies. *Npj Materials Degradation* (submitted).

Conference presentations

M. Meeusen, A. Lutz, I. De Graeve, J.M.C. Mol, H. Terryn. Micro-encapsulation of corrosion inhibitors. European Corrosion Congress – EUROCORR, Graz, Austria (September 2015) (Poster Presentation)

M. Meeusen, A.M. Homborg, B. Boelen, H. Terryn, J.M.C. Mol. Complementary use of EIS, Odd-Random-Phase EIS and Electrochemical Noise measurements to study corrosion systems. European Corrosion Congress – EUROCORR, Montpellier, France (September 2016)

M. Meeusen, L. Zardet, F. Andreatta, B. Boelen, H. Terryn, J.M.C. Mol. Studying possible synergistic effects between corrosion inhibitors for galvanized steel sheet. European Corrosion Congress – EUROCORR, Prague, Czech Republic (September 2017)

M. Meeusen, P. Visser, L.F. Macia, B. Boelen, H. Terryn, J.M.C. Mol. Use of Odd-Random-Phase EIS to study the protection mechanisms and performance of Cr(VI)-free inhibitor technology. International Workshop on Application of Electrochemical Techniques to Organic Coatings - AETOC, Billerbeck, Germany (April 2017)

M. Meeusen, L. Zardet, F. Andreatta, B. Boelen, H. Terryn, J.M.C. Mol. Methodology of studying corrosion inhibitor efficiency and synergy for coated galvanized steel sheet. European Corrosion Congress – EUROCORR, Krakow, Poland (September 2018)

M. Meeusen. Elektrochemische Impedantie Spectrsocopie (EIS) en Odd-Random-Phase Elektrochemische Impedantie Spectroscopie (ORP-EIS) als middel om elektrochemische systemen te bestuderen. Bond voor materialenkennis – Studiekern Corrosie, Delft, the Netherlands (October 2018)

M. Meeusen. Methodology of studying corrosion inhibitor efficiency and synergy for coated galvanized steel. Materials Innovation Institute – M2i Conference, Noordwijkerhout, the Netherlands (December 2018)

MATS MEEUSEN

Born on May 29th, 1991
Wilrijk (Antwerpen), Belgium

Education

2015-2019	**PhD in Materials Science and Engineering**, Delft University of Technology, Delft, the Netherlands
2012-2015	**MSc in Chemical and Materials Engineering**, Vrije Universiteit Brussel, Brussel, Belgium
2009-2012	**BSc in Chemical Engineering at Vrije Universiteit Brussel**, Brussel, Belgium
2003-2009	**Secondary education**, Koninklijk Lyceum Antwerpen, Antwerpen, Belgium

Working experience

2013	**Industrial internship**, Devan Chemicals, Porto, Portugal